LEABHARLANN CHOLÁISTE NA TRÍONÓIDE, BAILE ÁTHA CLIATH | TRINITY COLLEGE LIBRARY DUBLIN
Ollscoil Átha Cliath | The University of Dublin

Terms and Conditions of Use of Digitised Theses from Trinity College Library Dublin

Copyright statement

All material supplied by Trinity College Library is protected by copyright (under the Copyright and Related Rights Act, 2000 as amended) and other relevant Intellectual Property Rights. By accessing and using a Digitised Thesis from Trinity College Library you acknowledge that all Intellectual Property Rights in any Works supplied are the sole and exclusive property of the copyright and/or other IPR holder. Specific copyright holders may not be explicitly identified. Use of materials from other sources within a thesis should not be construed as a claim over them.

A non-exclusive, non-transferable licence is hereby granted to those using or reproducing, in whole or in part, the material for valid purposes, providing the copyright owners are acknowledged using the normal conventions. Where specific permission to use material is required, this is identified and such permission must be sought from the copyright holder or agency cited.

Liability statement

By using a Digitised Thesis, I accept that Trinity College Dublin bears no legal responsibility for the accuracy, legality or comprehensiveness of materials contained within the thesis, and that Trinity College Dublin accepts no liability for indirect, consequential, or incidental, damages or losses arising from use of the thesis for whatever reason. Information located in a thesis may be subject to specific use constraints, details of which may not be explicitly described. It is the responsibility of potential and actual users to be aware of such constraints and to abide by them. By making use of material from a digitised thesis, you accept these copyright and disclaimer provisions. Where it is brought to the attention of Trinity College Library that there may be a breach of copyright or other restraint, it is the policy to withdraw or take down access to a thesis while the issue is being resolved.

Access Agreement

By using a Digitised Thesis from Trinity College Library you are bound by the following Terms & Conditions. Please read them carefully.

I have read and I understand the following statement: All material supplied via a Digitised Thesis from Trinity College Library is protected by copyright and other intellectual property rights, and duplication or sale of all or part of any of a thesis is not permitted, except that material may be duplicated by you for your research use or for educational purposes in electronic or print form providing the copyright owners are acknowledged using the normal conventions. You must obtain permission for any other use. Electronic or print copies may not be offered, whether for sale or otherwise to anyone. This copy has been supplied on the understanding that it is copyright material and that no quotation from the thesis may be published without proper acknowledgement.

Genome Wide Investigation of Papillary Thyroid Carcinoma

A thesis submitted for the Degree of Doctor of Philosophy

by

Stephen Finn
BDS FDS MB BAO BCh BMedSc

Trinity College
University of Dublin

Trinity Term
2005

Supervisor: Dr. Orla Sheils, FAMLS, PhD

TRINITY COLLEGE
19 MAY 2005
LIBRARY DUBLIN
THESIS
7572.

Declaration

I declare that this thesis is my own work, and has not been submitted previously for a PhD degree at this or any other university. I agree that the library may lend or copy this thesis on request.

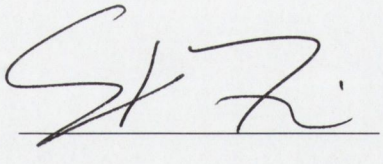

For my parents Patrick and Anne

Contents

Acknowledgements i

List of abbreviations iii

Publications vi

Summary xii

Chapter 1

General Introduction 1

1.1 Thyroid: Historical Context 2

1.2 Thyroid Embryology and Development 5

1.3 Anatomy and Histology of the thyroid gland 7

1.4 Primary Epithelial Thyroid Tumours 9

1.4.1 Classification of primary epithelial tumours of the thyroid 9

1.4.2 Pathology of primary epithelial tumours of the thyroid 10

1.4.2.1 Follicular Adenoma 10

1.4.2.2 Follicular Thyroid Carcinoma and variants 11

1.4.2.3 Papillary Thyroid Carcinoma and variants 13

1.4.2.4 Insular carcinoma/Poorly Differentiated Carcinoma 21

1.4.2.5 Anaplastic Carcinoma 22

1.4.2.6 Medullary thyroid Carcinoma 23

1.5 Epidemiology of thyroid cancer worldwide and in Ireland 24

1.6	Aetiology of thyroid cancer	27
1.6.1	Iodine	27
1.6.2	External Radiation	27
1.6.3	Other risk factors	30
1.7	Molecular Pathology of Papillary thyroid carcinoma	31
1.7.1	RAS	31
1.7.2	Tyrosine Kinase receptors	33
1.7.2.1	*Ret* proto-oncogene	33
1.7.2.2	Ret/PTC oncogenes	35
1.7.2.3	NTRK	37
1.7.2.4	MET	37
1.7.3	BRAF	38
1.7.4	Other Genes implicated in Thyroid carcinoma	39
1.7.4.1	Immediate early genes	39
1.7.4.2	p53	39
1.7.4.3	PTEN	40
1.7.4.4	PPARγ	40
1.8	Aims and Objectives	41
1.9	General References and Bibliography	43

Chapter 2

Methodology

2.1	Introduction	58
2.2	**Section 1**	**58**
2.2.1	Fresh Thyroid Tissue Archive	58

2.2.2	Formalin fixed paraffin embedded Tissue	59
2.3	**Section 2**	**60**
2.3.1	Cell Culture of N thy-ori cells	60
2.3.2	Formulation of N thy-ori culture media and other solutions	60
2.3.3	Thawing cells from stocks	61
2.3.4	Splitting Confluent flasks	61
2.3.5	Cryopreservation	62
2.3.6	Mycoplasma testing	63
2.3.6.1	Background	63
2.3.6.2	Mycoplasma Protocol	64
2.4	**Section 3**	**67**
2.4.1	Tissue preparation prior to nucleic acid extraction	67
2.4.2	Frozen Section cutting Protocol	67
2.4.3	Fixing and staining for Methyl green/H&E	68
2.4.4	Tissue Homogenisation	68
2.4.4.1	Mortar and pestle homogenisation of tissue	69
2.4.4.2	QIAshredder®	69
2.4.4.3	Microfuge pellet mixer	70
2.5	**Section 4**	**71**
2.5.1	Arcturus PixCell II Laser Capture Microdissection system	71
2.5.2	Background	71
2.5.3	Setting LCM Parameters	72

2.5.4	Protocol for LCM	74
2.6	**Section 5**	**79**
2.6.1	Nucleic acid extraction protocols	79
2.6.2.	Extraction of DNA from alcohol fixed frozen sections using Puregene® DNA Extraction Protocol	79
2.6.2.1	Cell Lysis and RNA digestion	79
2.6.2.2	Protein precipitation	79
2.6.2.3	DNA precipitation	80
2.6.2.4	DNA hydration	80
2.6.3	Extraction of RNA from laser captured cells using Purescript ® RNA extraction protocol	81
2.6.3.1	Cell Lysis	81
2.6.3.2	Protein/DNA precipitation	81
2.6.3.3	RNA precipitation	81
2.6.3.4	RNA hydration	82
2.6.4	Extraction of RNA from laser captured cells using Qiagen® Rneasy spin columns	82
2.6.4.1	Preparation for RNeasy column RNA extraction	82
2.6.4.2	Protocol for on column DNase digestion	84
2.6.4.3	Preparation for DNase digestion	84
2.6.4.4	DNase digestion Procedure	85
2.6.4.5	Washing and eluting RNA	86
2.6.5	Dual extraction of RNA and DNA from the same sample	87
2.6.5.1	Overview	87
2.6.5.2	Protein-DNA Pellet Resuspension	87

2.6.5.3	RNase Treatment	88
2.6.5.4	Protein Precipitation	88
2.6.5.5	DNA Precipitation	88
2.5.5.6	DNA Hydration	89
2.7	**Section 6**	**90**
2.7.1	Quantifying RNA and DNA Samples By UV Spectrophotometry	90
2.7.2	UV Spectrophotometry Background	90
2.7.3	Protocol for UV Spectrophotometry	91
2.8	**Section 7**	**93**
2.8.1	Assessing nucleic acid integrity by Agarose Gel Electrophoresis	93
2.8.2	Background	93
2.8.3	Protocol for Agarose Gel Electrophoresis	93
2.9	**Section 8**	**95**
2.9.1	Primer and Probe design	95
2.9.2	Background: Primer Express 1.5. Theory of Operation	95
2.9.3	Protocol for TaqMan Primer and probe design	96
2.9.4	Primer and probe sequences for ret/PTC-1, ret/PTC-3 and GAPDH	97
2.9.5	Design of primers and Probes for BRAF ^{V600E} allelic discrimination assay	97
2.10	**Section 9**	**99**
2.10.1	PCR and allelic discrimination Control Samples	99
2.10.2	ret/PTC-1	99
2.10.3	ret/PTC-3	99
2.10.3.1	Generation of cRNA positive control transcripts for ret/PTC-3	101
2.10.3.2	Bacterial Culture and transformation	101

2.10.3.3	Plasmid extraction	102
2.10.3.4	Linearisation and restriction digestion for diagnostic purposes	103
2.10.3.4	Purification of linearised DNA post restriction digestion	103
2.10.3.5	*In-vitro* Transcription	104
2.10.3.6	DNase treatment of cRNA reaction mixture	105
2.10.3.7	Purification of cRNA post DNase digestion	106
2.10.4	Allelic Discrimination Controls	107
2.11	**Section 10**	**107**
2.11.1	TaqMan RTPCR and Allelic Discrimination Assays	107
2.11.2	The Chemistry of TaqMan PCR assays	108
2.10.3.2	Minor groove Binder (MGB Probes)	111
2.10.4	RT-PCR	112
2.10.4	Allelic Discrimination Assay	112
2.12	**Section 11**	114
2.12.1	Background to Array CGH	114
2.12.2	Labelling Protocol	115
2.12.3	DNase Digestion and Labeled Probe Purification	116
2.12.3	Checking the Labeled DNA	117
2.12.4	Hybridisation Protocol	118
2.12.4.1	Preparing the Reagents	118
2.12.4.2	Preparing the Hybridisation Solution	119
2.12.4.3	Hybridisation	120
2.12.4.4	Washing the Microarrays	121
2.12.4.5	Image analysis	123

2.13	**Section 12 Applied Biosystems expression Microarrays**	**125**
2.13.1	Background. RT-IVT Protocol (The Eberwine Protocol)	126
2.13.1.1	RT IVT Protocol	128
2.13.1.2	Performing Second Strand Synthesis	129
2.13.1.3	Purifying cDNA	129
2.13.1.4	Performing *In Vitro* Transcription (IVT)	131
2.13.1.5	Purifying cRNA	132
2.13.2	Hybridisation and Chemiluminescence	135
2.13.2.1	Background	135
2.13.2.2	Prehybridising Microarrays	135
2.13.2.2	cRNA Fragmentation	137
2.13.2.3	Hybridising Samples to Microarrays	138
2.13.2.4	Preparing Wash Buffers and Reagents	139
2.13.2.4	Performing Hybridisation Washes	141
2.13.2.5	Performing Antibody Binding	142
2.13.2.6	Performing Antibody Washes	143
2.13.2.7	Performing the CL reaction	144
2.13.2.8	Performing the CL Detection	145
2.13.3	Array Controls	146
2.13.3.1	Assay Background Controls	147
2.13.3.2	Blank Features	148
2.13.3.3	Control Ladders	149
2.13.3.4	Hybridisation Controls	149
2.13.3.5	Internal Control	150
2.13.3.6	IVT Controls	151

2.13.3.7 Landmark Fiducials 152

2.13.3.8 RT Controls 152

2.13.3.8 Spatial Normalisation Controls 153

2.14 References 155

Chapter 3 **157**

Ret/PTC chimeric transcripts in an Irish cohort of sporadic Papillary Thyroid Carcinoma

3.1 Summary 158

3.2 Introduction 159

3.2.1 Papillary thyroid Carcinoma 159

3.2.2 Ret proto-oncogene 160

3.2.3 Ret rearrangements 161

3.3 Aims 164

3.4 Materials and Methods 164

3.4.1 Statistical approach 165

3.5 Results 166

3.5.1 Prevalence of ret rearrangements 166

3.5.2 Tumour morphology 167

3.5.2.1 Classic and Variant Morphology 167

3.5.2.2 Tall Cell Variant 168

3.6 Discussion 169

3.7 Conclusion 172

3.8 References 173

Chapter 4 **180**

Array CGH analysis of gamma irradiated human thyrocytes

4.1 Introduction 181

4.2 Summary 181

4.3 Radiation-induced thyroid carcinoma 182

4.4 Array CGH 183

4.5 *In vitro* studies of radiation on thyroid epithelium 184

4.6 Aims 185

4.7 Materials and Methods 186

4.7.1 Cell Culture 186

4.7.2 Gamma Irradiation of Thyroid cells 186

4.7.3 Nucleic acid extraction 187

4.7.4 TaqMan RT PCR 187

4.7.5 Array CGH 188

4.7.6 Reports and statistical analysis 188

4.8 Results 190

4.8.1 Effects of irradiation on cell proliferation 190

4.8.2 Morphological effects of irradiation on cells 190

4.8.3 TaqMan RT PCR for *ret*/PTC-1 and *ret*/PTC-3 192

4.8.3.1 Control n-thy-ori cells 192

4.8.3.2 Irradiated N-thy-ori cells 192

4.8.4 CGH array analysis 193

4.9 Discussion 196

4.10 Conclusion 202

4.11 References 204

Chapter 5 **212**

Assessment of DNA copy gain and loss in Papillary Thyroid Carcinoma using array CGH

5.1 Summary 213

5.2 Introduction 214

5.3 Comparative Genomic Hybridisation 215

5.3.1 Genosensor Array CGH (Vysis) 217

5.4 Aim 218

5.5 Materials and Methods 219

5.5.1 Tumours and Cell lines 219

5.5.2 Laser Capture Microdissection and DNA Extraction 219

5.5.3 Ret/PTC rearrangement analysis 220

5.5.4 BRAF Assay 220

5.5.4 CGH 221

5.5.5 Controls for CGH 221

5.5.5.1 Validation of technique using is a control DNA (COSH) 221

5.5.5.2 Validation of the sensitivity of the system using sex mismatched test and reference 222

5.5.5.3 Validation using previously described conventional CGH profiles of BCPAP cell line 225

5.6 Results 226

5.6.1 Analysis Cohort 226

5.6.2 Ret/PTC and BRAF mutation status 227

5.6.2 Array CGH 228

5.6.2.1 General Trends 228

5.6.2.2 Recurrent gains and losses 231

5.7 Discussion 236

5.8 Conclusion 242

5.9 References 243

Chapter 6 **249**

Biomarker discovery using microarray expression analysis of Papillary Thyroid Carcinoma and benign thyroid tissue

6.1 Summary 250

6.2 Introduction 252

6.2.1 Biomarkers of malignancy 254

6.2.2 Applied Biosystems® Human Genome Survey Microarray 254

6.3 Aims 256

6.4 Materials and methods 256

6.4.1 Specimens 256

6.4.2 RNA and DNA Extraction, *In vitro* transcription 257

6.4.3 RNA labelling, hybridisation to microarrays and the Chemiluminescence reaction 259

6.4.3.1 Reverse transcription 259

6.4.3.2 Second strand synthesis and cDNA purification 259

6.4.3.3 *In-vitro* transcription labeling and purification of cRNA 260

6.4.3.4 Chemiluminescence Reaction 260

6.4.3.5 Array Scanning 261

6.4.3.6 Data management 262

6.5 Analysis of Gene Chip Data using Spotfire Functional Genomics software 263

6.5.1 Normalisation 263

6.5.2 Statistical analysis 267

6.5.3 Data Mining and the Panther® Database 269

6.6 Results 271

6.6.1 Distinguishing benign thyroid lesions from PTC 271

6.6.2 Clustering and Bonferroni analysis 271

6.6.3 False Discovery Rate analysis 273

6.6.4 Distinction analysis 276

6.6.5 Benign and malignant follicular patterned lesions 281

6.6.6 Panther analysis 286

6.7 Discussion 288

6.8 Conclusion 293

6.9 References 295

Chapter 7 **305**

General Discussion, Future Work and Conclusions

7.1 Review of results and conclusions 306

7.2 Thyroid Cancer: A view of the future 316

7.2.1 The disappointment of the present 316

7.2.2 The promise of the future 317

7.2.3 Magic Bullets 318

7.3 References 320

Figures

Figure 1.1	Gross PTC	14
Figure 1.2	Classic PTC, Original magnification X 20	15
Figure 1.3	Follicular Variant PTC	18
Figure 1.4	Tall Cell variant	20
Figure 1.5	Incidence of thyroid cancer in Ireland	25
Figure 1.6	Death from Thyroid cancer in Ireland	26
Figure 1.7	Age and sex profile of Irish thyroid carcinoma from 1994-1997	26
Figure 1.8	The role of *RET* in thyroid carcinogenesis	34
Figure 2.1	Overview of LCM Process	73
Figure 2.2	Example of calls captured by LCM	74
Figure 2.3	Agarose gel electrophoresis of total RNA	95

Figure 2.4	Plasmid pcDNA3	100
Figure 2.5	Restriction map for ret/PTC-3 insert	100
Figure 2.6	Illustration of the principle of TaqMan PCR	109
Figure 2.7	Illustration of principle of allelic discrimination assay	113
Figure 2.8	Agarose Gel of purified labelled probe	118
Figure 2.9	Genosensor array 300 Report page	124
Figure 2.10	RT IVT Overview flowchart	127
Figure 2.11	Hybridisation and CL overview	136
Figure 2.12	Array Controls	147
Figure 3.1	Mechanisms of chromosomal rearrangements generating fusion-transforming genes in PTC	161
Figure 3.2	Most common ret rearrangements	162
Figure 3.3	TaqMan real time RT PCR amplification plot	165
Figure 4.1	Irradiated N thy-ori cells (Low)	191

Figure 4.2	Irradiated N thy-ori cells (High)	191
Figure 4.3	Distribution of statistically significant gains and losses according to locus	200
Figure 5.1	Schematic of array CGH	218
Figure 5.2	Allelic discrimination plot	221
Figure 5.3	Aberrations expressed as a percentage of loci analysed	229
Figure 5.4	Gains and losses as a percentage of total loci analysed	230
Figure 5.5:	Test to reference fluorescence ratios for all cases across all loci examined	231
Figure 6.1	Overview of Chemiluminescence chemistry	261
Figure 6.2	MA plot for median normalisation	266
Figure 6.3	MA plot for quantile normalisation	266
Figure 6.4	Hierarchical clustering of 1139 genes	272
Figure 6.5	Profile chart of genes showing increased and decreased expression in PTC with clear distinction patterns	276

Figure 6.6	Panther classification of genes in Table 6.5	280
Figure 6.5	Hierarchical clustering of 2639 genes	282
Figure 7.1	Signal transduction by PDGRF family kinases and BRAF	314

List of Tables

Table 1.1	Ret rearrangements	36
Table 2.1	LCM Settings	73
Table 2.2	Primer and probe sets for TaqMan PCR	97
Table 2.3	BRAF allelic discrimination primer/probe Sequences	98
Table 3.1	Tumour morphology	166
Table 3.2	Chimeric transcripts detected	167
Table 4.1	Copy gains and losses in irradiated and non-irradiated cells	195
Table 5.1	Case profiles	224
Table 5.2	Sex mismatched controls	225
Table 5.3	Rearranged ret and mutant BRAF status	228
Table 5.4	Recurrent gains	232
Table 5.5	Recurrent losses	233

Table 5.6	Recurrent Gains detected in surgical cases	234
Table 5.7	Recurrent losses detected in surgical cases	234
Table 5.8	Recurrent gains in relation to BRAF mutation status and Morphology	235
Table 6.1	Specimen morphology, ret and BRAF status	258
Table 6.2	Genes showing increased expression in malignancy after *t*-test and Bonferroni correction	273
Table 6.3	Genes with decreased expression in malignancy	274
Table 6.4	Genes with decreased expression in malignancy	275
Table 6.5	Genes with increased expression in PTC relative to benign conditions using the Distinction Calculation.	277
Table 6.6	Genes showing increased expression in FVPTC compared to normal thyroid tissue and benign follicular patterned thyroid lesions	284
Table 6.7	Functional comparison of genes showing increased expression in FVPTC and relative decreased expression in classic morphology PTC	286
Table 6.8	Functional comparison of genes showing increased expression in classic morphology and relative decreased expression in FVPTC	287

Acknowledgements

There are many people to acknowledge. At the top of the list, I would like to thank my supervisor Dr. Orla Sheils for all her help and encouragement, particularly for her highly positive attitude at critical and sometimes difficult times. I would also like to thank Professor John O'Leary for his enthusiasm and words of encouragement throughout the duration of the project. Thanks to both Orla and John for encouraging me to apply for a Health Research Board grant. Without their support, I know I would never have been successful.

I must also acknowledge the role played by the Health Research Board of Ireland. The Clinical Research Training Fellowship provided an opportunity for me to significantly advance my knowledge of the molecular basis of pathology and to gain expertise in innovative molecular technology. I intend to use this knowledge well in the future.

I must also thank my wife Esther for her constant support and love and probing questions!

There are many others:

Paul Smyth has been an absolute gem. He has educated me in the finer details of molecular techniques and with good humour and great craic, he has taught me everything from pipetting to advanced biostatistics! Thanks also to Dr. Richard Flavin and Susanne Cahill for their ideas, input and entertainment.

Thanks to Professor Con Timon and especially to his patients, without whom, none of the work for this thesis could have been done. I hope that the research done by this

group and others will be of significant benefit to other patients in the future. Thanks to Dr. Mary Toner for her role in tissue-banking and her expert histopathology input.

Thanks to all those at the research Laboratory in the Coombe Women's Hospital, especially for the help with cell culture and *in-vitro* transcription: Cara Martin, Niamh Murphy, Richard Shattock, Martina Ring and Cynthia Heffron. Thanks to Anya Milne for providing copies of many papers at short notice.

Many thanks to Professor Kingston Mills for his critical but constructive comments at the HRB interview and for allowing me the use of the gamma irradiation facilities at the Biochemistry Department in TCD.

I am very grateful to Teresa Ruffalo of Vysis for help with troubleshooting CGH array technique and Christopher Streck, Sergei Labur and David Howells of Applied Biosystems for the excellent training and bioinformatics assistance.

List of Abbreviations

β-ME	β-Mercaptoethanol
CDS	Celera Discovery System
CGH	Comparative Genomic Hybridisation
CL	Chemiluminescence
DAPI	4', 6-diamidino-2-phenylindole
DEPC	Diethylpyrocarbonate
DIG	Digoxigenin
DMSO	Dimethyl sulfoxide
DNA	Deoxyribonucleic acid
dNTP	Deoxynucleoside triphosphate
DTT	Dithiothreitol
ECACC	European cell and tissue culture collection
ELISA	Enzyme Linked Immuno Sorbent Assay
EST	Expressed sequence tag
EtBr	Ethidium Bromide
FAM	6-carboxyfluorescein
FCS	Foetal calf serum
FFPE	Formalin Fixed Paraffin Embedded
FISH	Fluorescent *In-Situ* Hybridisation
FMTC	Familial medullary thyroid carcinoma
FNAC	Fine Needle Aspiration Cytology
FRET	Forster-type energy transfer
FTC	Follicular thyroid carcinoma
FVPTC	Follicular variant papillary thyroid carcinoma

FWER	Family Wise Error Rate
GAPDH	Glyceraldehyde-3-phosphate dehydrogenase
H&E	Haematoxylin and Eosin
HHM	Hidden Markov Model
LB	Luria-Bertani medium
LBB	Luria-Bertani broth
LCM	Laser Capture Microdissection
MAPK	Mitogen activated protein kinase
MEN	Multiple Endocrine Neoplasia
MGB	Minor groove binder
MTC	Medullary thyroid Carcinoma
MW	Molecular Weight
NFQ	non-fluorescent quencher
NTC	No Template control
°C	Degrees centigrade
PBS	Phosphate Buffered Saline
PTC	Papillary thyroid Carcinoma
RNA	Ribonucleic acid
RPMI	Roslyn Park Memorial Institute
RT	Reverse transcription
SCID	Subacute combined Immunodeficiency
SV40	Simian virus 40
TAE	Tris/Acetic acid/EDTA
TAMRA	6-carboxy-tetramethyl-rhodamine
Tm	Melting temperature

TNS	Trypsin neutralising solution
UNG	Uracil-DNA glycosylase
UTP	Uridine triphosphate

Publications

Array CGH analysis of gamma irradiated human thyrocytes. 2004. Finn SP, Smyth P, O'Regan EM, Cahill S, Flavin R, O'Leary JJ, Sheils O. Virchow's archive 445:396-404

Ret/PTC chimeric transcripts in an Irish cohort of sporadic Papillary Thyroid Carcinoma. 2003. Finn SP, Smyth P, O' Leary JJ, Sweeney EC, Sheils OM. J Clin Endocrinol Metab 88(2):938-41

This paper was awarded The George Greene Medal by The Faculty of Pathology of the Royal College of Physicians of Ireland for the best paper published in a peer reviewed biomedical journal in the preceding year.

Real Time quantitative analysis of E-cadherin in ret/PTC-1 activated thyroid neoplasms. 2001. Smyth P, Sheils O, Finn SP, Martin C, O'Leary J, Sweeney EC. International Journal of Surgical Pathology 9(4): 265-72

Ret/PTC rearrangements in Hashimoto's Thyroiditis. 2002. Sheils O, Smyth P, Finn SP, Int J Surg Pathol. 10(2): 167-8; discussion 168-9.

Real-time analysis of Beta and Gamma-Catenin mRNA expression in ret/PTC-1 activated and nonactivated thyroid tissues. 2003. Smyth P, Finn SP, O'Leary J, Sheils O. Diagnostic Molecular Pathology 12(1): 44-49

Nucleic acid microarrays: an overview. 2003. Sheils OM, Finn SP, O'Leary J. Current Diagnostic Pathology 9(3): 155-158

Quality-control issues for PCR-based assays in the molecular laboratory. 2003. Sheils OM, Finn SP, O'Leary J. Current Diagnostic Pathology 9(3): 165-172

Ret/PTC and BRAF act as distinct molecular time dependent triggers in a sporadic cohort of papillary thyroid carcinoma. 2005. Smyth P, Finn SP, Cahill S, Flavin R, O'Regan EM, O'Leary JJ, Sheils OM. Int J Surg Pathol. 13(1): 1-8

Abstracts

In-vitro and in-vivo evidence of an association between ret/PTC expression and cell adhesiveness and morphology in thyroid neoplasia. Sheils OM, Smyth P, Finn SP, Martin C, O'Leary JJ. Poster presentation USCAP annual meeting, Chicago March 2002. Abstract published in Modern Pathology vol. 15 (1) 120

Ret/PTC Chimeric transcripts in sporadic papillary thyroid carcinoma: Correlation with tumour morphology. S. P. Finn, Smyth P, Sweeney E, O'Leary JJ, Sheils O. Platform presentation at International Association of Pathology Meeting, Amsterdam 2002. Abstract published

Ret/PTC–3 correlates with solid/follicular morphology in "sporadic" papillary thyroid carcinoma. S. P. Finn, Smyth P, Sweeney E, O'Leary JJ, Sheils O. Poster presentation at Annual meeting of Pathological Society of Great Britain and Ireland. July 2002. Abstract published in The Journal of Pathology.

Osteoclastoma like anaplastic thyroid carcinoma: molecular evidence of its histogenesis. EM O'Regan, Smyth P, Finn SP, Sheils O, O'Leary J, Toner M. Poster presentation at Annual meeting of Pathological Society of Great Britain and Ireland. July 2003. Abstract published in the Journal of Pathology.

Analysis of β-catenin expression in thyroid neoplasia. Smyth P, Finn SP, O'Leary JJ, Sheils O. Poster presentation at Annual meeting of Pathological Society of Great Britain and Ireland. July 2002. Abstract published in the Journal of Pathology.

E-cadherin expression in ret/PTC-1 activated thyroid neoplasms, detected by TaqMan RT-PCR. Smyth P, Finn SP, Martin C, Sweeney EC, Sheils O, O'Leary JJ
Poster presentation at Annual meeting of Pathological Society of Great Britain and Ireland. July 2001. Abstract published in The Journal of Pathology.

E-cadherin expression is reduced in ret/PTC-1 but not ret/PTC-3 activated thyroid neoplasms. Smyth P, Finn SP, O'Leary JJ, Sheils OM. Poster presentation at Annual meeting of Pathological Society of Great Britain and Ireland. July 2002. Abstract published in The Journal of Pathology.

Expression of p16INK4A in serous lesions of the female genital tract.

Heffron C, Murphy N, Finn SP, Shiels O, O'Leary JJ. Poster presentation 19th European Congress of Pathology, September 2003. Abstract published: Virchows Archive 443 (3) 324.

Ret/PTC-1 a novel~Chimeric transcript occurring in Ovarian Serous surface Carcinomas: Preliminary Results. Flavin RJ, Finn SP, Smyth P, O'Regan EM, Gaffney E, O'Leary JJ, Sheils OM. Poster presentation at USCAP meeting March 2004. Abstract published Modern Pathology Vol. 17 no. 1 (Supplement).

Microarray Comparative Genomic hybridisation analysis of Head and Neck Squamous Cell Carcinomas occurring in young patients. O' Regan EM, Smyth PA, Finn SP, Sheils O, Flavin RJ, O'Leary JJ, Toner M. Poster presentation at USCAP meeting March 2004. Abstract published Modern Pathology Vol. 17 no. 1 (Supplement). Winner of best Poster Head and Neck Section of USCAP 2004.

Induction of ret/PTC chimera by gamma irradiation of immortalised human Thyrocytes.

Finn SP, Smyth P, O'Regan EM, Flavin R, O'Leary JJ, Sheils OM. Poster presentation at USCAP meeting March 2004. Abstract published Modern Pathology Vol. 17 no. 1 (Supplement).

Array Comparative Genomic Hybridisation analysis of gamma irradiated human thyrocytes. Finn SP, Smyth P, O'Regan EM, Flavin R, O'Leary JJ, Sheils OM. Poster presentation at USCAP meeting March 2004. Abstract published Modern Pathology Vol. 17 no. 1 (Supplement).

Array CGH profiling of laser capture microdissected Papillary Thyroid Carcinoma tumours and clonal cell lines. Finn SP, Smyth P, O'Regan EM, Cahill S, Toner M, Timon C, O'Leary JJ, Sheils OM. Poster presentation at the summer meeting of The Pathological Society of Great Britain and Ireland, Amsterdam, 2004. Abstract published in Journal of Pathology.

Analysis Of Head And Neck Squamous Cell Carcinoma In Young Patients Using Microarray Comparative Genomic Hybridisation. O'Regan EM, Sheils OM, Smyth P, Finn SP, Cahill S, Flavin RJ, Toner M, O'Leary JJ. Platform presentation at the summer meeting of The Pathological Society of Great Britain and Ireland, Amsterdam, 2004. Abstract published in Journal of Pathology.

Temporal Trends in BRAF T1796A and ret/PTC oncogene detection in Irish thyroid neoplasms. Smyth P, Finn SP, Cahill S, Flavin RJ, O'Regan EM, O'Leary JJ, Sheils OM. Poster presentation at the summer meeting of The Pathological Society of Great Britain and Ireland, Amsterdam, 2004. Abstract published in Journal of Pathology.

Identifying biomarkers of papillary thyroid carcinoma using genome wide cDNA expression microarrays. Finn SP, Smyth P, Cullen M, O'Regan EM, Timon C, Toner M, Cahill S, Streck CP, Howells D, O'Leary JJ, Sheils O. Poster presentation at the 30th annual meeting of the European Thyroid Association, Istanbul 2004. Abstract published.

Gene expression profile of PTC: Comparison of follicular variant and classic morphology PTC with benign follicular patterned lesions. 2005. SP Finn, PC Smyth, EM O'Regan, S. Cahill, M. Toner, C. Timon, RJ Flavin, JJ O'Leary, O Sheils. Poster presented at USCAP meeting, San Antonio 2005. Abstract published Laboratory Investigation. Vol 85, Supplement 1.

Book Chapters

High Density SNP and cDNA array analysis.

Prosser J, Picton S, Howells D, Sherlock J, Martin C, Smyth P, Finn SP, O' Regan E, Sheils O, O'Leary J. In The Science and art of laboratory Diagnosis (2nd Edition, John Wiley)

CGH array analysis of human tissues

O'Regan E, Finn SP, Martin C, Smyth P, Sheils O, O'Leary J.

In The Science and art of laboratory Diagnosis (2nd Edition, John Wiley)

Summary

In recent years, there has been a technological explosion in the fields of molecular pathology and molecular oncology. The genome, transcriptome and increasingly the proteome of diverse tumours can now be analysed in minute detail. Thyroid cancer has come to the forefront of molecular pathology as a result of the sad consequences of the Chernobyl disaster and the recognition of the role of ret mutations in familial and sporadic medullary thyroid carcinoma and ret/PTC rearrangements in papillary thyroid carcinoma.

The purpose of this project was to use novel genome wide analysis to enhance our understanding of Papillary thyroid carcinoma, the most common thyroid carcinoma.

The project began with an assessment of ret/PTC rearrangements in a sporadic cohort of Irish PTC using TaqMan RTPCR. A significant minority of this Irish cohort of PTC express the radiation specific rearrangement ret/PTC-3 (18%). An association was noted between variant morphology and ret/PTC-3. Soon after completion of this part of the project, the role of BRAF (T1799A) as a possible alternative event in the pathogenesis of PTC was demonstrated and a separate study in our laboratory confirmed the association of specific morphology with specific genetic mutations.

The occurrence of radiation signature ret/PTC-3 activation in our cohort prompted further research into the effects radiation on thyroid epithelial cells using array Comparative Genomic Hybridisation. Gamma radiation has been largely overlooked as a potential cause of ret rearrangements, with Iodine 131 favoured as the cause of PTC developing post-Chernobyl. Our in-vitro experiments have shown for the first time that gamma irradiation was capable of inducing a ret rearrangement, specifically ret/PTC-3 and that no evidence of ret/PTC-1 activation could be demonstrated. We conclude that specific types of radiation influence the resulting specific

rearrangements. Array CGH demonstrated a predominant pattern of loss of DNA occurring in this thyroid radiation carcinogenesis model and that chromosome 10 may represent a hotspot for radiation damage in thyroid follicular epithelium.

Array CGH was also used to assess thyroid carcinoma cell lines and laser capture microdissected papillary thyroid carcinoma cells for genomic instability. The primary finding was that DNA copy gain and loss appears to occur in all cases of PTC using this technological approach. This conflicts with previous literature but confirms the previous impression that copy gain and loss does not occur at high levels. The occurrence of copy gain of Platelet derived growth factor receptor β exclusively in a subset of PTC without evidence of ret/PTC or BRAF abnormalities suggests that amplification of this gene may provide yet another mechanism of mitogen activated protein kinase pathway (MAPK) activation. In fact, increasingly, the role of a variety of molecular "lesions" affecting varying components of the MAPK cascade, as a final common pathway, has become central to the molecular pathogenesis of PTC.

Approximately 10% of the population develop thyroid nodules during their lifetime. The diagnostic tools available to distinguish benign from malignant neoplasms are not always reliable. The identification of biomarkers of PTC and other thyroid carcinomas could significantly improve diagnostic accuracy and prognostic information. The final part of the project involved using expression microarray technology to identify a panel of biomarkers that distinguish PTC from benign lesions. It is hoped that some of these biomarkers may prove useful for diagnostic purposes in Fine needle aspiration cytology samples in the future.

The data presented in this thesis demonstrates the evolution of the molecular biology of PTC away from a narrow focus on specific molecular lesions such as ret/PTC rearrangements to a pan genomic approach.

Chapter 1

General Introduction

1.1 Thyroid: Historical Context

In 1656, Thomas Wharton (1641-1673) is said to have coined the term thyroid. The word is derived from the Greek "thyros", meaning, "shield" because the gland was originally thought to be a protective shield for the larynx. However, historical references to the thyroid gland appeared much earlier in medical history. In 1600 BC, the Chinese were using burnt sponge and seaweed for the treatment of goitres. The word goitre itself is derived from the Latin term 'guttur', which means throat. Celsus, in his book 'De Re Medicina', first described a bronchoceole (literally a tracheal outpouch) in 15 AD. Also around that time Pliny the Elder referred to epidemics of goitre in the Alpine regions and again the use of burnt seaweed was mentioned in their treatment, in the same way as the Chinese had done 1600 years earlier. In 150 AD Galen, the Greek born physician and famed chronicler of Greco-Roman medicine again referred to 'spongia usta' (burnt sponge) for the treatment of goitre. He also suggested (incorrectly as it turned out) that the role of the thyroid was to lubricate the larynx. He was not, however, the first person to entertain a colourful opinion about the role of the gland. Throughout medical history such opinions have been prominent. The thyroid was believed to have a cosmetic function in women and paintings, some going back to ancient Egypt, have emphasised the size of the thyroid gland in women. In the early 1800s, the thyroid was thought to be a vascular shunt to divert the blood flow from the brain (Hamdy, 2002).

Rush reported in 1820 that the thyroid gland is larger in women because it is "necessary to guard the female system from the influence of the more numerous causes of irritation and vexation of mind to which they are exposed than the male

sex." (Rush, 1820). Also in 1820, Hofrichter stated: "If it were indeed true that the thyroid contains more blood at some times than at others, this effect would be visible to the naked eye; in this case women would certainly have long ceased to go about with bare necks, for husbands would have learned to recognize the swelling of this gland as a danger signal of threatening trouble from their better halves." (Hofrichter, 1820). However, not all historical observations about the thyroid gland were so inaccurate. The Dublin doctor Robert James Graves was the first physician to fully describe exophthalmic goitre in conjunction with the classic symptoms of the disease entity now known as Graves' disease or sometimes Basedow's disease.

He described in detail three patients with palpitations and enlargement of thyroid. One of the patients had eye symptoms: "The eyeballs were visibly enlarged, to such a degree the eyelids were unable to shut during sleep and when trying to close the eye. When the eyes were open the white of the eyes could be seen in the breadth of several lines around all of cornea."

Cretinism (congenital hypothyroidism) was described in 1871. In 1874, Gull noted the clinical changes associated with atrophy of the thyroid gland, and 4 years later, William Ord coined the term myxoedema (Greek: myxa, mucus) because he felt that excessive mucus formation and deposition under the skin were responsible for the characteristic thickening of the subcutaneous tissue, characteristic of this disease.

In Europe, Theodore Kocher (1841-1917), a Swiss surgeon, is claimed to be the first surgeon to excise the thyroid gland for the treatment of goitre (1876). However, Rehn is also said to have carried out the first thyroidectomy (removal of the thyroid

gland) for exophthalmic goitre in 1880. In any case, Kocher was prolific and had performed 5,000 thyroid excisions by 1912 with impressively reduced mortality (from 18 percent to less than 0.5 percent) (DuBose, 2004).

Kocher was awarded the Nobel Prize for Medicine in 1909 for his work. Around the same time, in the United States, Charles Horace Mayo (co-founder, with his brother, of the Mayo clinic) became the leading authority on thyroid surgery. In 1891, a 26-year-old English physician, George Murray, reported to the British Medical Association that he had cured a case of hypothyroidism by injecting sheep's thyroid gland into the patient. Shortly afterward, Howitz, Mackenzie, and Fox independently found that thyroid extracts were effective when administered orally. The usual dose was one-half of a sheep's thyroid served raw taken once a week!

In 1895 Adolph Magnus-Levy (1865–1955) introduced an experimental method of determining thyroid disturbances. He fed desiccated animal thyroids to normal men and made the observation that their metabolic rate was subsequently considerably increased. He also produced the first systematic study of the basal metabolism of normal individuals from childhood to old age and established that the function of the thyroid is to maintain the proper level of metabolism. Edward Kendall, professor of physiological chemistry at the Mayo Clinic, isolated thyroxine in crystalline form in 1915, and established that the crystalline form had the same effects as the thyroid extract from which it was obtained. A decade later, in 1926, Harington defined the chemical formula of thyroxine, and a year later synthesized the hormone.

The presence of thyroid-stimulating antibodies in Graves' disease was determined in 1956, and that of thyroid antibodies in Hashimoto disease in 1957. Hashimoto disease (struma lymphomatosa) was described in 1912. Medullary thyroid carcinoma was recognized as a distinct entity in 1959. The definition of the exact role of the thyroid gland in calcium metabolism had to wait for the discovery of calcitonin in 1961.

1.2 Thyroid Embryology and Development

The thyroid gland is the first of the body's endocrine glands to develop at 24-28 days gestation. The gland develops from the fusion of three distinct ectodermal structures. These consist of a single median anlage, and paired lateral anlagen. The median anlage accounts for the greater proportion of the thyroid gland and can be identified developing from the base of the tongue in the foramen caecum. The median anlage forms a diverticulum, grows laterally to form a bilobed structure, which descends from the tongue to its final position in the anterior neck. The initial descent of the thyroid gland occurs anterior to the pharyngeal gut. At this point, the thyroid is still connected to the tongue via the thyroglossal duct. The tubular duct later solidifies and subsequently obliterates entirely (during gestational weeks 7-10). Nonetheless, in some individuals, remnants of this duct may still persist. Ectopic thyroid tissue can occur anywhere along this course of development.

The foramen caecum represents the opening of the thyroglossal duct into the tongue; its remains may be observed as a small blind pit in the midline between the anterior two thirds and posterior third of the tongue.

A pyramidal lobe of the thyroid may be observed in up to 50% of adults. This lobe represents a persistence of the inferior end of the thyroglossal duct that has failed to obliterate. As such, the pyramidal lobe itself may be attached to the hyoid bone, similar to a thyroglossal duct cyst.

Further descent of the thyroid gland carries it anterior to the hyoid bone and, subsequently, anterior to the laryngeal cartilages. As the thyroid gland descends, it forms its mature shape, with a median isthmus connecting 2 lateral lobes. The thyroid completes its descent in the seventh gestational week, coming to rest in its final location immediately anterior to the trachea.

Parafollicular cells are also known as C cells. These cells are a special subset of cells within the thyroid gland that secrete calcitonin, a hormone necessary for the regulation of calcium.

The parafollicular cells arise from the ultimobranchial body. This body represents the last structure derived from the branchial pouches, hence its name. The ultimobranchial body arises from the fifth pharyngeal pouch, which is alternately described as the ventral portion of the fourth pharyngeal pouch. (Whether a fifth pharyngeal pouch actually exists is debatable.)

Migrating cells from the neural crest region infiltrate the ultimobranchial body (neuro-ectoderm). This structure is then incorporated into the thyroid gland. The C

cells of the thyroid, which give rise to medullary thyroid carcinoma, therefore, are of neural crest origin.

1.3 Anatomy and histology of the thyroid gland

In adults the thyroid gland consists of a bilobed gland lying in the anterior triangle of the neck united in front over the second, third and fourth thyroid cartilages by the isthmus. The thyroid is completely enveloped by a continuous fibrous capsule, with septa that divide the gland incompletely into lobules.

The normal weight of the gland lies between 15-25 g. At birth the gland weighs 1-2 g, and in pubertal children between 10-15g. In the elderly atrophy may occur, with the gland assuming its pubertal weight again.

Blood supply is from the superior thyroid arteries, arising from the external carotid artery and from the inferior thyroid arteries, which arise as branches of the thyrocervical trunk extending from the brachiocephalic artery. Venous drainage includes the brachiocephalic, internal jugular and occasionally the anterior jugular veins. Lymphatic drainage is to upper and lower deep cervical nodes. Lymphatic dissemination of papillary thyroid carcinoma is particularly common.

The nerve supply to the gland comprises the sympathetic vasomotor supply from the middle cervical ganglion and a parathyroid supply of no known function via the tenth cranial nerve (Vagus).

An important anatomic relation is the recurrent laryngeal nerve, which lies in a groove between the thyroid gland and the oesophagus and is vulnerable during thyroid and parathyroid surgery.

The parathyroid glands normally lie behind the lateral lobe of the thyroid gland, and may be either internal or external to the thyroid's capsule of pre-tracheal fascia. Usually there are four parathyroid glands, the 2 superior glands having more constant location behind the thyroid level with the first tracheal ring. The inferior parathyroid glands are more variable in position, which probably reflects their longer path of descent during development.

Histologically, the thyroid gland consists of lobules consisting of 20-40 follicles, supplied by an arterial branch and surrounded by inconspicuous connective tissue. The follicles are the functional unit of the thyroid and consist of a closed sac, average diameter 200nm, lined by a single layer of epithelium. The height of the follicular epithelial cells varies from low cuboidal to high columnar according to the functional activity of the gland. The lumen of the follicle contains a viscous material known as colloid, containing concentrated eosinophilic staining thyroglobulin.

The thyroid gland also contains a small percentage of calcitonin-producing C-cells. C-cells are present in the middle to upper thirds of the lateral lobes. They are inconspicuous, although they may be seen in small clusters. In normal adults the numbers of C-cells should be less than 50 per 100 X field.

1.4 Primary Epithelial Thyroid Tumours

The major focus of this thesis is Papillary Thyroid Carcinoma (PTC), however, the other epithelial tumours will be briefly considered in order to place the pathobiology of PTC in context.

1.4.1 Classification of primary epithelial tumours of the thyroid

At the time of writing the new WHO classification (DeLellis, in press) is about to be published and the brief synoptic classification presented here represents interpretation of the older WHO and AFIP classifications.

Follicular Cell Tumours:

Benign — Follicular Adenoma and variants

Malignant — Differentiated Carcinomas

- Follicular Carcinoma
- Papillary Carcinoma and variants

Poorly Differentiated

- Insular

Undifferentiated

- Anaplastic Carcinoma

Tumours of C Cells:

- Medullary Thyroid carcinoma and variants

1.4.2 Pathology of primary epithelial tumours of the thyroid

1.4.2.1 Follicular Adenoma

Follicular adenoma is a benign encapsulated neoplasm composed of a collection of follicular epithelium that usually shows uniform architecture. Microscopically follicular adenomas show a variety of patterns (trabecular, microfollicular, macrofollicular and normofollicular). The lesions have a thin capsule, which contrasts with the thick capsules often seen in association with carcinomas. In the absence of previous diagnostic intervention (Fine Needle Aspiration Cytology FNAC), mitotic activity is low. Variation in nuclear size may be evident and occasionally bizarre atypical cells may be seen. Degenerative features may be present and include myxoid degeneration, cystic degeneration, recent or older haemorrhage, calcification and ossification. Necrosis is rarely seen in the absence of previous FNA.

Differential Diagnosis: Follicular adenomas may be difficult to differentiate from adenomatous follicular nodules (the distinction is clinically irrelevant), minimally invasive follicular carcinomas and follicular variant of PTC. With regard to follicular carcinoma, careful examination of the capsule for true capsular and vascular invasion is necessary. True capsular invasion is rare in the absence of angioinvasion. Although the presence of nuclear atypia, mitotic activity and even necrosis may suggest malignancy, these features are never diagnostic. The differential diagnosis of follicular adenoma and follicular variant of PTC is based on the appreciation of the typical nuclear features of PTC. However, it must be

acknowledged that partially or incompletely developed nuclear features of PTC may occur and the differential diagnosis can be extremely difficult. Interobserver variation is a significant problem (Hirokawa, 2002). The Chernobyl Pathologists group has controversially suggested designating such difficult lesions as 'well differentiated thyroid tumour of uncertain malignant potential' (Williams, 2000). They argue, convincingly, that it is more appropriate to recognise the difficulty in deciding whether or not the nuclei are typical than to arbitrarily place well-differentiated encapsulated tumours with a follicular architecture and subtle or minor nuclear changes of PTC, in a definite benign or malignant category. The new WHO classification will includes similar terminology and uses the term 'well differentiated tumour of uncertain malignant potential' when there is no definite evidence of invasion, and 'well-differentiated carcinoma, not otherwise specified' when invasion is present.

1.4.2.2 Follicular Thyroid Carcinoma and Variants

Follicular Thyroid carcinoma (FTC) is a malignant epithelial tumour showing evidence of follicular cell differentiation and not belonging to any of the other distinctive types of thyroid malignancy. The lesion occurs predominantly in women (75%) and affects patients approximately 10 years older than those affected by PTC. FTC is associated with iodine deficiency. Clinically, it presents usually as a solitary thyroid nodule that appears "cold" on radionuclide scan. In contrast to PTC, lymphatic spread is unusual but haematogenous metastasis may occur with involvement of lungs, liver, bone. Unlike PTC, FTC is almost never occult. Distant

metastases are common in grossly invasive variants: 50% if associated with vascular and capsular invasion, 75% if local invasion and vascular or capsular invasion.

Grossly, FTC is usually a single encapsulated nodule, gray-tan-pink in colour, focally hemorrhagic with variable levels of fibrosis and calcification. Larger lesions are often infiltrative.

Microscopically, convincing evidence of invasion of adjacent thyroid parenchyma, vessels (medium sized veins or larger in or beyond the capsule) or capsule is present. The nuclear features of papillary carcinoma must be absent. Cytologically, the cells are usually uniform, and form small follicles with colloid.

Variants of FTC

- Minimally invasive (encapsulated) FTC and Angioinvasive FTC

Minimally invasive (encapsulated) FTC is grossly encapsulated (usually thicker and more irregular than adenoma) and show unequivocal capsular and/or vascular invasion. Capsular invasion must be full thickness with the tumour expanding in a mushroom-like fashion into the adjacent area. In real clinical practice this type of invasion is rare in the absence of angioinvasion. Vascular invasion is a much more reliable sign of malignancy than mere capsular invasion and requires invasion of vessels of venous calibre in or immediately outside the capsule (not within the tumour). Vascular invasion can be recognized, regardless of the presence or absence of an associated thrombus, whenever the intravascular, neoplastic nests are lined by endothelium. The evaluation of the degree of angioinvasiveness should be included

in pathology reports. Some have advocated using the term 'very angioinvasive' if invasion of more than one vessel can be demonstrated.

- Widely invasive FTC

There is widespread infiltration of blood vessels or adjacent tissue, without encapsulation. The features may overlap considerably with those of poorly differentiated carcinoma (Insular) and the behavior and prognosis is similar.

1.4.2.3 Papillary Thyroid Carcinoma and Variants

PTC usually presents as painless nodule or mass in neck or cervical node; usually appearing cold on radionuclide scans. Lymph node involvement is often present but not clinically apparent due to the small size of involved nodes with consistency similar to normal lymph nodes. The 10-year survival is 98%, similar to the general population (92% for follicular carcinoma) and 100% if the patient is aged 20 or less at diagnosis, even when nodal metastases are present. Cervical node involvement does not appear to affect prognosis.

The prognosis of conventional PTC and most of its variants depends mainly on the adequacy of primary excision and radioiodine therapy, the age of the patient and the stage of the disease. Poorer prognosis is associated with age > 40, macroscopic extra thyroidal extension, distant metastases (bone worse than lung) and large tumour size also known as the AMES criteria (Cady, 1998).

Grossly the lesion may be solid or cystic, often white in colour and with firm consistency Figure (1.1). It may be encapsulated (10%) or more often infiltrative. Fibrosis and calcification may also occur.

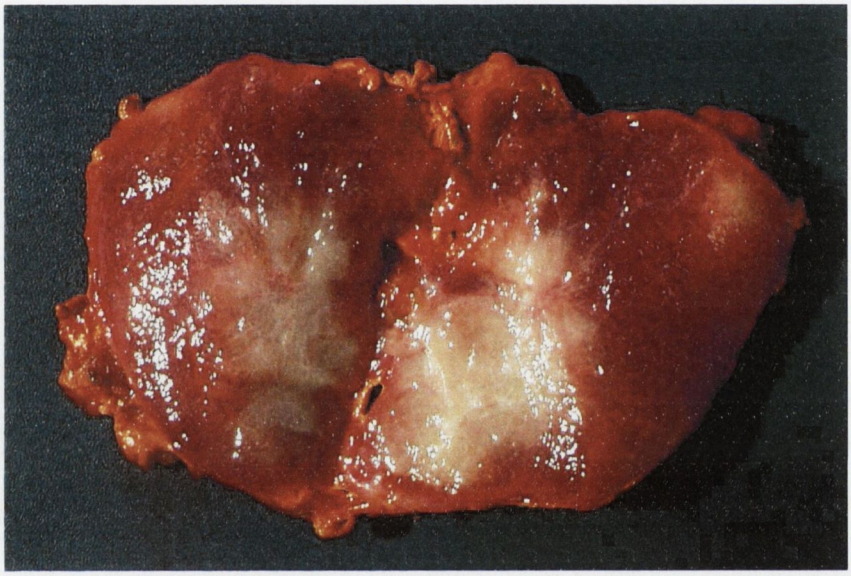

Figure 1.1 Image of cut surface of PTC

Microscopically, complex, branching papillae with fibrovascular cores associated with follicles are seen in conventional PTC. The key to the diagnosis is the identification of characteristic nuclear features, which include enlarged overlapping and irregular nuclei with finely dispersed optically clear chromatin (so called ground-glass or Orphan-Annie nuclei), eosinophilic intranuclear inclusions (representing cytoplasmic invaginations) and longitudinal nuclear grooves (representing folds of redundant nuclear membrane) Figure 1.2.

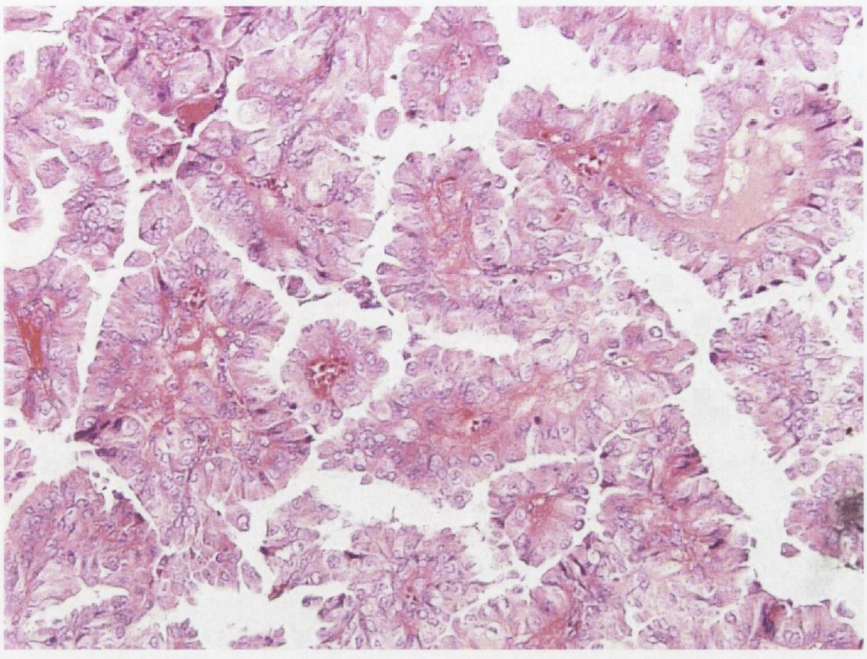

Figure 1.2 Classic morphology PTC, Original magnification X 20

Psammoma bodies are present in 50% of cases either in the papillary stalk or associated with fibrous stroma between tumour cells. They are fairly specific for papillary carcinoma, and are thought to represent necrosis of tumour cells or tips of papillae. Microscopically, PTC may often be multifocal, and traditionally this has been thought to be due to intraglandular lymphatic spread, however multifocality may also represent true multifocal disease. Vascular invasion may be seen.

Fibrosis, squamous metaplasia, solid areas, lymphocytes, histiocytes, Langerhans' cells are variably present. Mitotic figures and mucinous metaplasia may occur rarely.

Morphological Variants of PTC

- Papillary Microcarcinoma

The description of clinically undetectable thyroid cancer has evolved over time. Initially the term 'lateral aberrant thyroid' was used to describe thyroid tissue in the area of cervical lymph nodes in patients with clinically apparently normal thyroid glands. Eventually these were found to represent metastatic PTC from undetected intrathyroidal lesions smaller than 1.5cm. The concept of 'occult papillary carcinoma' evolved and was used to represent a focus of PTC < 1.5cm in maximum dimension. With improved imaging technology and increasing use of FNA, PTCs smaller than 1 cm are now commonly identified and are therefore no longer considered occult lesions. They are classified as thyroid 'papillary microcarcinomas' although the term microtumour has been advocated because of the clinical irrelevance associated with these lesions (Rosai, 2003). They are usually detected at autopsy or as incidental findings in thyroid removed for other disease or as lymph node metastasis of papillary carcinoma.

- Encapsulated classic variant

The encapsulated variant of PTC accounts for approximately 10% of all PTCs. This lesion is characterized by the gross appearance of an adenoma and the histological appearance of an encapsulated papillary neoplasm. The lesion displays classic PTC nuclear features and may or may not invade (usually only focally) into the associated capsule. This variant is thought to have a better prognosis than usual papillary cancers, although metastasis to lymph nodes may occur. The frequency of nodal

metastasis is approximately 25%, whereas usual PTC has a node metastasis rate of 50%. The main differential diagnosis is with follicular adenoma with papillary hyperplasia.

- Follicular Variant PTC

This designation is given to PTCs with an exclusively or almost exclusively follicular pattern of growth (Figure 1.3). The lesion is usually infiltrative with fibrous trabeculation, psammoma bodies and strongly eosinophilic colloid with scalloping. Occasionally the follicles are very large, with an appearance that simulates nodular hyperplasia. This appearance has been referred to as the macrofollicular variant of PTC. The follicular variant has the same prognosis as typical papillary carcinoma with metastases that are usually nodal, not distant, and more often showing classic papillary morphology rather than the follicular morphology of the primary neoplasm.

Sobrinho-Simões has described a diffuse form of the follicular variant of PTC, characterized by diffuse involvement of the entire thyroid (without discernible nodularity) associated with aggressive behaviour (Sobrinho-Simões, 1990).

- Encapsulated follicular variant

This variant combines the features of two variants. It is an encapsulated neoplasm (with of without capsular and/or vascular invasion) with the cytoarchitectural features of the follicular variant of PTC.

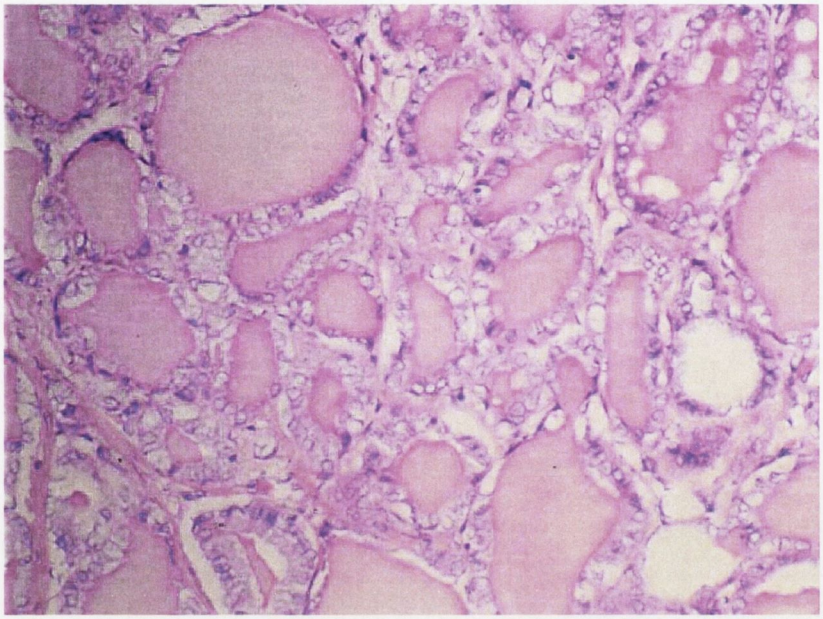

Figure 1.3 Follicular Variant PTC

- Solid/trabecular Variant

The term solid/trabecular variant is used when all or almost all of a tumour not belonging to any of the other variants has a solid/trabecular appearance. This variant is rare although it is the most common variant associated with ret rearrangements in the post-Chernobyl cohort. Necrosis is absent. It is associated with a less favorable prognosis than conventional PTC with slightly more distant metastases, however it does have a better prognosis than a poorly differentiated thyroid cancer.

- Diffuse Sclerosis Variant

This variant occurs more often in younger patients and children and is characterized by diffuse involvement of one or both lobes in association with dense sclerosis, frequent psammoma bodies, extensive solid foci, squamous metaplasia and prominent lymphocytic infiltration. Nodal and lung metastases are common and the tumour cells are not reactive for thyroglobulin.

- Tall and columnar cell variants

Tall cell variant of PTC (Figure 1.4) has been said to have a poorer prognosis than other variants, although some authorities dispute this. It usually affects older men and tends to be large. Extrathyroid extension is common and there is a greater incidence of vascular invasion. The papillae are well formed and covered by cells that are twice as tall as they are wide. The cytoplasm is abundant and eosinophilic. Mitoses are frequent.

Columnar cell carcinoma is very rare and shows the presence of nuclear stratification in association with clear cytoplasm. The features are more consistent with a colonic appearance rather than thyroid follicular cells.

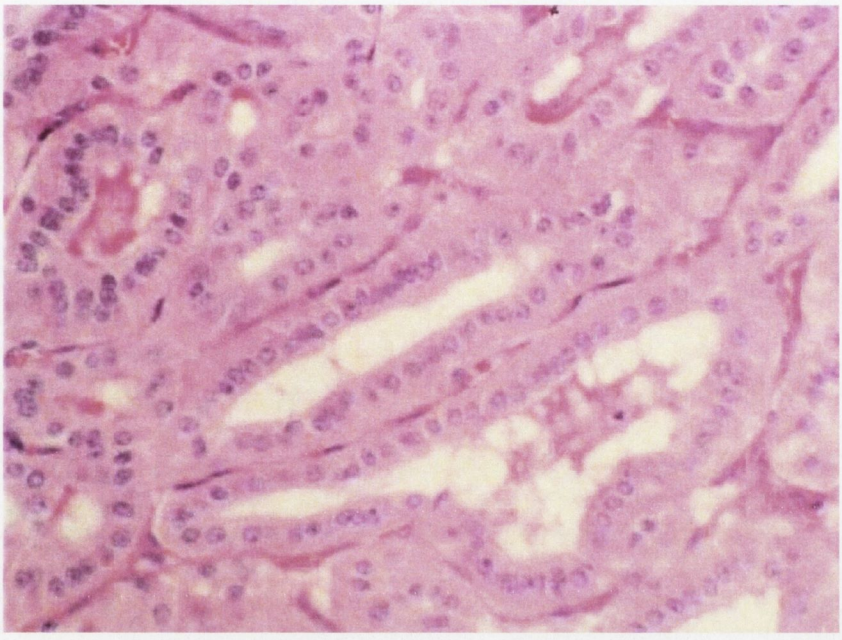

Figure 1.4 Tall Cell variant

- Cribriform-morular

This variant is associated with sporadic or germline (familial adenomatous polyposis) mutations of APC gene. It is usually found in young women (age 16-30). The tumours are encapsulated or circumscribed with a cribriform pattern, follicles without colloid and papillary formations of tall cells with abundant eosinophilic cytoplasm and pseudostratification. Spindle cells, hyperchromatic nuclei with grooves and pseudoinclusions, morular (squamoid) metaplasia with nuclear clearing resembling viral inclusions vascular and capsular invasion are common.

- Nodular fasciitis like stroma

This is a rare form where exuberant stroma obscures classic tumour features.

- Oncocytic

This variant is composed of oncocytic cells with classic nuclear features of papillary carcinoma. The affected patients are usually women and the lesion is frequently associated with autoimmune thyroiditis.

- Warthin-like

This rare variant, again usually affecting women, resembles the salivary gland tumour. It is circumscribed, papillary, often centrally cystic, has papillary nuclear features with oncocytic cytoplasm, with a brisk lymphoplasmacytic infiltrate in papillary stalks.

1.4.2.4 Insular carcinoma/Poorly Differentiated Carcinoma (PDC)

In 1984, Carcangiu and Rosai described what they termed 'poorly differentiated carcinoma' (Rosai, 1990). They also used the term insular carcinoma to describe the growth pattern of this neoplasm, which appeared to have a survival rate between that of the differentiated thyroid cancers, and anaplastic carcinoma. It appears that this category of thyroid tumour encompasses at least two major groups of tumours: the so-called insular carcinomas which resemble widely invasive follicular carcinomas, and a heterogeneous group that also fit the overall descriptive designation of PDC often with a trabecular or a solid growth pattern with morphologic and molecular features more characteristic of PTC (Sobrinho-Simoes 2002; Soares, 2004). However, in practical terms subclassification of poorly differentiated carcinoma is not advocated currently. PDCs may be challenging from the differential diagnostic

point of view. It can be difficult to distinctly separate PDC from PTC mainly composed of trabecular or solid areas especially when the nuclear features of PTC are subtle and incompletely developed. It may also be difficult to separate PDC from FTC with a predominant microfollicular/trabecular or solid growth pattern. Presence of necrosis and a high mitotic rate may be suggestive of PDC.

1.4.2.5 Anaplastic Carcinoma

This is a relatively rare, undifferentiated thyroid tumour with a mean age of 65 years at presentation. In 50% of cases the patients have prior multinodular goitre, 20% have prior differentiated carcinoma and 20% have concurrent differentiated carcinoma. The tumour probably arises as anaplastic transformation of papillary carcinoma or other well-differentiated tumour. The presentation is dramatic with rapidly enlarging, bulky neck mass that invades adjacent structures causing hoarseness, dysphagia, and dyspnoea. There is no effective treatment and death usually ensues within 1 year (mean survival 6 months). Grossly the tumour invades adjacent structures with necrosis and haemorrhage. Microscopically there are three main patterns:

1) Large, pleomorphic giant cells resembling osteoclasts;

2) Spindle cells resembling sarcoma; or

3) Squamoid – undifferentiated but epithelial with occasional focal keratinisation.

1.4.2.6 Medullary thyroid Carcinoma

Medullary thyroid carcinoma (MTC) is a neuroendocrine tumour derived from C cells (also known as parafollicular cells), which secrete calcitonin.

In 80% of cases the tumour is sporadic and presents in middle-aged patients as a solitary mass often accompanied by dysphagia, hoarseness and paraneoplastic syndromes (diarrhea from VIP, Cushing's syndrome).

In approximately 20% of cases the tumour is familial, associated with syndromes such as Multiple Endocrine Neoplasia (MEN) types 2A and 2B, familial medullary thyroid carcinoma syndrome, Von Hippel-Lindau syndrome or neurofibromatosis. Familial cases arise in younger patients (mean age 35) and tend to be bilateral, multicentric or diagnosed by serum calcitonin levels or peripheral blood mutational analysis.

MEN 2A occurs due to germ line mutations in RET proto-oncogene. RET is normally expressed in C cells; carcinomas may have germline point mutations causing constitutive activation of receptor. The tumour invades locally with metastases occurring to cervical and mediastinal nodes, lung, liver and bone.

1.5 Epidemiology of thyroid cancer worldwide and in Ireland

Carcinoma of the thyroid gland is an uncommon cancer although it is the most common malignancy of the endocrine system. Generally, thyroid cancer accounts for approximately 1% of total cancers in developed countries. There are about 122,000 new cases per year worldwide (Stewart, 2003). In Europe and the United States there are approximately 28,000 new cases each year and an estimated 376,000 existing cases of primary thyroid carcinoma. Well-differentiated (follicular and papillary) thyroid carcinoma accounts for 80% to 90% of these cases. Thyroid cancer is more common in women than in men (2-3:1). It is among the most curable neoplasms, but 5% to 20% of survivors develop local or regional recurrences, and <5% to 10% distant metastases, generally in the first years of follow-up, but sometimes after many years (Sclumberger, 1999).

Incidence of the disease is particularly high in Iceland and Hawaii (Kolnell, 1990; Ferlay, 2001). Thyroid tumours are rare in children, less than one case per million per year in most developed countries; the age specific incidence rates increase rapidly with age. For the past 30 years, incidence rates have been increasing in most developed countries, while mortality rates have been slowly decreasing. In the year 2000, the annual mortality rate per 100,000 people was 0.3 for men and 0.6 for women.

Unfortunately, the epidemiology of thyroid cancer in Ireland, prior to 1994, is poorly documented. The Irish National Cancer Registry (http://www.ncri.ie/ncri/index.shtml) was only set up in 1991 and did not begin to

register cancers nationwide until January 1994. For these reasons long term trends in thyroid cancer incidence and mortality in Ireland are regretably not available. In addition the data makes no distinction between different types of cancer such as PTC, FTC, UTC and MTC, although as in most other datasets PTC is the commonest type. The available figures are for 1994 -1999. The incidence for both sexes has remained at 55-65 cases per year with females outnumbering males as seen in Figure 1.5. Deaths from thyroid cancer are uncommon and average at about 25 cases per year. (Figure 1.6). The increasing incidence with older age and the sex profile for the years 1994-1997 are seen in Figure 1.7.

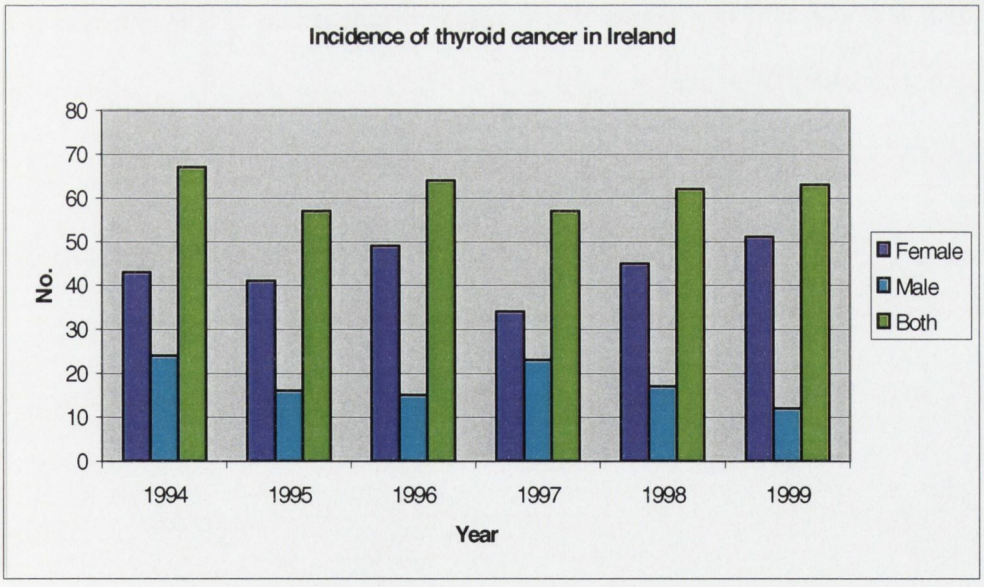

Figure 1.5 1994-1999 Incidence of thyroid cancer in Ireland

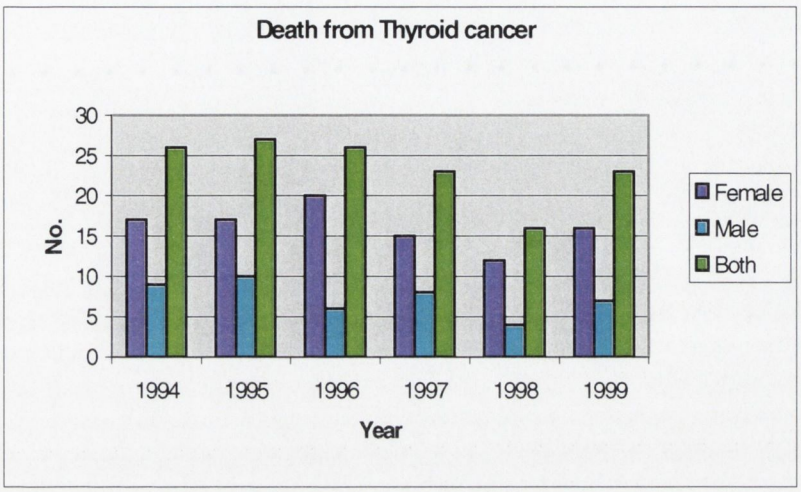

Figure 1.6. Mortality from thyroid Cancer in Ireland between 1994 and 1999

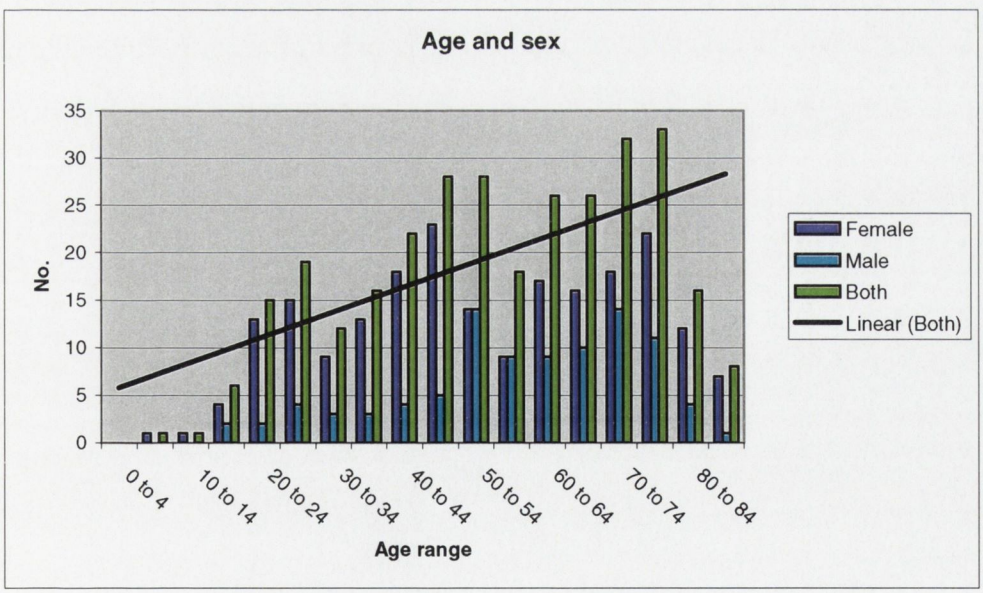

Figure 1.7 Age and sex profile of thyroid carcinoma from 1994-1997

1.6 Aetiology of thyroid cancer

The aetiology of thyroid carcinoma is not fully understood. Most cases cannot be associated with a specific aetiology. However, some specific risk factors, particularly for PTC, have been clearly identified.

1.6.1 Iodine

The development of papillary carcinoma in animals and humans has been associated with an excess of iodine in the diet (Harach, 1985). The apparent increased frequency was noticed after the introduction of iodine in the diet (Hofstadter, 1980). In addition a relative decrease in follicular carcinomas was also identified in these areas.

1.6.2 External Radiation

Exposure to radiation especially exposure occurring during childhood is a well-known risk factor for papillary thyroid carcinoma.

Marshall Islanders: Misjudgements about weather forecast and bomb yield led to contamination of the inhabited islands of Rongelap, Ailinginae and Utrik Atolls after the BRAVO test on Bikini Atoll conducted in 1954. By the end of 1990, 29 of the 86 (34%) people resident on Rongelap and Ailinginae had developed thyroid nodules. Six of these 29 developed thyroid cancer (Hamilton, 1997). This rate was higher than the rate of 4% observed in a comparison group of 227 Rongelap people who were not living on Rongelap at the time of the BRAVO test.

Nevada Test Site exposures: In the period 1951 to 1962, nearly 100 atmospheric tests were conducted at the Nevada Test Site with maximum exposures occurring in the years 1952, 1953, 1955, 1957. Subsequent studies revealed a non-statistically significant association between dose and thyroid cancer (one tailed $p = 0.019$). The estimated excess relative Risk per Gray (ERR Gy^{-1}) was 7.9. The association became statistically significant (one tailed, $p = 0.0019$) when malignant and benign thyroid neoplasms were combined with an estimated ERR Gy^{-1} of 7.0. (Gilbert, 2002)

Medical exposure to Iodine 131: There are several studies of persons exposed to I131 for diagnostic and therapeutic medical reasons. Most of these studies address exposure occurring in adulthood, whereas evidence of excess thyroid cancer risk from external exposure to radiation has been confined to childhood. In a very large study of patients who had administration of I 131 in Sweden for medical reasons, there was no evidence of excess thyroid cancer risk when analysis was confined to those exposed for reasons other than suspected thyroid cancer. This study showed no evidence of a dose response (Hall, 1996). Other studies failed to show statistically significant risk. Overall exposure of the thyroid to radiation from internal sources (i.e. Diagnostic and therapeutic doses of 131I) has not been consistently associated with increased risk of carcinogenesis.

Chernobyl Accident: On the 26th of April 1986, operators at the Chernobyl plant in the Ukraine were carrying out an engineering test of the unit 4 reactor when a succession of errors both human and mechanical led to a series of explosions and total destruction of the nuclear reactor (Moysich, 2002). Concentrated areas of

radiation contamination were spread in a spotty pattern over Ukraine, Belarus, Russia and into Europe. The most heavily contaminated areas, in which measurements of 137-caesium exceeded 37 $kBqm^2$, were in Belarus, the Russian Federation and Ukraine. Heavy rains exacerbated the radionuclide fallout, resulting in contamination of groundwater and soil. Initial ionising radiation exposure consisted of 131-Iodine (The radio-iodine shock), whereas later phases of environmental contamination were mainly due to 137 Cs, 134 Cs and 90-Strontium. The release of radioactive iodine isotopes was a cause of immediate concern but given the rather short half-life of 131I (8 days), exposure to Caesium isotopes was thought to be a more important factor in long term consequences for health.

Large increases in thyroid cancer incidence have occurred in Belarus, Ukraine, and Russia among persons under 20 years of age who were apparently exposed to I131 as result of the Chernobyl accident (Demidchik, 1996; Tsyb, 1996; Tronko, 1999). At first it was suspected that the apparent increase in incidence might be explained by improved thyroid screening that has been conducted in the affected areas, but it was later determined that most of the cancers were sufficiently aggressive that they would have been highly unlikely to have been missed with conventional reporting methods (Bleuer, 1996). The increase in thyroid cancer was most marked in the Gomel district of Belarus, which was also the most contaminated, and therefore consistent that these cancers were related to Chernobyl related radiation. It was also noted that the thyroid tumours from Belarus were unusually aggressive compared to those presumed to arise sporadically.

According to a recent United Nations Scientific Committee on the Effects of Atomic Radiation report (UNSCEAR, http://www.unscear.org/), the doses of radiation to the thyroids of children from contaminated areas in the former Soviet Union varied considerably. Doses varied from <0.02 Gy to >2 Gy in a sample of 32,000 children from Belarus and in a Russian sample average doses were between 0.35 Gy and 0.7 Gy, with some children receiving a dose as high as 4 Gy (Gilbert, 2002).

Overall there is good evidence from descriptive and analytic epidemiological studies that Chernobyl-related ionising radiation exposure is related to thyroid cancer in children. However, the association is much less clear in adults with longer follow up needed for increased thyroid cancer rates to become apparent. It seems that the adult thyroid gland may be less sensitive to radiation.

1.6.3 Other risk factors

Papillary carcinoma may arise in association with autoimmune thyroid disease. Although a statistically significant association has never been shown, the demonstration of cancer specific gene rearrangements (Sheils, 2002; Wirtschafter, 1999) and patterns of LOH (Hunt, 2002) have strengthened this association.

Papillary carcinoma may arise in association with several genetic syndromes. Interesting associations of PTC with some of the familial polyposis syndromes (Gardner's syndrome and Cowden's syndrome) have been noted (Harach, 1995).

1.7 Molecular Pathology of Papillary thyroid carcinoma

Carcinogenesis is a multi step process that leads to uncontrolled growth of cells with unchecked potential for proliferation. Cancer is caused by the activation or amplification of oncogenes, or by the deactivation or loss of genes that protect against cancer, such as tumour suppressor genes and DNA repair genes. In relation to thyroid carcinoma, particularly PTC, ionizing radiation is the most well described initiator of carcinogenesis. In general, radiation is more likely to induce DNA strand breaks rather than point mutations. When DNA strand breaks occur, especially double stranded breaks, the ability to fully repair the sequence is limited and the consequences are chromosomal rearrangements such as inversions, translocations, gains and deletions. If these consequences are non-lethal for the cell and cannot be otherwise reversed, they may lead to malignant transformation via altered gene expression, formation of chimeric genes, or loss of tumour suppressor gene function.

1.7.1 RAS

Ras proteins represent protein products of the 3 different RAS genes, H-RAS, K-RAS and N-RAS. These proteins (p21) are linked to the inner portion of the cytoplasmic membrane. They have GTPase activity and exist in two forms: an inactive form linked to guanosine diphosphate (GDP); and an active form, which is able to bind and activate guanosine triphosphate GTP by hydrolysis. Their function is to modulate signals from receptor tyrosine kinases on the cell membrane, e.g. Epidermal growth factor receptor (EGFR), to a cascade of mitogen-activated

phosphokinases (MAPK). These in turn are responsible for the activation of transcription of target genes (typically c-*fos* and c-*jun*) resulting in cell proliferation. In neoplasia ras becomes activated usually by point mutations and ras mutations are the most common abnormalities of dominant oncogenes in human cancer (30% of human cancers). Hotspots for these mutations occur in exon 1 (codons 12 or 13) of the GTP-binding domain and in exon 2 (codon 61) of the GTPase domain. The effect of these mutations is to "lock" the protein in its active, GTP bound from leading to constitutive activation of downstream MAPK pathways.

Mutations of all three ras proto-oncogenes have been described in association with thyroid neoplasia. There is variation in the literature regarding the prevalence of ras mutations among different types of thyroid tumours, however, it is believed that oncogenic ras is more common in follicular rather than papillary carcinoma and in those tumours occurring in iodine-deficient areas. The frequency of ras mutations is much higher in FVPTC than in conventional PTC and may provide a link between FVPTC and FTC (Zhu, 2003). In rat models thyroid tumours induced by chemical carcinogens are more commonly associated with H-*ras* whereas K-*ras* is seen in 60% of radiation-related tumours (Lemoine, 1998).

The role of ras mutations in thyroid tumour progression is unclear with conflicting literature. However, ras protein overexpression appears to be associated with poor prognosis in PTC (Basolo, 1994). Transgenic mice with thyroid specific ras expression develop thyroid hyperplasia and both follicular and papillary thyroid carcinoma. (Rochefort, 1996). Ras mutations have not been found to have a role in

carcinogenesis occurring after the Chernobyl accident (Nikiforov, 1996; Suchy, 1998)

1.7.2 Tyrosine Kinase receptors

1.7.2.1 *Ret* proto-oncogene

The RET proto-oncogene (c-RET) is located on chromosome 10q11.2 and encodes a transmembrane growth factor receptor with an intracellular tyrosine kinase domain. The ligands for RET belong to the glial cell line-derived neurotropic factor (GDNF) family. This family of ret ligands includes GDNF itself and its congeners neurturin, persephin, and artemin. The GDNF proteins signal through a multicomponent receptor complex that includes membrane bound ligand-binding GDNF family receptors (α GFR's) and RET. In conjunction with each α GFR, RET operates as an intracellular signal-transducing element. The extracellular domain of RET consists of a juxtamembrane cysteine rich region and a domain with homology to cadherins.

RET is normally expressed in cells of neural crest origin such as neural and ganglion cells. Tumours of neural crest origin such as neuroblastoma, phaeochromocytoma and medullary thyroid carcinoma also express RET. Recently ret expression by macrophages has been demonstrated. It is clear that RET plays a significant role during embryogenesis particularly with development of the neural and excretory systems. Mouse knockout models for RET have demonstrated major defects of the peripheral nervous system and kidney.

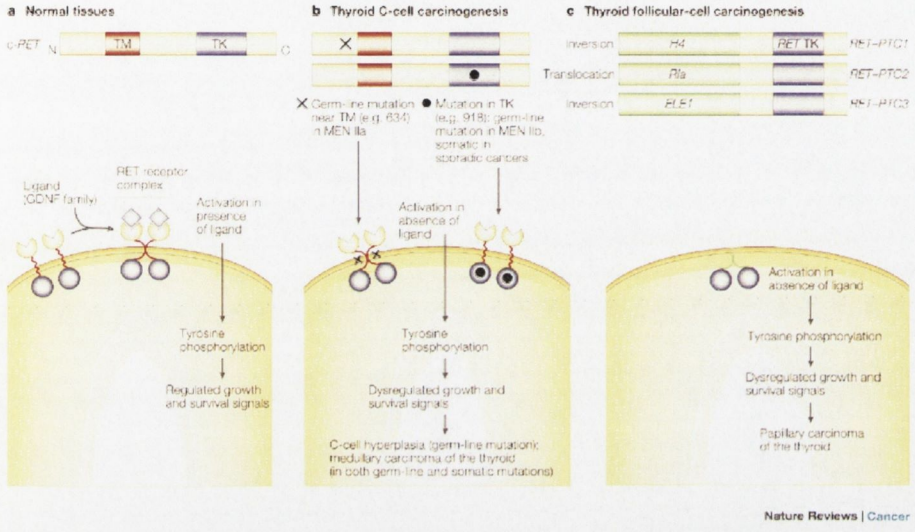

The role of *RET* in thyroid carcinogenesis.
A) The receptor tyrosine kinase c-*RET* is normally expressed in the developing neural-crest-derived tissues, including thyroid C cells. It binds to members of the glial-derived neurotrophic factor (GDNF) family of ligands, leading to dimerization of c-RET and activation of its tyrosine kinase activity. Downstream signalling events lead to growth and survival signals that are controlled by receptor occupancy, as well as crosstalk with other ligand–receptor interactions.
B) Germ-line or somatic point mutations either close to the transmembrane (TM) or in the tyrosine kinase (TK) regions of c-*RET* contribute to thyroid C-cell carcinogenesis. These mutations cause c-RET to dimerize independently of ligand or have kinase activity that is independent of dimerization. Germ-line point mutations are a feature of multiple endocrine neoplasia type II syndrome (MEN II), which predisposes to phaeochromocytoma, in addition to thyroid carcinoma. The mutations are dominant; normal receptors are not shown.
C) By contrast, somatic rearrangements of c-*RET* contribute to thyroid follicular-cell carcinogenesis: inversions or translocations fuse the part of c-*RET* that encodes the tyrosine kinase domain with one of several genes that encode coiled-coil-domain-containing proteins. Fusion to *H4* (a gene of unknown function), *RI* α (which encodes a regulatory subunit of protein kinase A) and *ELE1* (a transcriptional co-activator of the androgen receptor) are the most commonly involved, giving rise to the *RET-PTC1*, *RET-PTC2* and *RETPTC3* oncogenes, respectively. *H4* and *ELE1* are also involved in rare rearrangements with differing breakpoints. The resulting coiled-coil-domain-containing fusion protein dimerizes, leading to a constitutively active c-RET tyrosine kinase.

Figure 1.8 (Williams Nature Reviews Cancer 2002 (2) p542-549)

Mutations of *ret* have been found in Hirschprung's disease *ret* has been identified as the susceptibility gene for multiple endocrine neoplasia type 2 (MEN 2A; MEN 2B and familial medullary carcinoma, FMTC) syndromes and point mutations have been identified in sporadic medullary thyroid carcinoma and phaeochromocytoma. Genetic diagnosis of MEN is now possible by DNA analysis for *ret* mutations, which makes it possible to select patients for early thyroidectomy before the clinical development of MTC.

1.7.2.2 Ret/PTC oncogenes

In 1987 the demonstration of an activating oncogene specific for papillary thyroid carcinoma was first shown with NIH 3T3 transfection assays (Fusco, 1987). This oncogene was shown to be a rearranged form of *ret* called ret/PTC (RET/PTC is an acronym for REarranged during Transfection/Papillary thyroid carcinoma). This nomenclature was coined before the role of *ret* in Medullary thyroid carcinoma MTC was first recognised. (Grieco, 1990). The rearrangements described to date consist of fusion of the *ret* tyrosine kinase domain to the 5' terminal of various so-called donor genes. At least 15 chimeric mRNA's involving 10 distinct donor genes have been described. The commonest described are ret/PTC-1 and ret/PTC-3. Table 1.1 tabulates the known rearrangements involving *ret*. The association of ret rearrangements with radiation is strong. The strongest evidence again derives from Chernobyl. Numerous studies have demonstrated ret/PTC activation in post-Chernobyl thyroid papillary carcinoma.

Genes	*Translocation*
RET/PTC1 RET - H4/D10S170 (Smanik, 1995)	**Inv (10;10)(q11.2;q21)**
RET/PTC2 RET - PRKAR1A (Smanik, 1995)	**t(10;17)(q11.2;q23)**
RET/PTC3 (Santoro, 1994) RET/PTC4 or 3R2 (Fugazzola 1996) RET - ELE1/RFG Post Chernobyl Tumour	**Inv (10;10)(q11.2q23)**
RET/PTC5 in RET - RET-II/RFG5 Post Chernobyl Tumour	**14q22.1**
RET - ELKS (Yokata, 2000)	**t(10;12)(q11;p13)**
RET/PTC8 RET - KTN1 (Salassidis, 2000)	**RFG8 (18q21-22)** **t(10;14)(q11.2;q22.1)**
RET/PTC6 RET - TIF1 Post Chernobyl Tumour	**7q32-34**
RET/PTC7 RET - RFG7 Post Chernobyl Tumour	**1p13.1**
RET/PTC9 PTC8 bis RET - RFG9	**Rearrangement (18q21-22) RET/RFG9**
PCM1 - RET (Corvi, 2000)	**t(8;10)(p21-22;q11)**

Table 1.1 Ret rearrangements with references

1.7.2.3 NTRK

The proto-oncogene *NTRK1* or *Trk* (Chromosome 1q22) is similar in many ways to *ret* and also codes for a transmembrane tyrosine kinase receptor for neural growth factor (NGF), which is normally restricted to neural crest derived cells. In the same way as described for ret, *NTRK1* becomes activated in thyroid follicular epithelial cells by chromosomal rearrangements that lead to fusion of the *NTRK1*-TK domain to the 5'–terminal of heterologous genes. The resulting chimeric protein is constitutively activated. The heterologous donor genes include two resulting from intrachromosomal rearrangements: the non-muscular tropomyosin gene (*TPM3*) (Butti, 1995) on 1q31 and the 5' end of promoter regions mapped to 1q25 (TRK-T1 (Greco, 1995) and TRK-T2 (Beimfohr, 1999)). The third described rearrangement results from fusion of NTRK-TK domain to the 5' sequence of TRK fused gene (TFG). TRK rearrangements are restricted to PTC but occur at a lower prevalence than that of ret/PTC (<10% of cases).

1.7.2.4 MET

Met protein is a transmembrane receptor with tyrosine kinase activity. Its ligand is known to be HGF/SF (multifunctional cytokine hepatocyte growth factor/scatter factor). HGF/SF is a powerful mitogen for epithelial cells, including thyroid follicular cells. The oncogene is constitutively activated by amplification of the gene or through mutational change. *MET* overexpression is associated with PTC Scarpino, 2004). Stromal cells of the thyroid are known to secrete HGF and paracrine regulation of MET has been proposed (Ivan, 1997). Both Ret and Ras have

been shown to modulate MET overexpression in primary thyroid cell cultures (Ivan, 1997). The clinicopathological consequence of elevated met expression is presently unclear.

1.7.3 *BRAF*

BRAF (chromosome 7q24, v-raf murine sarcoma viral oncogene homolog B1) is a member of the *raf* family and is the first cancer-causing gene identified by The Sanger Institute in their Cancer Genome Project. Recently, mutations of this gene have been implicated in a variety of cancers, including, melanoma, colonic, borderline ovarian tumours, non-small cell carcinoma of the lung, cholangiocarcinoma and PTC. The *BRAF* gene encodes a cytoplasmic serine/threonine kinase that is regulated by binding to *Ras*. The V600E mutation is believed to mimic the phosphorylation in the activation segment by insertion of an acidic residue close to a site of regulated phosphorylation at serine 598. V600E was previously misnamed V599E.

Most mutations are found to be adjacent to the activating component of the kinase domain, thereby increasing the kinase activity of *BRAF*, leading to activation of ERK. The commonest mutation described involves a thymine-to-adenine transversion at nucleotide position 1796, which results in a valine-to-glutamate substitution at codon 600 (V600E). Recent papers have suggested that $BRAF^{V600E}$ is the most frequent mutation consistently associated with PTC, and not associated with any other thyroid tumour (apart from poorly differentiated and anaplastic carcinomas arising in PTC (Soares, 2004; Kimura, 2003; Kimura, 2004; Xing 2004).

In this context the mutation appears to occur as an alternative event to ret/PTC activation (Soares, 2003). This is consistent with the concept that *BRAF* acts along the RET/PTC-RAS-BRAF-MAPK pathways in thyroid cells. BRAF mutations do not seem to be associated with radiation induced thyroid carcinoma (Lima, 2004). Recently, a distinct BRAF mutation (K601E) has been detected in 9% of cases of the follicular variant of PTC (Trovisco, 2004).

1.7.4 Other Genes implicated in Thyroid carcinoma

1.7.4.1 Immediate early genes

The products of the proto-oncogenes c-*myc*, c-*jun* and c-*fos* are nuclear transcription factors, which activate the expression of several target genes normally involved in the control of cell growth and differentiation. These genes are known as the immediate early genes because of their rapid induction by various stimuli. Although these genes are known to be overexpressed in thyroid carcinoma amplifications and rearrangements have not been described in the literature (Tallini, 2002) and it may be that their increased expression is a reflection of a molecular event upstream of their activation.

1.7.4.2 p53

The *p53* is a tumour suppressor gene (TSG) mapping to chromosome 17p13. It encodes for a nuclear phosphoprotein that as a tetramer acts as a transcription factor and plays a major role as a cell cycle regulator. *p53*-mediated cell cycle arrest

frequently occurs in the G1 (also G2) phase in response to DNA damage. This allows the cell to repair damaged DNA when possible or to promote cell death when repair is not possible. Cancer cells with deficient *p53* function are likely to permit accumulated genetic damage and present a selective advantage for clonal expansion. Alterations in the *p53* TSG are the most common genetic damage in human cancer, usually occurring as a late genetic event.

In thyroid tumours, *p53* gene mutations are restricted to poorly differentiated and undifferentiated tumours and *p53* is thought to play a role in the dedifferentiation process in thyroid carcinogenesis. In PTC, *p53* point mutations are relatively uncommon, with reported mutation rates usually less than 10% (Ho, 1996).

1.7.4.3 *PTEN*

PTEN is a tumour suppressor gene mapped to 10q22-23. It encodes a dual-specificity phosphatase and has the ability negatively regulate the PI3-kinase/AKT pathway. Heterozygous *PTEN* +/- transgenic mice develop thyroid tumours, some of which have features of PTC. *PTEN* mutations have been identified in up to 25% of sporadic follicular adenomas and carcinomas and rarely in PTC (Dahia, 1997; Bruni, 2000).

1.7.4.4 PPARγ

PPARγ is a member of the nuclear hormone receptor superfamily that includes thyroid hormone, retinoic acid, and androgen and oestrogen receptors. These

receptors share common features, including a central DNA binding domain (DBD) and a carboxyl-terminal domain responsible for dimerisation, ligand binding, and transcriptional activation.

PAX 8 encodes a transcriptional factor required for the genesis of thyroid follicular cell lineages and regulation of thyroid-specific gene expression. In FTC with evidence of a t (2;3)(q13;p25) chromosomal translocation, a chimeric product characterised by in frame fusion of exon 7, 8 or 9 of *PAX*8 with exon 1 of *PPARγ* has been demonstrated (Kroll, 2000).

This rearrangement is not found in PTC and was touted as a potential biomarker of malignancy in the differential diagnosis of follicular patterned lesions of the thyroid. Unfortunately, other studies have shown the presence of the translocation in a number of follicular adenomas (Marques, 2002).

1.8 Aims and Objectives

The overall aim of this study was to provide a genome wide assessment of papillary thyroid carcinoma. The specific objectives were to:

1) Map ret/PTC chimeric transcripts in a sporadic cohort of PTC and correlate tumour morphology with specific ret rearrangement.
2) To investigate the effect of radiation on the genome of human thyroid cells.
3) To investigate global DNA copy gain and loss in Papillary Thyroid Carcinoma.

4) To analyse the expression profile of Papillary Thyroid Carcinoma in order to describe the pathobiology of PTC and identify potential biomarkers and therapeutic targets.

1.9 General References and Bibliography

Basolo F, Pinchera A, Fugazzola L, Fontanini G, Elisei R, Romei C, Pacini F. 1994. Expression of p21 ras protein as a prognostic factor in Papillary thyroid carcinoma. Eur J Cancer 30:171-174

Baverstock K, Egloff B, Pinchera A, Ruchti C, Williams D. 1992. Thyroid cancer after Chernobyl. Nature; 359: 21-22

Beimfohr C, Klugbauer S, Demidchik EP, Lengfelder E, Rabes HM. 1999. NTRK1 re-arrangement in papillary thyroid carcinomas of children after the Chernobyl reactor accident. Int J Cancer. 15;80(6):842-7

Bleuer JP, Averkin YI, Okeanov AE, Abelin T. 1997. The epidemiological situation of thyroid cancer in Belarus. Stem Cells 15:251-254

Bruni P, Boccia A, Baldassarre G, Trapasso F, Santoro M, Chiappetta G, Fusco A, Viglietto G. 2000. PTEN expression is reduced in a subset of sporadic thyroid carcinomas: evidence that PTEN-growth suppressing activity in thyroid cancer cells mediated by p27kip1. Oncogene. 19(28): 3146-55

Butti MG, Bongarzone I, Ferraresi G, Mondellini P, Borrello MG, Pierotti MA. 1995. A sequence analysis of the genomic regions involved in the rearrangements between TPM3 and NTRK1 genes producing TRK oncogenes in papillary thyroid carcinomas. Genomics. 28(1):15-24

Cady B, Rossi R. 1998. An expanded view of risk factor definition in differentiated thyroid carcinoma. Surgery 104:947-953

Cohen Y, Xing M, Mambo E, Guo Z, Wu G, Trink B, Beller U, Westra WH, Ladenson PW, Sidransky D. 2003. BRAF mutation in papillary thyroid carcinoma. J Natl Cancer Inst 95(8): 625-7

Corvi R, Berger N, Balczon R, Romeo G. 2000. RET/PCM-1: a novel fusion gene in papillary thyroid carcinoma. Oncogene 19(37):4236-42

Dahia PL, Marsh DJ, Zheng Z, Zedenius J, Komminoth P, Frisk T, Wallin G, Parsons R, Longy M, Larsson C, Eng C. 1997. Somatic deletions and mutations in the Cowden disease gene, PTEN, in sporadic thyroid tumors. Cancer Research 57 (21):4710-3.

DeLellis R. 2004. Tumours of the thyroid and parathyroid. In: Tumours of Endocrine Organs. Lyon. World Health Organisation Classification of Tumours (in press).

DiRenzo MF, Olivero M, Serini G, Orlandi F, Pilotti S, Belfiore A, Costantino A, Vigneri R, Angeli A, Pierotti MA. 1995. Overexpression of the c-MET/HGF receptor in human thyroid carcinomas derived from the follicular epithelium. J Endocrinol Invest.18 (2): 134-9.

Demidchik EP, Drobyshevskaya IM, Cherstvoy LN, Astakhova LN, Okeanov AE, Vorontsova TV, Germenchuk M. 1996. Thyroid cancer in children in Belarus. In: Karaoglou A, Desmet G, Kelly GN, Menzel HG, Eds. The radiological consequences of the Chernobyl Accident. Luxembourg: EUR 16544 EN; 1: 677-682

DuBose J, Barnett R, Ragsdale T. 2004. Honest and sensible surgeons: the history of thyroid surgery. Curr Surg 61(2): 213-219

Ferlay J, Bray F, Parkin DM, Pisani P, eds (2001) Globocan 2000: Cancer Incidence and Mortality Worldwide. IARC Cancer Bases No. 5, Lyon, IARCPress
Stewart BW, Kleihues P. World Cancer Report.

Fugazzola L, Pierotti MA, Vigano E, Pacini F, Vorontsova TV, Bongarzone I. 1996. Molecular and biochemical analysis of RET/PTC4, a novel oncogenic rearrangement between RET and ELE1 genes, in a post-Chernobyl papillary thyroid cancer. Oncogene 13(5):1093-7

Fukushima T, Suzuki S, Mashiko M, Ohtake T, Endo Y, Takebayashi Y, Sekikawa K, Hagiwara K, Takenoshita S. 2003. BRAF mutations in papillary carcinomas of the thyroid. Oncogene 22(41): 6455-7.

Fusco A, Grieco M, Santoro M, Berlingieri MT, Pilotti S, Pierotti MA, Della Porta G, Vecchio G. 1987. A new oncogene in human thyroid papillary carcinomas and their lymph node metastases. Nature 328:170-72

Gilbert ES, Land CE, Simon SL. 2002. Health effects from Fallout. Health Physics. 82(5): 726-735

Gimm O. 2001. Thyroid cancer. Cancer Lett. 163(2): 143-56

Greco A, Mariani C, Miranda C, Lupas A, Pagliardini S, Pomati M, Pierotti MA. 1995. The DNA rearrangement that generates the TRK-T3 oncogene involves a novel gene on chromosome 3 whose product has a potential coiled-coil domain. Mol Cell Biol. 15(11):6118-27.

Grieco M, Santoro M, Berlingieri MT, Melillo RM, Donghi R, Bongarzone I, Pierotti MA, Della Porta G, Fusco A, Vecchio G. 1990. PTC is a novel rearranged form of the ret proto-oncogene and is frequently detected in vivo in human papillary thyroid carcinomas. Cell 1990;60:557-63

Hall P, Mattson A, Boice JD, Jr. 1996. Thyroid cancer after diagnostic administration of iodine-131. Radiat Research 145:86-92

Hamdy RC. The thyroid gland. A brief historical perspective. 2002. South Med J 95(5):471-473

Hamilton TE, Van Belle G, LoGerfo JP. 1987. Thyroid carcinoma in Marshall Islanders exposed to nuclear fallout. JAMA 258:629-636

Harach HR, Escalante DA, Onativia A, Lederer Outes J, Saravia Day E, Williams ED. 1985. Thyroid carcinoma and thyroiditis in an endemic goitre region before and after iodine prophylaxis. Acta Endocrinol 108:55

Harach HR, Williams GT, Williams ED. 1995. Familial adenomatosis associated thyroid carcinoma: a distinct type of follicular cell neoplasm. Histopathology 25; 549

Hirokawa M, Carney JA, Goellner JR, DeLellis RA, Heffess CS, Katoh R, Tsujimoto M, Kakudo K. 2002. Observer variation of encapsulated follicular lesions of the thyroid gland. Am J Surg Pathol.26(11):1508-14

Ho YS, Tseng SC, Chin TY, Hsieh LL, Lin JD. 1996. p53 gene mutation in thyroid carcinoma. Cancer Lett. 103(1):57-63.

Hunt JL, Baloch ZW, Barnes L, Swalsky PA, Trusky CL, Sesatomi E, Finkelstein S, LiVolsi VA. 2002. Loss of heterozygosity mutations of tumour suppressor genes in cytologically atypical areas in chronic lymphocytic thyroiditis. Endocr Pathol. 13(4): 321-30

Hofrichter, 1990, quoted by Haynes RC Jr: Thyroid and antithyroid drugs. Goodman and Gilman's The Pharmacological Basis of Therapeutics, 8th Ed. Gilman AG, Rall TW, Niew As, et al (eds). Pergamon Press, p1361

Hofstadter F. 1980. Frequency and morphology of malignant tumours of the thyroid before and after the introduction of iodide prophylaxis. Virchows A Pathol Anat 385:263

Huang Y, Prasad M, Lemon WJ, Hampel H, Wright FA, Kornacker K, LiVolsi V, Frankel W, Kloos RT, Eng C, Pellegata NS, de la Chapelle A. 2001.Gene expression in papillary thyroid carcinoma reveals highly consistent profiles. Proc Natl Acad Sci U S A. 98(26): 15044-9.

Ivan M, Bond JA, Prat M, Comoglio PM, Wynford-Thomas. 1997. Activated ras and ret oncogenes induce over-expression of c-met (hepatocyte growth factor receptor) in human thyroid epithelial cells. Oncogene 14(20): 2417-23

Kazakov VS, Demidchik EP, Astakhova LN. 1992.Thyroid cancer after Chernobyl. Nature 359: 21

Kim DS, McCabe CJ, Buchanan MA, Watkinson JC. 2003. Oncogenes in thyroid cancer. Clin Otolaryngol. 28(5): 386-95.

Kimura ET, Nikiforova MN, Zhu Z, Knauf JA, Nikiforov YE, Fagin JA. 2003. High prevalence of BRAF mutations in thyroid cancer: genetic evidence for constitutive

activation of the RET/PTC-RAS-BRAF signaling pathway in papillary thyroid carcinoma. Cancer Res.63 (7): 1454-7

Kimura ET, Vanvooren V, van Sande J, Nikiforov YE, Fagin JA. 2004. Autonomously functioning thyroid nodules are not associated with BRAF mutations. Clin Endocrinol (Oxf). 60(3): 394-6

Kolonel LN, Hankin JH, Wilkens LR, Fukunaga FH, Hinds MW. 1990. An epidemiologic study of thyroid cancer in Hawaii. Cancer Causes Control 1:223-34

Kroll TG, Sarraf P, Pecciarini L, Chen CJ, Mueller E, Spiegelman BM, Fletcher JA. 2000. PAX8-PPARgamma1 fusion oncogene in human thyroid carcinoma. Science. 289(5483):1357-60

Lemoine NR, Mayall ES, Williams ED, Thurston V, Wynford-Thomas D. 1988. Agent-specific ras oncogene activation in rat thyroid tumours. Oncogene. 3(5): 541-4

Lima J, Trovisco V, Soares P, Maximo V, Magalhaes J, Salvatore G, Santoro M, Bogdanova T, Tronko M, Abrosimov A, Jeremiah S, Thomas G, Williams D, Sobrinho-Simoes M. 2004. BRAF mutations are not a major event in post-Chernobyl childhood thyroid carcinomas. J Clin Endocrinol Metab. 89(9):4267-71.

LiVolsi VA, Asa SL, eds. Endocrine Pathology. 2002. Churchill Livingstone.

Marques AR, Espadinha C, Catarino AL, Moniz S, Pereira T, Sobrinho LG, Leite V. 2002. Expression of PAX8-PPAR gamma 1 rearrangements in both follicular thyroid carcinomas and adenomas. J Clin Endocrinol Metab. (8):3947-52

McMihn RMH. 1994. Last's Anatomy, Regional and Applied. Ninth Edition. Churchill Livingstone.

Moysich KB, Menezes RJ, Michalek AM. 2002. Chernobyl-related ionising radiation exposure and cancer risk: an epidemiological review. The Lancet Oncology 3(5): 269-279

Namba H, Nakashima M, Hayashi T, Hayashida N, Maeda S, Rogounovitch TI, Ohtsuru A, Saenko VA, Kanematsu T, Yamashita S. 2003. Clinical implication of hot spot BRAF mutation, V599E, in papillary thyroid cancers. J Clin Endocrinol Metab. (9): 4393-7

Nikiforov YE, Nikiforova MN, Gnepp DR, Fagin JA. 1996. Prevalence of mutations of ras and p53 in benign and malignant thyroid tumors from children exposed to radiation after the Chernobyl nuclear accident. Oncogene.13(4):687-93

Nikiforova MN, Kimura ET, Gandhi M, Biddinger PW, Knauf JA, Basolo F, Zhu Z, Giannini R, Salvatore G, Fusco A, Santoro M, Fagin JA, Nikiforov YE. 2003. BRAF mutations in thyroid tumours are restricted to papillary carcinomas and

anaplastic or poorly differentiated carcinomas arising from papillary carcinomas. J Clin Endocrinol Metab. 88(11): 5399-404.

.

Piersanti M, Ezzat S, Asa SL. 2003. Controversies in papillary microcarcinoma of the thyroid. Endocr Pathol. 14(3): 183-191

Rochefort P, Caillou B, Michiels FM, Ledent C, Talbot M, Schlumberger M, Lavelle F, Monier R, Feunteun J. 1996. Thyroid pathologies in transgenic mice expressing a human activated Ras gene driven by a thyroglobulin promoter. Oncogene. 12(1): 111-8.

Rosai J, Carcangiu ML, DeLellis RA. 1992. Atlas of Tumour Pathology. Tumours of the thyroid gland. AFIP

Rosai J, LiVolsi VA, Sobrinho-Simoes M, Williams ED. 2003. Renaming papillary microcarcinoma of the thyroid gland: the Porto proposal. Int J Surg Pathol 11:249-251

Rush quoted by Haynes RC Jr. 1990. Thyroid and antithyroid drugs. Goodman and Gilman's The Pharmacological Basis of Therapeutics, 8th Ed. Gilman AG, Rall TW, Niew As, et al (eds). Pergamon Press, p1361

Salassidis K, Bruch J, Zitzelsberger H, Lengfelder E, Kellerer AM, Bauchinger M. 2000. Translocation t(10;14)(q11.2:q22.1) fusing the kinetin to the RET gene creates

a novel rearranged form (PTC8) of the RET proto-oncogene in radiation-induced childhood papillary thyroid carcinoma. Cancer Res. 60(11): 2786-9

Santoro M, Dathan NA, Berlingieri MT, Bongarzone I, Paulin C, Grieco M, Pierotti MA, Vecchio G, Fusco A. 1994. Molecular characterization of RET/PTC3; a novel rearranged version of the RET proto-oncogene in a human thyroid papillary carcinoma. Oncogene 9(2): 509-16

Scarpino S, Cancellario d'Alena F, Di Napoli A, Pasquini A, Marzullo A, Ruco LP. 2004. Increased expression of Met protein is associated with up-regulation of hypoxia inducible factor-1 (HIF-1) in tumour cells in papillary carcinoma of the thyroid. J Pathol.202 (3): 352-8

Sieben NL, Macropoulos P, Roemen GM, Kolkman-Uljee SM, Jan Fleuren G, Houmadi R, Diss T, Warren B, Al Adnani M, De Goeij AP, Krausz T, Flanagan AM. 2004. In ovarian neoplasms, BRAF, but not KRAS, mutations are restricted to low-grade serous tumours. J Pathol. 202(3): 336-40.

Schlumberger MJ. 1999. Diagnostic follow-up of well-differentiated thyroid carcinoma: historical perspective and current status. J Endocrinol Invest. 22(11 Suppl): 3-7

Sheils OM, O'Leary JJ, Uhlmann V, Lattich K, Sweeney EC. 2000. ret/PTC-1 Activation in Hashimoto Thyroiditis. Int J Surg Pathol. 8(3): 185-189

Smanik PA, Furminger TL, Mazzaferri EL, Jhiang SM. 1995. Breakpoint characterization of the ret/PTC oncogene in human papillary thyroid carcinoma. Hum Mol Genet. 4(12): 2313-8

Soares P, Trovisco V, Rocha AS, Lima J, Castro P, Preto A, Maximo V, Botelho T, Seruca R, Sobrinho-Simoes M. 2003. BRAF mutations and RET/PTC rearrangements are alternative events in the etiopathogenesis of PTC. Oncogene. (29): 4578-80.

Soares P, Trovisco V, Rocha AS, Feijao T, Rebocho AP, Fonseca E, Vieira de Castro I, Cameselle-Teijeiro J, Cardoso-Oliveira M, Sobrinho-Simoes M. 2004. BRAF mutations typical of papillary thyroid carcinoma are more frequently detected in undifferentiated than in insular and insular-like poorly differentiated carcinomas. Virchows Arch. 444(6): 572-6

Sobrinho-Simões M, Soares J, Carneiro F, Limbert E. 1990. Diffuse follicular variant of papillary carcinoma of the thyroid: report of eight cases of a distinct aggressive type of thyroid tumour. Surg Pathol 3: 189-203

Sobrinho-Simoes M, Sambade C, Fonseca E, Soares P. 2002. Poorly differentiated carcinomas of the thyroid gland: a review of the clinicopathologic features of a series of 28 cases of a heterogeneous, clinically aggressive group of thyroid tumours. Int J Surg Pathol 10:123-131

Stefaneanu L, Sasano H, Kovacs K, eds. Molecular and Endocrine Pathology. 2000. Arnold.

Stewart BW, Kleihues P. Eds: 2003. World Cancer Report. IARC Press. Lyon.

Suchy B, Waldmann V, Klugbauer S, Rabes HM. 1998. Absence of RAS and p53 mutations in thyroid carcinomas of children after Chernobyl in contrast to adult thyroid tumours. Br J Cancer. 77(6): 952-5

Tallini G. 2002. Molecular pathobiology of thyroid neoplasms. Endocr Pathol. 13(4): 271-88

Tronko MD, Bogdanova TI, Komissarenko IV, Epstein OV, Oliynyk V, Kovalenko A, Likhtarev IA, Kairo I, Peters SB, LiVolsi VA. 1999. Thyroid carcinoma in children and adolescents in Ukraine after the Chernobyl nuclear accident: Statistical data and clinicomorphologic characteristics. Cancer 86: 149-156

Trovisco V, Vieira de Castro I, Soares P, Maximo V, Silva P, Magalhaes J, Abrosimov A, Guiu XM, Sobrinho-Simoes M. 2004. BRAF mutations are associated with some histological types of papillary thyroid carcinoma. J Pathol. 202(2): 247-51

Tsyb AF, Parshkov EM, Shakhtarin VV, Stepanenko VF, Skvortsov VF, Chebotareva IV. 1996. Thyroid cancer in children and adolescents of Bryansk and

Kaluga regions. In: Karaoglou A, Desmet G, Kelly GN, Menzel HG, eds. The radiological consequences of the Chernobyl Accident. Luxembourg: EUR 16544 EN: 677-682

Williams ED, Doniach I, Bjarnason O, Michie W. 1977. Thyroid carcinoma in an iodine rich area. Cancer 39:215-222

Williams ED. 1993. Radiation induced thyroid cancer. Histopathology 23, 387-389

Williams ED. 2000. Two proposals regarding the terminology of thyroid tumours. Int J Surg Pathol 8:181-183

Wirtschafter A, Schmidt R, Rosen D, Kundu N, Santoro M, Fusco A, Multhaupt H, Atkins JP, Rosen MR, Keane WM, Rothstein JL. 1999. Expression of the RET/PTC fusion gene as a marker for papillary carcinoma in Hashimoto's Thyroiditis. Laryngoscope. 109(6): 1011-5

Xing M, Cohen Y, Mambo E, Tallini G, Udelsman R, Ladenson PW, Sidransky D. 2004. Early occurrence of RASSF1A hypermethylation and its mutual exclusion with BRAF mutation in thyroid tumourigenesis. Cancer Res 64(5): 1664-8

Xing M, Vasko V, Tallini G, Larin A, Wu G, Udelsman R, Ringel MD, Ladenson PW, Sidransky D. 2004. BRAF T1796A transversion mutation in various thyroid neoplasms. J Clin Endocrinol Metab 89(3): 1365-8

Xu X, Quiros RM, Gattuso P, Ain KB, Prinz RA. High prevalence of BRAF gene mutation in papillary thyroid carcinomas and thyroid tumour cell lines. 2003 Cancer Res 63(15): 4561-7

Yokota T, Nakata T, Minami S, Inazawa J, Emi M. 2000. Genomic organization and chromosomal mapping of ELKS, a gene rearranged in a papillary thyroid carcinoma. J Hum Genet. 45(1):6-11

Zhu Z, Gandhi M, Nikiforova MN, Fischer AH, Nikiforov YE. 2003. Molecular profile and clinical-pathologic features of the follicular variant of papillary thyroid carcinoma. An unusually high prevalence of ras mutations. Am J Clin Pathol. 120(1):71-7.

Chapter 2

Methodology

2.1 Introduction

This chapter provides a detailed account of all the methodologies used in this study. Background information and theoretical detail is included for several of the newer or more complex techniques. The descriptions of each technique are grouped in sections and are broadly listed in the order in which they appear in the text of the thesis.

2.2 Section 1

2.2.1 Fresh Thyroid Tissue Archive

All surgically removed thyroid tissue with appropriate consent was considered for tissue banking. On receipt, a pathologist was available at all times to dissect the specimen and harvest tissue for banking, in order to ensure no compromise of the diagnostic potential of the specimen.

1) A piece of normal tissue and tumour/diseased tissue was taken in all cases when appropriate. A new scalpel blade was used for each sample. The amount of tissue harvested depended on the size of the specimen or tumour.

2) Each slice was divided into separate smaller fragments (4mm x 4mm.) These fragments were then placed in Eppendorf or cryovial tubes labelled (in pencil) with the specimen number and whether normal (N) or tumour (T). If there were two separate tumours/nodules, they were labelled T1 and T2.

3) The eppendorfs were immersed in liquid Nitrogen for 2 minutes and then removed with a tweezers and placed in labelled containers.

These samples were immediately stored in a dedicated section of the freezer at -80°C.

4) In cases of known tumour, separate fragments were placed in cryovials/eppendorfs containing RNAlater®, a proprietary solution used for storing RNA without degradation. Tissues can be stored in RNAlater, a proprietary Stabilization Reagent, for up to 1 day at 37°C, 7 days at 18–25°C, 4 weeks at 2–8°C, or for archival storage at –20°C or –80°C.

2.2.2 Formalin fixed paraffin embedded Tissue

Formalin fixed (10% buffered) and paraffin embedded thyroid tumour samples were selected from the pathology files of St. James's Hospital, Dublin. Haematoxylin & Eosin (H&E) stained slides of all tumour samples were reviewed by a pathologist and classified according to appropriate criteria (Rosai, 1992).

2.3 Section 2

2.3.1 Cell Culture of N thy-ori cells

The human thyroid epithelial cell line (N thy-ori 3-1 ECACC number 90011609) is derived from normal thyroid tissue of an adult. The cells have been immortalized by transfection with a plasmid encoding for the Simian Virus 40 (SV40) large T antigen (Lemoine, 1989). N thy ori expresses specific features of thyroid epithelial function (iodide-trapping and thyroglobulin production). This cell line has been characterised in detail and found to be growth factor-independent, capable of anchorage-independent growth at low frequency but non-tumourigenic in nude mice.

N thy-ori cells were grown to confluence in a humidified atmosphere containing 5% CO_2 at 37°C.

2.3.2 Formulation of N thy ori culture media and other solutions

1. Culture media: RPMI, 10% Foetal Calf Serum (FCS), 2% Penicillin/ Streptomycin (5000 U/ml).

   e.g. Stock solution of 500mls of culture media (450 mls RPMI, 40 mls FCS and 10mls of Pen Streptomycin). Store at 4°C.
2. Trypsin Neutralising Solution (TNS) = RPMI/20%FCS. 10ml Aliquots. Store at -20°C.
3. Freezing Solution = RPMI/20%FCS/10% Dimethyl sulfoxide (DMSO) (e.g. 35ml/10ml/5ml). Store at -20°C.

4. The Trypsin is stored in 1ml aliquots at 10X. Dilute 1ml: 9 ml in Phosphate Buffered Saline (PBS) when splitting cells.

2.3.3 Thawing cells from stocks

1. Two T75 flasks were used. 15 mls of culture media was added to each and prewarmed to 37°C.
2. One cryovial of N thy ori cells were removed (1 ml in each) from liquid nitrogen and quickly brought to room temperature. 500μL of the thawed cells was added to each of the prewarmed flasks.

3. The medium was changed initially after 3 days (cells adherent) and at 3-day intervals until confluent.

2.3.4 Splitting Confluent flasks

THE MEDIUM WAS PREWARMED

1. Old medium was removed.
2. The cells were washed with 5ml Phosphate buffered saline (PBS).
3. The PBS was removed and discarded.
4. Five mls of Trypsin/EDTA (see above) was added to the flask and incubated at 37°C for 2-3 minutes.
5. Flasks were examined by phase microscopy to assess cell detachment.

6. Flasks were lightly tapped to encourage the release of cells from the plastic surface.
7. When > 90% of cells were detached, an equal volume 5 mls of Trypsin Neutralising Solution (TNS) was added.
8. The cell suspension was removed to a new 15 ml tube.
9. The flask was further washed with 5mls PBS and removed to the same 15ml tube.
10. The cells were then pelleted (5 min @ 1000rpm).
11. The supernatant was removed and discarded.
12. The cells were resuspended in 2ml RPMI (light tapping). New flasks were subsequently seeded with 25% (500µL, 1:4 split ratio) of the trypsinised cells.

2.3.5 Cryopreservation

1. After pelleting by centrifugation, the cells were resuspended in 2ml freezing solution in cryovials (1 ml in each cryovial).
2. The vials were placed on ice for 10 minutes, then at -20°C for 1 hour. Vials were then left overnight at -80°C. Vials were then transferred to a liquid nitrogen storage tank for long-term storage.

2.3.6 Mycoplasma testing

2.3.6.1 Background

Mycoplasma infection of cell cultures are persistent, tedious to detect, and difficult to remedy. First discovered as the aetiological agent of contagious bovine pleuropneumonia in 1898 and classified in the mid 1950s, Mycoplasma was found to have a broad range of hosts - humans, animals, insects, and plants. Statistics prove that 30 to 60% of all cell cultures are contaminated with mycoplasmas, resulting in alterations of growth rates, morphology, and cell viability. Furthermore, they may miss the real objectives and out-come of these experiments. Several different classical methods are used to detect Mycoplasma: DNA staining, microbiological culture, and biochemical detection. However, these methods are tedious, time consuming, and have limited sensitivity, which makes them unsuitable or at least too inconvenient for regular use in the laboratory.

The Mycoplasma Detection Kit (Roche) follows a standard Enzyme linked Immuno Sorbent Assay (ELISA) protocol. Results can be obtained in just one day with a limited number of handling steps. The kit is highly sensitive for the most common mycoplasmas (detection limit 104–107 cfu/ml, depending on the type of mycoplasma); it even detects contamination in cell supernatants diluted 1:10.

2.3.6.2 Mycoplasma Protocol

Stage 1 Enrichment of mycoplasma by centrifugation of the cell free supernatant, alkaline lysis (NaOH) and neutralization of the lysate

1) Transfer 1ml of culture supernatant into a centrifuge tube and pellet cells and/or cellular debris by centrifuging at 200Xg for 10 minutes at room temperature.
2) Transfer the supernatant into a fresh sterile tube and centrifuge at 13,000Xg for 10 minutes at 2-8°C. This sediments Mycoplasma.
3) Decant all of the supernatant. Leave the pellet and remove all medium.
4) Add 10µl of ultrapure water and 10µl of lysis reagent to the pellet and allow to solubilise.
5) Use 2 negative (10µl of water and 10µl of lysis reagent) and 1 positive controls (10µl of positive control DNA and 10µl of lysis reagent).
6) Incubate at 37° for one hour.
7) Add 30µl of neutralization reagent.

Stage 2 Mycoplasma PCR: Amplification of a conserved and mycoplasma-specific region of the DNA in the presence of digoxigenin-labelled dUTP (DIG-dUTP). The label is incorporated into the amplicon.

8) Transfer 25µl of PCR ready to go mix and 15µl of sterile water into PCR tubes. Instead of water UNG (Uracil-DNA glycosylase) may be used. UNG hydrolyses uracil-glycosidic bonds at dU-containing DNA sites and therefore destroys carry over products.
9) To each PCR tube add 10µl of Sample, Positive control or Negative control.
10) Transfer to the thermal cycler (PE 2400) and cycle as follows:

    Cycle 1: 95°C for 5 minutes

    Cycle 2-40: 94°C for 30 s, 62°C for 30 s, 72°C for 1 minute.

    Cycle 41: 72°C for 10 minutes.

    Hold at 8°C

Stage 3 Hybridisation and ELISA procedure

11) Add 40 µl of Denaturation reagent (bottle 4) into a suitable reaction tube using a Pipette with aerosol-preventive Pipette tips.
12) Transfer 10 µl of the amplification product per tube and incubate at 15-25°C for 10 minutes.
13) Add 450µl hybridisation reagent per tube and mix thoroughly.

14) Transfer 200µl of the mixture per well of the microplate

- Cover the wells with the self-adhesive cover foil.
- Incubate at 37°C on a shaker at 300rpm for 3 hours.

15) Remove hybridisation mixture by flicking and wash 3 times with 250µl washing buffer (1X) per well. Remove the washing buffer by flicking.

16) Add 200µl of anti-DIG-POD working dilution per well. Cover the wells with the self-adhesive cover foil. Incubate at 15–25°C on a shaker (300 rpm) for 30 minutes.

17) Remove anti-DIG-POD by flicking and wash five times with 250 µl Washing buffer (1×) per well. Remove the Washing buffer by flicking.

18) Add 100 µl of TMB substrate solution (bottle 10), prewarmed to 15-25°C, per well. Cover the wells with the self-adhesive cover foil. Incubate at 15–25°C on a shaker (300 rpm) for approx. 20 minutes.

19) Add 100 µl of Stop reagent (bottle 11) per well and measure absorbance using a microplate (ELISA) reader at 450 nm (reference wavelength approx. 690 nm) within 1 h after addition of the Stop reagent.

Interpretation of the results

Negative control The absorbance of the negative control should be lower than 0.25 A450 nm – A690 nm units. If values are higher, the whole experiment (amplification included) should be repeated.

Positive control The absorbance of the positive control should be higher than 1.2 A450 nm – A690 nm -units. If values are lower, the whole experiment (including amplification) should be repeated.

Samples Subtract the mean of the absorbance readings of the negative controls from those of the samples. Samples are regarded as mycoplasma-contaminated if the difference in absorbance (A) is higher than 0.2 A450 nm – A690 nm -units.

2.4 Section 3

2.4.1 Tissue preparation prior to nucleic acid extraction

2.4.2 Frozen Section cutting Protocol

1) The frozen tissue fragment was placed on a corkboard in a large drop of sterile ultrapure H2O. The corkboard was placed on a freezing microtome chuck.
2) The tissue, cork and chuck were immersed in liquid nitrogen and frozen.
3) The chuck was then transferred to the cold plate of the microtome. The block was "faced off" initially at a cutting depth of 30μm.

4) After facing off, ribbon sections were cut at 8μm thickness.

2.4.3 Fixing and staining for Methyl green/H&E

After cutting the frozen sections, the slides were fixed in alcohol and stained rapidly as follows.

1) Alcohol 70% - 15 dips.
2) H2O – 1 dip.
3) MG/Haematoxylin – 15 dips.
4) H2O – 1 dip.
5) Alcohol 70% - 10 dips.
6) Alcohol 95% - 15 dips.
7) Eosin – 15 dips (Omit this step if using Methyl Green).
8) Alcohol 95% - 15 dips.
9) Alcohol 100% (1) dips.
10) Alcohol 100% (2) – 15 dips.
11) Xylene (1) until clean.
12) Xylene Hold.

2.4.4 Tissue Homogenisation

Laser capture microdissected (LCM) cells requires no special homogenisation procedures. In contrast, homogenisation of the large fragments of banked thyroid tissue was a critical step, particularly prior to RNA extraction. A variety of

homogenisation techniques was evaluated. The best homogenisation procedure for snap frozen thyroid tissue was as follows.

2.4.4.1 Mortar and pestle homogenisation of tissue

The banked frozen or RNA later stabilised tissue was removed from the -80°C freezer and placed on dry ice during the extraction process. The mortar and pestle was autoclaved and treated with an RNase inhibitor (RNA Zap®) prior to homogenisation.

The mortar and pestle was pre-cooled with liquid nitrogen. Tissue was transferred directly from the dry ice to the mortar and pestle and immersed in liquid nitrogen. The liquid nitrogen may be allowed to evaporate, but the tissue should not be allowed to thaw.

The tissue was then thoroughly homogenised by grinding and the resultant powder and small fragments transferred to an RNase free Eppendorf tube, containing the appropriate lysis buffer (600μL). After vortexing, the sample was further homogenised using a Qiagen Shredder column.

2.4.4.2 QIAshredder®

Qiagen shredders are a commercially available spin column based shearing system. They can be used for further homogenisation of tissue initially homogenised by mortar and pestle and for cultured cells as the primary form of homogenisation.

Lysates were pipetted directly onto a QIAshredder spin column placed in 2 ml collection tube, and centrifuged for 2 min at maximum speed. The flow through was used for subsequent RNA extraction.

2.4.4.3 Homogenisation of Formalin Fixed Paraffin embedded tissue using a Microfuge pellet mixer

A Microfuge pellet mixer comprises plastic rods, which fit snugly into 1.5ml Eppendorf type tubes, and which can be attached to a hand held motorized rotor. They were used to partially homogenize formalin fixed paraffin embedded (FFPE) tissue samples prior to further digestion using Proteinase K.

2.5 Section 4

2.5.1 Arcturus PixCell II Laser Capture Microdissection system

2.5.2 Background

LCM is based on the selective adherence of visually targeted cells and tissue fragments to a thermoplastic membrane activated by a low energy infrared laser pulse. The system consists of an inverted microscope, a solid state near infrared laser diode, a laser control unit, a joystick controlled microscope stage with a vacuum chuck for immobilisation, a CCD camera, and a colour monitor. The LCM microscope is connected to a computer with additional laser control and image archiving.

The thermoplastic membrane used for the transfer of selected cells has a diameter of approximately 0.6cm and is mounted on an optically clear cap, which fits on standard 0.5ml microcentrifuge tubes for further processing (Figure 2.1).

The cap is suspended on a mechanical transport arm and positioned on the desired area of the dehydrated tissue section. Laser activation leads to focal melting of the ethylene vinyl acetate (EVA) membrane, which has its absorption maximum near the wavelength of the laser. The melted polymer expands into the section and fills the extremely small hollow spaces present in the tissue. The polymer re-solidifies within milliseconds and forms a composite with the tissue. The adherence of tissue to the activated membrane exceeds the adhesion to the glass slide and allows

selective removal of the cells. Laser impulses can be repeated multiple times, which allows rapid isolation of large numbers of cells. The selected cells are harvested by simple lifting of the cap, which is then transferred to a microcentrifuge tube containing the appropriate extraction lysis buffer.

Because the membrane absorbs most of the energy, the maximum temperatures reached by the tissue are in the range of 90°C for several milliseconds. The low energy of the infrared laser also avoids potentially damaging photochemical effects (Fend, 2000).

2.5.3 Setting LCM Parameters

The laser spot size can be adjusted to three sizes (<7.5μm, 15μm and 30μm). Further adjustable parameters include: pulse power, pulse width, threshold voltage and pulse duration. Laser pulse power and duration determine the size of the LCM transfer. Optimum transfers occur when, after firing the laser, the melted plastic film is similar in size to that of the target beam. Table 2.1 shows the most commonly used and best performing settings for LCM of thyroid tissue.

The total number of pulses in each case was approximately 700. For a 30μm spot size this yielded a tissue volume in the range of 10^{-7} to 10^{-6} μm^3. Examples of laser captured thyroid cells are seen in Figure 2.2.

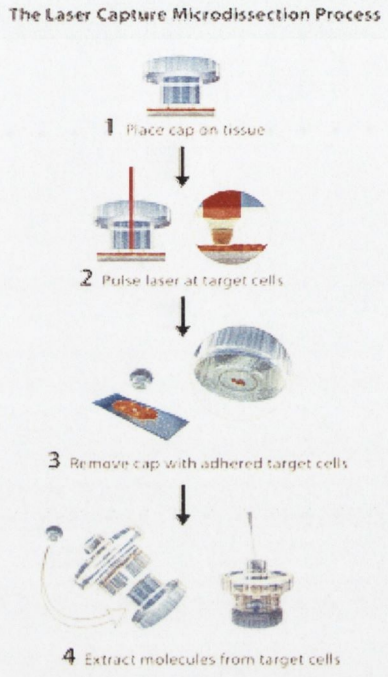

Figure 2.1 Overview of LCM Process

Spot Size	Power	Duration	Threshold Voltage
<7.5 μm	40mW	450μs	285MmV
~15 μm	25mW	1.5ms	285MmV
~30 μm	20mW	5ms	285MmV

Table 2.1 LCM Settings

1) Before Laser Capture Microdissection LCM

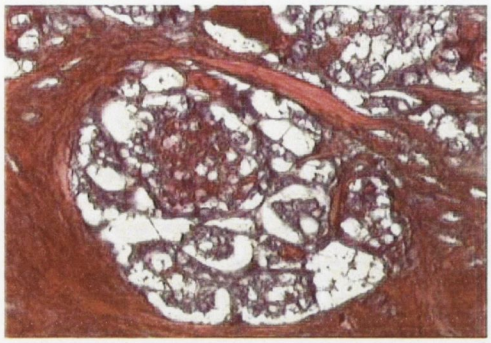

2) After LCM

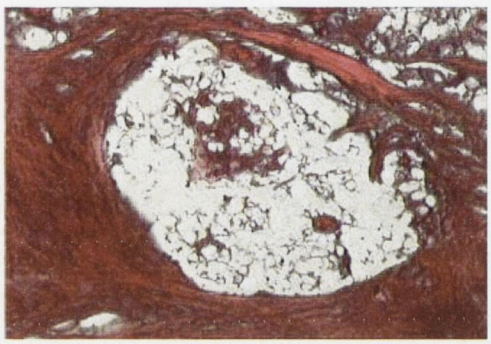

3) Microdissected Thyroid follicular cells

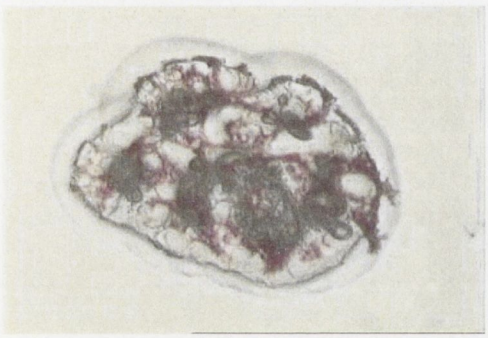

Figure 2.2 Example of calls captured by LCM

1. **Thyroid cells from FVPTC with dense stroma**
2. **After LCM**
3. **Microdissected FVPTC cells on captured on CapSure®**

2.5.4 Protocol for LCM

Cells may be captured from both FFPE H&E stained slides and alcohol fixed H&E stained frozen sections according to a standard protocol as follows:

After the system is powered up, the laser must be enabled via the key switch located on front of controller.

- Remove the CapSure cassette module from the PixCell 11 platform. It should slide out smoothly over the detents.
- Press down on the flanges of the cassette module. Press the end locking pins in to hold the plate down in the load position.
- Slide a CapSure cartridge, which holds four film carriers, into the cassette module until it hits a stop. The cassette loads from one end only.
- If more than four caps are required, load a second cartridge in the same manner, making sure there is no space between the two loaded cartridges.
- Press down on the flanges of the loaded cassette. Retract the locking pins and gently raise the cassette to its loaded position.
- The cartridge is now ready to be loaded into the PixCell 11.
- Slide the loaded CapSure cassette module to any detent position.
- After LCM, when the CapSure cartridges are empty, press down on the plate and lock into position by pushing the locking pins in. Carefully slide out the spent cartridges and discard.
- Move the joystick to the vertical position. This centres the translation stage, on the optical axis and ensures proper registration of the sample slide relative to the capture area. This also maximises the transfer area available for microdissection.
- Turn off the vacuum chuck via the switch located on the front of the controller.
- Place the slide on the translation stage, covering the vacuum chuck aperture. Manually position it to locate the transfer area in the centre of the field of view.

- Choose the appropriate objective for the desired magnification. Turn on the vacuum chuck.
- Adjust illumination control.
- Adjust focus control.
- Rotate the CapSure Placement Arm over the tissue sample.
- Insert the visualiser by pressing the silver plunger button located above the joystick. (The visualiser simulates the optical effect of coverslipping the slide and makes the image more defined)
- Adjust the microscope light source to obtain a good image on the monitor.
- To perform a microdissection, retract the visualiser by pressing the tab located below the plunger button, and re-adjust the microscope light source.
- Slide the CapSure cassette module to a detent position, making sure there is a CapSure at the load line.
- Rotate the placement arm to the CapSure pick-up position. The arm will automatically line up with the CapSure.
- Raise the placement arm vertically to remove the CapSure from the cassette module.
- Rotate the placement arm to transfer position over the slide. Release the placement arm. The CapSure will automatically lower onto the slide. Upon contact with the slide, the placement arm will seat the CapSure properly on the sample.

When the laser is enabled, an aiming beam is visible on the monitor.

- Select the laser spot size with the 'Spot Size Adjust' located on the left of the laser tower.

- Use the joystick or the XY controls to aim the laser beam on the capture region.

Use the front panel digital controls on the controller to adjust laser parameters.

- Fire the laser by pressing the remote thumb switch or the 'fire' button on the front of the controller.
- There is an audible beep when the laser fires. The activated portion of the transfer film will be visible as a ring of film fused to the tissue.
- Use the joystick to move to other areas in the tissue and capture other cells of interest.
- To remove the captured tissue, lift the placement arm in a smooth but swift motion.

The CapSure film carrier is designed to be placed immediately after LCM onto a reagent tube. This allows immediate digestion without any interim steps.

- Use an Eppendorf (0.5ml tube).
- Add the appropriate digestion buffer to the tube.
- With the CapSure in place, lift and rotate the placement arm to the unload platform.
- Lower the placement arm onto the unload platform – dropping the CapSure into the extraction slot.
- Rotate the placement arm to the rest position. The CapSure will be extracted form the arm and suspended in the unload platform.

- Slide the CapSure insertion tool onto the Unload platform. Make sure the open end of the insertion tool faces the suspended CapSure and the groove fits over the guide rail.
- Slide the insertion tool down the groove until the CapSure is engaged.
- Remove with CapSure attached.
- Insert CapSure onto reagent tube.
- Press down firmly to ensure an even seal.
- Continue extraction according to appropriate protocol.

2.6 Section 5

2.6.1 Nucleic acid extraction protocols

2.6.2. Extraction of DNA from alcohol fixed frozen sections using Puregene® DNA Extraction Protocol

2.6.2.1 Cell Lysis and RNA digestion

1. Add 0.3ml cell lysis solution to the dewaxed tissue/laser captured cells. For dewaxed tissue use the microfuge pellet mixer (30-50 strokes) for further homogenisation
2. Add 1.5 µl Proteinase K solution (20µg/ml) to the lysate, mix well and incubate at 55°C overnight. (With constant mixing)
3. Allow to cool to room temperature. Add 1.5µl RNase A solution (4µg/ml) to the cell lysate.
4. Mix by inverting x 25 and incubate at 37°C for 1 hour.

2.6.2.2 Protein precipitation

1. Cool sample to room temperature and add 100µl of the protein precipitation solution.
2. Vortex vigorously for 20 seconds to mix the protein precipitation solution evenly with cell lysate.
3. Centrifuge at 13,000-16,000 x g for 3 minutes.

2.6.2.3 DNA precipitation

1. Pour off the supernatant containing the DNA into 1.5ml microfuge tube containing 0.3ml 100% isopropanol. Mix by inverting x 50 times. If DNA yields are expected to be low, add a carrier such as glycogen (1µl, 20mg/ml).
2. Centrifuge at 13,000-16,000 x g for 5 minutes.
3. Pour off the supernatant and drain the tube on clean absorbent paper.
4. Add 0.3ml 70% alcohol and invert tube to wash the pellet. Centrifuge at 13,000 -16,000 x g for 1 min. Carefully pour off the alcohol.
5. Invert and drain the tube on clean absorbent paper and allow to air dry for 10-15 minutes.

2.6.2.4 DNA hydration

1. Add 20µl of the DNA hydration solution (This will give a concentration of 100ng/ml if the total yield is 2µg of DNA)
2. Rehydrate DNA by incubating the sample for 1 hour at 65°C.
3. Proceed to PCR assay or store DNA at -20°C. For future use the DNA may be aliquoted into 1µl volumes and stored at -20°C.

2.6.3 Extraction of RNA from laser captured cells using Purescript® RNA extraction protocol

2.6.3.1 Cell Lysis

1. Add 300 µl of cell lysis solution.
2. Add 1.5µl RNase-free Proteinase-K (20mg/ml).
3. Mix the sample by inversion 25 times.
4. Incubate the lysate overnight at 55°C with constant mixing, and then cool to room temperature.

2.6.3.2 Protein-DNA precipitation

1. Add 100µl of Protein-DNA precipitation solution to the cell lysate.
2. Invert the tube gently x 10 and place in an ice bath x 5 minutes.
3. Centrifuge the sample at 13,000-16,000g x 3 minutes to form a tight pellet of the precipitated proteins and DNA. If the pellet is not tight, repeat the centrifugation step.

2.6.3.3 RNA precipitation

1. Decant the supernatant containing the RNA into a clean 1.5 ml microfuge tube containing 300µl of ice-cold isopropanol, (leaving behind the precipitated protein-DNA pellet).
2. Add 1µl glycogen (20mg/ml).

3. Mix the sample by inversion 50 times.
4. Centrifuge the sample at 13,000-16,000g x 3 minutes; depending on the yield, the RNA may be visible as a small translucent pellet.
5. Pour off the supernatant and drain the tube briefly on clean absorbent paper. Add 300µl 70% ethanol and invert the tube several times to wash the RNA pellet.
6. Centrifuge the tube at 13,000-16,000g x 1 minute. Carefully decant the ethanol.
7. Invert the tube, drain on clean absorbent paper, and allow to air dry x 10-15 minutes.

2.6.3.4 RNA Hydration

1. Place tubes on ice and add 25µl RNA hydration solution (or DEPC water).
2. Hydrate RNA x 30 minutes in an ice bath. Alternatively, the RNA may be stored at -70 to –80°C until use.
3. Before use vortex the sample vigorously and pulse spin. Pipette the sample up and down several times to mix samples further.
4. Store RNA samples at –70 to –80°C

2.6.4 Extraction of RNA from banked tissue and cell lines samples using Qiagen RNeasy spin columns

2.6.4.1 Preparation for RNeasy column RNA extraction

A maximum amount of 30 mg tissue can generally be processed with RNeasy mini columns. For thyroid tissue, the binding capacity of the column (100 µg RNA) and the lysing capacity of Buffer RLT will not be exceeded by these amounts.

To process, do not allow tissue to thaw during weighing or handling prior to disruption in Buffer RLT.

β-Mercaptoethanol (β-ME) must be added to Buffer RLT before use. β-ME is toxic and should be dispensed in a fume hood and wearing appropriate protective clothing. Add 10 µl β-ME per 1 ml Buffer RLT. Buffer RLT is stable for 1 month after addition of β- ME.

Buffer RPE is supplied as a concentrate. Before using for the first time, add 4 volumes of ethanol (96–100%), as indicated on the bottle, to obtain a working solution.

All centrifugation steps are performed at 20–25°C in a standard microcentrifuge. The tissue or cells should be homogenized as discussed in Section 2.4.3.

1) After homogenisation, the tissue lysate should be centrifuged for 3 min at maximum speed in a microcentrifuge. Then carefully transfer the supernatant to a new microcentrifuge tube by pipetting. Use only this supernatant (lysate) in subsequent steps.

2) Add 1 volume (usually 600 µl for tissue) of 70% ethanol to the cleared lysate, and mix immediately by Pipetting. Do not centrifuge. Continue immediately with step 3.

Note! A precipitate may form after the addition of ethanol, but this will not affect the RNeasy procedure.

3) Apply up to 700 µl of the sample, including any precipitate that may have formed, to an RNeasy mini column placed in a 2 ml collection tube (supplied). Close the tube gently, and centrifuge for 15 s at >8000 x *g* (>10,000 rpm). Discard the flow through.

Reuse the collection tube.

If the volume exceeds 700 µl, load aliquots successively onto the RNeasy column, and centrifuge as above. Discard the flow-through after each centrifugation step.

2.6.4.2 Protocol for on column DNase digestion

Although the RNeasy silica-membrane technology efficiently removes most of the DNA without DNase treatment further DNA removal may be necessary for certain RNA applications that are sensitive to very small amounts of DNA (e.g., TaqMan RT-PCR analysis with a low-abundant target) and cDNA microarray.

2.6.4.3 Preparation for DNase digestion

Prepare DNase 1 stock solution before using the RNase-Free DNase Set for the first time. Dissolve the solid DNase I (1500 Kunitz units) in 550 µl of the RNase-free water provided. Take care that no DNase 1 is lost when opening the vial. Mix gently by inverting the tube.

DNase 1 is especially sensitive to physical denaturation and must not be vortexed. Mixing should only be carried out by gently inverting the tube. For long-term storage of DNase 1, remove the stock solution from the glass vial, divide it into

single-use aliquots, and store at –20°C for up to 9 months. Thawed aliquots can be stored at 2–8°C for up to 6 weeks. Do not refreeze the aliquots after thawing.

2.6.4.4 DNase digestion Procedure

Carry out lysis, homogenisation, and loading onto the RNeasy mini column as indicated in the protocols above.

1) Pipette 350 µl Buffer RW1 into the RNeasy mini column, and centrifuge for 15 s at ≥8000 x *g* (≥10, 000 rpm) to wash. Discard the flow-through.

2) Add 10 µl DNase I stock solution (see above) to 70 µl Buffer RDD. Mix by gently inverting the tube. Buffer RDD is supplied with the RNase-Free DNase Set.

3) Pipette the DNase 1 incubation mix (80 µl) directly onto the RNeasy silica-gel membrane, and place on the bench top (20–30°C) for 15 min.

Note: Make sure to Pipette the DNase 1 incubation mix directly onto the RNeasy silica-gel membrane. DNase digestion will be incomplete if part of the mix sticks to the walls or the O-ring of the RNeasy column.

4) Pipette 350 µl Buffer RW1 into the RNeasy mini column, and centrifuge for 15 s at ≥8000 x *g*. Discard the flow-through. Continue with the first Buffer RPE wash step.

2.6.4.5 Washing and eluting RNA

1) Transfer the RNeasy column into a new 2 ml collection tube (supplied). Pipette 500 µl Buffer RPE onto the RNeasy column. Close the tube gently, and centrifuge for 15 s at >8000 x *g* (>10,000 rpm) to wash the column. Discard the flow-through. Reuse the collection tube in the next step.

2) Add another 500 µl Buffer RPE to the RNeasy column. Close the tube gently, and centrifuge for 2 min at >8000 x *g* (>10,000 rpm) to dry the RNeasy silica-gel membrane.

To eliminate any chance of possible Buffer RPE carryover, continue first with step 3. It is important to dry the RNeasy silica-gel membrane since residual ethanol may interfere with downstream reactions. This centrifugation ensures that no ethanol is carried over during elution.

Note: Following the centrifugation, remove the RNeasy mini column from the collection tube carefully so the column does not contact the flow-through as this will result in carryover of ethanol.

3. Place the RNeasy column in a new 2 ml collection tube and discard the old collection tube with the flow-through. Centrifuge in a microcentrifuge at full speed for 1 minute.

4. To elute, transfer the RNeasy column to a new 1.5 ml collection tube. Pipette 30–50 µl RNase-free water directly onto the RNeasy silica-gel membrane. Close the tube gently, and centrifuge for 1 min at ≥8000 x *g* (≥10,000 rpm) to elute.

5. If the expected RNA yield is >30 µg, repeat the elution step (step 11) as described with a second volume of RNase-free water. Elute into the same collection tube.

To obtain a higher total RNA concentration, this second elution step may be performed by using the first eluate (from step 4). The yield will be 15–30% less than the yield obtained using a second volume of RNase-free water, but the final concentration will be higher.

2.6.5 Dual extraction of RNA and DNA from the same sample

2.6.5.1 Overview

To purify both DNA and RNA from the same sample, simply follow the appropriate Purescript® RNA Purification Kit protocol (Section 2.6.3), but save the Protein-DNA pellet for DNA purification. The DNA from this pellet can be recovered easily using the Puregene® DNA Purification Kit as described in the procedure below.

2.6.5.2 Protein-DNA Pellet Resuspension

1. Add 300 µl Puregene Cell Lysis Solution to the saved protein-DNA pellet from the protein-DNA precipitation step of the Purescript ® RNA Purification protocol.

2. Pipette up and down to resuspend the pellet. Usually no incubation is required; however, if cell clumps are visible after mixing, incubate at 37°C or room temperature until the solution is homogeneous.

2.6.5.3 RNase Treatment

1. Add 1.5 µl Puregene RNase A Solution (4 mg/ml) to the cell lysate.

2. Mix the sample by inverting the tube 25 times and incubate at 37°C for 15 minutes.

2.6.5.4 Protein Precipitation

1. Cool the sample to room temperature.

2. Add 100 µl Puregene Protein Precipitation Solution to the cell lysate.

3. Vortex vigorously at high speed for 20 seconds to mix the Puregene Protein Precipitation Solution uniformly with the cell lysate.

4. Centrifuge at 13,000-16,000 x g for 3 minutes. The precipitated proteins will form a tight pellet. If the protein pellet is not tight, repeat Step 3 followed by incubation on ice for 5 minutes and then repeat Step 4.

2.6.5.5 DNA Precipitation

1. Pour the supernatant containing the DNA (leaving behind the precipitated protein pellet) into a clean 1.5 ml tube containing 300 µl 100% Isopropanol (2-propanol).

2. Mix the sample by inverting gently 50 times.

3. Centrifuge at 13,000-16,000 x g for 1 minute; the DNA will be visible as a small white pellet.

4. Pour off supernatant and drain tube briefly on clean absorbent paper. Add 300 µl 70% Ethanol and invert the tube several times to wash the DNA pellet.

5. Centrifuge at 13,000-16,000 x g for 1 minute. Carefully pour off the ethanol. The pellet may be loose so pour slowly and watch pellet.

6. Invert and drain the tube on clean absorbent paper and allow to air dry 10-15 minutes.

2.5.5.6 DNA Hydration

1. Add 50 µl Puregene DNA Hydration Solution.

2. Rehydrate DNA by incubating sample 1 hour at 65ºC and/or overnight at room temperature. If possible, tap tube periodically to aid in dispersing the DNA.

4. Store DNA at 4°C. For long-term storage, store at -20°C or -80°C.

2.7 Section 6

2.7.1 Quantifying RNA and DNA Samples by UV Spectrophotometry

2.7.2 UV Spectrophotometry Background

All array experiments, both CGH and Expression arrays required accurate quantitation of DNA and RNA yields respectively by Spectrophotometry in advance.

Nucleic acids absorb UV light due to the conjugated aromatic nature of the bases; the sugar phosphate backbone does not contribute appreciably to the absorption. The wavelength of maximum absorption of light by both DNA and RNA is 260 nm (λ_{max}=260 nm), which is conveniently distinct from the λ_{max} of protein (280nm). The absorption properties of nucleic acids can be used for detection, quantitation, and assessment of purity. Quantitation of nucleic acids is possible by measuring the absorbance at 260 nm and by factoring in the appropriate extinction coefficient (RNA extinction coefficient = 40, DNA extinction coefficient = 50). The background absorbance at 320 nm should be close to zero and can be used to correct for background absorbance (e.g. A260 – A 320, True absorbance at 260 nm). The purity of nucleic acids may be estimated by determination of the ratio of absorbance at 260 and 280 nm A_{260}/A_{280}. Pure double stranded DNA has an A_{260}/A_{280} of 1.8, and pure RNA one of around 2.0. Protein with λ_{max} of 280 has an A_{260}/A_{280} of less than 1. Hence, if a DNA sample has an A_{260}/A_{280} greater than 1.8, this is suggestive of RNA contamination, whereas one less than 1.8 suggests protein contamination (Turner, 2000).

2.7.3 Protocol for UV Spectrophotometry

1) The UV Spectrophotometer must be switched on and the UV lamp activated 20 minutes prior to use in order to insure accuracy

2) Dilute samples as follows:

a) Gently vortex hydrated RNA/DNA samples 5 seconds and pulse spin.

b) Prepare dilution tubes by adding 95 µl ultrapure water to 1.5 ml tubes.

c) Remove 5 µl RNA/DNA from each sample (gently Pipette up and down 2 or 3 times before removing sample to mix) and mix with the ultrapure water to make a total volume of 100 µl, giving a 1:20 dilution.

d) To prepare blank solution, dilute 5 µl RNA/DNA Hydration Solution or RNA elution solution (i.e. use the same Hydration Solution that was used for the RNA isolation) with 95 µl ultrapurewater to make a 1:20 dilution.

e) Vortex all dilutions for 5 seconds and pulse spin.

3) Select the spectrophotometer program (e.g. dsDNA, RNA).

4) Rinse a clean, quartz cuvette twice with ultrapure water, tap on bench paper to blot, and wipe with a Kimwipe.

5) Pipette blank solution into cuvette and read absorbances at 320 nm (background), 280 nm, and 260 nm.

6) Rinse cuvette twice as described in step 4. Pipette first sample into the cuvette and read absorbances at 320 nm, 280 nm and 260 nm.

7) Continue by rinsing the cuvette as described in step 3 and reading additional samples at 320 nm, 280 nm and 260 nm.

8) To calculate RNA/DNA concentration of each sample: (A260-A320) x Extinction coefficient (40 for RNA and 50 for DNA) x dilution factor (*i.e.*100/5) x final sample volume = RNA/DNA yield in µg.

2.8 Section 7

2.8.1 Assessing nucleic acid integrity by Agarose Gel Electrophoresis

2.8.2 Background

Agarose is a polysaccharide derived from seaweed, which forms a solid gel when dissolved in aqueous solution at concentrations between 0.5% and 2% (w/v). When an electric field is applied to an agarose gel in the presence of a buffer solution, DNA/RNA fragments move through the gel towards the positive electrode at a rate, which is dependent on their size and shape. The nucleic acid is visualised after electrophoresis by staining with Ethidium bromide and illuminating the gel under UV light.

2.8.3 Protocol for Agarose Gel Electrophoresis

1) Dissolve 1.5g agarose in 100ml of 1x TAE buffer (1.5% gel). Heat in the microwave oven until the agarose has dissolved. (At full power for approx 2 minutes)

2) Allow the solution to cool (until the steam has disappeared) and add in 5µl of Ethidium bromide. This solution can be stored at 37°C.

3) Place a strip of tape across each end of the glass plate to seal the ends. This forms a mould. The gel can then be poured into the plate until it is level with the top of the plate (3 - 5mm thick).

4) Place an 8 well comb in position along one of the red lines. (This allows the wells to be seen clearly when loading the DNA).

5) Leave the gel to set for 10 minutes. When set, the comb can be removed and the tape removed from each end.

6) Prepare the electrophoresis tank by filling it with 1x TAE buffer, to cover the gel. Place the gel, still on the plate, into the tank with the wells to the left.

7) To load the DNA/RNA, it must first be stained with a loading buffer (supplied with the DNA ladder) at a ratio of 1µl loading buffer to 6µl of DNA. Load 5µl of the DNA ladder into one well to allow size comparisons of the bands. For best results, mix 10µl of DNA with 2µl of loading buffer and pipette directly into the well. One µl of formamide may be added to RNA samples to prevent secondary folding.

8) Close the lid on the tank and attach the leads to the terminals and to the EC 105 power pack, (negative to negative (black), positive to positive (red)). Turn the voltage to 100v and leave to run for approx 15 minutes. (Check there are bubbles rising from the electrodes to indicate there is current flowing). By this time, the dye front should be half way down the gel. Turn off the current and remove the leads from the tank.

The gel can now be removed from the tank and taken to the dark room for U.V. illumination and photographing, See Figure 2.3.

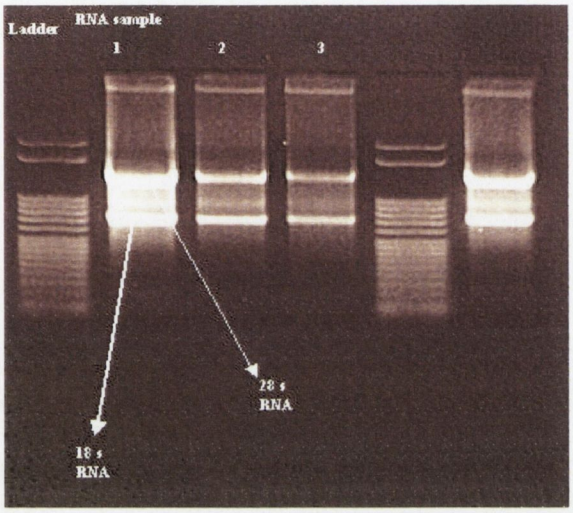

Figure 2.3 Agarose gel electrophoresis of total RNA. High quality RNA has 28S rRNA band: 18S rRNA ratio equal to 2:1 intensity and there is little or no genomic DNA carry-over (high MW).

2.9 Section 8

2.9.1 Primer and Probe design

2.9.2 Background: Primer Express 1.5. Theory of Operation

Primer Express finds PCR primer pairs by screening potential primer pairs against user supplied criteria, and only returns those pairs that meet these criteria. Criteria are embodied in a series of tests performed first on all candidate primer sequences, and further on those forward and reverse primers, which pass these tests, to find acceptable primer pairs. The primer selection process can be likened to a series of filters, since only those candidate primer sequences passing the first test are subjected to the second test, only those passing the second are subjected to the third, etc. The primer pair search effort takes place in three stages:

1. Acceptable forward primers are found.

2. Acceptable reverse primers are found.

3. Forward and reverse primers are tested in all possible combinations to find acceptable primer pairs.

All of the primer pairs that pass these tests are returned to the user. The specific algorithms for the test procedures are available from Applied Biosystems.

2.9.3 Protocol for TaqMan Primer and probe design

Import DNA/cDNA sequence into Primer Express.

Label intron/exon boundaries (if dealing with cDNA).

Select 'find primers/probes now'. Choose primer and probe sets so the probe traverses the intronic/rearrangement junction where possible (to eliminate potential signals from any contaminating DNA) according to the following manual criteria:

Primers

Tm 58°-60°C

20-80% GC content

Length 9-40 bases

<2°C difference in Tm between the two primers

Maximum of 2 G/C at 3'end

Probe

Tm > 10°C higher than primer Tm.

20-80% GC content

Length 9-40 bases

No G on the 5' end

Fewer than 4 contiguous G's

Must not have more G's than C's

Amplicon

50-150 base pair in length

3' end of primer as close to the probe as possible without overlapping

2.9.4 Primer and probe sequences for ret/PTC-1, ret/PTC-3 and GAPDH

REACTION		SEQUENCE
ret/PTC – 1	F	CGC GAC CTG CGC AAA
TaqMan™	P (5' FAM labelled)	TTA CCA TCG AGG ATC CAA
	R	ACC AAG TTC TTC CGA GGG AAT T
ret/PTC – 3	F	AAC CAA GTT CTT CCG AGG GAA T
TaqMan™	P (5' FAM labelled)	CCA CTT TGG ATC CTC CTG
	R	TGT TCT CCA AGG TCT GCT TTT G
GAPDH TaqMan™	F	CAT CCA TGA CAA CTT TGG TAT CGT
	P (5' VIC labelled)	ACT CAT GAC CAC AGT CC
	R	GGG TGG CAG TGA TGG CAT

F = Forward, P = probe, R = Reverse.

Table 2.2 Primer and probe sets for TaqMan PCR

2.9.5 Design of primers and Probes for BRAF ^{V600E} allelic discrimination assay

Primers and probes were designed by submitting the appropriate annotated sequence to the Assays by Design service provided by Applied Biosystems. The major advantage of this system is the high quality control provided by Applied Biosystems. In addition, assay design time is markedly reduced and all assays are provided in a one-tube format, designed for universal thermal cycling conditions without further need for optimization.

SNP genotyping assays include two TaqMan MGB 6-FAM™dye- and VIC dye-labelled probes and two matching primers. The probes are designed to incorporate MGB (minor groove binder) with NFQ (non-fluorescent quencher) technology. The details of the primers and probes used for Allelic Discrimination are seen in Table 2.3

Forward Primer name	BRAF-1-1796F
Forward primer sequence	CATGAAGACCTCACAGTAAAAATAGGTGAT
Reverse Primer name	BRAF-1-1796R
Reverse Primer Sequence	GGATCCAGACAACTGTTCAAACTGA
Wild type probe name	BRAF-1-1796V2
Wild type probe sequence	CCATCGAGATTTCACTGTAG
	Reporter VIC
Mutant type probe name	BRAF-1-1796M2
Mutant type probe sequence	CCATCGAGATTTCTCTGTAG
	Reporter FAM

Table 2.3: BRAF allelic discrimination primer/probe sequences.

2.10 Section 9

2.10.1 PCR and allelic discrimination Control Samples

2.10.2 ret/PTC-1

Positive control RNA for ret/PTC-1 rearrangement was generated by extracting RNA from stocks of the papillary thyroid carcinoma cell line TPC-1. This cell line constitutively expresses the rearranged chimera ret/PTC-1.

2.10.3 ret/PTC-3

For ret/PTC-3, plasmid DNA containing the ret/PTC-3 cDNA was donated as a gift from Professor Sissy Jhiang. Professor Jhiang had cloned ret/PTC-3 into a plasmid vector known as pcDNA 3 (Figure 2.4). Plasmids are circular molecules of DNA that can replicate in the host cell independently of the main bacterial chromosome. Engineered plasmids can contain a number of genes to confer antibiotic resistance and give high transformation efficiencies as well as polylinkers containing various unique restriction endonuclease cutting sites. The ret/PTC-3 insert size is 1.95 kb and can be excised from the plasmid by HindIII/EcoRV restriction endonuclease digestion. EcoRI will cut the insert at the rearrangement junction Figure 2.5.

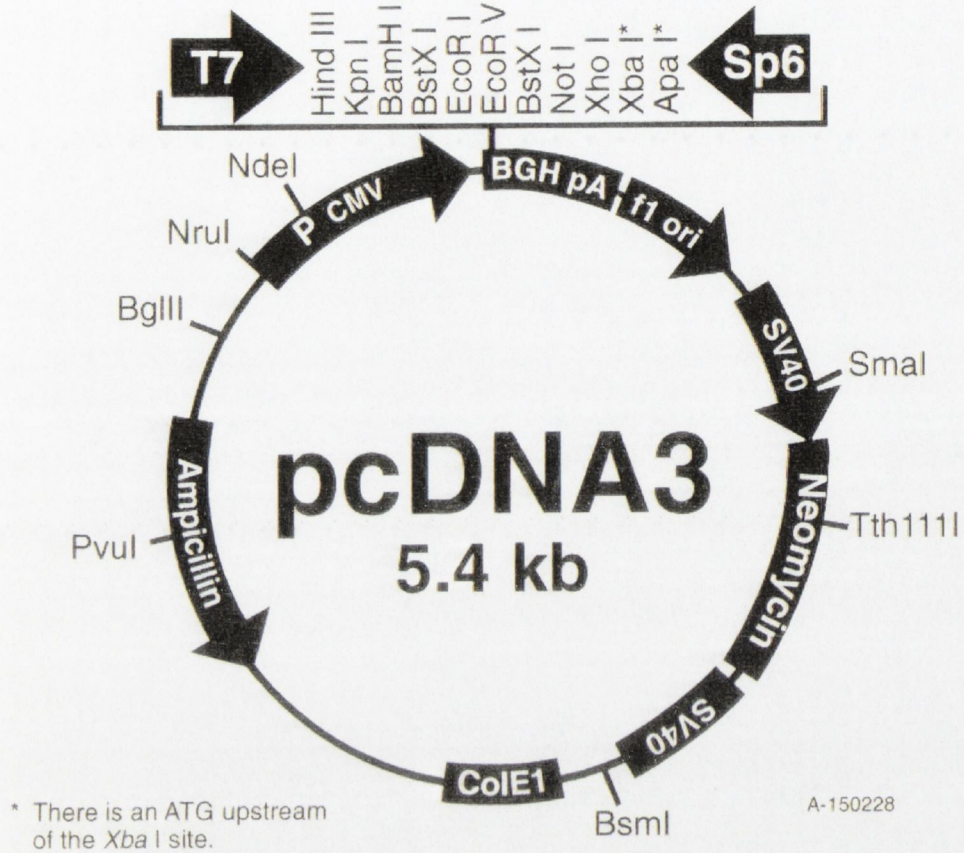

Figure 2.4 Plasmid pcDNA3

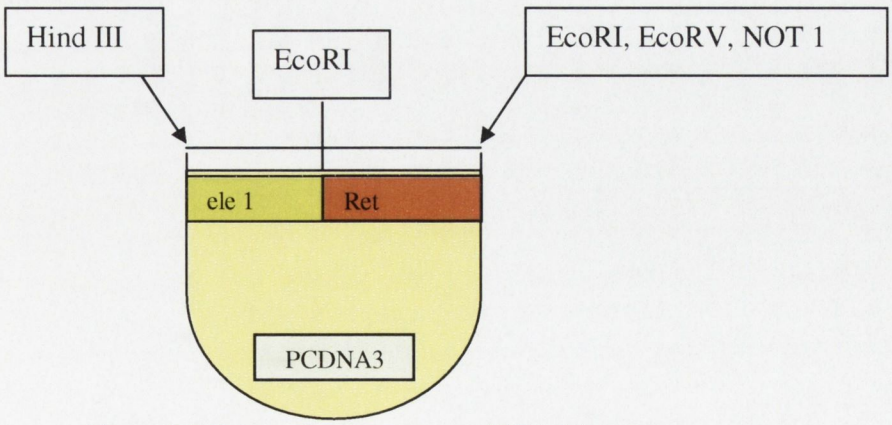

Figure 2.5 Restriction map for ret/PTC-3 insert

2.10.3.1 Generation of cRNA positive control transcripts for ret/PTC-3

Prior to performing *in vitro* transcription IVT to generate cRNA, stocks of PTC3 pcDNA3 were generated using the One Stop TOPO 10F' protocol (TOPO TA cloning ®, Invitrogen). Blue and white colony selection was not required, since the donated plasmid had a documented ret/PTC-3 insert. Ampicillin was used to select for E coli colonies containing the plasmid.

2.10.3.2 Bacterial Culture and transformation

1. Combine 2µl of plasmid with 1 vial of chemically competent E coli. (Do not Pipette up and down).
2. Incubate on ice for 30 minutes.
3. Heat shock for 30 seconds at 42°C.
4. Immediately transfer to ice.
5. Add 250µl of SOC medium.
6. Shake tube horizontally (200 rpm) at 37°C for 1 hour.
7. Spread 25µl and 50µl (add 20µl SOC to each) on LB (1.0% Tryptone, 0.5% yeast extract, 1.0% Sodium Chloride, pH 7.0) plates with 50µg/ml of ampicillin.
8. Grow at 37°C overnight.
9. Select 3 distinct colonies and transfer each to 5ml of LBB with ampicillin.
10. Grow overnight at 37°C with horizontal shaking.

11. Stocks are made by combining 0.8ml of the broth with 0.2ml of glycerol and freezing at -80°C.

2.10.3.3 Plasmid extraction

Agarose plates with Ampicillin are inoculated with E coli from the glycerol stocks and grown overnight at 37°C. Distinct colonies are harvested and resuspended in 50μl of sterile water. A PCR screening experiment is performed to verify presence of the plasmid containing ret/PTC-3. Colonies with positive PCR bands are further cultured overnight in 5 ml of LB broth with 40μl (50mg/ml) of Ampicillin.

Plasmid extraction

Plasmid extraction is performed using the QIAprep procedure (Qiagen).

1. Transfer 1.5ml of culture to a 1.5ml microcentrifuge tube. Centrifuge at 10,000 rpm for 2 minutes and discard supernatant. Repeat X 1.
2. Resuspend the pellet in 250μl of buffer P1, add 250μl of buffer P2, invert 5 times.
3. Add 350μl of buffer N3 and invert 5 times.
4. Centrifuge at 12,000 rpm for 10 minutes.
5. Transfer the supernatant to a QIAprep spin column.
6. Centrifuge at 12,000 rpm for 30 seconds.
7. Add 750μl of buffer PE and centrifuge at 12,000rpm for 30 seconds.
8. Remove the spin column and transfer to a clean 2ml collection tube and centrifuge at 12,000rpm for 1 minute.

9. Add 50µl of Buffer EB, incubate tubes for 1 minute and then centrifuge at 12,000 for 3 minutes.
10. The purified plasmid can be stored at -20°C.

2.10.3.4 Linearisation and restriction digestion for diagnostic purposes

PTC pcDNA3 can be linearised using the restriction endonuclease NOT-1, which cuts after the insert and therefore allows IVT to be performed. A double digest with restriction endonucleases EcorI and HIND III may be used diagnostically to verify that the plasmid contains the ret/PTC-3 insert.

NOT 1 Digestion reaction: In a 20µl reaction combine 2µl of Buffer (10X), 1µl of NOT 1, 10µl of plasmid and 7µl of water. Incubate at 37°C for 1 hour. Electrophoresis on a 1% agarose gel shows a band corresponding to linearised plasmid.

2.10.3.4 Purification of linearised DNA post restriction digestion

1. Pre-cool the centrifuge to 4°C.
2. Increase the volume of the linearization reaction to 100µL with TEB (1X).
3. Add 100µL of Phenol (pH = 8.0) and add 100µ of chloroform/isoamylalcohol (24:1) and vortex briefly.
4. Centrifuge at 13,000 rpm for 10 minutes at 4°C.

5. Remove the aqueous layer to a fresh tube containing 100µL chloroform/isoamylalcohol (24:1) and centrifuge at 13,000 rpm for 5 minutes at 4°C.
6. Remove the aqueous phase to a new tube with 200µL of 100% Ethanol and 10µL of Sodium Acetate (3M).
7. Freeze at -80°C for one hour.
8. Centrifuge at 13,000 rpm for 30 minutes at 4°C.
9. Remove the supernatant, add 100µL of ice cold 75% Ethanol and centrifuge at 13,000 rpm for 5 minutes at 4°C.
10. Remove the supernatant, pulse spin and remove the remaining liquid with a fine Pipette tip.
11. Air dry for 5 minutes.
12. Rehydrate with 12 µL of DEPC treated water.

2.10.3.5 *In-vitro* Transcription

1) Two reactions are set up, one a positive control (pGEM) and the second using the linearised plasmid as template.

2) Set up as follows

Reagents	Control pGEM µl	Linearised PTC pcDNA 3 in µl
Buffer 5X	4	4
DTT 100 mM	2	2
rNTPs (1µl of each)	4	4
Rnase inhibitor	0.5	0.5
T7 polymerase	1	1
PTC pc DNA 3	0	8
pGEM	1	0
Water	7.5	0.5

3) Incubate at 37°C for 4 hours.

4) Run the products on a 1% agarose gel to verify cRNA product.

2.10.3.6 DNase treatment of cRNA reaction mixture

1) Add 6µl of DNase (6 units) to 8µL of transcription reaction.

2) Incubate at 37°C for 30 minutes.

2.10.3.7 Purification of cRNA post DNase digestion

1) Pre-cool the centrifuge to 4°C.

2) Increase the volume of the DNase reaction to 100µl with TEB.

3) Add 100µL of Phenol (pH = 4.5) and add 100µ of chloroform/isoamylalcohol (24:1) and vortex briefly.

4) Centrifuge at 13,000 rpm for 10 minutes at 4°C.

5) Remove the aqueous layer to a fresh tube containing 100µL chloroform/isoamylalcohol (24:1) and centrifuge at 13,000 rpm for 5 minutes at 4°C.

6) Remove the aqueous phase to a new tube with 200µL of 100% Ethanol and 10µL of Ammonium Acetate (7M).

7) Incubate at -80°C for one hour.

8) Centrifuge at 13,000 rpm for 30 minutes at 4°C.

9) Remove the supernatant, add 100µL of ice cold 75% Ethanol and centrifuge at 13,000 rpm for 5 minutes at 4°C.

10) Remove the supernatant, pulse spin and remove the remaining liquid with a fine Pipette tip.

11) Air dry for 5 minutes.

12) Rehydrate with 20 µL of DEPC treated water.

13) Check concentration by UV Spectrophotometry.

14) Dilute and aliquot the cRNA appropriately.

2.10.4 Allelic Discrimination Controls

Cell line DNA was donated by Dr. Paula Soares for Allelic Discrimination assays.

DNA from B-CPAP cell line: Homozygous $BRAF^{V600E}$

DNA from K2 PTC cell line: Heterozygous $BRAF^{V600E}$

DNA from the TPC-1 cell line was used as a source of wild type BRAF.

2.11 Section 10

2.11.1 TaqMan RTPCR and Allelic Discrimination Assays

A TaqMan PCR-based system was selected for mRNA chimera detecion of ret/PTC-1 and ret/PTC-3 in this study. The Taqman system was chosen for a number reasons. Firstly, Taqman PCR and Reverse-Transcriptase (RT) PCR requires only a few nanograms of target RNA. This is highly significant since the amount of RNA extractable from formalin fixed and paraffin embedded archival material is low. Secondly, Taqman PCR and RT-PCR products are small (generally less than 200bp) and thus can be used to amplify partially degraded or fragmented RNA such as that obtained from archival material.

2.11.2 The Chemistry of TaqMan PCR assays

Real time quantitative PCR allows the detection of specific PCR products based on the use of a fluorescently labelled probe designed to hybridise within the target sequence of the PCR product. During PCR cycling the detection of increasing fluorescent signal is proportional to the accumulation of amplification products. Therefore, quantification of the original concentration of the target sequence is possible. The unique design of TaqMan probes, combined with the 5' – 3' exonuclease activity of *Taq* DNA polymerase allows direct detection of PCR product by the release of a fluorescent reporter during PCR. The fluorescent reporter dye is covalently linked to the 5'-end of the TaqMan probe and is quenched by TAMRA (6-carboxy-tetramethyl rhodamine) attached to the 3'-end of the oligonucleotide. When the probe is intact, the proximity of reporter to quencher dye results in suppression of the reporter fluorescence emission due to Forster-type energy transfer (FRET). During PCR, if the target of interest is present (Figure 2.6A), the probe anneals between the forward and reverse primer sites (Figure 2.6B). During the extension of the primers, *Taq* DNA polymerase cleaves the probe thus releasing the reporter from the quencher (Figure 2.6C). As a result, an increase in fluorescence emission is observed. Since the exonuclease activity of the *Taq* DNA polymerase acts only if the fluorogenic probe is annealed to the target and not if the probe is free in solution, the increase in fluorescence is proportional to the amount of specific product (Orlando, 1998).

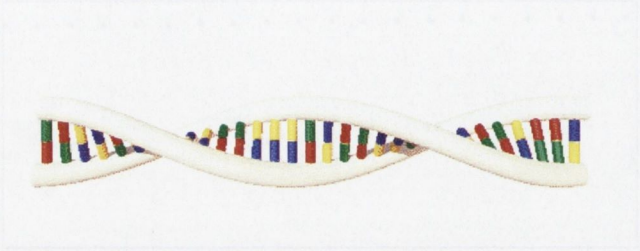

(A)

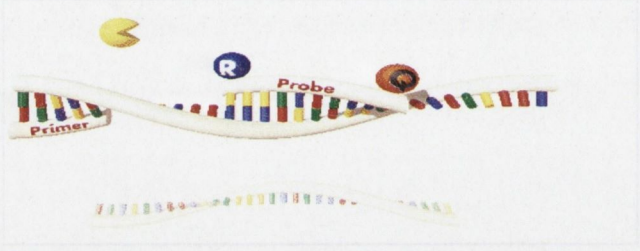

(B)

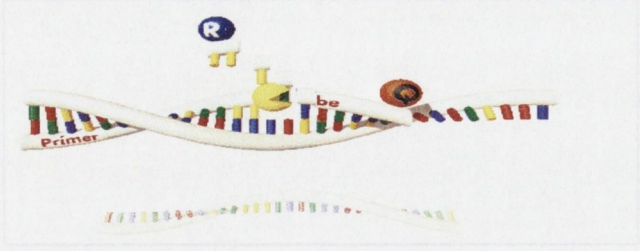

(C)

Figure 2.6 Illustration of the principle of TaqMan PCR

(A) Intact double strand of target DNA (B) Primer and TaqMan probe annealing
(C) Release of reporter molecule due to probe cleavage.

The superiority of this system to standard PCR lies in the fact that it guarantees specificity of the PCR product and the high sensitivity of the fluorescent signal allows the detection of PCR products starting from low quantities of starting templates. The TaqMan PCR procedure can be applicable both to the endpoint detection of PCR products and to the detection in real-time of product accumulation during cycling.

For end-point detection the increase of fluorescence is compared to the fluorescence of a "no template control NTC". To normalise for unavoidable pipetting errors and volume changes that may inevitably occur during PCR setup, the reporter fluorescence is divided by the quencher fluorescence to yield a ratio termed the RQ for each reaction.

The difference between the sample RQ (RQ+) and the NTC RQ (RQ-) is called the delta RQ (ΔRQ). This difference represents the amplification of a specific product, which has occurred during PCR. To assure a statistically high confidence level in the results generated by TaqMan PCR, the protocol should include a minimum of 3 NTCs (usually 6). Based on T distribution values any ΔRQ value above the threshold has a 99.7% confidence level of being a positive result.

The real-time assay procedure involves monitoring the fluorescence signal during each step of the PCR amplification and is automated in the ABI PRISM 7000/7700 Sequence Detector System (Applied Biosystems, Foster City, CA, USA). Real-Time PCR allows reactions to be characterised by the point in time at which amplified product becomes detectable, rather than the amount of PCR product that is accumulated after a fixed number of PCR cycles. The sensitive fluorescence detection by the 7000/7700 Sequence Detector allows the threshold cycle (C_T) to be

observed when PCR amplification is still in the exponential phase. This circumvents many of the problems associated with quantitation in the plateau stage of PCR amplification. This is the main reason why C_T is a more reliable measure of starting copy number than an end-point measurement of the amount of accumulated PCR product. Furthermore, well-to-well variations of fluorescence measurement can be normalised using a fluorescent reference dye. The system minimises carryover contamination employing a closed-tube system which allows both PCR cycling and data acquisition to occur simultaneously as well as subsequent analysis without further manipulation of the samples (Orlando, 1998).

In this study both end point detection and real time monitoring for quality control purposes were utilised. No formal quantitation was performed. However, both ret/PTC-1 and ret/PTC-3 are chimeric transcripts and their detection is significant even without quantitation. The presence of intact RNA template was confirmed in every case using glyceraldehyde-3-phosphate dehydrogenase (GAPDH) as an endogenous reference (housekeeping gene). In addition, exon/chimeric breakpoint spanning probes were used to ensure the detection of cDNA rather than genomic DNA.

2.10.3.2 Minor groove Binder (MGB Probes)

For mRNA target detection MGB (Minor Groove Binder) probes were employed. These are DNA probes which are conjugated to minor groove binder groups. MGB fluorogenic probes are superior to traditional probes for a number of reasons: MGB probes bind more tightly to their complement, this raises the annealing temperature of the probe allowing for more flexible assay design. MGB probes are more sequence specific than standard DNA probes, especially for single base mismatches

at elevated hybridisation temperatures MGB probes have a lower backround fluorescence and as a consequence, a greater signal to noise ratio. MGB probes stabilize A-T bonds more than G-C bonds in the DNA Duplex. This reduces the influence of target sequence on Tm (Kutyavin, 2000).

2.10.4 RT-PCR

For mRNA target detection Taqman RT-PCR (reverse transcription PCR) amplification was carried out using Taqman One step RT-PCR Master Mix. One-step RT-PCR performs RT as well as PCR in a single buffer system. The reaction proceeds without the addition of reagents between the RT and PCR steps. The RT-PCR reaction exploits the 5´ nuclease activity of AmpliTaq Gold® DNA Polymerase to cleave a TaqMan probe during PCR. MultiScribe™ Reverse Transcriptase is a recombinant Moloney Murine Leukemia Virus (MuLV) Reverse Transcriptase used for reverse transcription.

2.10.4 Allelic Discrimination Assay

Allelic discrimination using TaqMan chemistry is based on the design of two TaqMan probes, specific for the wild type allele and the mutant allele in question. Each of the two probes is labelled with a different fluorescent tag (usually FAM and VIC), and each is designed with the gene mutation affecting the middle part of the probe sequence. The binding efficiency of the wild type TaqMan probe to the mutant allele and vice versa is low due to the mismatch within the TaqMan probe and the target sequence; therefore, mismatched binding is highly reduced. The

TaqMan® probes contain the minor groove binder (MGB), which enhances the discrimination between match and mismatch by allowing the use of shorter probes a non-fluorescent quencher (NFQ) which allows better spectral discrimination between the reporter dyes (Figure 2.7).

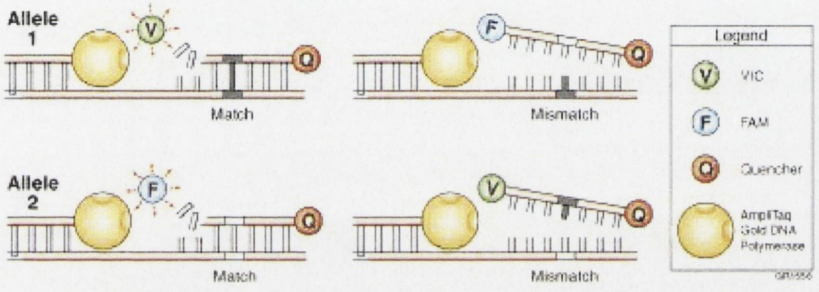

A substantial increase in....	Indicates
VIC Fluorescence only	Allele 1 is homozygous
FAM Fluorescence only	Allele 2 is homozygous
Both Fluorescent signals	Heterozygosity

Figure 2.7 Illustration of principle of allelic discrimination assay

2.12 Section 11

2.12.1 Background to Array CGH

Microarray based genomic analysis is a novel technique intended for rapid examination of human DNA for changes in copy number of specific sequences. The assay involves labelling of sample DNA with Cy3 (Perkin Elmer/NEN #NEL576) fluorophore. This is mixed with whole genomic reference DNA that is labelled with Cy5 (Perkin Elmer/NEN #NEL577) fluorophore and co-hybridized to a microarray in the presence of human Cot 1 DNA to suppress hybridisation of labelled probe to repeat sequences. The microarray contains target clone DNA (P1, PAC or BAC clones) representing regions that are important in cytogenetics and oncology. See Appendix 1 for a complete list of annotated clones. DNA clones comprising the desired target sequences are arrayed in target spots of approximately 75-125 μm in diameter, whereby 3 target spots represent each clone.

Following hybridisation and removal of unhybridised probe, target spots are counter-stained with a blue fluorophore included in the Array DAPI mounting solution and analyzed using the GenoSensor Reader System™. The GenoSensor Reader System is a large-field multicolour fluorescence imaging system which captures an image of the hybridised chip in 3 colour planes: Cy 3, Cy5 and DAPI blue. The included software automatically identifies each spot and, by analysis of the set of Cy3/C5 ratios on all targets, calculates the ratio most representative of the modal DNA copy number of the sample DNA. For each target, the normalised ratio, relative to the modal DNA copy number is calculated.

This normalised ratio of a target indicates the degree of gain or loss of copy number compared with the sample's modal copy number. Detection of copy ratio changes will be highly dependent on the purity of DNA in the extracted tissue specimen. Even a very highly amplified gene will not appear as such if tumour DNA represents only a small fraction of total extracted tissue DNA. For this reason LCM was performed to ensure truly homogenous cell populations

2.12.2 Labelling Protocol

1) In 1.5 ml DNase free snap lock tubes mix the following reagents for test and reference labelling reactions:

Cy-3 (Test)	Cy-5 (Reference)
Test DNA (25 ng/μL) 4.0 μL	
	Reference DNA (25 ng/μL) - 4.0 μL
TE Buffer 41.6 μL 41.6 μL	TE Buffer 41.6 μL 41.6 μL
2.5X Random Priming Mix 40 μL 40 μL	2.5X Random Priming Mix 40 μL 40 μL

2) Denature at 100°C, 10 minutes.

3) After denaturing the sample, immediately place tubes on ice for 10 minutes.

4) Spin down condensate inside tube.

5) Place tubes back on ice and add the following reagents test and reference tubes:

GenoSensor Array 300 Nucleotide Mix 10 µL
Klenow 2 µL
Cy-3 dCTP (1 mM) 2.4 µL (Test only)
Cy-5 dCTP (1 mM) - 2.4 µL (Reference only)

6) Mix gently by vortexing and quickly spin. Incubate at 37°C, 2 hours in the dark, then place tubes on ice.

2.12.3 DNase Digestion and Labelled Probe Purification

Set up DNase Reactions and 1:20 DNase I Amp Grade dilution on ice. Dilute DNase Amp Grade 1:20 using DNase Dilution Buffer provided (make immediately before use and discard unused portion of the diluted DNase). Add the following to the random priming reaction (100µL.

1. DNase Reaction Buffer 17 µL.

2.1:20 diluted DNase Amp Grade (prepared fresh on ice) 3 µL.

Then:

1) Incubate at 15°C, 1 hour in the dark.

2) Immediately following DNase digestion, place tubes on ice.

3) Quench reactions with 6 µL of Stop Buffer and then vortex.

4) Prepare a MicroSpin S-200 HR column, Amersham as described in the manufacturer's protocol (Procedure A: General Protocol). Make sure that there are no visible resin particles on the outside of the column, wipe off resin deposit with a lint-free paper tissue if present.

5) Slowly apply 126 µL of labelled probe to the column and spin the column according to the manufacturer's protocol.

6) To the column-purified probe, add 0.1 volume of 3 M Sodium Acetate (12 µL).

7) Add 1 µL of precipitation reagent, vortex briefly.

8) Add 2.5 volumes of cold (-20°C) 100% Ethanol (350 µL), vortex briefly.

9) Incubate at – 20°C, 1 hour

10) Centrifuge at 16,000 rcf, 30 minutes at 4°C

11) Remove supernatant and then air-dry pellets (do not vacuum dry the pellet).

12) Resuspend pellets in 4.0 µL of 10 mM Tris pH 8.0. Gently vortex to facilitate resuspension, incubate at room temperature for 30 min prior to setting up gel, hybridisation, or storage.

13) Quickly spin the tubes to collect the sample at the bottom of the tube.

14) Probe may be stored at –20°C if not used immediately for a gel analysis or hybridisation reaction.

2.12.3 Checking the Labelled DNA

Check the labelled probe on a 2% agarose gel. If there is no DNA trailing above 200 base pairs, do not use the probe in array hybridisation. See Figure 2.8

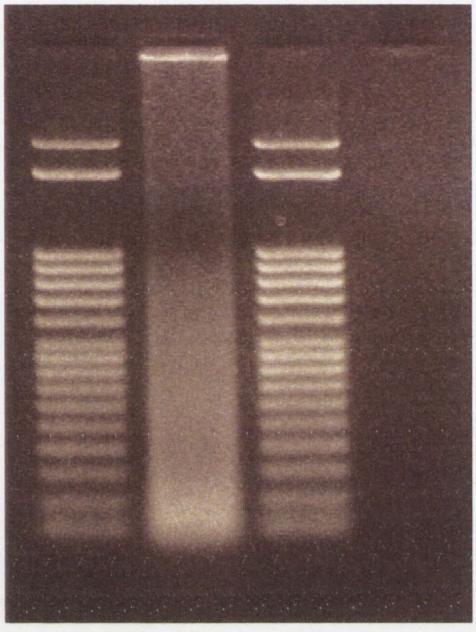

Figure 2.8 Agarose Gel of purified labelled probe

2.12.4 Hybridisation Protocol

2.12.4.1 Preparing the Reagents

20X SSC Mix thoroughly 66 g (entire bottle) of 20X SSC in 250 mL purified H2O. Store at ambient temperature no longer than 6 months.

2X SSC/50% formamide wash Mix thoroughly 105 mls formamide, 21 mls 20X SSC and 84 mls purified H2O. Label three glass Coplin jars with lids, "1", "2", "3." Pour enough formamide wash solution into each to cover the arrays but not so much

as to immerse the labels on the microarray holder. Between uses, store covered at 2-8 °C. Discard after washing 30 microarrays or after 2 weeks of storage.

1X SSC Add 50 mL 20X SSC to 950 mL purified H2O. Pour enough wash solution (see above, "formamide wash") into each of four glass Coplin jars with lids. Label the jars "4", "5", "6", and "7". Individual washes should be discarded after use. Stock wash solution should be stored at ambient temperature for no longer than 6 months.

Array DAPI Solution Store the Array DAPI solution at -20°C in the dark. Allow solution to warm to room temperature prior to pipetting.

2.12.4.2 Preparing the Hybridisation Solution

Pre-warm the hybridisation buffer to 37°C for 30 min, vortex and spin prior to use to ensure that the solution is uniform. Note: It is extremely important that the hybridisation buffer is well dissolved. Due to high concentration of Cot-1 DNA in hybridisation buffer, the solution may appear cloudy or opalescent. Some cloudiness in the buffer after pre-warming is acceptable as long as there are no visible clumps of precipitate. Quickly spin the tube to collect the solution at the bottom of the tube. Hold the hybridisation buffer at 37°C until immediately before use.

Combine the following in a 0.5 mL or 1.5 mL Eppendorf microfuge tube:

1. Microarray Hybridisation Buffer 25 µL. Note: Prior to addition, probes should be microcentrifuged at 12,000 – 16,000 rcf for 1 min. When Pipetting probe avoid any precipitate that may be at the bottom of the tube.

2. Test DNA Probe (Cy-3 dCTP) 2.5 µL

3. Reference DNA Probe (Cy-5 dCTP) 2.5 µL

4. Vortex and quickly spin the sample

2.12.4.3 Hybridisation

1. Place the microcentrifuge tube containing the hybridisation mixture into an 80°C water bath and incubate for 10 minutes to denature the DNA.

2. Remove from the water bath and centrifuge at 12,000 – 16,000 rcf for 5 seconds.

3. Quickly transfer the microcentrifuge tubes containing the hybridisation mixture to a 37°C incubator or covered heating block, incubate in the dark for 1 hour.

4. Remove the necessary number of microarrays from their protective packaging using the tear marks. Place the microarrays in a 37°C dry air incubator for 30 min prior to use.

5. Place a paper towel folded in half on the bottom of a sealable (air-tight) box. To the bottom of this box add 14-16 ml of 50% formamide/ 2XSSC wash solution to saturate the paper towel. Place the box in 37°C dry air incubator for 30 min – 1-hour prior to use.

Note: Complete steps 6 - 8 on one array before beginning the next one. Do not allow tubes to sit at room temperature. If multiple hybridisations are to be set up at one time use a 37°C heating block to hold tubes.

6. Carefully remove the cover protecting the microarray hybridisation area and discard.

7. Remove the tube containing the hybridisation solution from the 37°C heating block. Mix gently and quickly spin. Draw the full amount of hybridisation mixture into a pipette tip and slowly add the hybridisation mixture onto the corner of the

array. Be very careful not to touch the Pipette tip on the DNA array area or introduce air bubbles (leave the microarray on the slide warmer).

8. Using forceps, carefully remove a Hybridisation Coverslip from the bag. Remove lint or dust from the Hybridisation Coverslip using a Kimwipe. Holding the Hybridisation Coverslip at an angle, contact the hybridisation solution on the microarray with the painted side of the Hybridisation Coverslip touching the solution and slowly lower the Hybridisation Coverslip to ensure that no air bubbles are introduced.

9. Place microarray in pre-warmed box in 37°C incubator

10. Repeat steps 5 - 8 for the remaining microarrays

11. Hybridise arrays for 60-72 hours

2.12.4.4 Washing the Microarrays

Do not wash more than 5 microarrays at one time. Optimally, washes should be done in reduced light if possible. Array labels are resistant but not impervious to formamide wash solution and immersion should be as limited as practical. Replace wash solutions after washing about 30 microarrays, or two weeks of use. Adequate washing is vital to assay performance. Prior to transferring microarrays from one bath to the next, agitate the microarray with a back and forth motion (approx. 10 times). This will help ensure proper washing.

The microarrays should not be allowed to dry at any step upon completion of the hybridisation. Do not allow the microarrays to dry between washes, i.e. move chips quickly from one wash to the next without examining them. Avoid areas with high airflow when processing arrays. Do not allow chips to dry after the final rinse.

Never apply force when washing chips. Avoid twisting the arrays in the Coplin jars. Be careful when moving chips up and down in the grooves of the Coplin jars, to prevent cracking or dislodging of the chip from its holder.

If washes have been stored at 4°C, allow them to warm to room temperature. Place formamide washes (#1-3) in 40°C water bath allowing them to equilibrate approximately 30 minutes. Prior to washing arrays use a thermometer to check washes are at 40°C±1°. Place Coplin jars (#4 -7) containing 1X SSC and another jar (#8) containing distilled water at room temperature.

1. Remove one microarray from the box in the incubator.

Using fine tip forceps, remove the Hybridisation Coverslip by grabbing the overhanging edge and gently lifting up. Immediately immerse the microarray in 50% 2XSSC/formamide wash solution at 40°C (Coplin jar #1) and agitate briefly.

2. Repeat for remaining microarrays (up to 5), one at a time. Incubate the microarrays in Coplin jar #1 for 10 minutes

3. After incubation, agitate each microarray in turn and transfer to Coplin jar #2 (formamide wash at 40°C). Incubate microarrays in Coplin jar #2 for 10 minutes

4. After incubation, agitate microarrays and transfer, in succession as above, to Coplin jar #3 (formamide wash at 40°C). Incubate microarrays in Coplin jar #3 for 10 minutes

5. Agitate as above and transfer to Coplin jar #4 (1X SSC at room temperature). Incubate microarrays in Coplin jar #4 for 5 minutes

6. Agitate as above and transfer to Coplin jar #5 (1X SSC at room temperature). Incubate microarrays in Coplin jar #5 for 5 minutes

7. Agitate as above and transfer to Coplin jar #6 (1X SSC at room temperature). Incubate microarrays in Coplin jar #6 for 5 minutes

8. Agitate as above and transfer to Coplin jar #7 (1X SSC at room temperature). Incubate microarrays in Coplin jar #7 for 5 minutes.

9. After removing array from last wash, rinse in distilled H2O for 1-2 seconds.

10. Briskly shake chip twice to get rid of the excess water ensuring the array area itself remains wet.

11. Quickly apply coverslip-containing DAPI mounting solution to the wet chip.

Chips should be stored in the dark for 45 minutes prior to reading on the Genosensor instrument.

2.12.4.5 Image analysis

The Genosensor Reader Software automatically captures 3 images of each microarray, specific for the DAPI (counterstain), the Test DNA (green), and the reference DNA (red), respectively. The software uses the blue image to identify target spots and their location in the grid.

Once all spots are identified, the program analyzes each pixel within each spot for its intensity in each of the remaining colour planes. An algorithm is employed to determine the local background for each of these colours, which is subtracted from the intensity of each colour. The background-corrected intensities are then used to determine the ratio of Test Intensity (green) to Reference Intensity (red), which after further normalisation can be used to estimate the relative abundance of a specific

target sequence in the test DNA. The software generates a report page for each array. (Figure 2.9)

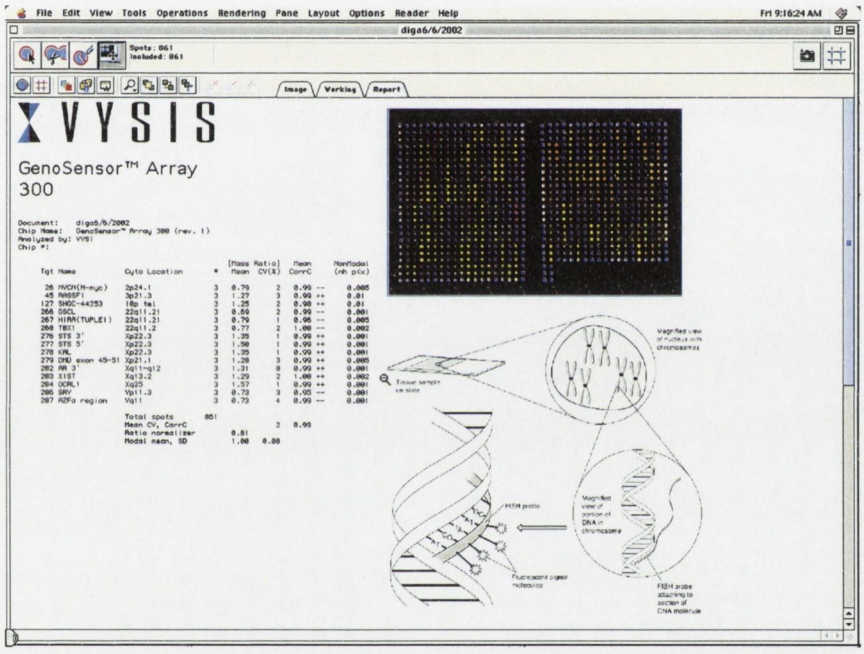

Figure 2.9 Genosensor array 300 Report page

2.13 Section 12 Applied Biosystems expression Microarrays

In general, there are two types of microarray platforms depending on the method of nucleic acid deposition on the chip surface: robotically spotted or *in situ* synthesis by photolithography, a technology that is commonly used in computer chips fabrication. The latter is commercially available from Affymetrix™. Historically the robotically spotted microarrays were referred to as cDNA microarrays because the nucleic acids being spotted were PCR products amplified from cDNA libraries. The photolithographically synthesized arrays were commonly called oligonucleotides arrays or oligoarrays because shorter oligonucleotides (~25mers) were placed on the arrays and each gene is represented by multiple oligos. It is inaccurate to use the type of probes on arrays to differentiate different platforms because researchers now also prepare oligoarrays by robotically spotting oligonucleotides (~50 to 70mers) on the slide e.g. Applied Biosystems Human Genome Survey.

Applied Biosystems microarrays are 2.5 inches X 3 inches. The microarrays contain 96 subgrids containing 19 X 19 features, for a total of 34,656 features on the microarray. Each feature measures 150μm in diameter and is spaced at 225μm (centre to centre). The probe sequences on the microarrays are optimised by using high quality sequences from multiple sources:

- Celera expert-curated sequences
- Publicly available, validated mRNA sequences
- Wet chemistry-validated sequences.

The probes are designed with the following features.

Attribute	*Probe Design*	*Design Result*
Length	60 base pairs long	• High Specificity • Optimal performance
Placement	Biased towards the 3' end	High sensitivity because DIG-labelling is more efficient at the 3' end
Coverage	• Common regions between alternative transcripts • 3' end defined as the most upstream polyadenylation site if possible	• Gene Level Coverage • Gene Specificity
Number	One probe per gene	Genome-wide coverage
Overlap	Low probe overlap	Multiple independent measurements of mRNA levels

2.13.1 Background. RT-IVT Protocol (The Eberwine Protocol)

The purpose of the Applied Biosystems Chemiluminescent RT-IVT Labelling Kit is to convert RNA into digoxigenin (DIG)-labelled cRNA for hybridisation to Applied Biosystems 1700 microarrays. The starting quantity of total RNA must be between 1-10μg of total RNA. (This corresponds to 0.05-2μg mRNA). The protocol uses a procedure developed by Van Gelder and Eberwine in the late 1980s, which amplifies mRNA using T7 RNA polymerase (Van Gelder, 1990). The Eberwine procedure converts mRNA into cDNA and then into amplified RNA, in a manner that allows up to 10^6 amplification of the starting material (Schena, 2003).

Messenger RNA is isolated from the cells or tissue of interest. The isolated mRNA is hybridised with an oligo-dT primer that contains additional sequences corresponding to one strand of the T7 RNA polymerase promoter. The oligo-dT

primed mRNA is converted into single stranded cDNA with reverse transcriptase and then into double stranded cDNA with DNA polymerase. Because each double stranded cDNA molecule contains a T7 promoter, large quantities of amplified RNA can be synthesized from the cDNA mixture with RNA polymerase. (Figure 2.10)

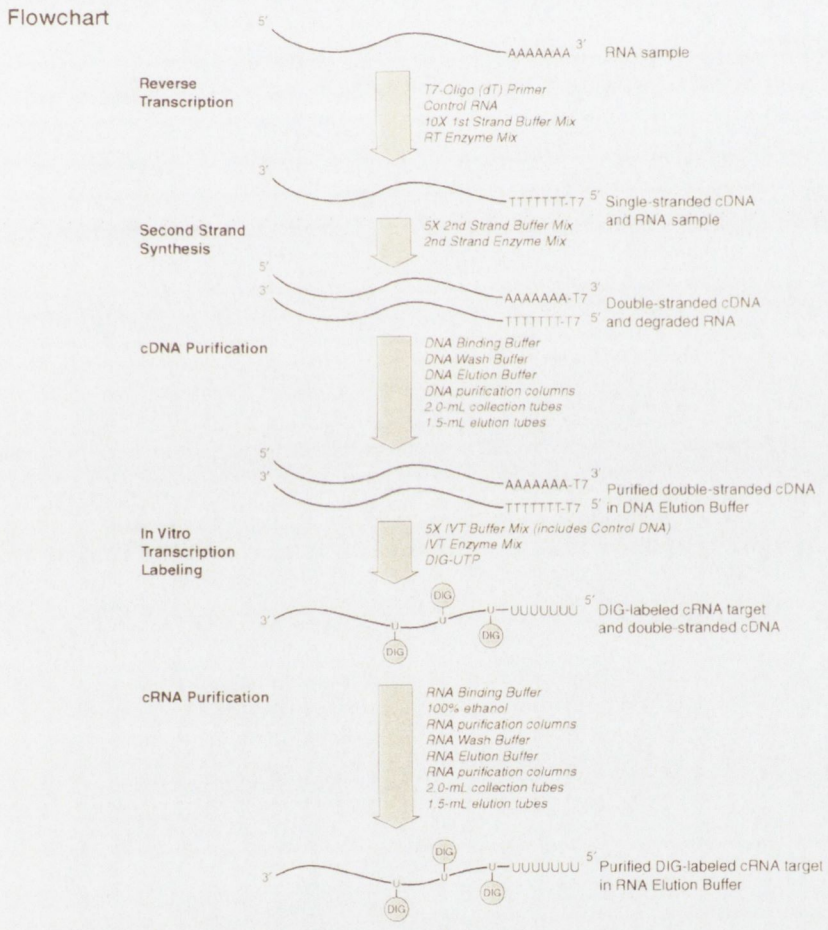

Figure 2.10 RT IVT Overview flowchart

2.13.1.1 RT IVT Protocol

1) Thaw sample and reagents on ice. Mix sample and reagents by vortexing and then centrifuge the tubes briefly.

Pipette components into 0.2-mL MicroAmp reaction tube on ice.

Component	Volume (µL)
T7-Oligo (dT) primer	2.0
Control RNA	4.0
Sample (made up with nuclease free water)	9.0 (1-10µg total RNA)
Total	15.0

2) Heat and cool the RNA and primer mixture in the Thermal cycler. (ABI 9600).

Stage	Temperature	Time	Reaction Volume
1	70°	5 Minutes	15µL
2	4°C	Indefinite hold	

3) Place tubes on ice after the run is complete.

4) Check **10X 1st Strand Buffer Mix** for precipitates. (Warm to 37°C and vortex if present). Add reverse transcription reagents to the reaction tube.

Component	Volume (µL)
10X 1st Strand Buffer Mix	2.0
RT Enzyme Mix	3.0

5) Run reverse transcription in a thermal cycler.

Stage	Temperature	Time	Reaction volume
1	25°C	10 Minutes	20µL
2	42°C	2 hours	
3	70°C	15 minutes	
4	4°C	Indefinite hold	

2.13.1.2 Performing Second Strand Synthesis

1) Add components to the cDNA mixture on ice.

Component	Volume (µL)
Nuclease free water	95.0
5X 2nd Strand Buffer Mix	30.0
2nd Strand Enzyme Mix	5.0

2) Run second strand synthesis in a thermal cycler.

Stage	Temperature	Time	Reaction volume
1	16°C	2 hours	150µL
2	70°C	15 minutes	
3	4°C	Indefinite hold	

3) Place the tubes on ice after the run is complete.

2.13.1.3 Purifying cDNA

1. In a new 1.5-mL nuclease-free microcentrifuge tube, combine:

• **DNA Binding Buffer**: 150 µL

• Entire 2nd strand synthesis reaction: 150 µL

2. Begin the purification:

a. Insert a DNA purification column into a 2-mL collection tube.

b. Transfer the reaction-DNA Binding Buffer mixture (300 µL) to the column.

c. Cap the tube, then centrifuge the column and tube at 13,000 × *g* for 1 minute.

d. Remove the column from the tube, discard the liquid, and reinsert the column into the tube.

3. Wash the cDNA (1):

a. Add 700 µL of **DNA Wash Buffer** to the column.

b. Cap the tube, then centrifuge the column and tube at 13,000 × *g* for 1 minute.

c. Remove the column from the tube, discard the liquid, and reinsert the column into the tube.

4. Wash the cDNA (2):

a. Add 700 µL of **DNA Wash Buffer** to the column.

b. Cap the tube, then centrifuge the column and tube at 13,000 × *g* for 1 minute.

c. Remove the column from the tube, discard the liquid, and reinsert the column into the tube.

d. Cap the tube, then centrifuge the column and tube at 13,000 × *g* for 1 minute.

5. Elute the cDNA (1):

a. Transfer the column to a new 1.5-mL elution tube.

b. Add 30 µL of DNA Elution Buffer to the fibre matrix at the bottom of the column.

Note: Do not let the Pipette tip touch the fibre matrix.

c. Cap the tube, then incubate the column at room temperature for 1 minute.

d. Centrifuge the column and tube at 13,000 × *g* for 1 minute for an elution volume of 30 µL.

6. Elute the cDNA (2):

a. Add 30 µL of DNA Elution Buffer to the fibre matrix at the bottom of the column.

Note: Do not let the Pipette tip touch the fibre matrix.

b. Cap the tube, then incubate the column at room temperature for 1 minute.

c. Centrifuge the column and tube at 13,000 × *g* for 1 minute for an elution volume of 60 µL.

7. Elute the cDNA (3):

a. Add 30 µL of DNA Elution Buffer to the fibre matrix at the bottom of the column.

Note: Do not let the Pipette tip touch the fibre matrix.

b. Cap the tube, then incubate the column at room temperature for 1 minute.

c. Centrifuge the column and tube at 13,000 × *g* for 1 minute for a final elution volume of 90 µL.

2.13.1.4 Performing *In Vitro* Transcription (IVT)

1. Calculate the volume of cDNA output to use, based on mRNA input:

Volume of cDNA output to use (µL) = 4.5 ÷ (µg of mRNA input)

Note: If you used total RNA, assume that 3% is mRNA.

2. If the volume of cDNA output required is:

• Greater than 24 µL, concentrate the volume to 24 µL:

Use a vacuum concentrator to concentrate the required volume of cDNA output to 24 µL.

• Less than 24 µL, increase the volume to 24 µL: Add nuclease-free water to the required volume of cDNA output until the total volume is 24 µL.

3. Check **5X IVT Buffer Mix** for precipitate. If precipitate is present:

    a. Warm **5X IVT Buffer Mix** at 37 °C for 2 to 3 minutes.

    b. Vortex briefly.

4. Combine IVT components at room temperature:

Component	Volume (µL)
CDNA output	24
5 X IVT Buffer Mix	8.0
Dig UTP (14 nmol)	4.0
IVT Enzyme Mix	4.0
Total	40.0

5. Perform IVT in the thermal cycler:

Stage	Temperature	Time	Reaction volume µL
1	37°C	9 hours	
2	4°C	Indefinite	40

6) After the run remove the tube from the thermal cycler

2.13.1.5 Purifying cRNA

Procedure

1. In a new 1.5-mL nuclease-free microcentrifuge tube, combine:

• Nuclease-free water: 20 µL

• Entire IVT reaction: 40 µL

2. Add to the IVT reaction mix and mix by pipetting:

• **RNA Binding Buffer**: 200 µL

• **100% ethanol**: 140 µL

3. Begin the cRNA purification:

a. Insert an RNA purification column into a 2-mL collection tube.

b. Transfer the IVT reaction-RNA Binding Buffer-ethanol mixture (400 µL) to the column.

c. Cap the tube, then centrifuge the column and tube at 13,000 × *g* for 1 minute.

d. Remove the column from the tube, discard the liquid, and reinsert the column into the tube.

4. Wash the cRNA (1):

a. Add 500 µL of **RNA Wash Buffer** to the column.

b. Cap the tube, then centrifuge the column and tube at 13,000 × *g* for 1 minute.

c. Remove the column from the tube, discard the liquid, and reinsert the column into the tube.

5. Wash the cRNA (2):

a. Add 500 µL of **RNA Wash Buffer** to the column.

b. Cap the tube, then centrifuge the column and tube at 13,000 × *g* for 1 minute.

c. Remove the column from the tube, discard the liquid, and reinsert the column into the tube.

d. Cap the tube, then centrifuge the column and tube at 13,000 × *g* for 1 minute.

6. Elute the cRNA (1):

    a. Transfer the column to a new 1.5-mL elution tube.

    b. Add 50 µL of RNA Elution Buffer to the fibre matrix at the bottom of the column.

    Note: Do not let the Pipette tip touch the fibre matrix.

    c. Cap the tube, then incubate the column at room temperature for 2 minutes.

    d. Centrifuge the column and tube at 13,000 × *g* for 1 minute for an elution volume of 50 µL.

7. Elute the cRNA (2):

    a. Add 50 µL of RNA Elution Buffer to the fibre matrix at the bottom of the column.

    Note: Do not let the Pipette tip touch the fibre matrix.

    b. Cap the tube, then incubate the column at room temperature for 2 minutes.

    c. Centrifuge the column and tube at 13,000 × *g* for 1 minute for a final elution volume of 100 µL.

8. Discard the column and cap the tube.

8. Store the cRNA product on ice while you assess the quantity (UV Spectrophotometry) and quality (agarose gel electrophoresis).

2.13.2 Hybridisation and Chemiluminescence

2.13.2.1 Background

Figure 2.11 presents an overview flowchart of the hybridisation and Chemiluminescence steps. Briefly, the DIG labelled cRNA is hybridised to the array. After appropriate blocking and washing, Anti-digoxigenin-alkaline phosphatase (AP) is added to bind to digoxigenin in the cRNA. Further microarray rinses remove any unbound antibody and prepare the microarray for the chemiluminescence reaction. Enhancing solution is then added to the microarray to increase the quantum yield of the chemiluminescent reaction. With the addition of substrate, the alkaline phosphatase in the anti-digoxigenin-AP conjugate dephosphorylates the substrate. This chemical reaction emits light. The microarray is loaded onto the heated stage of the Applied Biosystems 1700 Chemiluminescent Microarray Analyzer. The temperature of the stage is the optimal temperature for the chemiluminescent reaction. The 1700 analyzer focuses on the microarray. The 1700 analyzer obtains fluorescent and chemiluminescent images of the microarray.

13.2.2 Prehybridising Microarrays

Note! Power on the hybridisation oven and set the temperature to 55 °C.

Note: The oven may take up to 3 hours to heat up and equilibrate to 55 °C.

1. Make sure that the oven temperature is 55 °C.

2. Prepare reagents:

    a. Equilibrate reagents to room temperature 1 hour before use:

        • Hybridisation Denaturant

        • Blocking Reagent 1

        • Blocking Reagent 2

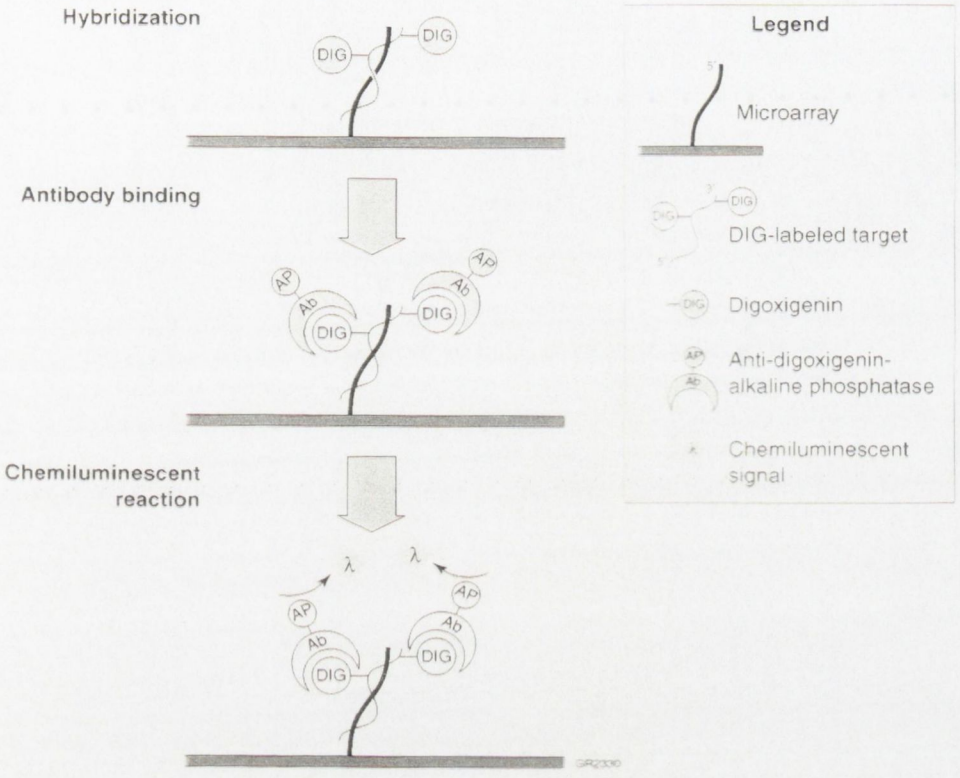

Figure 2.11 Hybridisation and CL overview

b. Warm the Hybridisation Buffer at 37 °C for 30 minutes and then vortex to dissolve precipitates.

4. Prepare hybridisation mixture in a nuclease-free tube and vortex to mix:

Component	Volume (µL)/Microarray
Nuclease Free Water	150
Hybridisation Buffer	330
Hybridisation Denaturant	100
Blocking Reagent	420
Total/Microarray	1000

4. Transfer prehybridisation mixture into each microarray cartridge:

a. Remove the foil wrapping from a cartridge.

b. Remove the plug and Pipette the prehybridisation mixture (1 mL) into the port.

c. Dry the port surface with lint-free tissue and seal the port with the plug. Turn the plug to secure it.

d. Place the cartridge in the oven, making sure that the cartridge is level and held securely by the clamps.

5. Incubate cartridge(s) in the oven:

- Temperature: 55 °C
- Agitation: 100 rpm
- Time: 1 hour

2.13.2.2 cRNA Fragmentation

During prehybridisation, fragment the cRNA.

1. Allow reagents to equilibrate to room temperature 1 hour before use:

- cRNA Fragmentation Buffer
- cRNA Fragmentation Stop Buffer

2. Combine components into a 0.2-mL MicroAmp reaction tube on ice.

Component	Volume (μL)
cRNA fragmentation buffer	10.0
10μg DIG-labelled cRNA and nuclease free water	90.0
Total	100.0

3. Heat the tube in a thermal cycler at 60°C for 30 minutes.

4. Neutralise the reaction:

a. Remove the tube from the thermal cycler and place it on ice.

b. Add 50 µL of cRNA Fragmentation Stop Buffer and mix by Pipetting up and down.

5. Centrifuge the tube briefly and place it on ice.

2.13.2.3 Hybridising Samples to Microarrays

1. Vortex Hybridisation Controls then centrifuge the tube briefly.

2. For each microarray prepare hybridisation mixture in a nuclease-free microcentrifuge tube:

Component	Volume (µL)/Microarray
Nuclease-free water	100
Hybridisation Buffer	170
Hybridisation Controls	30
Fragmented cRNA targets	150
Hybridisation Denaturant	50
Total/Microarray	500

3. Vortex the hybridisation mixture, then centrifuge the tube briefly.

4. Take to the hybridisation oven:

- Tube(s) with hybridisation mixture
- 1000-µL Pipettor
- 1000-µL tips
- Lint-free tissues

5. Transfer hybridisation mixture into each microarray cartridge:

IMPORTANT! Do not allow cartridges to cool. Add hybridisation mixture quickly.

a. Remove one cartridge from the oven and close the door.

b. Remove the plug and Pipette hybridisation mixture (500 µL) into the port.

c. Dry the port with lint-free tissue and seal it with the plug.

d. Return the cartridge to the hybridisation oven.

6. Incubate cartridge(s) in the oven.

- Temperature: 55 °C
- Agitation: 100 rpm
- Time: 16 hours

IMPORTANT! Do not vary the incubation time. Variations may affect reproducibility.

2.13.2.4 Preparing Wash Buffers and Reagents

Volumes provided are for one set of washes with one to eight microarrays in one wash tray.

1. Equilibrate to room temperature before use:

- Hybridisation Wash Buffer Concentrate
- Hybridisation Wash Detergent Concentrate
- Chemiluminescence Rinse Buffer Concentrate
- Enhancing Rinse

- Nuclease-free deionised water

2. Prepare hybridisation wash buffer 1:

Component	Volume (mL)
Hybridisation Wash Buffer Concentrate	60
Hybridisation Wash Detergent Concentrate	120
Nuclease-free deionised water	420
Total	600

3. Prepare hybridisation wash buffer 2:

Component	Volume mL
Hybridisation Wash Buffer Concentrate	3
Nuclease-free deionised water	597
Total	600

4. Prepare CL rinse buffer:

Component	Volume mL
Chemiluminescence Rinse Buffer Concentrate	125
Nuclease-free deionised water	2375
Total	2500

5. Prepare enhancing rinse buffer:

Component	Volume mL
Chemiluminescence Rinse Concentrate	10
Nuclease-free deionised water	190
Total	200

2.13.2.4 Performing Hybridisation Washes

IMPORTANT! Do not allow the microarrays to dry out. After completing a step, *immediately* proceed to the next step.

1. Add 600 mLs hybridisation wash buffer 1 to a clean wash tray.
2. Wash microarrays in hybridisation wash buffer 1:
    a. Open the oven, remove a cartridge, and close the door.
    b. Open the cartridge and take the microarray out.
    c. Make sure that the two gaskets are intact and that the hybridisation volume (1 mL) is still present.
    d. Decant hybridisation mixture and place the microarray in buffer. Make sure that it is submerged in buffer.
    e. Repeat steps 2a through d for each cartridge.
    f. Agitate on an orbital shaker set at 80 rpm for 5 minutes.
    g. Drain the buffer.
3. Wash microarrays in hybridisation wash buffer 2:
    a. Add 600 mLs hybridisation wash buffer 2 to the wash tray.
    b. Agitate on an orbital shaker set at 80 rpm for 5 minutes.
    c. Drain the buffer.
4. Perform CL rinse 1:
    a. Add 400 mLs CL rinse buffer to the wash tray.
    b. Agitate on an orbital shaker set at 80 rpm for 5 minutes.
    c. Drain the buffer.
5. Perform CL rinse 2:
    a. Add 400 mLs CL rinse buffer to the wash tray.
    b. Agitate on an orbital shaker set at 80 rpm for 5 minutes.

c. Cover the wash tray, remove it from the orbital shaker, and place it on the bench top.

Note: You may leave the microarrays in CL rinse buffer at room temperature for up to 1 hour.

2.13.2.5 Performing Antibody Binding

1. Centrifuge the anti-digoxigenin-AP at full speed for 5 minutes.

2. Combine components for the CL blocking buffer/antibody mixture in a nuclease free tube and mix well by inversion. Do not vortex.

Component	Volume/Microarray
Nuclease free water	2.8mL
Chemiluminescence Rinse buffer Concentrate	0.2mL
Blocking Reagent	1.0mL
Anti-digoxigenin-AP	15μL
Total/Microarray	4.015mL

3. Add the CL blocking buffer/antibody mixture (repeat for each microarray)

a. Remove one microarray from the wash tray, shape and tap it gently, and place it on the rocking platform shaker.

b. Immediately add 4 mL CL blocking buffer/antibody mixture to the microarray.

Complete this step for all microarrays within 2 minutes.

4. Cover the arrays with the wash tray cover, and then agitate on the rocking platform shaker for 20 minutes at room temperature.

2.13.2.6 Performing Antibody Washes

1. Perform CL rinse 1:

    a. Add 500 mL CL rinse buffer to a clean wash tray.

    b. For each microarray, decant CL blocking buffer/antibody mixture, shake and tap the microarray gently, then place it in the wash tray. Make sure that all microarrays are submerged in buffer.

    c. Cover the wash tray, then agitate on the rocking platform shaker for 10 minutes.

    d. Drain the buffer from the wash tray.

2. Perform CL rinse 2:

    a. Add 500 mL CL rinse buffer to the wash tray, then make sure that all microarrays are submerged in buffer.

    b. Cover the wash tray, then agitate on the rocking platform shaker for 10 minutes.

    c. Drain the buffer from the wash tray.

3. Perform CL rinse 3:

    a. Add 500 mL CL rinse buffer to the wash tray, then make sure that all microarrays are submerged in buffer.

    b. Cover the wash tray, then agitate on the rocking platform shaker for 10 minutes.

4. Cover the wash tray and place it on the bench top.

Note: You may leave the microarrays in the CL rinse buffer at room temperature for up to 3 hours

2.13.2.7 Performing the CL reaction

The chemiluminescent reaction is time-dependent. Perform this procedure with only one microarray at a time.

1. Power on the Applied Biosystems 1700 Chemiluminescent Analyzer at least 10 minutes before using it.
2. Perform a CL enhancing rinse:
    a. Place 100 mL CL enhancing rinse buffer in a 10.2 × 12.7-cm (4 × 5-inch) tray.
    b. Remove one microarray from the wash tray, decant the CL rinse buffer, shake and tap the microarray gently, then place it in the small tray with 100 mL CL enhancing rinse buffer.
    c. Agitate on the rocking platform shaker for 10 minutes.
    d. Stop the agitation of the rocking platform shaker.
3. Perform the enhancing step:
    a. Remove the microarray from the small tray, decant CL enhancing rinse buffer, shake and tap the microarray gently, then place it vertically on the rocking platform shaker.
    b. *Quickly* add 4 mL of **Chemiluminescence Enhancing Solution** to the microarray.
    c. Agitate on the rocking platform shaker for 20 minutes.
4. Perform a CL enhancing rinse:
    a. Place 100 mL CL enhancing rinse buffer in a second 10.2 × 12.7-cm (4 × 5-inch) tray.

b. Decant the enhancing solution from the microarray, then shake and tap the microarray gently.

c. Place the microarray in the second small tray with

100 mL CL enhancing rinse buffer.

d. Agitate on the rocking platform shaker for 5 minutes.

5. Add substrate:

a. Remove the microarray from the small tray, decant the CL enhancing rinse buffer, then shake and tap the microarray gently.

b. Wipe the bottom of the microarray with lint-free tissue.

c. Add 3.5 mL of **Chemiluminescence Substrate** to the microarray.

IMPORTANT! The chemiluminescent reaction is time dependent.

After you perform this step, proceed with performing CL detection immediately.

2.13.2.8 Performing the CL Detection

1. Power on the 1700 instrument.

2. Load the microarray into the instrument:

a. Dry any excess liquid from the sides and bottom of the microarray with lint-free tissue.

b. Open the instrument door.

c. Orient the microarray so that the end bar code is at the top and the side bar code is on the right, then place the microarray on the heated stage of the instrument.

d. Lock the bar, then close the door.

3. Perform the read:

a. On the computer, select **Start > Programs > Applied Biosystems > AB1700 Software** to start the software.

b. Enter the Login Name and Password.

c. Select cartridge settings: Microarray Type, Chemistry Method, Reader Method, Analysis Method, Folder, Sample Name/ID

d. Click **Start** and wait for the instrument to obtain the images.

5. Analyze the data.

2.13.3 Array Controls

Numerous controls are present on the array. These provide the ability to monitor the performance of each array and each experimental condition and to generate Quality Control Reports. (Figure 2.12)

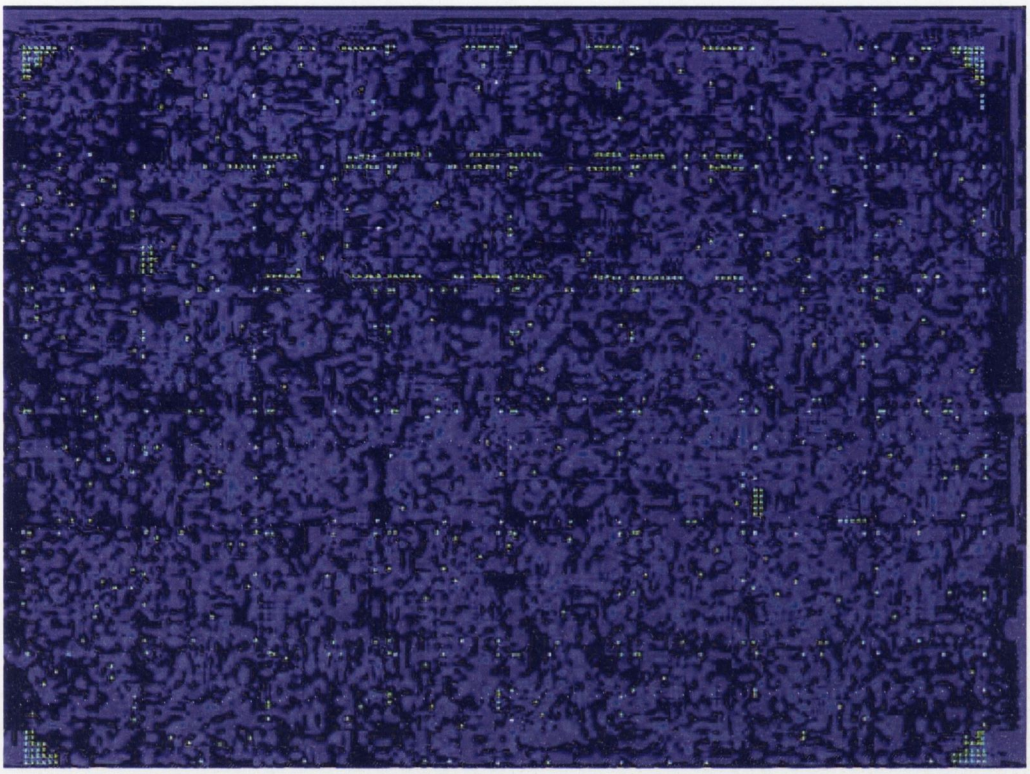

Figure 2.12 Array Controls. The green spots represent the various array and other controls on half of the microarray grid

2.13.3.1 Assay Background Controls

Purpose: The assay background controls provide information about non-specific background signals from all probes on the microarray.

Definition: The assay background controls consist of oligos designed to have low cross reactivity with the genome being tested. The design strategy:

1. Applied Biosystems performed BLAST® (Basic Local Alignment Search Tool) searches with random sequences.

2. Sequences were ranked according to low predicted reactivity with the genome sequence of interest.

4. Sequences were refined further based upon empirical data generated at Applied Biosystems. The microarray contains 196 features, 2 copies of 98 unique 60-mer probes placed throughout the array. Function Non-specific binding to the assay background controls results in signal. Non-specific binding can result from cross-hybridisation, binding of alkaline phosphatase enzyme, or other chemical processes that lead to background chemiluminescent signal. The software calculates the amount of background chemiluminescent signal and uses the correction to measure all other chemiluminescent signals on the microarray.

2.13.3.2 Blank Features

Purpose: The amount of signal produced at the blank features provides information about:

- The background signal for every region of the microarray
- Cross-talk from adjacent spots

Definition: 1633 spots on the microarray are blank. The features are located between the image zones and between the 19x19 subgrids on the microarray. Function Non-specific binding of DNA or RNA, antibodies, alkaline phosphatase enzyme, or other chemical or mechanical processes can result in background signal. Signals from the blank features indicate the level of non-specific signal generated from the assay. The software calculates the amount of background chemiluminescent and fluorescent signals from the blank features and uses the correction to measure all other chemiluminescent and fluorescent signals on the microarray.

2.13.3.3 Control Ladders

Purpose: The control ladders are used to:

- Perform quality checks of array spotting and chemistry
- Compare reproducibility of spotting across batches and many arrays.
- Perform quality checks of chemiluminescent detection chemistry
- Demonstrate sensitivity and dynamic range of chemiluminescent detection chemistry.

Definition: The fluorescent fiducial ladder consists of probes labelled with LIZ® dye and spotted on the microarray in a five-fold dilution series: 625X, 125X, 25X, 5X, and 1X

The chemiluminescent fiducial ladder consists of DIG-labelled probes spotted on the microarray in a five-fold dilution series: 625X, 125X, 25X, 5X, and 1X. There are two copies of each ladder in each image zone.

Function: Because the labelled probes are attached to the microarray, fiducial control ladders are independent of labelling and hybridisation. Signal indicates that the chemiluminescent reaction was successful. Signal intensity variability indicates spotting and attachment efficiencies across various batches of manufactured arrays.

2.13.3.4 Hybridisation Controls

Purpose: The hybridisation controls can be used to:

- Indicate successful hybridisation
- Indicate hybridisation stringency
- As a spatial normalisation control

Definition: The hybridisation controls consist of:

• Three DIG-labelled 60-mer oligo control targets supplied with the CL detection kit

– HYB_Control_1_Ct

– HYB_Control_2_Ct

– HYB_Control_3_Ct

• Three unlabelled probes spotted on the microarray:

– HYB_Control_1_Cp

– HYB_Control_2_Cp

– HYB_Control_3_Cp

Function: The DIG-labelled oligo targets are added to the microarray with the DIG-labelled cDNA or cRNA targets. The three hybridisation controls on the microarray are designed to hybridize to all of the DIG-labelled oligo targets:

• Presence of signal indicates hybridisation occurred.

• Signal strength indicates hybridisation stringency.

2.13.3.5 Internal Control

Purpose: The internal control can be used to:

• Grid all features on the microarray

• Normalise the CL signal

Definition: This control consists of:

• Internal control target (ICT) supplied with the CL detection kit: 24mer oligo labelled with LIZ dye

• Internal control probe (ICP) on the microarray: 24mer co spotted at every feature in the microarray that contains a 60mer gene expression probe

Function: The ICT is added to the hybridisation mixture. When hybridisation occurs, the ICTs hybridize to every ICP to produce a fluorescent signal.

2.13.3.6 IVT Controls

Purpose: When using the RT-IVT labelling kit, the IVT controls indicate whether the *in vitro* transcription labelling reaction worked and how well the reaction worked. The IVT controls are not used when using the RT labelling kit.

Definition: The IVT controls consist of:

• Three synthetic double-stranded cDNA with a T7 promoter and bacterial control gene sequences:

– *bioB* — 1000-nt ds-cDNA with T7 promoter

– *bioC* — 750-nt ds-cDNA with T7 promoter

– *bioD* — 600-nt ds-cDNA with T7 promoter

• A total of 120 features on the microarray:

– Fifteen probes on the microarray: five for each bacterial control gene, *BioB*, *BioC*, and *BioD*.

– Each probe is spotted eight times: four times in each image zone.

Function: The synthetic control cDNAs are added to the RNA sample when using the RT-IVT labelling kit. The control cDNA undergoes *in vitro* transcription in the presence of DIG to produce DIG-labelled cRNA. The DIG-labelled control cRNAs hybridize to the probes on the microarray and, after a successful chemiluminescent reaction, generate signal.

2.13.3.7 Landmark Fiducials

Purpose: The landmark fiducial controls are used by the system software to:

• Confirm that the placements of a subset of the features are in the correct position after manufacturing

• Determine the orientation of plates and of the array

• Define the edges and corners of the array

• Align the fluorescent and chemiluminescent images

Definition: The landmark fiducial controls consist of probes on the microarray:

• Probes labelled with LIZ dye

• Probes labelled with DIG

Function: The fluorescent landmark fiducial controls provide strong signals independent of labelling, hybridisation, and the chemiluminescent reaction.

After a successful chemiluminescent reaction, the chemiluminescent landmark fiducial controls provide strong signals independent of labelling and hybridisation.

2.13.3.8 RT Controls

Purpose: The RT controls indicate:

• With the RT labelling kit, whether the reverse transcription labelling reaction worked and how well the reaction worked.

• With the RT-IVT labelling kit, whether the reverse transcription reaction worked and how well the reaction worked.

Definition: The RT controls consist of:

• Three synthetic mRNAs with bacterial control gene sequences:

– *lys*— 1000-nt mRNA with poly (A) tail

– *phe* — 1400-nt mRNA with poly(A) tail

– *dap* — 1900-nt mRNA with poly(A) tail

• A total of 120 features on the microarray:

– Fifteen probes on the microarray: five for each bacterial control gene *DAP*, *LYS*, and *PHE*.

– Each probe is spotted eight times: four times in each image zone.

Function: The synthetic mRNAs are added to the reverse transcription reaction with the RNA sample when using the RT labelling kit or the RT-IVT labelling kit:

• With the RT labelling kit, the control RNA undergoes reverse transcription in the presence of DIG-dUTP to produce DIG-labelled cDNA.

• With the RT-IVT labelling kit, the control RNA undergoes reverse transcription and second strand synthesis into double-stranded cDNA. The control sequences then undergo *in vitro* transcription in the presence of DIG-dUTP to produce DIG-labelled cRNA.

The DIG-labelled control cDNAs (RT labelling kit) or DIG-labelled control cRNAs (RT-IVT labelling kit) hybridize to the probes on the microarray and, after a successful chemiluminescent reaction, generate signal.

2.13.3.9 Spatial Normalisation Controls

Purpose: The software uses the spatial normalization control signal to:

• Compare the signals within one image zone and calculate the percent coefficient of variation (%CV) within the image zone

• Compare the signals across the array and calculate the percent coefficient of variation (%CV) across the array

Definition: The spatial normalization controls consist of:

• Three DIG-labelled oligo control targets supplied with the CL detection kit

• HYB_Control_3_Cp, unlabelled probe spotted on the microarray

Function The unlabelled probe is spotted on at least one corner of each 19x19 subgrid on the microarray (117 features total).

The DIG-labelled oligo targets are added to the microarray with the DIG-labelled cDNA or cRNA targets. The spatial normalization control probe on the microarray is designed to hybridise to all of the DIG-labelled oligo targets.

2.14 References

Fend F, Raffield M. 2000. Laser Capture microdissection in pathology. J Clin Pathol 53:666-672

Kutyavin IV, Afonina IA, Mills A, Gorn VV, Lukhtanov EA, Belousov ES, Singer MJ, Walburger DK, Lokhov SG, Gall AA, Dempcy R, Reed MW, Meyer RB, Hedgpeth J. 2000. 3'-minor groove binder-DNA probes increase sequence specificity at PCR extension temperatures. Nucleic Acids Res.15; 28(2): 655-61.

Lemoine NR, Mayall ES, Jones T, Sheer D, McDermid S, Kendall-Taylor P, Wynford-Thomas D. 1989. Characteristics of human thyroid epithelial cells immortalized *in vitro* by simian virus 40 DNA transfection. Br J Cancer 60:897-903

Orlando C, Pinzani P, Pazzagli M. Developments in quantitative PCR. 1998. Clin Chem Lab Med. 36(5): 255-69.

Rosai J, Carcangiu ML, DeLellis RA. 1992. Atlas of tumour Pathology: Tumours of the Thyroid gland, 3rd series. Washington, DC: Armed Forces Institute of Pathology

Schena M. 2003. Microarray analysis. Wiley and Sons

Turner PC, McLennan AG, Bates AD, White MRH. 2000. Instant notes Molecular Biology. 2nd Edition. BIOS Scientific Publishers Limited.

Van Gelder RN, von Zastrow ME, Yool A, Dement WC, Barchas JD, Eberwine JH. 1990. Amplified RNA synthesized from limited quantities of heterogeneous cDNA. Proc Natl Acad Sci U S A. 87(5): 1663-7

Chapter 3

Ret/PTC chimeric transcripts in an Irish cohort of PTC

3.1 Summary

The focus of this chapter was to assess the prevalence of the most commonly described ret rearrangements (*ret*/PTC-1 and *ret*/PTC-3) in PTC accessioned over a prolonged time period (1982-2002) at St. James's Hospital. *Ret*/PTC-3 is strongly associated with childhood PTC occurring after radiation exposure. In this context (post radiation exposure), *ret*/PTC-3 has been correlated with solid/follicular variant morphology, poorer prognosis and aggressive tumour behaviour.

The cohort described in this chapter represents a "sporadic" group in terms of radiation exposure, with no known history of radiation exposure documented in this population during the time period. A second aim of this chapter was to assess whether the morphology of the tumours in this sporadic group could be associated with either of these two rearrangements.

Thyroid follicular cells were laser capture microdissected from sections of archival PTC (N=28). Total RNA was extracted and analysed, by TaqMan RT PCR for expression of the housekeeping gene GAPDH, to confirm the integrity of the extracted RNA. Subsequently, each sample was analysed for expression of *ret*/PTC-1 and *ret*/PTC-3, using breakpoint-spanning probes to ensure detection of the rearranged chimera.

Ret/PTC rearrangements were detected in 60% of the PTC cases examined. Specifically, transcripts of *ret*/PTC-1 and *ret*/PTC-3 were detected in 43% and 18% of PTCs respectively. *Ret*/PTC-3 correlated with a group of tumours showing variant

morphology (including Follicular variant, Hurthle Cell Variant and Tall Cell variant) and was not detected in classic morphology PTC. A single case of Tall Cell Variant demonstrated expression of both *ret*/PTC-1 and *ret*/PTC-3 within the same tumour (Chimera heterogeneity).

The study shows a high prevalence of the two common *ret* rearrangements in an Irish cohort of PTC. Correlation of tumour morphology with rearrangement status suggests a link between variant morphology and *ret*/PTC-3.

3.2 Introduction

3.2.1 Papillary thyroid Carcinoma

Papillary thyroid carcinoma (PTC) is the most common malignant tumour of the thyroid gland and represents up to 80% of all thyroid cancer (Rosai, 1992). The morphological appearance of PTC is not homogenous, with several distinct histological variants described.

The diagnosis of classical PTC is primarily based on recognising typical nuclear morphological features, which include nuclear hypochromasia/ground glass appearance, nuclear grooves, and nuclear inclusions in association with papillary architecture. Classification of other variants requires the integration of tumour architecture, other cell and cytoplasmic features, and tumour stroma. Variants include follicular variant, diffuse sclerosis, solid variant, Hurthle cell PTC, Tall cell

variant, and columnar variant. These morphological variants are likely to reflect variations in tumour biology, which have yet to be clearly defined.

3.2.2 *Ret* proto-oncogene

The c-*ret* proto-oncogene (chromosome 10q11.2) has 21 exons and encodes a transmembrane receptor with cytoplasmic tyrosine kinase (Takahashi, 2001) activity. The protein product of the *ret* gene is a functional receptor for its ligand, glial cell line-derived neurotropic factor (GDNF). The gene was first identified as a novel oncogene in 1985 following transfection of NIH 3T3 cells with DNA from a human T-cell lymphoma (Takahashi, 1985). The transforming gene resulted from a recombination event between two unlinked DNA sequences, which occurred during the transfection process; hence, the name *ret*, for 'rearranged during transfection'. The resulting chimeric gene encoded a fusion protein comprising an amino-terminal region that displayed a putative zinc finger motif fused to a tyrosine kinase domain. Subsequently, the name *ret* was retained to designate the gene coding for the tyrosine kinase. Germline point mutations of the *ret* proto-oncogene are associated with the dominantly inherited cancer syndromes multiple endocrine neoplasia types 2A and 2B (MEN 2A and MEN 2B) and familial medullary thyroid carcinoma (FMTC). Somatic mutations in *ret* have been found in a proportion of patients with sporadic MTC (Komminoth, 1997). Point mutations of the *ret* gene are also associated with both sporadic and familial cases of Hirschsprung disease (Aganglionic megacolon) (Attie, 1995).

3.2.3 Ret rearrangements

In PTC, c-*ret* is activated by somatic gene rearrangements rather than point mutations (Figure 3.1). These rearrangements lead to juxtaposition of the region coding for the tyrosine kinase with the 5'- terminal of otherwise unrelated genes (Manie, 2001). These rearrangements were thought to be specific for PTC; however, they are not ubiquitously detected and vary in frequency according to the tumour population studied and the detection technology employed (Chung, 1999; Tallini, 2001). Ret rearrangements (*ret*/PTC-1) have also been detected associated with Hashimoto's thyroiditis (Wirtschafter, 1997; Sheils, 2000).

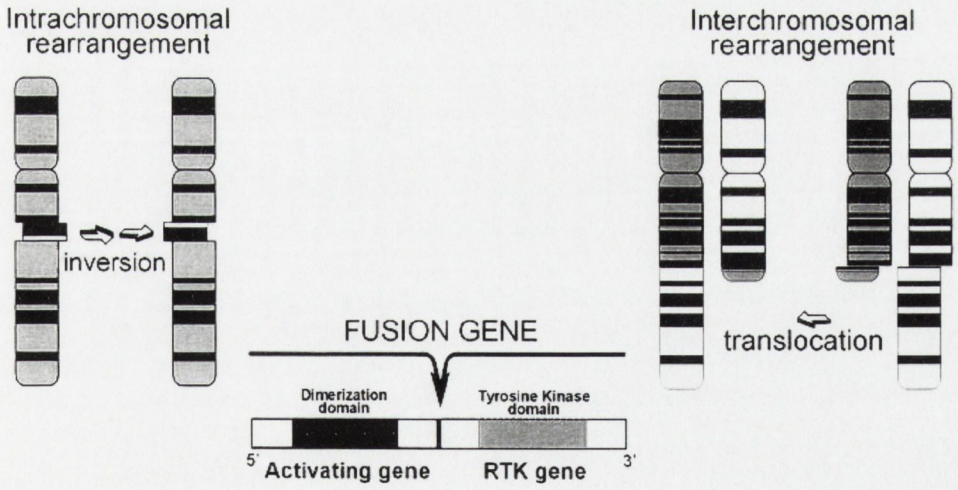

Figure 3.1 Mechanisms of chromosomal rearrangements generating fusion-transforming genes in PTC (Pierotti, 2001). RTK (Receptor tyrosine kinase)

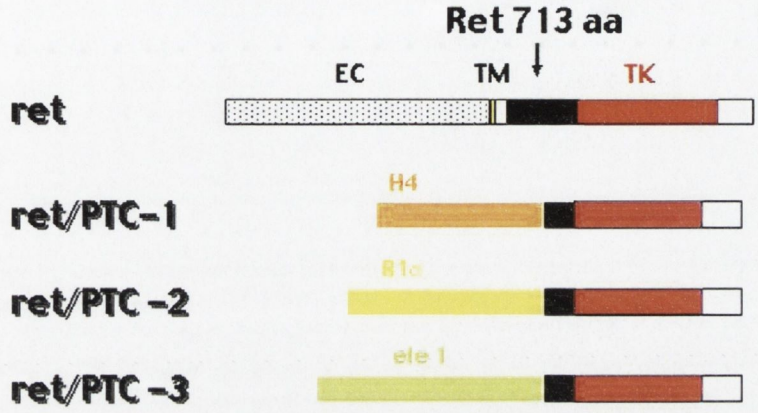

Figure 3.2 The three most common *ret*/PTC gene rearrangements.

The top portion represents the intact ret receptor, with an extracellular region (EC), a transmembrane domain (TM) and a tyrosine kinase domain (TK). The rearrangements involve a breakpoint at amino acid 713 and encode the distal portion of ret including the tyrosine kinase. The upstream portions are regulated by the promoters of other genes, H4, R1a and ELE, and encode fusion proteins as shown (Asa, 2001).

The most prevalent rearranged chimeric transcript detected is *ret*/PTC-1, resulting from fusion of the tyrosine kinase-encoding region of c-ret to the 5' terminal sequences of a gene termed *H4* on chromosome locus 10q21 (Sozzi, 1991). Ret/PTC2 is generated through fusion of *ret* with the *PRKAR1A* gene encoding RI-alpha and situated on chromosome 17 (Bongarzone, 1993), however, the second most common rearrangement is not *ret*/PTC-2 but *ret*/PTC-3 involving fusion of *ret* to a gene known as *ELE-1* on Chromosome 10q11.2, also known as ret fused gene (*RFG*) (Bongarzone, 1994).

The two most common rearrangements occur as a result of paracentric inversion of chromosome 10 leading to juxtaposition of either *H4* or *ELE-1* adjacent to the ret tyrosine kinase domain. *Ret*/PTC-3 was first described in children exposed to ionising radiation as a consequence of the Chernobyl accident (Bongarzone, 1997). In this setting *ret*/PTC-3 has been correlated with poorer prognosis, aggressive tumour behaviour and distinct solid morphology (Thomas, 1999).

To date, at least 15 chimeric mRNAs involving 10 different genes have been described (Tallini, 2001). The prevalence of specific rearrangements varies according to geographical location (Chung, 1999, Tallini, 2001) and history of radiation exposure (Fenton, 2000). It is also becoming more apparent that the morphology of PTC variants is associated with specific *ret*/PTC rearrangements (Nikiforov, 1997, Santoro, 2000, Nikiforov, 2001). In particular, *ret*/PTC-1 appears to be associated with PTC of classical and diffuse sclerosing morphology and *ret*/PTC-3 with solid variant morphology. *Ret*/PTC-3 is associated with poorer prognosis, more aggressive tumour behaviour and may well be a marker for radiation-induced carcinoma particularly in children.

3.3 Aims

The objective of this study was to assess the prevalence of the two common *ret* chimeric transcripts (*ret*/PTC-1 and *ret*/PTC-3) in a group of "sporadic" PTC in Ireland, using highly sensitive TaqMan technology and to correlate tumour morphology with these two specific *ret* rearrangements.

3.4 Materials and Methods

Twenty-eight archival cases of formalin fixed paraffin embedded PTC were analysed. These cases represented material accessioned between 1982 and 2001 at St. James's Hospital, Dublin. Haematoxylin and Eosin (H&E) stained sections were reviewed by two histopathologists and classified according to a recognised system (Rosai, 1992), (Table 3.1). Laser capture microdissection was utilised to obtain pure populations of thyrocytes. Extracted RNA was subjected to RT PCR using break point spanning MGB probes to ensure detection of expressed chimera. The sequences of the primers and probes are described in the materials and methods chapter (Section 2.9.4). The integrity of the extracted RNA was confirmed by demonstrating amplification of GAPDH housekeeping gene. PCR products were detected in real time, Figure 3.2.

3.4.1 Statistical approach

Fisher's exact test was used to determine the associations between *ret*/PTC-1 and *ret*/PTC-3 expression and tumour morphology.

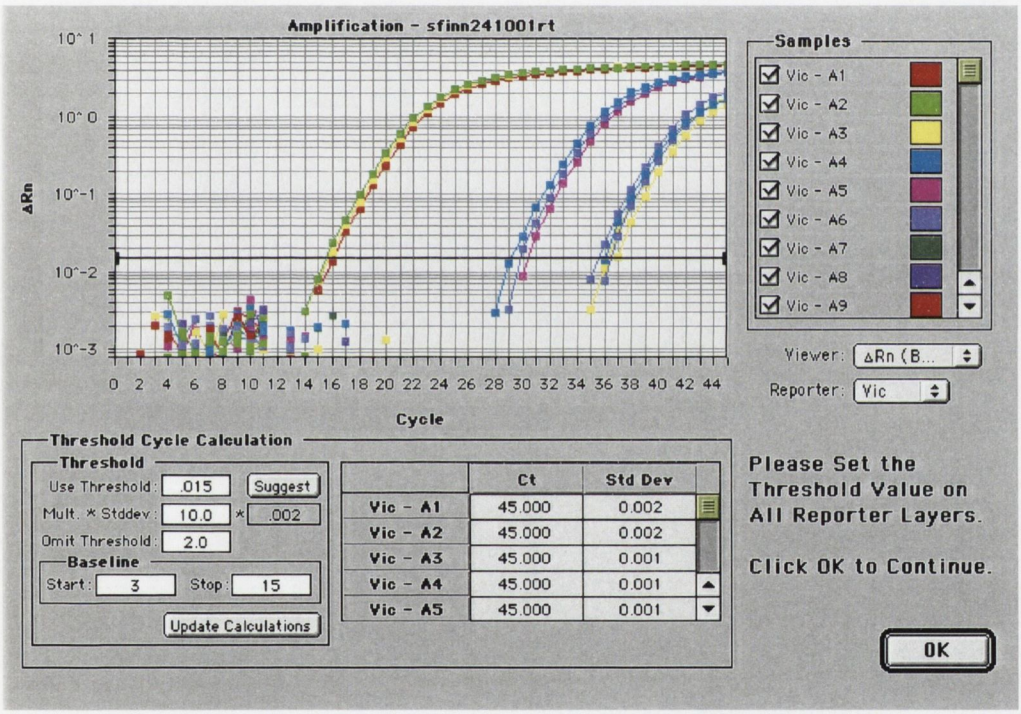

Figure 3.3 TaqMan real time RT PCR amplification plot.

The lower the C_T the more target is present. Each curve above represents an individual sample.

Morphology	Number of cases examined	Number of patients
Classical morphology PTC	**17**	**17**
Follicular variant PTC	**5**	**5**
Hurthle cell PTC	**1**	**1**
Tall Cell Variant	**5**	**2***

* 3 recurrences

Table 3.1 Tumour morphology

3.5 Results

3.5.1 Prevalence of *ret* rearrangements (Table 3.2)

In all 28 tumours were analysed. The housekeeping gene *GAPDH* was amplified in all cases (in 4 cases repeat laser microdissection and RNA extraction was required. The initial samples were discarded). These 28 specimens represented surgical resection material from 25 different patients, because one patient suffered 3 recurrences of an aggressive Tall Cell Variant PTC. A total of 17 *ret* rearrangements were detected in the 28 tumours examined (60%). Specifically, *ret*/PTC-1 and *ret*/PTC-3 transcripts were detected in 12/28 (43%) and 5 of 28 (18%) of all PTCs examined respectively.

3.5.2 Tumour morphology

3.5.2.1 Classic and Variant Morphology

The spectrum of morphological subtypes in this cohort of PTC is shown in Table 3.1.

Ret/PTC-3 was detected in 3 of 5 (60%) of FV PTC and was not detected in conventional PTC. *Ret*/PTC-1 was detected in a single case of follicular variant PTC and in 9 of 17 (53%) of conventional PTC. By subdividing the morphological groups into two major categories, classical morphology and variant morphology (Including FVPTC, Tall Cell variant and Hurthle Cell variant), and using Fisher's Exact test it was possible to show associations between *ret*/PTC-1 expression and classical morphology PTC (p=0.019) and a statistically significant association between *ret*/PTC-3 expression and variant morphology (p=0.004).

Morphology	Ret/PTC-1	Ret/PTC-3	Neither	Both
Classical PTC N=17	9	0	8	0
Follicular variant PTC n=5	1	3	1	0
Hurthle Cell PTC N=1	0	0	1	0
Tall cell variant N=5**	2	2	1	1

**Chimeric transcripts of both *ret*/PTC-1 and *ret*/PTC-3 detected in the same tumour.

Table 3.2 Chimeric transcripts detected

3.5.2.2 Tall Cell Variant

In one of two cases of tall cell variant the tumour behaved aggressively and recurred on 3 occasions, accounting for 4 separately accessioned surgical specimens for this individual patient. Each specimen was examined for *ret*/PTC-1 and *ret*/PTC-3 rearrangements. In this patient's case thyrocytes from the initial resection demonstrated *ret*/PTC-1 positivity. In the subsequent first recurrence neither *ret*/PTC-1 nor *ret*/PTC-3 could be detected. Examination of the second recurrence showed positivity for both *ret*/PTC-1 and *ret*/PTC-3. Thyrocytes microdissected from the third and final recurrence showed positivity for *ret*/PTC-3 only.

3.6 Discussion

The prevalence of *ret* rearrangements has been examined in cohorts of papillary carcinomas in many countries and geographical locations throughout the world. The prevalence has shown a marked geographic discordance. Low prevalence rates have been demonstrated in Saudi Arabia (3%) (Zou, 1994), Germany (8%) (Mayr, 1998), Japan (only ret/PTC-1 assessed, ranging from 0% to 9%) (Namba, 1991; Wajjwalku, 1992; Ishizaka, 1991), France (11%) (Santoro, 1992). The highest rates have been reported in papillary thyroid carcinomas, which occurred after the Chernobyl accident (overall prevalence 87%) with *ret*/PTC-3 the most common rearrangement detected (58%) followed by *ret*/PTC-1 (16%) and *ret*/PTC-2 (3%) (Nikiforov, 1997).

Comparisons of these prevalence rates may not be appropriate. Many of the cohorts studied are numerically small and in addition the methods employed to detect ret status have varied widely and have included Southern blot RT PCR, Southern blot transfection assays, *in-situ* hybridisation, interphase FISH and TaqMan RT PCR.

However, as discussed by Tallini (Tallini, 2001), the existence of true geographic variability is shown by comparison of the prevalence of *ret*/PTC activation in different studies of sporadic papillary carcinomas which have used broadly similar methods, usually RT PCR followed by hybridisation with chimera specific probes. In certain cases the heterogeneity of reported prevalence rates is striking. For example, taking 2 Australian series, Learoyd et *al* used RT PCR and direct sequencing of amplicons to demonstrate an incidence of 4.2% in 1998 (Learoyd,

1998). In comparison however, a second Australian study by Chua *et al,* published in 2000 showed an 85% prevalence of ret rearrangements in their cohort of Caucasian Australians (Chua, 2000).

In our cohort, we looked for *ret*/PTC-1 and *ret*/PTC-3 only, knowing that these represent the commonest rearrangements in the literature. We found a combined prevalence of these 2 rearrangements of 60%, which is comparable with the highest rates detected in non-radiation exposed populations. The combination of laser capture microdissection to ensure pure populations of malignant thyrocytes, the highly sensitive and specific TaqMan chemistry and the use of MGB probes flanking the breakpoint region may favour detection of these rearrangements, even at low copy number. As discussed by Chua *et al* (Chua, 2000), other studies that demonstrated high prevalence rates utilised almost pure cell populations as substrates and combined this with highly sensitive detection methods.

A prominent feature of the post Chernobyl papillary thyroid carcinomas was the correlation between the morphological variant of the carcinoma and the type of rearrangement detected. The solid variant, which is rare in sporadic papillary thyroid carcinoma, is frequently found in the Chernobyl population of paediatric papillary thyroid carcinomas and is associated with *ret*/PTC-3 and a poorer prognosis (Thomas, 1999). The histological parameters for its diagnosis overlap with those of the follicular variant and poorly differentiated thyroid carcinomas but the nuclei retain the features of PTC (Nikiforov, 2001). In our series, as might be expected for a cohort of sporadic tumours, we had no case of solid PTC. However, *ret*/PTC-3 chimeric transcripts were detected in three of five (60%) of follicular variant PTC

and were not detected in any case of conventional PTC. *ret*/PTC-1 was detected in a single case of follicular variant carcinoma and in nine of 17 (53%) of conventional PTC. This is suggestive of a link between *ret*/PTC-3 with the follicular variant of papillary thyroid carcinoma in our cohort. The association of *ret*/PTC-3 with solid papillary thyroid carcinoma in post-radiation populations and with Tall cell variant (Basolo, 2002) coupled with the predominance of *ret*/PTC-1 associated with classical morphology must reflect variation in the underlying molecular morphogenesis of these tumours

However, the relationship of a specific rearrangement to a morphological variant is not definitive. This is highlighted in our cohort by a single patient presenting with Tall Cell variant PTC. In this case, the tumour behaved aggressively and recurred on 3 separate occasions. In the initial resection specimen, transcripts of *ret*/PTC-1 only were detected. Examination of a subsequent resection failed to reveal any *ret* rearrangement (in spite of successful RNA extraction and control gene positivity). At the second recurrence, transcripts of both *ret*/PTC-1 and *ret*/PTC-3 were present. In the final recurrence, chimeric transcripts of *ret*/PTC-3 only were detected. The occurrence of multiple ret rearrangements within the same tumour has been noted previously (Sugg, 1998). Indeed the study by Chua *et al* demonstrated single tumours with up to 3 distinct *ret* rearrangements (Chua, 2000) and they have postulated that these findings may represent a polyclonal origin for at least some of these tumours. The sequential findings in our own case are more difficult to rationalise but may be accounted for by geographical variation and clonal heterogeneity within the tumour.

Evidence also suggests that *ret*/PTC-3 is associated with a more aggressive tumour biology and worse prognosis. Basolo *et al* demonstrate increased mitogenic signalling activity of *ret*/PTC-3 in the Tall Cell variant and have correlated this with elevated MAPK activation (Basolo, 2002). Monaco *et al* speculate that protein interactions, mediated by protein products of the genes fused to ret at the 5' terminal (*H4* and *ELE-1*), affect the signalling of the specific *ret*/PTC isoforms (Monaco, 2002). We have previously demonstrated consistently reduced expression of E-cadherin in *ret*/PTC-1 positive cohorts in comparison to normal thyroid tissue (Smyth, 2001). A comparable study assessing expression levels of E-cadherin in *ret*/PTC-3 positive and negative normal controls failed to demonstrate a significant reduction (unpublished data). Thus, the emerging literature is beginning to elucidate parallel but distinct pathways of PTC mitogenesis associated with the two common *ret* rearrangements.

3.7 Conclusion

In conclusion, this study has demonstrated a high prevalence of the common *ret* rearrangements in an Irish cohort of PTC (Finn, 2003). We have correlated tumour morphology with the common *ret* rearrangements in order to contribute to the emerging literature suggesting that tumour morphology is in some way related to the underlying specific rearrangements involved. The link between variant morphology and ret/PTC-3 and radiation has been seen in other studies in the literature and suggests a role for radiation in the pathogenesis of a subset of the PTCs described in the current study.

3.8 References

Asa S. 2001. How Familial Cancer Genes and Environmentally Induced Oncogenes Have Changed the Endocrine Landscape. Mod Pathol; 14(3): 246–253

Attie T, Pelet A, Edery P, Eng C, Mulligan LM, Amiel J, Boutrand L, Beldjord C, Nihoul-Fekete C, Munnich A, Ponder BAJ, Lyonnet S. 1995. Diversity of RET proto-oncogene mutations in familial and sporadic Hirschsprung disease. Hum. Molec. Genet. 4: 1381-1386

Basolo F, Giannini R, Monaco C, Melillo RM, Carlomagno F, Pancrazi M, Salvatore G, Chiappetta G, Pacini F, Elisei R, Miccoli P, Pinchera A, Fusco A, Santoro M. 2002. Potent mitogenicity of the RET/PTC3 oncogene correlates with its prevalence in Tall-Cell Variant of papillary thyroid carcinoma. AJP 160: 247-254

Bongarzone I, Butti MG, Coronelli S, Borrello MG, Santoro M, Mondellini P, Pilotti S, Fusco A, Della Porta G, Pierotti MA.1994. Frequent activation of *ret* proto-oncogene by fusion with a new activating gene in papillary thyroid carcinomas. Cancer Research 54(11): 2979-85

Bongarzone I, Butti MG, Fugazzola L, Pacini F, Pinchera A, Vorontsova TV, Demidchik EP, Pierotti MA. 1997. Comparison of the breakpoint regions of ELE-1 and RET genes involved in the generation of RET/PTC3 oncogene in sporadic and in radiation-associated papillary thyroid carcinomas. Genomics 42:252-9

Bongarzone I, Monzini N, Borrello MG, Carcano C, Ferraresi G, Arighi E, Mondellini P, Della Porta G, Pierotti MA. 1993. Molecular characterization of a thyroid tumour-specific transforming sequence formed by the fusion of ret tyrosine kinase and the regulatory subunit RI alpha of cyclic AMP-dependent protein kinase A. Mol Cell Biol. 13(1): 358-66.

Chua EL, Wu WM, Tran KT, McCarthy SW, Lauer CS, Dubourdieu D, Packham N, O'Brien CJ, Turtle JR, Dong Q. 2000. Prevalence and distribution of ret/ptc 1, 2, and 3 in papillary thyroid carcinoma in New Caledonia and Australia. J Clin Endocrinol Metab 85:2733-2739

Chung JH, Hahm JR, Min YK, Lee MS, Lee MK, Kim KW, Nam SJ, Yang JH, Ree HJ. 1999. Detection of RET/PTC oncogene rearrangements in Korean papillary carcinomas. Thyroid 9:1237-1243

Fenton CL, Lukes Y, Nicholson D, Dinauer CA, Francis GL Tuttle RM. 2000. The ret/PTC mutations are common in sporadic papillary thyroid carcinoma of children and young adults. J Clin Endocrinol Metab 85:1170-5

Finn SP, Smyth P, O'Leary J, Sweeney EC, Sheils O. 2003. Ret/PTC chimeric transcripts in an Irish cohort of sporadic papillary thyroid carcinoma. J Clin Endocrinol Metab. 88(2): 938-41

Ishizaka Y, Kobayashi S, Ushijima T, Hirohashi S, Sugimura T, Nagao M. 1991. Detection of ret/PTC transcripts in thyroid adenomas and adenomatous goitre by an RT-PCR method. Oncogene 6:1667-72

Komminoth P. 1997. The RET proto-oncogene in medullary and papillary thyroid carcinoma. Molecular features, pathophysiology and clinical implications. Virchows Arch 431:1-9

Learoyd DL, Messina M, Zedenius J, Guinea AI, Delbridge LW, Robinson BG. 1998. RET/PTC and RET tyrosine kinase expression in adult papillary thyroid carcinomas. J Clin Endocrinol Metab 83:3631-35

Manie S, Santoro M, Fusco A, Billaud M. 2001. The RET receptor: function in development and dysfunction in congenital malformation. Trends in Genetics 17:580-58

Mayr B, Potter E, Goretzki P, Ruschoff J, Dietmaier W, Hoang-Vu C, Dralle H, Brabant G. 1998. Expression of ret/ptc1, -2, -3, - delta 3and – 4 in German papillary thyroid carcinoma. Br J Cancer 77:903-6

Monaco C, Visconti R, Barone MV, Pierantoni GM, Berlingieri MT, De Lorenzo C, Mineo A, Vecchio G, Fusco A, Santoro M. 2001. The RFG oligomerisation domain mediates kinase activation and re-localization of the RET/PTC3 oncoprotein to the plasma membrane. Oncogene 20:599-608

Namba H, Yamashita S, Pei HC, Ishikawa N, Villadolid MC, Tominaga T, Kimura H, Tsuruta M, Yokoyama N, Izumi M. 1991. Lack of PTC gene rearrangements in human thyroid tumours. Endocrinol Jpn 38:627-32

Nikiforov YE, Erickson LA, Nikiforova MN, Caudill CM, Lloyd RV. 2001. Solid variant of papillary carcinoma. Incidence, clinical-pathologic characteristics, molecular analysis, and biologic behaviour. Am J Surg Pathol 25:1478-1484

Nikiforov YE, Rowland JM, Bove KE, Monforte-Munoz H, Fagin JA. 1997. Distinct pattern of ret oncogene rearrangements in morphological variants of radiation-induced and sporadic thyroid papillary carcinomas in children. Cancer Res 57:1690-1694

Pierotti MA. 2001. Chromosomal rearrangements in thyroid carcinomas: a recombination or death dilemma. Cancer Lett. 166(1):1-7

Rosai J, Carcangiu ML, DeLellis RA. 1992. Atlas of tumour pathology: tumours of the thyroid gland, 3rd series. Washington, DC: Armed Forces Institute of Pathology

Santoro M, Thomas GA, Vecchio G, Williams GH, Fusco A, Chiappetta G, Pozcharskaya V, Bogdanova TI, Demidchik EP, Cherstvoy ED, Voscoboinik L, Tronko ND, Carss A, Bunnell H, Tonnachera M, Parma J, Dumont JE, Keller G, Hofler H, Williams ED 2000 Gene rearrangements and Chernobyl related thyroid cancers. British Journal of cancer 82:315-322

Santoro M, Carlomagno F, Hay ID, Herrmann MA, Grieco M, Melillo R, Pierotti MA, Bongarzone I, Della Porta G, Berger N. 1992. RET oncogene activation inn human thyroid neoplasms is restricted to the papillary carcinoma subtype. J Clin Invest 89:1517-22

Sheils OM, O'Leary JJ, Uhlmann V, Lattich K, Sweeney EC. 2000. Ret/PTC-1 activation in Hashimoto thyroiditis. International Journal of Surgical Pathol 8:185-189

Smyth P, Sheils O, Finn S, Martin C, O'Leary JJ, Sweeney EC. 2001. Real-time quantitative analysis of E-cadherin expression in ret/PTC-1 activated thyroid neoplasms. Int J Surg Pathol 9:265-72.

Sozzi G, Pierotti MA, Miozzo M, Donghi R, Radice P, De Benedetti V, Grieco M, Santoro M, Fusco A, Vecchio G, Mathew CGP, Ponder BAJ, Spurr NK. 1991. Refined localization to contiguous regions on chromosome 10q of the two genes (H4 and RET) that form the oncogenic sequence PTC. Oncogene 6(2): 339-42

Sugg SL, Ezzat S, Rosen IB, Freeman JL, Asa SL. 1998. Distinct multiple ret/ptc gene rearrangements in multifocal papillary thyroid neoplasia. J Clin Endocrinol Metab 83:4116-4122

Takahashi M, Ritz J, Cooper GM. 1985. Activation of a novel human transforming gene, ret, by DNA rearrangement. Cell. 42(2): 581-8.

Takahashi M. 2001. The GDNF/RET signalling pathway and human diseases. Cytokine Growth Factor Rev 12:361–373

Tallini G, Asa SL. 2001. RET oncogene activation in Papillary Thyroid Carcinoma. Adv Anat Pathol 8:345-354

Thomas GA, Bunnell H, Cook HA, Williams ED, Nerovnya A, Cherstvoy ED, Tronko ND, Bogdanova TI, Chiappetta G, Viglietto G, Pentimalli F, Salvatore G, Fusco A, Santoro M, Vecchio G. 1999. High prevalence of RET/PTC rearrangements in Ukrainian and Belarusian post-Chernobyl thyroid papillary carcinomas: a strong correlation between RET/PTC3 and the solid-follicular variant. J Clin Endocrinol Metab 84:4232-8

Wajjwalku W, Nakamura S, Hasegawa Y, Miyazaki K, Satoh Y, Funahashi H, Matsuyama M, Takahashi M. 1992. Low frequency of rearrangement of the ret and trk proto-oncogenes in Japanese thyroid papillary carcinomas. Jpn J Cancer Res 83:671-5

Wirtschafter A, Schmidt R, Rosen D, Kundu N, Santoro M, Fusco A, Multhaupt H, Atkins JP, Rosen MR, Keane WM, Rothstein JL. 1997. Expression of RET/PTC fusion gene as a marker for papillary carcinoma in Hashimoto's thyroiditis. Laryngoscope 107:95-100

Zou M, Shi Y, Farid NR. 1994. Low rate of ret proto-oncogene activation (PTC/ret^{TPC}) in papillary thyroid carcinomas from Saudi Arabia. Cancer 73:176-80

Chapter 4

Array CGH analysis of gamma irradiated human thyrocyte

4.1 Introduction

4.2 Summary

The susceptibility of thyroid epithelium to radiation-induced carcinogenesis is well recognized. In this context, thyroid carcinogenesis is associated with specific somatic *ret*/PTC rearrangements and morphologically with the papillary phenotype. Previous studies have demonstrated the possibility of inducing ret rearrangements in vitro using X-rays. The purpose of this study was to assess whether gamma radiation using a Caesium 137 source can induce specific *ret* rearrangements in a human thyroid epithelial cell culture model. We further hypothesized that if radiation induced thyroid carcinogenesis is associated with non-random rearrangement events then DNA copy gain and loss induced by irradiation may also occur in a non-random manner.

We irradiated SV40 (Simian virus 40) immortalized human thyroid epithelial cells (N thy-ori) with incremental doses of γ-radiation and using TaqMan RT PCR looked for the presence of the common ret rearrangements. Cohorts showing evidence of *ret*/PTC chimeric transcripts were further analyzed using microarray Comparative Genomic Hybridization (CGH) to detect copy gain and loss associated with radiation.

Four Gy of γ-radiation was sufficient to induce *ret*/PTC-3. In this model, transcripts of *ret*/PTC-1 were not detected and we suggest that the type of radiation may influence the resulting rearrangement that occurs. Using array CGH we have demonstrated a predominant pattern of subtelomeric deletions occurring in association with this radiation cohort and raise the possibility that chromosome 10 may be a hotspot for

radiation-induced damage for as yet unknown reasons. This pattern has been described in other tumours and it would be rewarding in the future to carry out array CGH on a cohort of post Chernobyl PTC with associated *ret*/PTC-3 rearrangement.

4.3. Radiation induced thyroid carcinoma

The susceptibility of the thyroid gland to radiation-induced carcinogenesis is well recognized, particularly when radiation exposure occurs at a young age. This applies especially to papillary thyroid carcinoma (PTC) developing in children. The evidence from epidemiological and molecular studies carried out both before and particularly after the Chernobyl nuclear disaster is compelling (Rubino, 2002). The excess relative risk per Gray (Gy) delivered to the thyroid has been estimated to be 7.7 (Ron, 1995) and this has been confirmed in subsequent studies (Lundell, 1994; De Valthaire, 1999). Exposure to radioactive iodine isotopes has correlated with increased incidence of PTC in contaminated children as occurred in the Marshall Islands (BRAVO thermonuclear test) in 1954 (Hamilton, 1987) and in Belarus and the Ukraine after the Chernobyl disaster in 1986 (Kazakov, 1992; Shibata, 2001).

In Papillary Thyroid Carcinoma we have seen that current molecular evidence indicates a major role for somatic rearrangements involving the *ret* proto-oncogene (chromosome 10q11.2) and to a lesser extent the *N-trk* gene (chromosome 1), in the pathogenesis of PTC. The emerging role of *BRAF* mutations is also currently being recognized (Kimura, 2003, Soares, 2003, Xu, 2003), with mutation of the *BRAF* gene now being recognised as the most common of all molecular genetic alterations in PTC

occurring as an alternative event to *ret* activation. However, as of yet no association between radiation induced PTC and *BRAF* mutations has been described (Xing, 2004; Nikiforova, 2004; Smyth, 2004).

Ret rearrangements have been discussed in Chapters 1 and 3. It is clear from the literature that ret rearrangements, particularly ret/PTC-3, are very likely to represent a radiation signature because of their prevalence in PTC occurring in children after the Chernobyl disaster (Thomas, 2001).

4.4 Array CGH

Comparative Genomic hybridization (CGH) is a technique that allows the detection of chromosomal copy number changes (gains and losses) across the entire genome. Array CGH in principle broadly conforms to traditional chromosomal CGH (Kallioniemi, 1992) but uses DNA target clones (P1, PAC or BAC clones) spotted onto a glass slide and therefore obviates the need for metaphase spreads and expert cytogenetic input (Hui, 2001; Pollack, 2002; Wilhelm, 2002). Microarray CGH is more sensitive than conventional CGH and shows higher resolution with precise mapping of amplicon boundaries and simplified data analysis. The Genosensor array 300 system (Vysis, Downer's Grove, Illinois) is a recently developed system and consists of an array of 287 DNA clones (spotted in triplicate) representing genomic regions that are important in cytogenetics and oncology. The array provides a powerful tool for genome wide evaluation of genomic instability manifest as copy gain and loss. However, as with conventional CGH, array CGH cannot detect structural chromosomal abnormalities not involving copy number changes, such as

balanced translocations, inversions, or ring chromosomes (Weiss, 1999). For conventional CGH, the resolution (minimal size of the DNA aberration that can be detected) is between 5MB-10MB and is homogeneous along the chromosomes (except around the centromeres).

For GenoSensor, the resolution can be as low as 100kb, but is not homogeneous along the chromosome. The targets used on the microarray have been selected on the basis of providing information on known regions of interest and the approximate coverage for each chromosome is 40Mb. A fully annotated list of the targets is available in appendix 1.

4.5 *In-vitro* studies of radiation on thyroid epithelium

Studies have demonstrated that previously non-neoplastic human thyroid cells can be transformed by single and fractionated doses of γ-irradiation in the range of 0.5 to 4.0 Gy and that these irradiated cells become tumourigenic in nude mice (Riches, 1994). Chromosomal instability has been described in a similar model of radiation-induced thyroid tumourigenesis using conventional cytogenetics, spectral karyotyping and conventional CGH (Zitelsberger, 2001). However, although these experiments demonstrated that previously non-tumourigenic thyroid cells became tumourigenic in nude mice after irradiation and elegantly describe the resulting cytogenetic profiles, the authors did not demonstrate the radiation signature of rearranged *ret* in the tumours examined. Work by Mizuno *et al* has demonstrated the possibility of inducing ret rearrangements *in vitro* using X-radiation (Ito, 1993, Mizuno, 2000). However, the type (X-irradiation) and dose (50 Gy) of radiation used in Mizuno's

experiment does not approximate Chernobyl conditions, where the major sources of radiation comprised predominantly Beta irradiation with a significant but smaller component of gamma radiation from various isotopes (Williams, 2002). In addition, the average dose received was lower (Gavrilin, 1999). There is no previous report of γ-irradiation induced ret rearrangements *in vitro* in the literature.

4.6 Aims

We decided to investigate if gamma (γ) irradiation at a dose comparable to the average dose at Chernobyl could induce either of the 2 common ret rearrangements. A Caesium 137 (^{137}Cs) source was used given that Caesium is a known contaminant persisting post Chernobyl, as an appropriate source of γ-radiation. (^{137}Cs is the second most abundant of three major radioactive isotopes released as a result of the Chernobyl disaster, the other two being Iodine 131 and Strontium 90, both of which release ß radiation). A further objective was to describe the pattern of DNA copy gain and loss in γ-irradiated cells using induction of rearranged *ret* as a surrogate endpoint

4.7 Materials and Methods

4.7.1 Cell Culture

The human thyroid epithelial cell line (N thy-ori 3-1 ECACC number 90011609) is derived from normal thyroid tissue of an adult. The cells have, however, been immortalised by transfection with a plasmid encoding for the Simian Virus 40 (SV40) large T antigen (Lemoine, 1989). It is of interest that SV40-like DNA sequences have previously been linked to papillary thyroid carcinoma although not in a causative role (Pacini, 1998).

4.7.2 Gamma Irradiation of Thyroid Cells

Irradiation was performed using the Gammacell 3000 Elan (MDS Nordion, Ottawa, Canada), which uses a ^{137}Cs γ source. During irradiation, the cells were passaged and resuspended briefly in PBS/10%FCS. Four irradiation cohorts were selected: 0Gy (control), 2Gy, 3Gy and 4 Gy. This range approximates the average doses received by children in the Belarus region of the Ukraine.

4.7.3 Nucleic acid extraction

Co-extraction of RNA and DNA was performed for each of the cell culture experiments using the Purescript and Puregene Gentra protocols respectively. Extracted total RNA was subsequently used for One Step TaqMan RTPCR (Applied Biosystems, Foster City, CA) to detect chimeric transcripts of the two most common ret rearrangements (*ret*/PTC-1 and *ret*/PTC-3).

4.7.4 TaqMan RT PCR

Reverse transcription and PCR of extracted total RNA was performed using a TaqMan One Step Reverse Transcription Reagent kit (Applied Biosystems, Foster city, CA). Target specific Primers and probes were designed using ABI Prism Primer Express 1.5 software (Applied Biosystems, Foster city, CA). Probes were designed to span the fusion points of the chimeric transcripts of *ret*/PTC-1 and *ret*/PTC-3 See Table 2.2, Section 2.9.4).

All probes used in the TaqMan™ reactions were designed to have non-fluorescent quenchers and minor groove binding (MGB) modifications. As previously described in chapter 2, MGB probes have low background fluorescence and bind more tightly to their target. This raises the T_m of the probes and allows for a more flexible assay design. Six negatives were included in each TaqMan run. These included 4 no template controls and 2 no amplification controls. *GAPDH* was used to confirm the integrity of the extracted RNA. Two replicates were run for each assay. For *ret*/PTC-1

detection, RNA from the cell line TPC-1 was included as a positive control. For *ret*/PTC–3 plasmid derived *ret*/PTC-3 cRNA transcripts were used. Thermal cycling was performed on an ABI PRISM 7000 Sequence Detection system (Applied Biosystems, Foster City).

4.7.5 Array CGH

Array CGH was performed as previously described in the materials and methods chapter (Section 2.12).

4.7.6 Reports and statistical analysis

The Vysis Array 300 software generates a report for each array. This report tabulates among other variables: the assigned target number, target clone name, cytogenetic location, and the number of spots included, mass to mean ratio (the mean over the number of contributing spots of the normalised per-spot test to reference ratios. Each spot's test to reference ratio is computed by first dividing the spot's total test intensity by its total reference intensity. This "raw ratio" is then converted to a normalised ratio by dividing by a normaliser whose value ensures that targets with modal DNA copy number in both the test and reference samples have ratios close to 1.0), the mass ratio coefficient of variation CV % (sample standard deviation/sample mean), and the p value for non-modality (for targets which apparently are non-modal, this is the p-value of the Null Hypothesis that the target has modal DNA copy number.

P-values for non-modal copy number are only computed for targets with at least two included spots. Only p-values less than 0.01 are displayed. With circa 300 targets on a chip, a p-value of 0.01 can be expected to occur randomly for about three modal targets. For this reason, in this study loci were only accepted as being reliably amplified or deleted on the following stringent conditions: The p value for the null hypothesis was <0.005 and all 3 spots are included and the mass ratio CV is less than or equal to 7.0%.

Two cohorts were examined. We selected non-irradiated N-thy-ori cells as the control and demonstrated absence of ret rearrangements in this control group. N-thy-ori cells irradiated with 4 Gy γ-radiation, in which ret rearrangements were demonstrable by RT PCR, were used to assess the effects of γ-irradiation. Both cohorts were of identical passage number. The normalised mass to mean ratio for each locus was tabulated for each of the 2 cohorts. Thresholds for gain of 1.2 and 0.8 for a loss were validated by Vysis. A control experiment was run in tandem with the experiment using with cell line DNA (CoSH mixture comprising three cell lines) provided by the manufacturer with known documented amplifications of a variety of oncogenes. The results generated were exactly concordant with those described by Vysis.

4.8 Results

4.8.1 Effects of irradiation on cell proliferation

Immediately after irradiation increased numbers of dead cells were noted in the irradiated flasks in comparison to control flasks. All of the irradiated cohorts suffered a lag period before achieving confluence again. During this post irradiation lag period the media was replaced at regular 3-day intervals. The period for the cells to become confluent varied in proportion to the dose of gamma radiation received i.e. 0 Gy cohort first sub-confluent at 5 days, 2 Gy cohort first sub-confluent at 18 days, 3 Gy cohort first sub-confluent at 24 days and 4 Gy cohort first sub-confluent at 27 days. This phenomenon reflects the increasing numbers of cells killed at the outset of the experiment due to an incremental dose of radiation (with a resultant smaller pool for regeneration) After this first long passage period the cells became sub-confluent more quickly and at the same rate as for non-irradiated cells (4-5 days). Each cohort of cells was grown for 50 days (10 passages each) after reaching their first post-radiation sub-confluence.

4.8.2 Morphological effects of irradiation on cells

Striking morphological differences became apparent between the irradiated cells and their non-irradiated counterparts. Irradiated cells showed marked elongation (spindling) and concordant cytomegaly and nucleomegaly (without marked increase in nuclear: cytoplasmic ratio. This appearance is often seen by pathologists in the radiation phenotype of cells reacting to radiation damage). The nuclear membranes of

the irradiated cells showed coarse irregularities and each nucleus contained increased numbers of nucleoli (Figures 4.1 and 4.2).

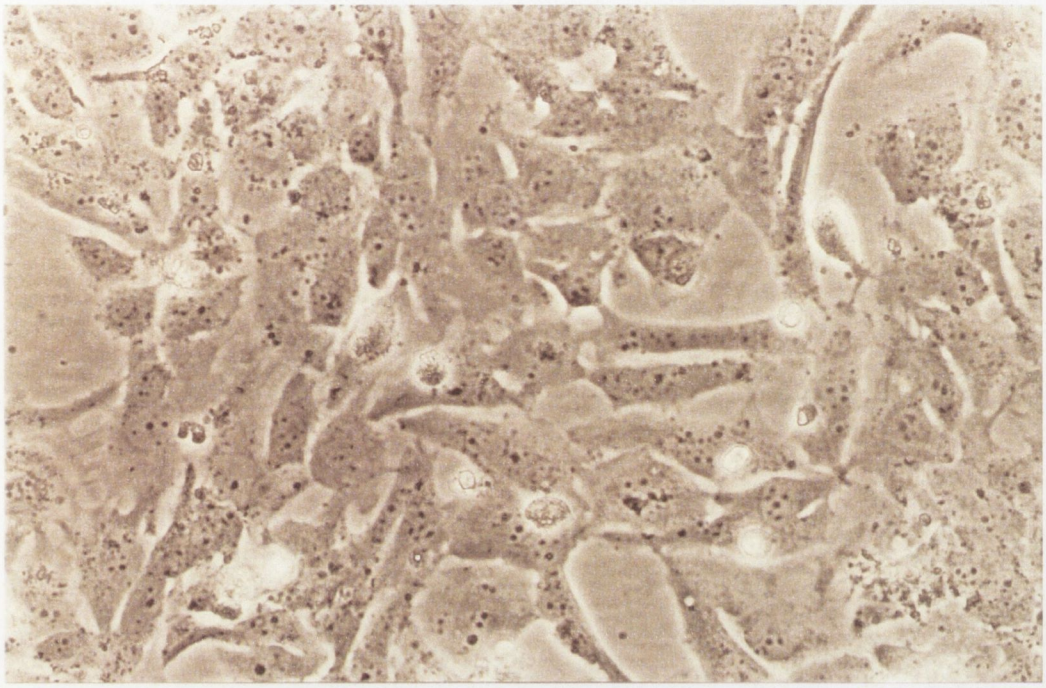

Figure 4.1 Irradiated cells Original magnification 20X

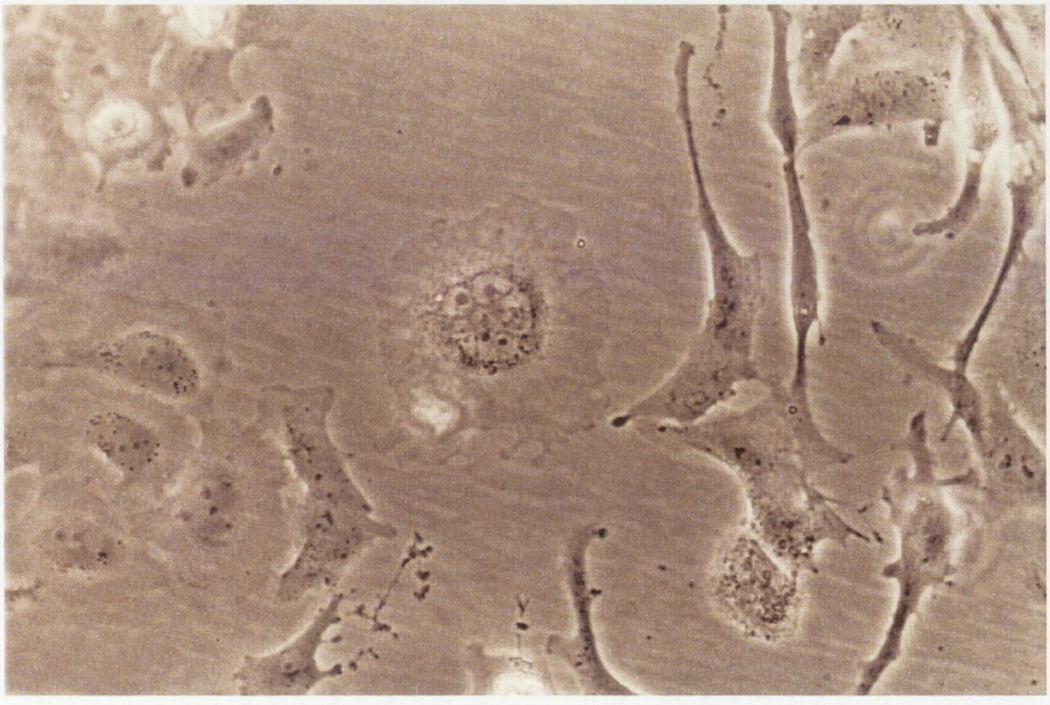

Figure 4.2 Irradiated Cells Original Magnification 40X

4.8.3 TaqMan RT PCR for *ret*/PTC-1 and *ret*/PTC-3

4.8.3.1 Control n-thy-ori cells

Neither ret/PTC-1 nor ret/PTC-3 was demonstrated in the non-irradiated control cell group at any time during the course of the experiment.

4.8.3.2 Irradiated N-thy-ori cells

Ret/PTC-1: The presence of chimeric transcripts of *ret*/PTC-1 could not be demonstrated in any of the 3 irradiated cell cohorts examined at any time before or after irradiation using sensitive RT TaqMan PCR. This applied both to aliquots of the cultured cells and to supernatants of the cell culture.

Ret/PTC-3: Chimeric transcripts of *ret*/PTC-3 were detected exclusively in the cohort of cells which received 4Gy γ-irradiation. *ret*/PTC-3 was detected in RNA extracted from cell aliquots and not from supernatants. Because rearranged *ret* is not expressed in normal cells an end point plus/minus (Presence or absence) TaqMan® assay was utilised at 99.9% confidence intervals. Expression of *ret*/PTC-3 was detectable after the first passage and until the third passage but not thereafter.

4.8.4 CGH array analysis

The results of the array CGH experiments are seen in Table 4.1. The gains and losses seen in the unirradiated cells represent the effects of SV40 mediated transformation. All amplifications were at a low level (1.2 to 3.0). The cytogenetic consequences of the immortalising effect of SV40 are reflected in the striking concordance of gain and loss at numerous loci. Additional statistically significant gains and losses occurred only in the irradiated cells. The irradiated cells show prominent loss of DNA sequences with occasional gains. Of the 23 additional aberrations or presumed aberrations in the irradiated cell line 87% (20 of 23) were deletions and 45% (9 of 20) of these deletions occurred distally on the chromosome at unique sub telomeric loci.

Target Number and Name	Non- irradiated N Thy-ori	Irradiated N thy-ori	Cytogenetic locus
006 D1S2660	Normal	Loss	1p36.32
038 D2S447	Loss	Loss	2q tel
039 3PTEL25	Loss	Loss	3p tel
040 3PTEL01,CHL1	Normal	Loss	3p tel
046 FHIT	Loss	Loss	3p14.2
048 D3S1274, ROBO1	Loss	Loss	3p12-3p13
053 TP63	Loss	Loss	3q27-q29
058 D4S114	Normal	Loss	4p16.3
064 PGRMC2	Loss	Loss	4q26
067 D4S2930	Loss	Loss	4q tel
071 DAB2	Normal	Loss	5p13
076 NIB1408	Gain	Gain	5q tel
077 5QTEL70	Gain	Gain	5q tel
078 9PTEL48	Gain	Gain	6p tel
079 PIM1	Normal	Loss	6p21.2
087 ESR1	Loss	Loss	6q25.1
089 G31341	Gain	Loss	7p tel
093 RFC2, CYLN2	Gain	Gain	7q11.23
099 stSG48460	Gain	Gain	7q tel
100 7QTEL20	Gain	Gain	7q tel
116 MTAP	Normal	Loss	9p21.3
126 10QTEL006	Gain	Normal (Loss)	10p tel
127 SHGC-44253	Gain	Normal (Loss)	10p tel
128 D10S249, D10S533	Gain	Normal (Loss)	10p15
131 BMI1	Normal	Loss	10p13
137 stSG27915	Gain	Gain	10q tel
138 10QTEL24	Gain	Normal (Loss)	10q tel
139 11PTEL03	Normal	Loss	11p tel
146 MEN1	Gain	Gain	11q13
154 MLL	Loss	Loss	11q23
155 WI-6509	Loss	Loss	11q tel
156 AF240622	Loss	Loss	11q tel
157 8M16/SP6	Gain	Gain	12p tel
158 SHGC-5557	Gain	Gain	12p tel
160 CDKN1B (p27)	Gain	Gain	12p13.1-p12
163 CDK2, ERBB3	Normal	Gain	12q13
172 D13S319	Normal	Loss	13q14.2
178 IGH (D14S308)	Gain	Gain	14q tel
182 UBE3A, D15S10	Loss	Loss	15q11-q13
185 FES	Normal	Loss	15q26.1
187 PACE4C	Normal	Loss	15q tel
189 16PTEL03	Gain	Normal (Loss)	16p tel

Target Number and Name	Non- irradiated N Thy-ori	Irradiated N thy-ori	Cytogenetic locus
190 stSG48414	Normal	Loss	16p tel
200 stSG30213	Normal	Loss	16q tel
209 D17S1296, D17S1523	Loss	Normal (Gain)	17p12-p11.2
214 BRCA1	Normal	Gain	17q21
241 AKT2	Normal	Loss	19q13.1-q13.2
244 20PTEL18	Gain	Gain	20p tel
245 SOX22	Gain	Gain	20p tel
246 JAG1	Gain	Gain	20p12.1-p11.23
247 MKKS, SHGC-79896	Gain	Gain	20p12.1-p11.23
248 TOP1	Gain	Gain	20q12-q13.1
249 NCOA3 (AIB1)	Gain	Gain	20q12
250 MYBL2	Gain	Gain	20q13.1
251 CSE1L (CAS)	Gain	Gain	20q13
252 PTPN1	Gain	Gain	20q13.1-q13.2
253 STK6 (STK15)	Gain	Gain	20q13.2-q13.3
254 ZNF217(ZABC1)	Gain	Gain	20q13.2
255 CYP24	Gain	Gain	20q13.2
256 TNFRSF6B (DCR3)	Gain	Gain	20q13
257 TPD52L2, TOM	Gain	Gain	20q tel
258 20QTEL14	Gain	Gain	20q tel
260 RUNX1 (AML1)	Gain	Gain	21q22.3
261 DYRK1A	Normal	Gain	21q22
263 PCNT2 (KEN)	Gain	Gain	21q tel
264 21QTEL08	Gain	Gain	21q tel
265 D22S543	Gain	Normal (Loss)	22q11
266 GSCL	Normal	Gain	22q11.21
268 TBX1	Normal	Gain	22q11.2
273 ARSA	Loss	Loss	22q tel
274 22QTEL31	Gain	Loss	22q tel
275 DXYS129	Normal	Loss	X/Yp tel
279 DMD exon 45-51	Loss	Loss	Xp21.1
280 DXS580	Loss	Loss	Xp11.2
281 DXS7132	Normal	Loss	Xq12
286 SRY	Loss	Loss	Yp11.3
287 AZFa region	Loss	Loss	Yq11

Table 4.1 Copy gains and losses in irradiated and non-irradiated cells

Note: The p value for the null hypothesis is <0.005 and all 3 spots are included and the mass ratio CV is less than or equal to 7.0%. (Gain or loss in brackets indicates a suggested gain or loss in comparison with the control cells).

Colour Key

Losses common to both:

Gains common to both:

Losses exclusive to Irradiated cells:

Gains exclusive to irradiated cells:

4.9 Discussion

The predominant exposure occurring after the Chernobyl accident was to ^{131}I with emission of β-radiation. Ingestion of contaminated milk by children with actively growing thyroid glands in the context of moderate Iodine deficiency is assumed to be the most likely reason for the marked increase in PTC that subsequently occurred (Williams, 2002). However, a significant and somewhat overlooked source of irradiation resulted from exposure to ^{137}Cs with release of γ-irradiation. The aims of this study were twofold. Firstly, to assess whether γ-irradiation is capable of inducing ret-rearrangements at a dose corresponding to the dose received by children in the Belarus area after the Chernobyl disaster and using a source of γ radiation (^{137}Cs) known to have been released and to have persisted after the initial radio-iodine shock.

Secondly, although post-irradiation and sporadic PTC is strongly associated with chromosomal rearrangements, a number of other genome wide biological consequences may result from exposure to ionizing radiation (Wright, 1999). We assessed the pattern of DNA copy gain and loss in irradiated immortalised thyroid cells showing evidence of *ret*/PTC-3 chimeric transcripts by RT-PCR, using the GenoSensor array system. Detection of a radiation specific rearrangement was used as the most appropriate available surrogate endpoint for an experiment investigating the effects of γ-irradiation on the genome of thyroid cells.

The present study shows for the first time that γ radiation can induce a ret rearrangement, namely *ret*/PTC-3. Induction of ret rearrangements by γ irradiation has

not been shown previously *in-vitro*. Although Riches *et al* demonstrated the tumourigenicity of γ irradiation (Riches, 1994, Zitelsberger, 2001, Riches, 2001) *ret* rearrangements were not described in the tumours that derived. Previously, cell culture models have shown that *ret*/PTC-1 could be induced in *"in-vitro"* X-ray treated tumour cell lines not showing *ret* activation/rearrangement prior to irradiation (Ito, 1993). Following this the *ret*/PTC-3 rearrangement was induced in normal human thyroid tissue transplanted into SCID mice after 50 Gy of X-ray exposure (Mizuno, 2000). However, in that study *ret*/PTC-1 was observed more frequently and persisted throughout the observation period of up to 60 days. The reasonable conclusion drawn by these authors is that although *ret*/PTC-3 can be induced by X-irradiation, *ret*/PTC-1 rearrangement appears to be preferentially induced by X-irradiation.

Like Mizuno, this study demonstrates transient expression of *ret*/PTC-3. This may be explained either by selective loss of the cells bearing the *ret*/PTC-3 rearrangement or alternatively by transcriptional silencing of expression of the rearranged genes. Some have argued that *ret* rearrangements are merely needed to initiate thyroid malignancy but may not play a central role in tumour progression and itis possible that silencing of expression may occur in this context.

Remarkably, we failed to demonstrate chimeric transcripts of *ret*/PTC-1 at any stage or in any cohort of γ irradiated cells. It is clear that *ret* rearrangements are highly specific for thyroid carcinogenesis. *ret*/PTC-3 is strongly associated with aggressive post Chernobyl PTC with a specific solid morphology occurring in children (Thomas et al., 2001) and with short latency (Smida, 1999). Indeed *ret*/PTC-3 may well be a

radiation specific signature, notwithstanding that it can be detected at a lower rate in sporadic PTC (Finn, 2003). The matter is complicated, however, by the findings of another important study (Bounacer, 1997). In this study the authors assessed the ret status of thyroid tumours developing in patients who had received radiation therapy (most commonly X-irradiation) for benign or malignant conditions during childhood or young adulthood. The most frequent rearrangement detected in this series was *ret*/PTC-1 (63%), not *ret*/PTC-3 (10%). In another review paper the question is begged as to why the types of ret rearrangement seen in PTC associated with accidental (Chernobyl) and therapeutic irradiation should be so different? These authors suggest that it may be explained because of the different types of radiation received (Sarasin, 1999), specifically X-irradiation related to therapeutic intervention and radioactive isotopes in relation to Chernobyl. Although the design and methodology of the current study and that of Mizuno *et al* are different, both studies, when considered together, raise the possibility that the *ret*/PTC-3 rearrangement may be associated with γ irradiation and/or β irradiation and the *ret*/PTC-1 rearrangement with X-ray irradiation. This interpretation would allow us to rationalise the conflicting literature regarding which rearrangement is more commonly associated with radiation.

The results of the CGH microarray analysis has to be interpreted carefully with due regard to the limitations of the experimental design. Our data provides a single snapshot of dominant gains and losses occurring in a cell culture system using demonstration of expression of the *ret*/PTC-3 rearrangement as a marker of the appropriate dose of irradiation. It must be acknowledged that this *in vitro* model cannot reflect *in vivo* selection processes that may operate in PTC. Furthermore, the data from the irradiated cells almost certainly represents an overall view of multiple

clones rather than a single clone and patterns of gain and loss reflect the dominant profile in the cells examined. For these reasons the pattern of gains and losses is likely to be more informative than specific loci involved.

The irradiated and non-irradiated cells are of equal passage number in order to allow for control of cell culture induced aberrations. The CGH profiles (Table 4.1) are identical at the majority of the loci examined and this reflects genomic instability induced in the normal thyroid cells by SV40 large T antigen transfection. This SV40 and cell culture mediated genomic stability is highlighted when comparison is made to Zitelsberger's conventional CGH data for the same cell line (Zitelsberger, 2001). Although the CGH profiles and array CGH profiles are in part coincident (Gains at chromosomes 5, 7, 10, 11q13, 12p, 16p, 20q13, 21, 22 and losses at 3p, 4q, and X) at certain loci, mutually exclusive aberrations are noted in both data sets. Figure 4.2 highlights the additional gains (Green) and losses (Red) seen in the irradiated cells in comparison to the non-irradiated cells.

In this model, gamma - irradiation appears to be predominantly associated with a pattern of loss of genetic material, which occurs relatively evenly spread out across the genome. However, it is noteworthy that the loss of DNA occurred mainly at sub-telomeric loci (40% of all losses). Although the clones are specific for unique regions at telomeres, the data is suggestive that the larger telomere itself may be susceptible to radiation damage. This is concordant with Zitelsberger's CGH study of tumours resulting from gamma irradiated thyroid epithelial cells. Telomeres cap chromosome ends and prevent end-to-end fusions and subsequent chromosome instability. Latre *et al* have demonstrated that chromosomes with shortened telomeres fuse to radiation-

induced DNA breaks and interfere with the correct rejoining of the broken ends (Latre, 2003).

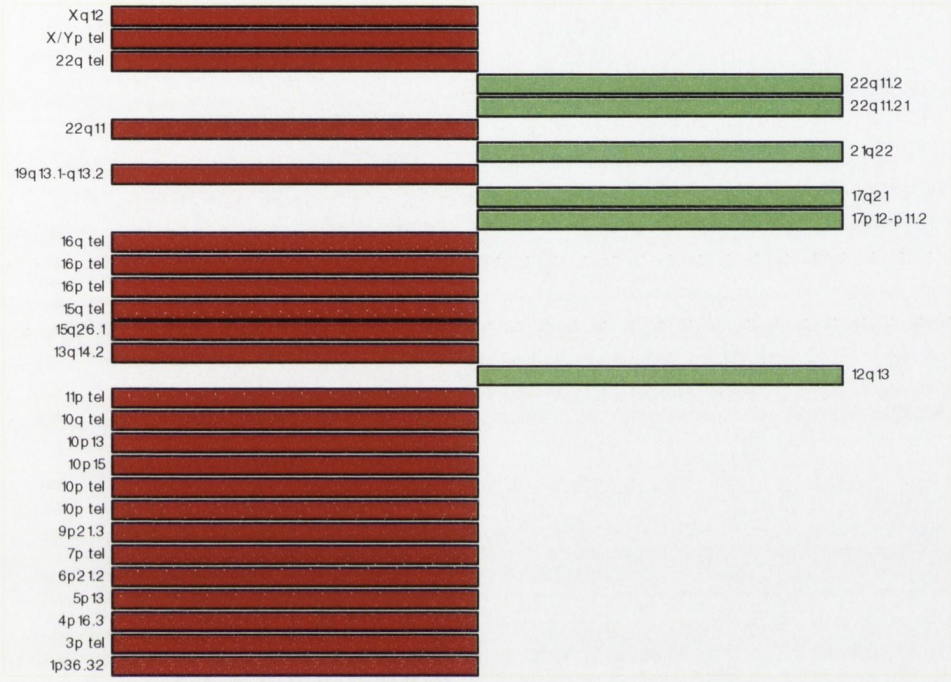

Figure 4.3 Irradiated cells: Distribution of statistically significant gains (Green) and losses (Red) according to locus

It is possible that radiation induced loss of telomeric DNA may explain the propensity for chromosomal rearrangements that occurs in PTC associated with radiation. It has also been shown that genomic instability occurs in successive generations of cells exposed to radiation. This instability preferentially affects telomeres and may play a role in radiation-induced carcinogenesis (Sabatier, 1995). Another study examined telomerase activity and telomere length in benign and malignant human thyroid tissues finding statistically significant telomere shortening in differentiated thyroid malignancies and follicular adenomas. This appears to occur even when telomerase is reactivated (Jones, 1998; Kammori, 2000).

It is also noteworthy that chromosome 10 appears to represent a "susceptible" chromosome in this radiation model. Given the known tendency for chromosome 10 to become involved in illegitimate rearrangements in radiation induced papillary thyroid carcinoma and its strong representation as a site of deletions in these data, it may well be that chromosome 10 is, for as yet unknown reasons, a hotspot for radiation induced thyroid carcinogenesis. Riches *et al* have shown high level amplification of 10p11.2 associated with a deletion of the remaining short arm segment of chromosome 10 distal to 10p11.2 in epithelial cells exposed to low dose γ-radiation (Riches, 1994). However, Zitelsberger's study shows gains associated with chromosome 10p rather than losses and it must be acknowledged that the occurrence of radiation-induced aberrations on chromosome 10 may be an entirely stochastic phenomenon (Zitelsberger, 2001), especially when one considers that the non-irradiated cells show over representation of amplifications of DNA on chromosome 10, consequently presenting a higher probability of sustaining irradiation induced damage.

In the present data, amplifications are uncommon (5 loci only). Although this may reflect sample heterogeneity, this is unlikely when one considers the abundance of deletions present. The detection of deletions is far more sensitive to sample heterogeneity than the detection of amplifications. Hence, it is reasonable to say that amplifications are uncommon in this model. Of interest, amplification of 17q21 (BRCA1) lie in proximity to 17q23 locus (not represented on the Vysis array 300 system). This locus (17q23) provides the donor gene (regulatory subunit RI-alpha of protein kinase A) for a rearrangement known as *ret*/PTC-2, which is implicated in minority of PTC (Bongarzone, 1994). TaqMan RTPCR is, however, sequence specific

and *ret* rearrangement assays used cannot detect the more rare *ret* rearrangements associated with radiation. Such detection would require many separate assays.

Previous conventional CGH studies of thyroid carcinoma tumours demonstrated that DNA copy number changes were rare in papillary carcinoma (Hemmer, 1999) (12% in one series) and when demonstrated were all shown to be gains and occurred in elderly patients. Our experience using this array system in sporadic PTC (Chapter 5) suggests that while copy number changes are low, both gains and losses occur. CGH data on radiation associated PTC is limited. One conventional CGH study included two cases of papillary thyroid carcinoma associated with a history of radiation (Kjellman, 2001). One of the two cases showed a gain on 17q, which correlates with the *in-vitro* data seen in this experiment. A second study performed extensive karyotyping (Zitelsberger, 1999) of Chernobyl related tumours by conventional cytogenetics, however, only one tumour had CGH and SKY performed and there are no large studies providing CGH profiles of post Chernobyl solid PTC associated with *ret*/PTC-3 rearrangement.

4.10 Conclusion

In conclusion, the current study demonstrates, for the first time, γ-irradiation induction of *ret*/PTC-3 *in-vitro* using a dose and a source of radiation that closely compares to what was received by those exposed to Chernobyl fallout. A true *in-vitro* model of post Chernobyl conditions is difficult to achieve requiring a mixture of radiation including both β-irradiation from ^{131}I and γ-irradiation from ^{137}Cs. However, this model more closely approximates an ideal model than previous X-irradiation based models. The failure to detect *ret*/PTC-1 is remarkable and, taken in the context

of the literature suggests that the type of radiation influences the type of *ret* rearrangement that evolves. Using array CGH we have demonstrated a clear pattern of deletion of genomic DNA with subtelomeric deletions occurring prominently.

4.11 References

Bongarzone I, Butti MG, Coronelli S, Borrello MG, Santoro M, Mondellini P, Pilotti S, Fusco A, Della Porta G, Pierotti MA. 1994. Frequent activation of ret proto-oncogene by fusion with a new activating gene in papillary thyroid carcinomas. Cancer Res 54:2979-85

Bounacer A, Wicker R, Caillou B, Cailleux AF, Sarasin A, Schlumberger M, Suarez HG. 1997. High prevalence of activating ret proto-oncogene rearrangements, in thyroid tumors from patients who had received external radiation. Oncogene 15:1263-73

De Vathaire F, Hardiman C, Shamsaldin A, Campbell S, Grimaud E, Hawkins M, Raquin M, Oberlin O, Diallo I, Zucker JM, Panis X, Lagrange JL, Daly-Schveitzer N, Lemerle J, Chavaudra J, Schlumberger M, Bonaiti C. 1999. Thyroid carcinomas after irradiation for a first cancer during childhood. Arch Int Med 159:2713-2720

Finn SP, Smyth P, O' Leary JJ, Sweeney EC, Sheils OM. 2003. Ret/PTC chimeric transcripts in an Irish cohort of sporadic Papillary Thyroid Carcinoma. J Clin Endocrinol Metab. 88:938-41

Gavrilin YI, Khrouch VT, Shinkarev SM, Krysenko NA, Skryabin AM, Bouville A, Anspaugh LR. 1999. Chernobyl accident: reconstruction of thyroid dose for inhabitants of the Republic of Belarus. Health Phys. 76(2):105-19.

Hamilton TE, Van Belle G, LoGerfo JP. 1987. Thyroid carcinoma in Marshall Islanders exposed to nuclear fallout. JAMA 258:629-636

Hemmer S, Wesenius VM, Knuutila S, Franssila K, Joensuu H. 1999. DNA copy number changes in thyroid carcinoma. American Journal of Pathology 154:1539-1547

Hui AB, Lo KW, Yin XL, Poon WS, Ng HK. 2001. Detection of multiple gene amplifications in glioblastoma multiforme using array based comparative genomic hybridization. Lab Invest. 81:717-23

Ito T, Seyama T, Iwamoto KS, Hayashi T, Mizuno T, Tsuyama N, Dohi K, Nakamura N, Akiyama M. 1993. In vitro irradiation is able to cause RET oncogene rearrangement. Cancer Res 53: 2940-2943

Jones CJ, Soley A, Skinner JW, Gupta J, Haughton MF, Wyllie FS, Schlumberger M, Bacchetti S, Wynford-Thomas D. 1998. Dissociation of telomere dynamics from telomerase activity in human thyroid cancer cells. Exp Cell Res 240:333-9

Kallioniemi A, Kallioniemi OP, Sudar D, Rutovitz D, Gray JW, Waldman F, Pinkel D. 1992. Comparative Genomic Hybridization for molecular cytogenetic analysis of solid tumours. Science 258:818-821

Kammori M, Takubo K, Nakamura KI, Furugouri E, Endo H, Kanauchi H, Mimura Y, Kaminishi M. 2000. Telomerase activity and telomere length in benign and malignant human thyroid tissues. Cancer Letters 159:175-181

Kazakov, VS, Demidchik EP, Astakhova LN. 1992. Thyroid cancer after Chernobyl. Nature 359:21-22

Kimura ET, Nikiforova MN, Zhaowen Z, Knauf J, Nikiforov YE, Fagin JA. 2003. High prevalence of BRAF mutations in Thyroid carcinoma: Genetic evidence for constitutive activation of the RET/PTC-RASBRAF signaling pathway in papillary thyroid carcinoma. Cancer Res 63:1454-1457

Kjellman P, Lagercrantz S, Hoog A, Wallin G, Larsson C, Zedenius J. 2001. Gain of 1q and loss of 9q21.3-q32 are associated with a less favorable prognosis in papillary thyroid carcinoma. Genes, Chromosomes & Cancer 32:43-49

Latre L, Tusell L, Martin M, Miro R, Egozcue J, Blasco MA, Genesca A. 2003. Shortened telomeres join to DNA breaks interfering with their correct repair. Exp Cell Res. 287:282-8

Lemoine NR, Mayall ES, Jones T, Sheer D, McDermid S, Kendall-Taylor P, Wynford-Thomas D. 1989. Characteristics of human thyroid epithelial cells immortalized *in vitro* by simian virus 40 DNA transfection. Br J Cancer 60:897-903

Lundell M, Hakulinen T, Holm LE. 1994. Thyroid cancer after radiotherapy for skin hemangioma in infancy. Radiat Res 140:334-339

Mizuno T, Iwamoto KS, Kyoizumi S, Nagamura H, Shinohara T, Koyama K, Seyama T, Hamatani K. 2000. Preferential induction of RET/PTC1 rearrangement by X-ray irradiation. Oncogene 19:438-443

Nikiforova MN, Ciampi R, Salvatore G, Santoro M, Gandhi M, Knauf JA, Thomas GA, Jeremiah S, Bogdanova TI, Tronko MD, Fagin JA, Nikiforov YE. 2004. Low prevalence of BRAF mutations in radiation-induced thyroid tumors in contrast to sporadic papillary carcinomas. Cancer Lett. 209(1):1-6

Pacini F, Vivaldi A, Santoro M, Fedele M, Fusco A, Romei C, Basolo F, Pinchera A. 1998. Simian virus 40-like DNA sequences in human papillary thyroid carcinomas. Oncogene 16:665-9

Pollack JR, Sørlie T, Perou CM, Rees CA, Jeffrey SS, Lonning PE, Tibshirani R, Botstein D, Børresen-Dale AL, Brown PO. 2002. Microarray analysis revels a major direct role of DNA copy number alteration in the transcriptional program of human breast tumors. PNAS 99:12963-12968

Riches AC, Herceg Z, Bryant PE, Wynford-Thomas D. 1994. Radiation-induced transformation of SV40-immortalized human thyroid epithelial cells by single and fractionated exposure to γ-irradiation *in vitro*. Int J Radiat Biol 66:757-765

Riches A, Peddie C, Rendell S, Bryant P, Zitzelsberger H, Bruch J, Smida J, Hieber L, Bauchinger M. 2001. Neoplastic transformation and cytogenetic changes after Gamma irradiation of human epithelial cells expressing telomerase. Radiat Res 155:222-229

Ron E, Lubin JH, Shore RE, Mabuchi K, Modan B, Pottern LM, Schneider AB, Tucker MA, Boice JD Jr. 1995. Thyroid cancer after exposure to external radiation: a pooled analysis of seven studies. Radiat Res 141:259-277

Rubino C, Cailleux AF, De Valthaire F, Schlumberger M. 2002. Thyroid cancer after radiation exposure. European Journal of Cancer 38:645-647

Sabatier L, Lebeau J, Dutrillaux B. 1995. Radiation-induced carcinogenesis: individual sensitivity and genomic instability. Radiat Environ Biophys 34:229-32

Sarasin A, Bounacer A, Lepage F, Schlumberger M, Suarez HG. 1999. Mechanisms of mutagenesis in mammalian cells. Application to human thyroid tumours. C R Acad Sci III. 322(2-3): 143-9

Shibata Y, Yamashita S, Masyakin VB, Panasyuk GD, Nagataki S. 2001. 15 years after Chernobyl: New evidence of thyroid cancer. Lancet 358:1965-1966

Smida J, Salassidis K, Hieber L, Zitzelsberger H, Kellerer AM, Demidchik EP, Negele T, Spelsberg F, Lengfelder E, Werner M, Bauchinger M. 1999. Distinct

frequency of ret rearrangements in papillary thyroid carcinomas of children and adults from Belarus. Int J Cancer. 80:32-8

Smyth P, Finn SP, Cahill S, O'Regan EM, Flavin R, O'Leary JJ, Sheils O. 2005. Timeline trends in ret/PTC and mutant BRAF expression in an Irish cohort of PTC. International Journal of Surgical Pathology 13(1): 1-8

Soares P, Trovisco V, Rocha AS, Lima J, Castro P, Preto A, Maimo V, Botelho T, Seruca R, Sobrinho-Simoes M. 2003. BRAF mutations and RET/PTC rearrangements are alternative events in the etiopathogenesis of PTC. Oncogene 22:4578-80.

Thomas GA, H. Bunnell, Cook HA, Williams ED, Nerovnya A, Cherstvoy ED, Tronko ND, Bogdanova TI, Chiappetta G, Viglietto G, Pentimalli F, Salvatore G, Fusco A, Santoro M, Vecchio G. 2001. High Prevalence of RET/PTC Rearrangements in Ukrainian and Belarusian Post-Chernobyl Thyroid Papillary Carcinomas: A Strong Correlation between *RET*/PTC3 and the Solid-Follicular Variant. J Clin Endocrinol Metab. 84:4232-8

Weiss M, Hermsen MAJA, Meijer GA, van Grieken NCT, Baak JPA, Kuipers EJ, van Diest PJ. 1999. Demystified... Comparative genomic hybridization. J Clin Pathol: Mol Pathol, 52:243-51

Williams ED. 2002. Cancer after nuclear fallout: lessons from the Chernobyl accident. Nature Reviews Cancer 2: 543-549

Wilhelm M, Veltman JA, Osshen AB, Jain AN, Moore DH, Presti JC, Kocacs G, Waldman FM. 2002. Array-based Comparative Genomic Hybridization for the differential diagnosis of renal cell cancer. Cancer Research 62:957-60

Wright EG. 1999. Inherited and inducible chromosomal instability: a fragile bridge between genome integrity mechanisms and tumourigenesis. J Pathol 187:19-27

Xing M, Vasko V, Tallini G, Larin A, Wu G, Udelsman R, Ringel MD, Ladenson PW, Sidransky D. 2004. BRAF T1796A transversion mutation in various thyroid neoplasms. J Clin Endocrinol Metab. 89(3): 1365-8

Xu X, Quiros RM, Gattuso P, Ain KB, Prinz RA. 2003. High prevalence of BRAF gene mutations in papillary thyroid carcinoma and thyroid tumor cell lines. Cancer Res 63:4561-4567

Zitelsberger H, Bruch J, Smida J, Hieber L, Peddie CM, Bryant PE, Riches AC, Fung J, Weier HU, Bauchinger M. 2001. Clonal chromosomal aberrations in Simian virus 40-transfected thyroid cells and in tumors developed after in vitro irradiation. Int. J. Cancer (Radiat, Oncol. Invest) 96:166-177

Zitelsberger H, Lehmann L, Hieber L, Weier HG, Janish C, Fung J, Negele T, Spelsberg F, Lengfelder E, Demidchik E, Salassidis K, Kellerer AM, Werner M, Bauchinger M. 1999.Cytogenetic changes in radiation induced tumors of the thyroid. Cancer Research 59, 135-1

Chapter 5

Assessment of DNA copy gain and loss in Papillary Thyroid Carcinoma using array Comparative Genomic Hybridisation

5.1 Summary

Previous conventional Comparative Genomic Hybridisation (CGH) studies of Papillary thyroid carcinoma (PTC) have demonstrated a low prevalence of copy gain and loss, with the majority of tumours showing no evidence of chromosomal instability. The technique of CGH has been improved, however, by the introduction of array CGH and by the use of laser capture microdissection to ensure pure cell populations for analysis.

In this chapter array CGH profiles of laser-captured thyrocytes from 11 well-characterised PTC with known *ret*/PTC and *BRAF* mutation status are described. The cohort includes 5 classic and 3 follicular variant tumours. In addition, three clonal PTC cell lines were examined. Results indicate that copy gain and loss occurs in all of the tumour cases and cell lines examined albeit at a low rate in surgical cases of PTC. Cell lines, as would be anticipated, show a higher number of aberrations than surgical tumour samples.

The most common recurrent aberrations involve gains on chromosomes 1, 5, 7, 11, 15, 17 and 22 with recurrent deletions occurring on chromosomes 4, 18 and 19. Independent analysis of the data from the eight tumour samples shows that amplifications of *TP73* (1p36.33), *SNRPN* (15q12) and *PDGFRB* (22q13.1) occur exclusively in tumours with a wild type *BRAF* status and variant morphology. None of the 8 tumour samples showed either of the 2 common *ret*/PTC rearrangements. This reflects the predominant prevalence of mutated BRAF that has been apparent in tumours occurring in Ireland since 1997 (Smyth, 2004).

This study of PTC shows a higher prevalence of aberrations than previously described in the literature. Recurrent patterns of gains and losses are seen with potential oncogenes identified in tumours with no currently well-described molecular trigger. Oncogenes and tumour suppressor genes, which may potentially act synergistically with *BRAF*^{V600E} mutation (resulting from base substitution T1799A), in the multistep pathogenesis of PTC are identified. The combination of laser capture microdissection and arrayed clones optimises studies utilizing CGH.

5.2 Introduction

PTC is thought to be a relatively genome stable neoplasm. In contrast to FTC, almost all PTCs are diploid (Johannessen, 1981). PTCs have been shown to be microsatellite stable (Soares, 1997) and generally show low levels of LOH (Kitamura, 2000; Gillespie, 2000). However, there is at least some evidence that allelic loss may occur and may be related to poor prognosis (Kitamura, 2000).

The literature has shown that PTC is associated with several specific molecular genetic events, the best documented of which are *ret*/PTC rearrangements and the more recently described *BRAF*^{V600E} mutation. Although activating point mutations of the *RAS* oncogene are also considered to account for the development of a small subset of adult sporadic PTCs (Namba, 1990), the true relevance of *RAS* mutations to the pathogenesis of PTC is undermined when one considers that similar mutations of the RAS gene have been documented at an even higher prevalence in nodules from benign multinodular goitres (21%) and benign microfollicular adenomas (25%) (Namba, 1990).

BRAF^{V600E} now appears to be the leading genetic event in adult sporadic (Non-radiation exposed) papillary thyroid carcinomas (Puxeddu, 2004; Kimura, 2003) and shows strong concordance with classic papillary phenotype. *Ret*/PTC and *BRAF* mutations appear to largely occur in a mutually exclusive manner (Soares, 2003), although overlap, the significance of which is currently unknown, occurs in a minority of cases (Smyth, 2004 in press; Nikiforov, 2004). Thus, *BRAF* mutations are the most frequent genetic aberration found in sporadic PTCs, and the mutation of one of the intermediates of the RET/PTC-RAS-BRAF pathway accounts for a genetic event, potentially involved in tumour initiation, in two thirds of PTCs (Kimura, 2003; Soares 2003). However, the genetic trigger(s) for the remaining one third of PTCs remains unknown. Furthermore, the Multistep Theory of Tumourigenesis predicts that more than one genetic or epigenetic event is associated with the subsequent development of carcinoma. Further work on the genetic events associated with initiation and progression of PTC is needed.

5.3 Comparative Genomic Hybridisation

Comparative Genomic Hybridisation (CGH) was first described in 1992 (Kallioniemi, 1992). CGH is a technique that allows comprehensive analysis of multiple DNA copy number gains and losses across the entire genome, in one single experiment. Genome wide analysis of DNA copy number changes by CGH has revealed a spectrum of recurrent chromosomal changes in cancer. Genes affected by

these chromosomal alterations are likely to be primary mediators of cancer initiation and progression.

The rationale of CGH is based on the assumption that the ratio of the binding of test and control DNA is proportional to the ratio of the number of sequences in the two samples. CGH incorporates the sensitivity of *in-situ* techniques and overcomes many of the disadvantages of conventional cytogenetic studies, as it bypasses the need for *in-vitro* tumour culture.

However, in conventional/classic CGH the identification of genes involved in chromosomal aberrations has been difficult. The difficulties in the identification of target genes for the recurrent chromosomal aberrations identified by CGH are partly due to the limited mapping resolution of this technique, which does not allow precise localization of the genetic aberrations (Kallioniemi, 1994; Bentz, 1998). The sensitivity of CGH can be adversely affected by contamination of tumour material with normal cells and a tumour component representing a minimum of 70% of the DNA extracted from the tissue is highly desirable. The use of laser capture microdissection or another microdissection technique is indispensable by ensuring near 100% tumour content for CGH experiments.

The sensitivity of CGH depends on the level and size of the copy number changes. Simulation experiments indicate that a copy number increase of 50% should be detectable if the region is 2 megabase pairs (Mb) or larger, and an amplified region (amplicon) of 250 kilobase pairs (kb) would need a 400% copy number increase to be detectable with conventional CGH (Joos, 1993). The lower limit of detection is determined by the product of the excess copy number and the size of the amplified

region. When a deletion is 100% (no copies present), a resolution of 1-2Mb can be achieved (Piper, 1995).

The use of arrayed DNA fragments, such as large-insert genomic clones or cDNA clones, as hybridisation targets has dramatically increased the resolution of CGH (Pinkel, 1998). Array-based CGH offers a higher resolution (down to ~ 100kb). A schematic of the array CGH concept is shown in Figure 5.1. The format of arrayed clones provides other advantages over the use of metaphase chromosomes, including the possibility of higher throughput and the facility to directly map aberrations to the genome sequence. In addition, the technique obviates the requirement for expertise in karyotyping. However, there are limitations. Array CGH is limited to a given number of genome loci and for this reason does not currently give information that is homogenous across the entire genome. A significant disadvantage is that there is a limitation to the degree to which the results obtained from conventional CGH and from array CGH can be directly compared.

5.3.1 Genosensor Array CGH (Vysis)

The Vysis Array 300 microarray contains triplicates of 287-target clone DNAs (P1 and BAC clones). Therefore, there are 861 discrete spots on the array. Appendix 1 details the clone names, cytogenetic location and Genbank accession number of these clones. The manufacturer has chosen clones that represent the most common oncogenes and tumour suppressor genes encountered in the scientific literature. In addition, the array includes clones, which mark known areas of loss of heterozygosity in cancer and loci of common microdeletions and unique

subtelomeric sequences relevant to other genetic diseases. Although the array provides an average of 40Mb coverage of each chromosome, it must be emphasised that this coverage is not homogenous along the chromosome and effectively amounts to 1% coverage of the entire genome. For this reason comparison between the Vysis array 300 and the results of conventional CGH are not straightforward. However, the Vysis array remains a powerful tool for investigating the pathobiology of cancer.

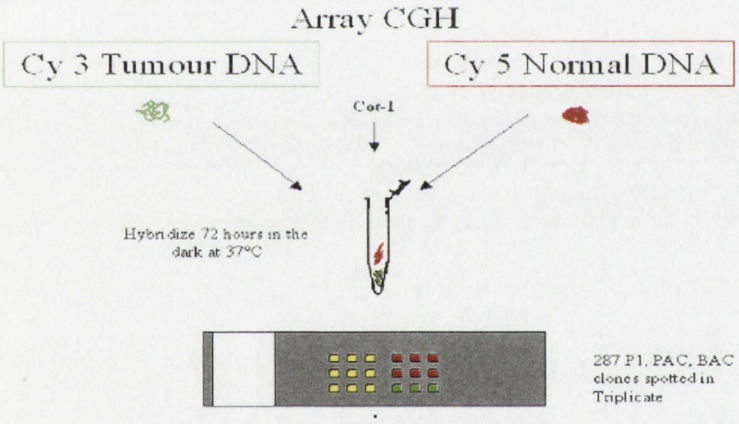

Figure 5.1 Schematic of array CGH

5.4 Aim

The aim of this chapter was to assess DNA copy number gain and loss in PTC tumour samples and clonal cell lines using the Genosensor array CGH platform. Cells from prospectively accessioned PTC were laser capture microdissected to ensure near 100% tumour content. The BRAF status and ret/PTC status of each of

the cases was assessed by TaqMan allelic discrimination assay and TaqMan RT PCR respectively. These molecular triggers are well described in PTC and the utility of array CGH analysis is enhanced because identification of candidate oncogenes and tumour suppressor genes in PTC with none of the well described molecular triggers is likely to reveal new molecular triggers and contribute to the understanding of the molecular pathogenesis of PTC. In those tumours with either ret/PTC or mutant BRAF recurrent aberrations may shed light on the multistep pathogenesis of PTC.

5.5 Materials and Methods

5.5.1 Tumours and Cell lines

Samples of PTC were prospectively collected and snap frozen at -80° C. Prior to laser capture microdissection and DNA extraction frozen section was performed to confirm presence and morphology of frozen tumour samples. PTC tumour cell lines were cultured and DNA harvested for CGH. Growth conditions and cell culture protocols were described in Chapter 2. Table 5.1 shows the details of the specimens and cell lines included in the study.

5.5.2 Laser Capture Microdissection and Nucleic acid Extraction

Laser capture microdissection was performed on frozen sections stained with HE and both DNA and RNA were extracted from the pure tumour cell populations captured. Nucleic acid extraction was performed using Gentra protocols as described in Chapter 2.

5.5.3 Ret/PTC rearrangement analysis

Chimeric transcripts of ret/PTC-1 and ret/PTC-3 were detected using breakpoint-spanning probes with minor groove binding modifications as described in chapter 2. Amplification of PCR products was detected in real time. Positive control material included the use of the TPC-1 cell line, which is known to express ret/PTC-1 transcripts and cRNA derived from a previously cloned ret/PTC-3 containing plasmid.

5.5.4 BRAF Assay

An allelic discrimination type TaqMan® assay was used to type the presence and zygosity of $BRAF^{V600E}$. Laser capture microdissection ensured pure populations of malignant cells to prevent contamination by normal cells with wild type BRAF sequences. The primer sequences and cycling conditions for this assay are described in Chapter 2. Positive control material was provided by Dr. Paula Soares (IPATIMUP, Portugal) in the form of cell lines of known BRAF mutation status:

K2	Heterozygous for $BRAF^{V600E}$
BCPAP	Homozygous for $BRAF^{V600E}$
TPC1	Wild type BRAF

Figure 5.2 shows the typical data output from the Allelic discrimination assay.

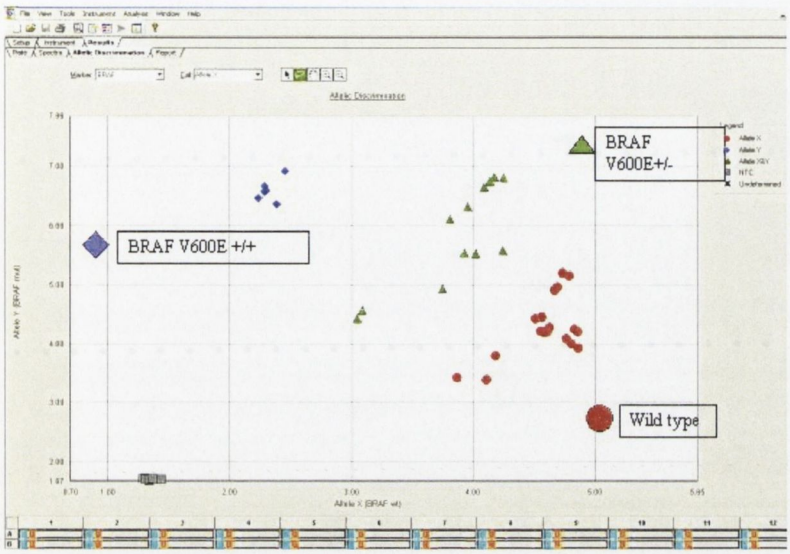

Figure 5.2: Allelic discrimination plot

5.5.4 CGH

Array CGH was performed as described in the Chapter 2. TPC-1, BCPAP and K2 Papillary Thyroid Carcinoma cell lines, which had been used as sources of control material were also analysed by CGH. Laser capture microdissection was used to ensure homogeneous populations of tumour cells.

5.5.5 Controls for CGH

5.5.5.1 Validation of technique using a control DNA (COSH)

CoSH is a control and validation DNA provided by Vysis. The DNA consists of a mixture of DNAs extracted from 3 tumor cell lines (COLO 320 HSR, SJSA-1 and BT-474). The mixture of cell lines has known amplifications of MYC, GLI and MDM2, among others. Array CGH of COSH was used as an external validation of

operator technique for each batch of experiments. Array CGH performed on COSH revealed amplifications of these genes in accordance with the data from Vysis.

5.5.5.2 Validation of the sensitivity of the system using sex mismatched test and reference

There is no internal control clone or group of clones with the Vysis Genosensor system that can be used for internal experimental validation. One potentially useful way to incorporate an internal control is to use reference DNA of the sex opposite to that of the sample being arrayed (i.e. Male Sample, XY: Female Reference XX). In cases where the sex chromosomes are unaffected by tumour associated aberrations, the results will indicate loss of the X chromosome loci with gain of the Y chromosome loci. This strategy is straightforward for pre/post-natal clinical samples. With oncology samples, more discrepancies are seen within the sex markers, and fewer markers may be detected than with a normal blood. For the sex markers there are five of the 11 X chromosome loci and both the Y chromosome loci that can be reliably used to determine the confidence in the results. The reliable loci on the X chromosome are STS 3' (Xp22.3), STS5' (Xp22.3), KAL (Xp22.3), AR 3' (Xq11-q12) and XIST (Xq13.2). The two Y loci on the array are SRY (Yp11.3) and AZFa (Yq11). Of course true tumour associated aberrations may affect these loci and anomalous results may therefore occur. The other markers are not always detected due to some homology between X and Y for those specific clones (Personal Communication, Dr. Teresa Ruffalo, Vysis). For these reasons and because the sex of the cell lines was not known in two cases (Cases 1 and 2) amplifications and deletions involving the X and Y chromosome were not included in the results.

To determine the variations in the ratios of the spots in normal control DNA, comparative hybridisations using test and reference DNA from three normal samples were performed. This approach has been used previously by many other groups (Albrecht, 2004; Schraml, 2003; Hui, 2001). Mean ratio of the normal array CGH was 1.01 for each of the 3 hybridisations. The standard deviation was 0.09. A value of the mean ratio +/- two standard deviations was set as the cut-off level for normal gene copy number. Ratios of higher than 1.19 and lower than 0.81 were considered to have copy gain and copy loss respectively. This correlates closely with the manufacturer recommended figures of 0.8 and 1.2 for a loss and a gain respectively.

Case	1	2	3	4	5	6	7	8	9	10	11
Description	Cell Line K2	Cell Line TPC1	Cell Line BCPAP	Surgical	Surgical	Surgical	Surgical	Surgical	Surgical	Surgical	Surgical
Age	NA	NA	76	26	51	39	30	73	36	23	37
Sex	NA	NA	F	F	F	M	F	M	F	F	M
Tumour Size cm	NA	NA	NA	2	2.5	1.2	6.0	2.5	1.9	2.2	1.3
Morphology	NA	NA	NA	Classic	Classic	Classic	Classic	Mixed	FV	FV	FV

NA-Non applicable.
FV-Follicular Variant

Table 5.1 Case profiles

Case		7	11
Test/Reference		Female/Male XX/XY	Male/Female XY/XX
Target number/Name	Chromosome	T/R Ratio	T/R Ratio
276 STS 3'	X	1.456	0.755
277 STS 5'	X	1.318	0.653
278 KAL	X	1.068	0.723
282 AR 3'	X	1.396	0.562
283 XIST	X	1.212	0.791
286 SRY	Y	1.180	1.713
287 AZFa region	Y	0.800	1.891

T/R-Normalised Test to Reference fluorescence ratio

Table 5.2 Sex mismatched controls

Internal validation was performed in two of the cases (Cases 7 and 11), Table 5.2. In Case 7 (Female Test and Male reference) 4 of 5 expected gains on the X chromosome and 1 of 2 expected deletions on the Y chromosome were detected. In Case 11 (Male Test and Female Reference) 5 of 5 expected losses and 2 of 2 expected gains were detected. In cases where the sexes were matched, occasional aberrations of the X and Y loci were identified and this may rationalise the anomalous ratios for KAL and SRY that occurred in case 7.

5.5.5.3 Validation using previously described conventional CGH profiles of BCPAP cell line

Corso *et al* have published conventional metaphase CGH profiles of the cell line BCPAP (Corso, 2002). Although, as discussed above, strict and exact comparisons between metaphase CGH and array CGH are difficult some conclusions can be

drawn. Corso demonstrated gains of chromosome 1 (1p11~p31.2), chromosome 5 (5p14~q22), chromosome 11 (11p11~p14.2 and 11q14-q22.5) and chromosome 20 (20p13~q13). Losses were demonstrated on chromosome 7 (7q21.3~q22), chromosome 9 (9p13.2~p24). All of these aberrations were reproduced by the Vysis system. Discordant aberrations were also noted which serve to illustrate the inherent instability and variation of cell lines and the difficulty of comparing two different techniques.

Terminology. In the literature, the term gain usually refers to an additional 1, 2 or 3 copies of a particular region. Amplification typically refers to an increase of greater than three copies.

5.6 Results

5.6.1 Analysis Cohort

The cohort analysed consisted of three cell lines and 8 prospectively accessioned PTCs comprising 4 classic morphology PTC, 3 follicular variant PTC and a single case of PTC (Case 8) with multi divergent differentiation including areas of classical morphology, follicular variant morphology, diffuse sclerosis and mucoepidermoid differentiation. With regard to this case, all of these areas were separately micro dissected and no evidence of expression of either of the two common ret rearrangements or of mutant BRAF was detected in any of the distinct morphologic areas. CGH was performed on DNA from a single sample acquired from cells from all these variable areas.

5.6.2 Ret/PTC and BRAF mutation status (Table 5.3)

Chimeric transcripts of ret/PTC-1 were detected in the TPC-1 cell line, which is known to express ret/PTC-1. No surgical tumour case showed evidence of ret/PTC-1. Ret/PTC-3 was detected in none of the 11 samples. Homozygousmutations of BRAF (V600E) were detected in the homozygous control cell line (BCPAP) and in 3 surgical cases (Cases 4, 5 and 6). The occurrence of $BRAF^{V600E}$ was seen in association with 3 of 4 classic variant PTCs and not in any of the 3 cases of FVPTC. Heterozygous mutation of BRAF was detected in the heterozygous control K2 cell line (Case 2).

Case Number		Rearranged ret Status	Mutated BRAF Status	Morphology
1	K2	Negative	V600E+/-	Cell line
2	TPC-1	Ret/PTC-1	Wild Type	Cell line
3	BCPAP	Negative	V600E+/+	Cell line
4		Negative	V600E+/-	Classic
5		Negative	V600E+/-	Classic
6		Negative	V600E+/-	Classic
7		Negative	Wild	Classic
8		Negative	Wild	Multidivergent
9		Negative	Wild	FV
10		Negative	Wild	FV
11		Negative	Wild	FV

V600E+/+ Homozygous for mutant BRAF
V600E+/- Heterozygous for mutant BRAF
Wild both alleles wild type BRAF
FV Follicular Variant

Table 5.3 rearranged ret and mutant BRAF status

5.6.2 Array CGH

5.6.2.1 General Trends

Array CGH revealed DNA sequence copy number changes in all 3-cell lines and all 8 surgical cases of PTC examined. The numbers of amplifications and deletions were expressed as a percentage of the number of somatic loci on the array (N=273). With array CGH, this approach more accurately reflects the degree of genetic

instability than the total number of aberrations per case commonly used in presenting metaphase CGH data results. Results from the 13 sex chromosome loci were not included because sex chromosomes were used for validation as discussed above. A single somatic cell locus was excluded because although present on three of the arrays it was not reliably spotted on later array batches.

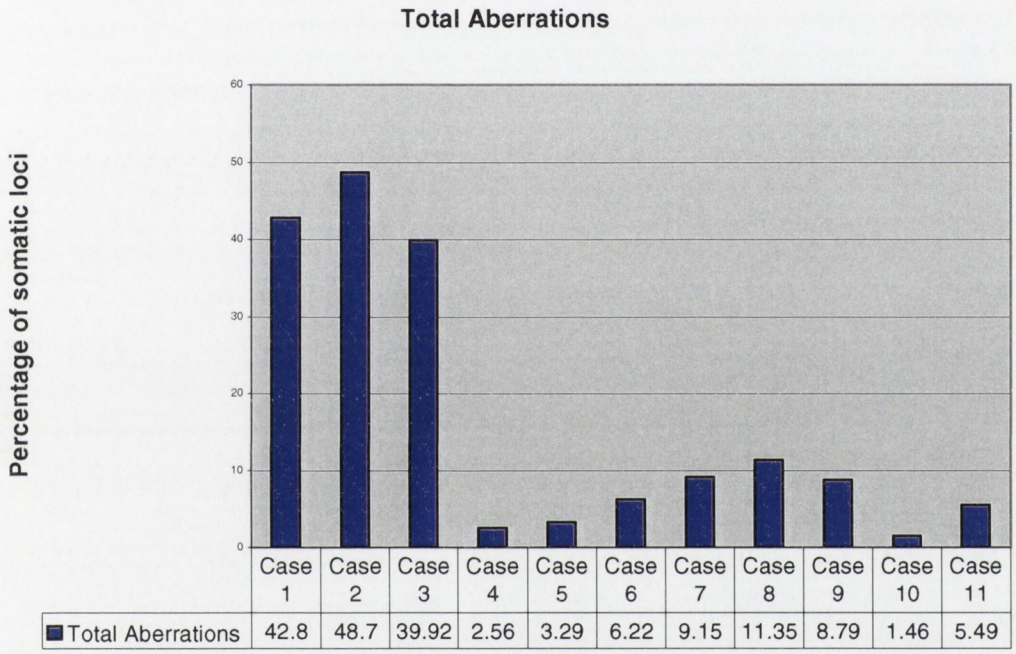

Figure 5.3 Aberrations expressed as a percentage of loci analysed

Aberrations (including both gains and losses) were detected in all cases and aberrations were detected at a higher rate in cell lines (Mean 43.8%) than in surgical tissue samples (Mean 6%). See Figure 5.3. The percentage of aberrations detected per locus examined in the tissue samples showed no significant association with either the morphological subtype (Follicular variant or classic PTC) or the mutation status (*BRAF* wild type v *BRAF* ^{V600E}).

Figure 5.4 demonstrates the percentage of gains and losses per case analysed and demonstrates that both gains and losses occurred in each tumour and cell line with no significant predominance of one versus the other.

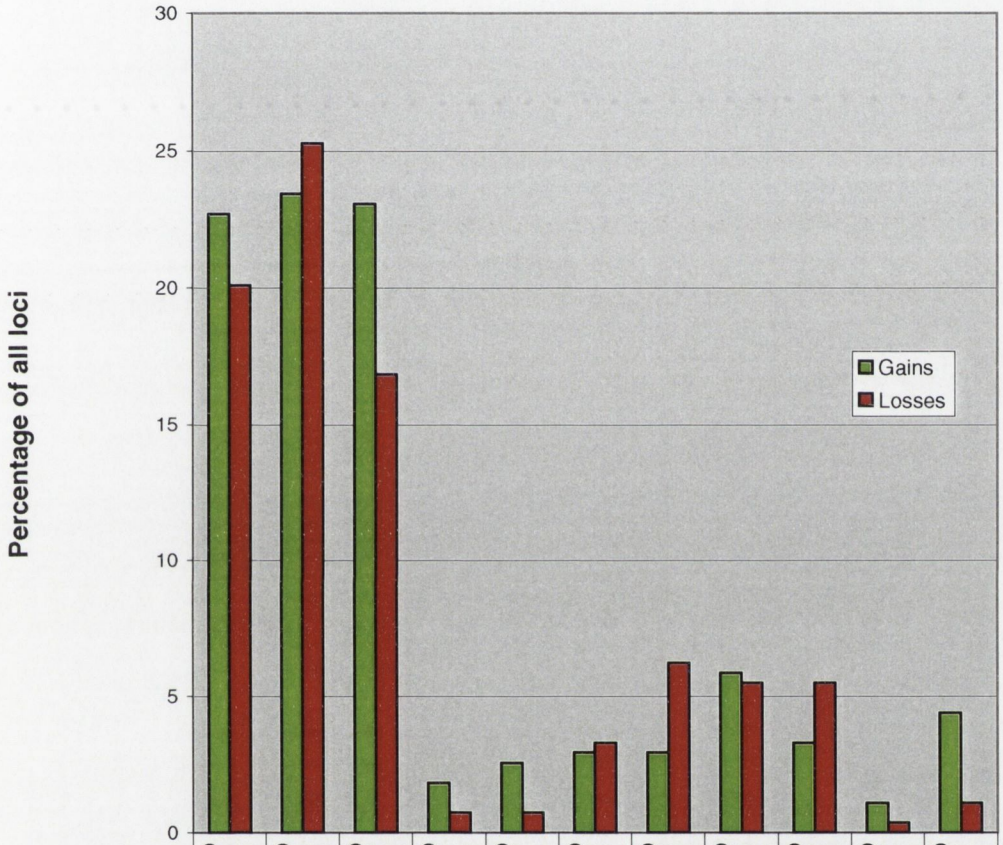

	Case 1	Case 2	Case 3	Case 4	Case 5	Case 6	Case 7	Case 8	Case 9	Case 10	Case 11
Gains	22.7	23.44	23.07	1.83	2.56	2.93	2.93	5.86	3.29	1.09	4.39
Losses	20.1	25.27	16.84	0.73	0.73	3.29	6.22	5.49	5.49	0.36	1.09

Figure 5.4 Gains and losses as a percentage of total somatic loci analysed

Figure 5.5 shows the fluorescence ratios for all the cases examined across all the somatic loci. Large amplifications only occurred in cell lines (High peaks in cases 1 and 2). For all other cases, the maximum fluorescence ratio for a gain never

exceeded 2.5. This indicates that no high-level amplifications of any of the loci occurred in surgical tissue samples.

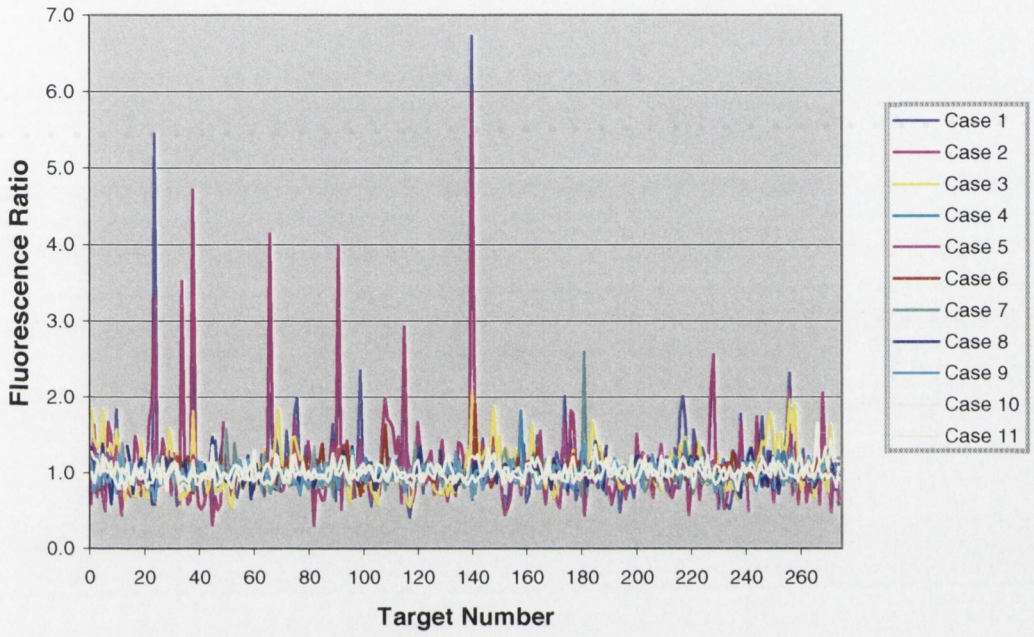

Figure 5.5 Test to reference fluorescence ratios for all cases across all loci examined

5.6.2.2 Recurrent gains and losses

Tables 5.4 and 5.5 show recurrent gains and losses respectively occurring in all the cell lines and tissues examined. An arbitrary cut off threshold of 20% was used to exclude common aberrations occurring at low frequency.

Locus	Target Number and Name	Percentage of all cases with gains	Comment
1p tel	001 CEB108/T7	27.27%	Sub Tel
1p tel	002 1PTEL06	27.27%	Sub Tel
1p36.33	005 TP73	36.36%	
1p36.2-p36.1	010 FGR (SRC2)	40.00%	Oncogene
2p tel	024 U32389	27.27%	Sub Tel
2q tel	038 D2S447	27.27%	Sub Tel
3p21.3	045 RASSF1	27.27%	TSG
3q21-q22	049 RBP1, RBP2	22.22%	
4q tel	066 4QTEL11	20.00%	Sub Tel
5p tel	068 C84C11/T3	36.36%	Sub Tel
5q33-q35	075 CSF1R	36.36%	
7p tel	089 G31341	27.27%	Sub Tel
7p12.3-p12.1	091 EGFR	36.36%	Amp/Gain
7q11.23	093 RFC2, CYLN2	36.36%	
7q tel	099 stSG48460	27.27%	Sub Tel
8p22-q21.3	108 E2F5	27.27%	Amp
9ptel	115 D9S913	27.27%	Sub Tel
11p tel	140 INS	27.27%	Sub Tel
11p15.5	141 HRAS	27.27%	Amp
11p15.5	142 CDKN1C (p57)	36.36%	TSG
11q13	147 CCND1	27.27%	Amp
11q13	148 FGF4, FGF3	36.36%	Amp
12p tel	157 8M16/SP6	20.00%	Sub Tel
12q13	163 CDK2, ERBB3	27.27%	Amp
13q tel	174 D13S327	27.27%	Sub Tel
14q32.32	177 AKT1	27.27%	Amp
15q12	181 SNRPN	36.36%	
15q26.1	185 FES	27.27%	Amp
17q11.2	217 THRA	30.00%	Amp
17q21-q22	218 TOP2A	36.36%	Amp
18p11.32	228 TYMS (TS)	20.00%	Amp
20q13	256 TNFRSF6B (DCR3)	27.27%	Amp
20q tel	258 20QTEL14	27.27%	Sub Tel
22q11.2	268 TBX1	20.00%	
22q13.1	271 PDGFRB (SIS)	36.36%	Amp

Amp -Cancer Amplicon previously described in the literature
TSG - Tumour Suppressor Gene
Oncogene - Known Oncogene
Sub Tel - Sub Telomeric sequence

Table 5.4 Recurrent gains

Locus	Target Number and Name	Percentage of all cases with losses	Comment
1p36	003 CDC2L1 (p58)	27%	
1p13.2	015 NRAS	27%	Amp
1q tel	023 1QTEL10	27%	Sub Tel
2q23-q37	033 TBR1	27%	
2q33.3-q34	036 ERBB4 (HER-4)	27%	Oncogene
3p12-3p13	048 D3S1274, ROBO1	20%	LOH
3q26.3	052 PIK3CA	36%	Amp
5q tel	077 5QTEL70	27%	Sub Tel
8p22	103 CTSB	27%	Amp
9p11.2	118 AFM137XA11	27%	
10p tel	127 SHGC-44253	20%	Sub Tel
10p13	131 BMI1	27%	
10q23.3	134 PTEN	27%	TSG
12q23	167 DRIM, ARL1	27%	
17p13.3	206 PAFAH1B1 (LIS1)	20%	
18q21.3	233 BCL2 3'	30%	Amp
19p tel	237 stSG42796	45%	Sub Tel

Amp -Cancer Amplicon previously described in the literature
TSG - Tumour Suppressor Gene
Oncogene - Known Oncogene
Sub Tel - Sub Telomeric sequence

Table 5.5 Recurrent losses

Because of the great number of aberrations seen in the 3 cell lines in comparison with prospectively collected tissue samples and also because of the known inherent genomic instability of cell lines, the data for the tissue samples was independently analysed for recurrent aberrations occurring exclusively in the 8 tissue samples. Recurrent gains and losses present in the 8 laser capture micro dissected surgical cases are presented in Tables 5.6 and 5.7 respectively.

Locus	Target Number and Name	Percentage of surgical cases with gains	Number of cases	Comment
7q21.3-q22	096 SERPINE1	25%	2/8	
11q13	148 FGF4, FGF3	25%	2/8	Amp
15q12	181 SNRPN	38%	3/8	
15q26.1	185 FES	25%	2/8	
22q13.1	271 PDGFRB (SIS)	38%	3/8	Amp

Table 5.6 Recurrent Gains detected in surgical cases

Locus	Target Number and Name	Percentage of surgical cases with losses	Numbers of cases	Comment
1p tel	002 1PTEL06	25%	2/8	Sub Tel
1q tel	023 1QTEL10	38%	3/8	Sub Tel
2p tel	024 U32389	25%	2/8	Sub Tel
2p13-p12	028 REL	25%	2/8	Amp
2q tel	038 D2S447	25%	2/8	Sub Tel
4p16.3	059 WHSC1	25%	2/8	
5q tel	077 5QTEL70	38%	3/8	Sub Tel
11p tel	140 INS	25%	2/8	Sub Tel
15q tel	188 WI-5214	25%	2/8	Sub Tel
19p tel	237 stSG42796	38%	3/8	Sub Tel
20p tel	244 20PTEL18	25%	2/8	Sub Tel

Table 5.7 Recurrent losses detected in surgical cases

A stated aim of this study was to look for potential molecular triggers in those PTC lacking either mutant BRAF or ret/PTC activation. Table 5.8 demonstrates that gains of PDGFRB (22q13), TP 73 (1p36.33) and SNRPN (15q12) were exclusively detected in tumours without these known molecular triggers.

Case number	PDGFRB (Sis) Gain 22q13	TP73 Gain 1p36.33	SNRPN Gain 15q12	BRAF Status	Morphology
4	Normal	Normal	Normal	V600E+/-	Classic
5	Normal	Normal	Normal	V600E+/-	Classic
6	Normal	Normal	Normal	V600E+/-	Classic
7	Normal	Normal	Gain	Wild	Classic
8	Gain	Gain	Gain	Wild	Mixed
9	Gain	Gain	Gain	Wild	FV
10	Normal	Normal	Normal	Wild	FV
11	Gain	Gain	Normal	Wild	FV

Table 5.8 Recurrent gains (Highlighted) in relation to BRAF mutation status and morphology

5.7 Discussion

The aim of these experiments was to perform an assessment of DNA copy gain and loss occurring in both Papillary Thyroid Carcinoma cell lines and prospectively collected surgical samples of PTC. The rearranged ret and BRAF mutation status of each case was analysed so as to allow any candidate genes to be assessed with reference to the already known classic molecular triggers of PTC. No case showed expression of ret/PTC-3. Only the TPC-1 cell line showed the expected expression of ret/PTC-1. All of the cases were collected over the last two years and the absence of ret activation reflects a temporal trend that our group has noted in PTC accessioned over the last 20 years. This temporal trend has shown ret/PTC chimera detected for the most part pre-1997 and BRAF mutations being more prevalent post-1997. The results suggest that some environmental/etiological agent(s) may have influenced the pathobiology of thyroid tumour development, among the population examined, over time (Smyth, 2004). In this cohort of PTC mutant BRAF was exclusively detected in tumours of classic papillary morphology. This finding is consistent with the recent literature.

Previous studies in the literature have used varying technological approaches to identify candidate oncogenes and tumour suppressor genes in PTC. Classic cytogenetic studies identified abnormalities in 27% of cases, with the most common recurrent changes involving inv (10) (q22.2q21.2) in 7%, t (10; 17) (q11.2; q23) in 3% and chromosome 1 aberrations in 3% of cases (Pierotti, 1996; Ward, 1998). Losses of Heterozygosity (LOH) studies have also yielded a low rate of detection of aberrations (23%) without any identifiable predilection to specific chromosomal loci

(Ward, 1998; Hermann 1991). However, Califano showed higher levels of LOH (Califano et al, 1996) than other groups.

CGH is a powerful molecular cytogenetic method that provides enhanced ability to screen solid tumours for genetic aberrations without prior knowledge of potential aberrations, as is required for LOH studies. Previous CGH studies of PTC have yielded varying results. All of the previous studies have used conventional metaphase CGH. Chen identified several novel copy number changes at a low prevalence in 16 cases of PTC, including gains at chromosome arms 1p34 (4 cases), 1p36 (5 cases) 1q42 (4 cases), 2p21 (3 cases), 2p13 (3 cases), 5q31 (3 cases), 5q33-34 (4 cases), 9q32-34 (4 cases), 14q32 (5 cases), 16q22-24 (4 cases), 19q13.1 (8 cases) and a loss at 16q12-q13 (3 of 16 cases) (Chen, 1998).

In the present study it was possible to corroborate Chen's findings at several loci including the gains of 1p34, 1p36, 5q31, 5q33-34, 14q32 and the loss at 16q12-13 (Tables 5.4 and 5.5). In some cases the Vysis array does not contain clones mapping to loci detected by Chen e.g. 1q42, 2p21, and 9q32-34. The most common gain in PTC described in Chen's data is 19q13.1, however, although a candidate gene (AKT2) from this locus is represented on the Vysis array, amplification was not detected in any of the 11 cases examined in the present study. These points again emphasise some of the limitations of making direct comparisons of array CGH and classic CGH data.

In another study by Singh *et al* of 21 cases of PTC, genetic abnormalities were identified by CGH in less than half of the cases. A recurrent pattern of aberrations

was seen in cases where genetic changes were detected, involving losses at chromosome arms 1p and 9q and chromosomes 17, 19, 22, and gains of chromosome 4 and chromosome arms 5q, 6q, 9q, and 13q. Loss of chromosome 22 was unique to younger patients (P=0.05) and was associated with a higher rate of regional lymphatic metastasis (19% v 80%, P = 0.02) (Singh, 2000). Again, the data in the present study partly corroborates the findings of Singh's study, showing the losses of distal 1p, and gains of 5q and 13 q but the full length chromosomal losses and gains have not been reproduced in the present data. Furthermore, the loss of the entire length of chromosome 22, which was associated with younger patients and regional node metastasis, is not seen in any of the 11 cases in the present study.

Hemmer reported that CGH abnormalities were rare in PTC (3 of 26 cases, 12%). All of the aberrations in this study were gains, including 5q14-23.3, 5q23.3-qter, gain of the entire lengths of chromosomes 7 and 17, and gains 21q22.1-qter and 1q23-qter (Hemmer, 1999). The presence of these aberrations was correlated with older age and the presence of cervical nodal metastasis. Hemmer's data shows no obvious overlap with the current data presented here; however, the case with the most number of aberrations detected in our cohort (11.35% of all loci) was aged 73 at diagnosis. All of the other patients were young (<40 years) at diagnosis and had small numbers of genomic aberrations. Hemmer also analysed follicular carcinoma and found loss of the entire length of chromosome 22 was commonly associated with this type of thyroid carcinoma but not with PTC. In regard to chromosome 22 Hemmer and Singh's data is clearly conflicting.

In a study of 25 cases, with varying histopathological and clinical features, from the Karolinska Institute, chromosomal imbalances were detected at a higher rate than in other studies (Kjellman, 1999). Our data shows a similar high rate of aberrations, 100% of 11 cases v 84% of Kjellman's 25 cases. All of the other studies indicate that aberrations occur in a small minority of cases. Gains and losses were approximately equally frequent (54% v 46%), a feature also notable in our data (See Figure 5.3).

In Kjellman's series, the most frequent alteration was gain of 9q33-qter (7 of 25 cases) (28%). Other recurring alterations were gain of the entire X chromosome (20%), of 1q (16%), of 17q (16%), and of 22q (12%). High-level amplification was detected at distal 1q in one case. Losses were most frequently detected on 22q (12%) and on 9q21.3 –q32 (12%).

By comparison, the data presented in this chapter shows no gains of 9q33-qter or 1q but the gains on 17 q and 22q are seen. The gain of chromosome X occurring in male patients was not seen in the 2 male patients (Cases 6 and 8) that had identically sex matched reference DNA in our cohort. None of the losses described by Kjellman are reproduced in our cohort.

Bauer *et al* analysed 15 cases by CGH (Bauer, 2002). Only four (27%) showed aberrations with an average of 3.25 aberrations per case (Range 2-4). All PTC samples with abnormal CGH had vascular or capsular invasion. There was significant correlation between the presence of chromosomal aberrations and invasion. All four cases with CGH abnormalities had a partial or complete gain of

chromosome 20 and 3 of the 4 also had a partial or complete loss of chromosome 13. Possible loss at chromosome 4q was observed in cases with younger age. A gain of chromosome 12q24 was observed in a case of a patient with a history of external beam radiation. A single tall Cell variant had a gain of chromosome 15. MSI was not detected in any case.

The primary finding of the current study is that DNA copy gain and loss appears to occur in all cases of PTC when tumours are examined using a combination of laser capture microdissection and sensitive array based CGH. Copy gain and loss is more frequent in cell lines, which no doubt reflects the ease with which aggressivelybehaving tumours can be maintained in immortal culture, which leads to a selection bias for highly genomically unstable tumours, and the artificial effects of prolonged culture and passage. Taking the surgical cases, which more accurately reflect true biology, aberrations occur at a low percentage of all the loci examined with a mean percentage of aberrations of 6% of all loci examined (Range, 1.45%-11.35%).

In the current study, taking amplified genes occurring in more than 36% of the cases as a threshold, (Table 5.4) the most common amplifications involve loci of well-described oncogenes related to the mitogen activated protein kinase pathway (MAPK), including FGR/SRC2 on 1p36.2-p36.1 (FGR- Gardner Rasheed Feline Sarcoma viral oncogene homolog, a protein tyrosine kinase), EGFR on 7p12.3-p12.1 (epidermal growth factor receptor, a protein tyrosine kinase), FGF4 on 11q13 (Fibroblast Growth Factor 4, a classical activator of the MAPK pathway) and PDGFRB on 22q13.1 (Platelet derived growth factor receptor B SIS, another

classical activator of the MAPK pathway). This finding is significant when one considers that activating mutations of ret/PTC and BRAF all modulate the MAPK pathway. Clearly, the MAPK pathway plays a central role in the pathogenesis of PTC.

It can be seen from reviewing the literature that CGH data on PTC has yielded disparate results and conclusions. PTC is clearly a morphologically heterogeneous neoplasm and shows molecular heterogeneity. It may well be that DNA copy gain and loss occurs as a secondary event to established molecular triggers such as ret/PTC activation and BRAF mutation. For this reason in the current study an attempt has been made to assess DNA copy gain and loss in very well characterised tumours. Also an attempt has been made to overcome the effect of normal cellular contamination by using laser capture microdissection and increasing the resolution of the technique by targeting specific known oncogenes and tumour suppressor genes using array CGH. In all of the previous conventional CGH studies cited above, no specific microdissection measures were utilised, which may go some way towards explaining the absence of aberrations detected in many studies.

The most potentially important findings of the current study are the recurrent amplifications of PDGFRB, TP73 and SNRPN occurring in those tumours without either of the common molecular triggers. It must be acknowledged that the numbers of cases are small and for this reason statistical significance cannot be inferred. However, other evidence points to a role in particular for PDGFRB in the pathogenesis of PTC. A recent expression microarray study identified PDGF expression as a possible diagnostic marker of PTC (Yano, 2004). Over expression of

the protein was confirmed by immunohistochemistry. It is possible that copy gain of this gene will lie behind the increased expression of the protein. Furthermore, PDGFRB is an attractive candidate for oncogenic activation because the expressed gene has a tyrosine kinase function and is known to contribute to the mitogen activated protein kinase pathway (MAPK). Yano et al also demonstrated over expression of FGF4 in their study. FGF 4, which activates MAPK, was the most commonly amplified oncogene in the 11 cases of PTC described in this chapter (Table 5.4). As discussed above activation of MAPK pathways is a feature of all the known PTC oncogenes discovered thus far.

5.8 Conclusion

The current study demonstrates that copy gain and loss occurs in more cases of PTC than heretofore seen in the literature. The combination of laser capture microdissection and array based CGH may be an optimal combination for detecting copy gain and loss in tumours. This study emphasises the central role played by the MAPK pathway in the pathogenesis of PTC. Amplification of PDGFRB occurs exclusively in tumours without mutation of BRAF or expression of ret/PTC chimeras. The mechanism of overexpression of both FGF 4 receptor and PDGF, recently described in the literature, may well be copy gain at the genomic level.

5.9 References

Antonini P, Venuat AM, Caillou B, Berger R, Schlumberger M, Bernheim A, Parmentier C. 1992. Cytogenetic studies on 19 papillary thyroid carcinomas. Genes Chromosomes Cancer. 5(3): 206-11.

Albrecht B, Hausmann M, Zitzelsberger H, Stein H, Siewert JR, Hopt U, Langer R, Hofler H, Werner M, Walch A. 2004. Array-based comparative genomic hybridisation for the detection of DNA sequence copy number changes in Barrett's adenocarcinoma. J Pathol. 203(3): 780-8

Bauer AJ, Cavalli LR, Rone JD, Francis GL, Burch HB, Tuttle RM, Ringel MD, Stratakis CA, Haddad BR. 2002. Evaluation of adult papillary thyroid carcinomas by comparative genomic hybridisation and microsatellite instability analysis. Cancer Genetics and Cytogenetics 135; 182-186

Bentz M, Plesch A, Stilgenbauer S, Dohner H, Lichter P. 1998. Minimal sizes of deletions detected by comparative genomic hybridisation. Genes Chromosomes Cancer. 2: 172-5

Califano JA, Johns MM 3rd, Westra WH, Lango MN, Eisele D, Saji M, Zeiger MA, Udelsman R, Koch WM, Sidransky D. 1996. An allelotype of papillary thyroid cancer. Int J Canc 69:442-444

Chen X, Knauf JA, Gonsky R, Wang M, Lai EH, Chissoe S. 1998. From amplification to gene in thyroid cancer: a high resolution mapped bacterial-artificial-chromosome resource for cancer chromosome aberrations guides gene discovery after comparative genomic hybridisation. Am J Hum Genet 63:625-37

Corso C, Ulucan H, Parry EM, Parry JM. 2002. Comparative analysis of two thyroid tumour cell lines by fluorescence in situ hybridisation and comparative genomic hybridisation. Cancer Genet Cytogenet. 137(2): 108-18.

Dettori T, Frau DV, Garcia JL, Pierantoni G, Lee C, Hernandez JM, Fusco A, Morton CC, Vanni R. 2004. Comprehensive conventional and molecular cytogenetic characterization of B-CPAP, a human papillary thyroid carcinoma-derived cell line. Cancer Genetics and Cytogenetics; 151:171-177

Gillespie JW, Nasir A, Kaiser HE. 2000. Loss of heterozygosity in papillary and follicular thyroid carcinoma: a mini review. In Vivo. 14(1):139-40

Hemmer S, Wasenius VM, Knuutila S, Franssila K, Joensuu H. 1999.DNA copy number changes in thyroid carcinoma. Am J Pathol; 154:1539-47

Herrmann M, Hay ID, Bartelt DH Jr, Ritland SR, Dahl RJ, Grant CS, Jenkins RB. 1991. Cytogenetic and molecular genetic studies of follicular and papillary thyroid cancers. J Clin Invest 88:1596-1604

Hui AB, Lo KW, Yin XL, Poon WS, Ng HK. 2001. Detection of multiple gene amplifications in glioblastoma multiforme using array-based comparative genomic hybridisation. Lab Invest. 81(5): 717-23

Johannessen JV, Sobrinho-Simoes M, Tangen KO, Lindmo T. 1981. A flow cytometric deoxyribonucleic acid analysis of papillary thyroid carcinoma. Lab Invest. 45(4):336-41.

Joos S, Scherthan H, Speicher MR, Schlegel J, Cremer T, Lichter P. 1993. Detection of amplified DNA sequences by reverse chromosome painting using genomic tumour DNA as probe. Hum Genet. 90(6): 584-9

Kallioniemi A, Kallioniemi OP, Sudar D, Rutovitz D, Gray JW, Waldman F, Pinkel D. 1992. Comparative genomic hybridisation for molecular cytogenetic analysis of solid tumours. Science. 258 (5083): 818-21

Kallioniemi A, Kallioniemi OP, Piper J, Tanner M, Stokke T, Chen L, Smith HS, Pinkel D, Gray JW, Waldman FM. 1994. Detection and mapping of amplified DNA sequences in breast cancer by comparative genomic hybridisation. Proc Natl Acad Sci U S A.; 91(6): 2156-60.

Kimura ET, Nikiforova MN, Zhu Z, Knauf JA, Nikiforov YE, Fagin JA. 2003. High prevalence of BRAF mutations in thyroid cancer: genetic evidence for constitutive activation of the RET/PTC-RAS-BRAF signalling pathway in papillary thyroid carcinoma. Cancer Res. 63(7): 1454-7

Kitamura Y, Shimizu K, Tanaka S, Ito K, Emi M. 2000. Association of allelic loss on 1q, 4p, 7q, 9p, 9q, and 16q with postoperative death in papillary thyroid carcinoma. Clin Cancer Res. 6(5):1819-25

Kjellman P, Lagercrantz S, Hoog A, Wallin G, Larsson C, Zedenius J. 2001. Gain of 1q and Loss of 9q21.3.q32 are associated with a less favourable prognosis in PTC. Genes, Chromosomes and Cancer 32:43-49

Lehmann L, Greulich KM, Zitelsberger H, Negele T, Spelsberg F, Bauchinger M, Weier HU. 1997. Cytogenetic and molecular genetic characterization of a chromosome 2 rearrangement in a case of human papillary thyroid carcinoma with radiation history. Cancer Genetics and Cytogenetics 96:30-36

Namba H, Rubin SA, Fagin JA. 1990. Point mutations of ras oncogenes are an early event in thyroid tumourigenesis. Mol Endocrinol. 4(10): 1474-9

Pierotti MA, Bongarzone I, Borello MG, Greco A, Pilotti S, Suzy G. 1996. Cytogenetics and molecular genetics of carcinomas arising from thyroid epithelial follicular cells. Genes Chromosomes and Cancer 16:1-14

Pierotti MA. 2000. Papillary thyroid carcinomas. Atlas Genet Cytogenet Oncol Haematol. Available at: http://www.infobiogen.fr/services/chromcancer/Tumors/PapilThyroidCarID5053.html

Pinkel D, Segraves R, Sudar D, Clark S, Poole I, Kowbel D, Collins C, Kuo WL, Chen C, Zhai Y, Dairkee SH, Ljung BM, Gray JW, Albertson DG. 1998. High-resolution analysis of DNA copy number variation using comparative genomic hybridisation to Microarrays. Nat Genet. 20(2): 207-11

Piper J, Rutovitz D, Sudar D, Kallioniemi A, Kallioniemi OP, Waldman FM, Gray JW, Pinkel D. 1995. Computer image analysis of comparative genomic hybridisation. Cytometry. 19(1): 10-26

Puxeddu E, Moretti S, Elisei R, Romei C, Pascucci R, Martinelli M, Marino C, Avenia N, Rossi ED, Fadda G, Cavaliere A, Ribacchi R, Falorni A, Pontecorvi A, Pacini F, Pinchera A, Santeusanio F. 2004. BRAF (V599E) mutation is the leading genetic event in adult sporadic papillary thyroid carcinomas. J Clin Endocrinol Metab. 89(5): 2414-20

Schraml P, Schwerdtfeger G, Burkhalter F, Raggi A, Schmidt D, Ruffalo T, King W, Wilber K, Mihatsch MJ, Moch H. 2003. Combined array comparative genomic hybridisation and tissue microarray analysis suggest PAK1 at 11q13.5-q14 as a critical oncogene target in ovarian carcinoma. Am J Pathol. 163(3):985-92

Singh B, Lim D, Cigudosa JC, Ghossein R, Ashok R, Shaha AR, Poluri A, Wreesman VB, Tuttle M, Shah JP, Rao PH. 2000. Screening for genetic aberrations in papillary thyroid cancer by using comparative genomic hybridisation. Surgery 128(6):888-894

Smyth P, Finn SP, Cahill S, Flavin R, O'Regan EM, O'Leary JJ, Sheils OM. 2005. Ret/PTC and BRAF act as distinct molecular time dependent triggers in a sporadic cohort of papillary thyroid carcinoma. Int J Surg Pathol. 13 (1): 1-8

Soares P, Trovisco V, Rocha AS, Lima J, Castro P, Preto A, Maximo V, Botelho T, Seruca R, Sobrinho-Simoes M. 2003. BRAF mutations and RET/PTC rearrangements are alternative events in the etiopathogenesis of PTC Oncogene. 22(29):4578-80

Soares P, dos Santos NR, Seruca R, Lothe RA, Sobrinho-Simoes M. 1997. Benign and malignant thyroid lesions show instability at microsatellite loci. Eur J Cancer. 33(2):293-6

Ward LS, Brenta G, Medvedovic M, Fagin JA. 1998. Studies of allelic loss in thyroid tumours reveal major differences in chromosomal instability between papillary and follicular carcinomas. J Clin Endocrinol Metab 83:525-30

Yano Y, Uematsu N, Yashiro T, Hara H, Ueno E, Miwa M, Tsujimoto G, Aiyoshi Y, Uchida K. 2004. Gene expression profiling identifies platelet-derived growth factor as a diagnostic molecular marker for papillary thyroid carcinoma. Clin Cancer Res. 10(6): 2035-43

Chapter 6

Biomarker discovery using microarray expression analysis of Papillary Thyroid Carcinoma and benign thyroid tissue

6.1 Summary

Papillary Thyroid Carcinoma (PTC), the most common thyroid malignancy, is a clinically and morphologically heterogeneous neoplasm, with a usually indolent, although sometimes unpredictable behaviour. Mutations of the BRAF (V600E) and rearrangements of the ret gene (ret/PTC) are strongly associated with PTC, however, in clinical practice analysis of tissue for these aberrations is unrewarding. The diagnosis of PTC and subsequent therapeutic approach would be greatly facilitated by the identification of clinically relevant biomarkers. In particular, the identification of a panel of biomarkers that distinguish benign and inflammatory conditions from malignancy would be advantageous.

DNA and RNA were extracted from fresh thyroid samples, comprising PTC (N=8, 4 classic and 4 follicular variants) and benign thyroid samples (N=5, 2 follicular adenomas, 2 normal thyroid and 1 Graves' disease). Ret rearrangement and BRAF mutation status was assessed by TaqMan RT-PCR and allelic discrimination assays respectively. We used a novel chemiluminescence expression array system to study the expression of 31,600 genes in our samples. Chemiluminescence provides improved performance by ensuring high signal to noise values in combination with low detection limits.

Mutant BRAF was exclusively associated with classic morphology PTC. Rearranged ret was not detected. Hierarchical clustering revealed distinct patterns of expression between benign and malignant groups. Using a distinction calculation method it was possible to identify the most informative up and down regulated

candidate biomarker genes, which, distinguish PTC from benign thyroid tissue, irrespective of ret or BRAF status. ANOVA with the stringent Bonferroni correction revealed 2 highly statistically significant candidate genes whose expression distinguished between PTC and benign thyroid tissue. Using a variety of statistical techniques, a considerable number of other potential biomarkers of thyroid malignancy have also been identified.

In conclusion, we have identified biomarkers of PTC, which although requiring further validation, have the potential to improve the diagnostic accuracy of thyroid carcinoma and in the longer term may lead to improved treatment strategies.

6.2 Introduction

It is clear that cancer results from changes of gene expression patterns that affect key cellular pathways involved in processes that include cell growth, differentiation, homeostasis, response to injury etc. Knowledge of these specific pathways and processes may lead to the identification of diagnostic biomarkers, prognostic biomarkers and potential targets for disease specific therapy. Until now classification of cancer has been based on histopathological assessment with clinicopathological correlation. These tried and trusted methods have been successfully utilised for decades; however, it is becoming apparent that new expression array technology will exponentially increase our knowledge about the molecular basis of all types of neoplasia. Definition of a genome wide expression pattern for disease states will also enhance our understanding of cell biology and may provide a link between molecular genetics and clinical practice (Van't Veer LJ, 2003; West, 1998; Mazzanti 2004).

For the promise of expression microarray technology to bear fruit, experiments must seek to answer key clinically relevant questions and eventually lead to improved patient care. With regard to thyroid carcinoma, correct treatment planning is vital in order to ensure good outcome. Thyroid nodules are common. It has been estimated that 5-10% of the population will develop a clinically significant thyroid nodule during their lifetime (Mazzaferri, 1993). The solitary thyroid nodule, defined as a palpably discrete swelling within an otherwise normal gland, is usually a benign lesion. However, in clinical practice concern about the possibility of thyroid cancer

is always encountered. In the United States, only about 12,000 new thyroid cancers are diagnosed every year and there are about 1000 deaths from the disease, yet investigation of the solitary thyroid nodule is very common and leads to a significant burden on health care systems.

Fine-needle aspiration cytology (FNAC) is the predominant method for triaging thyroid nodules into operative and non-operative lesions. FNAC is safe, inexpensive and leads to a better selection of patients for surgery than any other test (Mazzaferri, 1993). The results of FNAC are usually conclusive in cases of classic morphology PTC providing that sampling is adequate. However, the follicular variant and other follicular patterned lesions such as follicular carcinoma and follicular adenoma are difficult to diagnose preoperatively in all cases. The use of FNAC has halved the number of patients undergoing surgery, and in those who do, twice as many have been found to have cancer (Hamberger, 1982). However, there are limitations. Between 10-25% of all cytologic specimens are indeterminate, or suspicious (Goellner, 1987; Ravetto, 2000). Of these about 20% are from malignant nodules (Caruso, 1991). Twice as many patients are referred for surgery for a suspicious lesion (10%) as for a malignant lesion (5%). No effective method, however, has been found to cytologically identify truly malignant lesions that yield indeterminate cytologic results.

A second major question is how the surgical treatment of lesions noted to be indeterminate or suspicious should proceed. A compete thyroidectomy is preferred by many surgeons when dealing with a malignant lesion whereas thyroid lobectomy is performed for benign nodules. A suspicious/indeterminate preoperative FNA diagnosis treated with complete lobectomy would result in the majority of patients

undergoing either an unnecessary procedure or over aggressive treatment leading to a requirement for thyroid hormone replacement therapy for life. Conversely a lobectomy performed in suspicious/indeterminate cases would necessitate a repeat operation for completion in a proportion of malignant cases.

6.2.1 Biomarkers of malignancy

In recent years, there has been a great emphasis in the thyroid literature on the identification of biomarkers of thyroid tumours (Xing, 2004; Prasad, 2004; Volante, 2004; Saggiorata, 2004; Pisani, 2004, Rosai 2003; Feilchenfeldt 2003; Beesley, 2002; Herrmann, 2002; Lloyd 2001; Saggiorata, 2001; Bartolazzi, 2001; Inohara, 1999). However, no definitive biomarker or set of biomarkers has yet emerged in a meaningful way to combat the diagnostic and operative planning problems discussed above. Recently, gene expression microarray technology has been used to attempt to identify biomarkers of malignancy relevant to the thyroid (Mazzanti, 2004; Barden, 2003; Cerutti, 2004; Finley, 2004a; Finley 2004b) and such studies are likely to have the greatest potential for the identification of important biomarkers.

6.2.2 Applied Biosystems Human Genome Survey Microarray

Approaches using microarrays to interrogate gene activity have been limited by probes designed without the benefit of reference to a fully curated gene library of the total human genome. Researchers have attempted to overcome this limitation by designing probe sets against consensus-based expression sequence tag (EST)

libraries with partially curated gene libraries to approximate a total gene set. Curation refers to the quality of information associated with a particular gene or transcript and EST sequences are often partially curated and possibly associated with unreliable probe sequences. Therefore, rather than providing a uniform survey of gene activity, these probe sets are biased according to the abundance and visibility of ESTs that have already been observed in certain tissue types under certain conditions.

The human genome survey microarray from Applied Biosystems provides access to both the public databases and to the privately curated Celera human Genome database. For these reasons the Applied Biosystems microarray contains the most complete collection of genes available on any expression microarray platform. The array provides 31,700 probes for the interrogation of 27,868 genes. Of this high quality gene set, 28% have been curated exclusively by Celera genomics and are therefore not available in high quality format in the public domain. The most current version (March 2004) of the Celera Discovery System (CDS) catalogues 31,566 human genes. At the time of probe design for the current Human Genome survey array, approximately 2000 genes currently found in CDS were not found on the microarray. This is the reason why there are 27,868 genes targeted by the current microarray even though there are 33,202 probes which can be used for gene expression interrogation.

The oligonucleotide probes on the array are 60 base pairs (60 mers) and are designed to report an aggregate gene activity level from alternatively spliced transcripts of a gene. They are designed not to discriminate between the abundance levels of

alternative transcripts. Alternative transcripts can be identified subsequently using appropriate TaqMan RTPCR assays.

6.3 Aims

As can be appreciated from the introductory comments above, there is a clear need to develop more accurate diagnostic tests allied to traditional FNAC techniques in order to evaluate thyroid lesions. The diagnosis of the most common thyroid carcinoma, PTC, and subsequent therapeutic approach would be greatly facilitated by the identification of such clinically relevant biomarkers. In particular the identification of a panel of biomarkers that distinguishes benign and inflammatory conditions from malignancy would be advantageous. The aim of this chapter was to use a new highly curated chemiluminescent-based expression microarray platform to identify potential biomarkers of thyroid malignancy. This first step in the process is, of course, to identify biomarkers in well-characterised thyroid tumours and in the future to validate the accuracy of the biomarkers discovered by this technique in a blind manner prospectively on material from FNAC.

6.4 Materials and Methods

6.4.1 Specimens

All specimens for microarray analysis were collected fresh from theatre at St. James's Hospital and immediately snap frozen in liquid nitrogen. All specimens were collected prospectively. Diagnosis of the lesion was performed by a consultant pathologist using conventional formalin fixed paraffin embedded techniques. The

presence of lesional tissue in the banked frozen samples was confirmed by frozen section examination prior to nucleic acid extraction. Table 6.1 tabulates the samples, and provides detailed description of tumour morphology, BRAF status and ret rearrangement status.

6.4.2 RNA and DNA Extraction, *In vitro* transcription

RNA (for expression microarray studies and RTPCR for ret/PTC-1 and ret/PTC-3) and DNA extraction (for assessment of BRAF status) were performed as outlined in Chapter 2 (Section 2.6.1) using the Qiagen RNeasy and Gentra extraction protocols respectively. In all cases amplification of RNA was performed using the Eberwine procedure (Eberwine, 1996) in order to generate enough RNA to hybridise to the array. Between 1μg –10 μg of starting total RNA is recommended for input to the reverse transcription-in-vitro transcription reaction. Generally between 3μg-5μg total RNA was used. The integrity of extracted nucleic acid was verified by gel electrophoresis (Section 2.8.1) and nucleic acids were quantified by UV spectrophotometry (Section 2.7.3). BRAF mutation status and ret/PTC-1 and – 3 statuses were assessed as described in previous chapters.

Number	Array ID	Pathology No	Description	BRAF status by TaqMan Allelic Discrimination. Mutant v Wild	Ret rearrangement status	Tumour Subtype
1	HA003GG	H18/04	Benign Follicular Adenoma	BRAF Wild	Negative	NA
2	HA0012V	H1566/04	Benign Follicular Adenoma	BRAF Wild	Negative	NA
3	HA0020D	H1566/04	Benign Follicular Adenoma	BRAF Wild	Negative	NA
4	HA003GS	H8813/02	Normal thyroid tissue	BRAF Wild	Negative	NA
5	HA003GT	H3888/03	Normal thyroid tissue	BRAF Wild	Negative	NA
6	HA00354	H3334/04	Benign inflammatory lesion	BRAF Wild	Negative	Lymphocytic thyroiditis
7	HA001ZZ	H4989/03	Papillary thyroid carcinoma	BRAF Wild	Negative	Follicular Variant
8	HA003GP	H4989/03	Papillary thyroid carcinoma	BRAF Wild	Negative	Follicular Variant
9	HA003H5	H3113/03	Papillary thyroid carcinoma	BRAF Wild	Negative	Follicular Variant
10	HA00200	H787/04	Papillary thyroid carcinoma	BRAF Wild	Negative	Classic Morphology
11	HA003GZ	H948/04	Papillary thyroid carcinoma	BRAF Wild	Negative	Follicular Variant
12	HA0020E	H8813/02	Papillary thyroid carcinoma	Heterozygous Mutant BRAF	Negative	Classic Morphology
13	HA003HZ	H3888/03	Papillary thyroid carcinoma	Heterozygous Mutant BRAF	Negative	Classic Morphology
14	HA006D0	H3599/04	Papillary thyroid carcinoma	BRAF Wild	Negative	Follicular Variant
15	HA003GP	H8438/03	Papillary thyroid carcinoma	Heterozygous Mutant BRAF	Negative	Classic Morphology

Table 6. 1 Specimen morphology, BRAF status and ret status

6.4.3 RNA labelling and hybridisation to microarrays and the Chemiluminescence reaction

The specific details and protocols for RNA labelling and hybridisation are outlined in chapter 2 (Section 2.13).

6.4.3.1 Reverse transcription

The total RNA isolated from the samples contains approximately 3% messenger RNA, which by definition has a poly A tail. The first step is to reverse transcribe this poly A RNA into single stranded cDNA. This reaction is primed by using an oligo dT primer (which has a T7 promoter recognition sequence incorporated for use in subsequent IVT steps). The reverse transcriptase used in this reaction is a modified version of M-MLV reverse transcriptase (Molony murine leukemia virus reverse transcriptase). The modified reverse transcriptase has no RNase H activity (preventing RNA degradation). It also provides longer cDNA transcripts and higher yields than the wild type enzyme. RT Labeling Control RNA is added at this stage to allow assessment of the quality of reverse transcription at the end of the process.

6.4.3.2 Second strand synthesis and cDNA purification

The next step is performed in a single reaction. The template mRNA and the control RNA are hydrolyzed using sodium hydroxide and heat at 37 °C. The reaction is neutralized by the addition of 1M Tris, pH 7.0. A second strand synthesis complementary to the cDNA generated in the first step is performed and results in

double stranded cDNA, which is then purified and eluted from the degraded RNA and reaction reagents, which salts, buffers, unincorporated nucleotides and primers.

6.4.3.3 *In-vitro* transcription labeling and purification of cRNA

T7 RNA polymerase incorporates ribonucleotides and DIG-UTP to synthesize copy RNA (cRNA) from ds cDNA containing the T7 promoter site. This step results in 100-fold to 1000-fold amplification of targets. cRNA purification washes away salts, unincorporated nucleotides, primers, and cDNA. The cRNA is eluted in a solution suitable for hybridization of the cRNA to 1700 microarrays.

6.4.3.4 Chemiluminescence Reaction

Chemiluminescence is the generation of electromagnetic radiation in the form of light by the release of energy from a chemical reaction. While the light can, in principle, be emitted in the ultraviolet, visible or infrared region, it is most commonly emitted in the visible region of the spectrum. An overview of the chemiluminescence process is seen in Figure 6.1.

High signal strength and absence of background noise in chemiluminescent technology allows detection of extremely low levels of gene expression, compared with alternative fluorescent techniques.

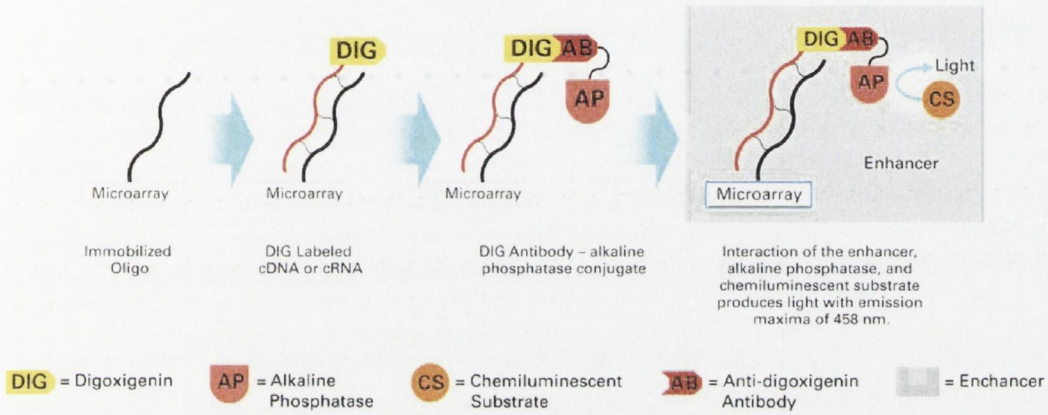

Figure 6.1 Overview of Chemiluminescence chemistry

The DIG labelled cRNA hybridises with its complementary immobilized 60-mer oligonucleotide probe on the microarray. An anti-digoxigenin antibody, to which alkaline phosphatase has been conjugated, in turn binds to the Digoxigenin labelled cRNA. Interaction of an enhancer, the alkaline phosphatase and chemiluminescent substrate produces light with emission maxima of 458 nm.

6.4.3.5 Array Scanning

The array scanning procedure, including pre-incubation and focus steps, takes 12 minutes per array. Light production on the microarray reaches a steady state within the first five minutes. During this time, the microarray is being focused and the temperature is raised to 35°C in order for the enzymatic reaction to reach a steady state. The chemiluminescent reaction emits light at a steady state for 60 minutes. A state-of-the-art CCD camera is used to acquire the images. A motorised chassis moves the loaded microarray into the optical path of the analyser to detect both chemiluminescent and fluorescent signals. The system software can then relate the resultant intensities to gene expression and perform accurate feature registration.

Multiple images are then taken to bring the microarray into focus and to measure, in turn, the fluorescent and chemiluminescent signals. Although the array system primarily uses a chemiluminescence technology, fluorescent images play a significant role.

A 24-mer oligo labelled with a fluorophore known as LIZ® is present during hybridisation. This oligonucleotide is complementary to one that is co-deposited at every feature on the array during the manufacturing process. This fluorescent signal is used in the gridding, normalisation and identification of every feature on the microarray, even in the absence of gene expression products binding to microarray probes. The microarray is imaged in both short (5 seconds) and long (25 seconds) read times. This extends the linear dynamic range of the chemiluminescent signals (> 1000-fold). The absence of an excitation background, together with the highly reproducible photon emissions, makes the signal-to-noise ratio produced from equivalent hybridisations superior to that found in alternative array systems.

6.4.3.6 Data management

The array system uses an Oracle® object-relational database to manage the huge amount of data associated with each of the millions of experimental data points produced over the course of a microarray gene expression project. The system provides an option to export data in MAGE-ML and flat file formats for secondary data analysis.

6.5 Analysis of Gene Chip Data using Spotfire Functional Genomics software

Microarray analysis is complicated. The entire area is novel, changes occur quickly, and so currently there are no standardised analysis approaches. The approach taken here is to analyse a number of ways to normalise the data, the priority being to extract the most meaningful data. The possibility of false positive results cannot be overlooked, but the analysis of these data has used a plethora of mathematical approaches to minimise this occurring. It is difficult in a thesis primarily concerned with pathobiology to delve into complex mathematics but the following paragraphs indicate the measures used to ensure the gene lists generated were as biologically relevant as possible.

6.5.1 Normalisation

Raw signal intensities are exported from the ABI 1700 to a proprietary data analysis platform (Spotfire, Decision Site for Functional Genomics). Additional statistical calculations were performed using the R statistical package (http://www.r-project.org/). The data was filtered to remove data with a Signal/noise ratio < 3 in all of the arrays, as recommended by the manufacturers.

For quality control purposes, Replicate Arrays were performed in selected cases, (Cases 2 and 3 are technical replicates of RNA from the same benign follicular adenoma sample and Cases 7 and 8 are technical replicates of the same PTC sample).

In any experiment, both random and systematic bias tends to occur. Arrays and samples have different variables (purity, reaction efficiency) that lead to different overall expression values on different arrays. One cannot remove the random bias but it is possible to minimise it by using replicates.

Normalisation is an attempt to correct for systematic bias in data. Various forms of global normalization are applicable to the data presented in this chapter. Compensation for systematic bias can be achieved by scaling the expression values of each array by a constant. There are many ways to select a scaling factor or global normalisation factor. Global normalisation makes an assumption that given a large enough sample the average signal intensity (corresponding to gene intensity level) doesn't change. Global normalisation methods that can be used include Median, Quantile, and Trimmed Mean etc. MA plots (Log2 ratios plotted (M) against average intensities (A)) are plots used to identify signal dependent biases and MA plots can be used to compare the effect of different normalisation methods.

Figure 6.2 shows an MA plot for the technical replicates Cases 2 and 3 (Benign Follicular Adenoma) using a median normalisation method. Figure 6.3 shows an MA plot for the same samples using a Quantile normalisation method. Both plots are symmetrical around zero and show no appreciable difference. There is 93% concordance in detected genes between the technical replicate arrays with 64% of genes detected on both arrays for both median normalised and quantile normalised data.

For these data either of these global normalisation methods is applicable. This is entirely in keeping with what would be expected for technical replicates.

A further normalisation method known as Z score transformation can be used to make gene expression intensity comparable across multiple arrays. This approach is particularly useful when using hierarchical clustering and when using visualisations that highlight trends of gene expression across numerous arrays (Cheadle, 2003).

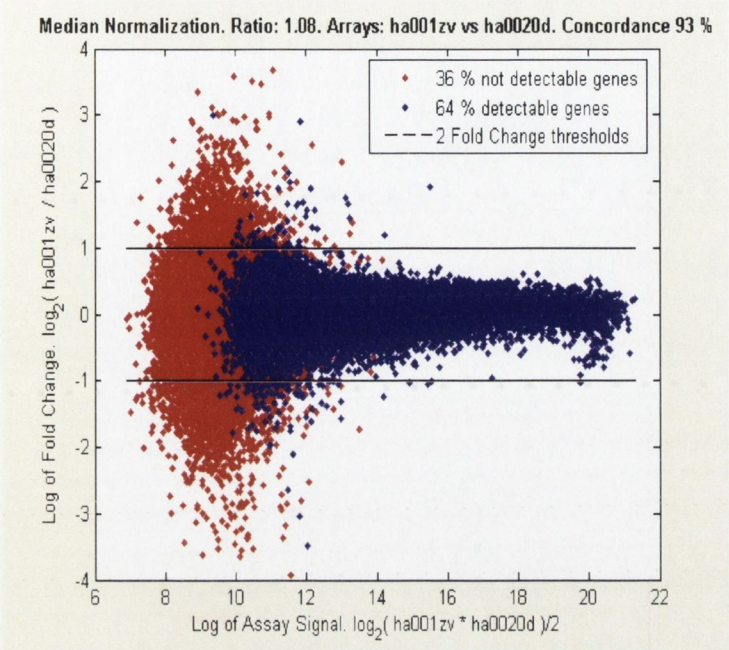

Figure 6.2 MA plot for technical replicates using median global normalisation
The blue dots on the MA plot represent detectable genes and the red dots not detectable genes. Almost all the blue dots lie within the 2-fold change threshold. Concordance is high between the replicate arrays (93%).

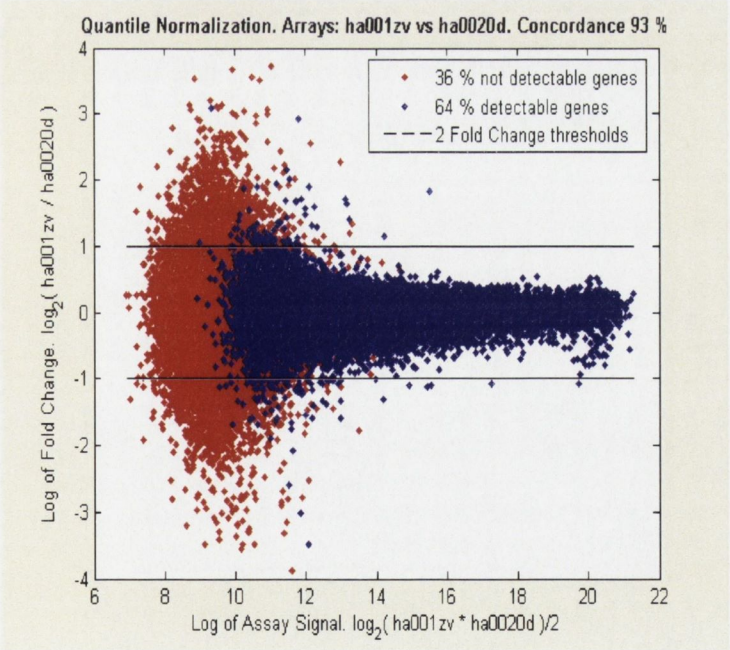

Figure 6.3 MA plot for technical replicates using quantile global normalisation The blue dots on the MA plot represent detectable genes and the red dots not detectable genes. Almost all the blue dots lie within the 2-fold change threshold. Concordance is high between the replicate arrays (93%)

6.5.2 Statistical analysis

The Treatment Comparison tool in Spotfire uses a *t*-test (for 2 groups) or ANOVA (more than 2 groups). For comparison of two conditions (e.g. Benign and Malignant or Wild type BRAF and mutated BRAF), a *t*-test is the method of choice. The *t*-test looks at the mean and variance of the sample and control distributions and calculates the probability that the observed difference in mean occurs when the null hypothesis is true. The null hypothesis states that the mean of the two distributions is equal.

A second way of looking for biomarkers is to use the distinction calculation (Golub, 1999) The distinction value is a measure of how distinct the difference in expression level is between different parts of a profile. This is particularly useful when looking for genetic biomarkers. An example would be a gene that shows high expression for a certain type of tumor cells but not for healthy cells.

One starts by dividing the variables into groups (e.g. Benign v Malignant). The aim is to look for genes that show a distinct difference in expression between the groups. While there should be a large difference in expression between the groups there should also be as little variation as possible within the groups. The profiles are compared to an idealized expression pattern in which the expression level is uniformly high in the first group and uniformly low in the second group, etc. The calculated distinction values are a measure of how similar each profile is with this ideal profile.

Profiles with high positive distinction values have high expression values in the first group and low expression values in the second group. Profiles with high negative

distinction values have low expression values in the first group and high expression values in the second group.

In the context of t-tests, setting a cut-off for differential expression is problematic because one has to balance the potential false positives (Type 1 error) and the false negatives (Type 2 error). Furthermore, performing statistical tests for tens of thousands of genes creates a multiple hypothesis-testing problem. For example, in an experiment with a 10 000 gene array in which significance level α is set at 0.05, 500 genes would be inferred as significant even if none was differentially expressed. Therefore, using a p value of 0.05 is likely to exaggerate Type 1 errors. The multiple hypothesis testing problem is conventionally tackled by conservative approaches that control the family-wise error rate (FWER), the probability of having at least one false positive among all testing hypotheses (Leung, 2003). A classical example is the Bonferroni correction (Bonferroni, 1936).

However, as argued by Benjamini and Hochberg (Benjamini, 1995), controlling the FWER in multiple testing settings may not always be appropriate. Indeed, in large-scale hypothesis generating studies such as microarray experiments, this criterion becomes so conservative that the probability of detecting any true association is, in some cases, almost nil. As an alternative and less stringent concept of error control, Benjamini and Hochberg introduced the false discovery rate (FDR). The FDR is the expected proportion of erroneously rejected null hypotheses among the rejected ones. The main reason for using the FDR is that it controls a quantity that is relevant and

leads to more powerful procedures than those relying on the FWER. Based on this concept, they initially developed a step-up procedure under the hypothesis of independence, which controls FDR at a pre-specified value. Extensions to the case of dependent tests have recently been proposed by Benjamini and Yekutieli (Benjamini, 2001). In their seminal paper, Benjamini and Hochberg also presented other error criteria such as the conditional expectation of the proportion of false discoveries given that at least one discovery, later called "positive False Discovery Rate" (pFDR) by Storey (Storey, 2001).

6.5.3 Data Mining and The Panther Database

The PANTHER™ Protein Classification System was designed to provide coarse-grained functional information for as many mammalian genes as possible using sophisticated bioinformatics techniques and expert human curation. The Panther browsable database was designed for high-throughput analysis of protein sequences. One of the key features of Panther is a simplified ontology of protein function, which allows browsing of the database by biological function. Biologist curators have associated the ontology terms with groups of protein sequences rather than individual sequences. Statistical models, known as Hidden Markov Models, are built from each of these groups (Thomas, 2003). The advantage of this approach is that new sequences can be automatically classified as they become available. This database classifies protein products of genes into functional categories allowing researchers to browse or analyse large sets of genes by their known or inferred functions. The website (http://panther.appliedbiosystems.com) includes numerous tools for navigating and analyzing lists of genes and associated information such as proteins

and protein families for identifying specific Applied Biosystems TaqMan® Gene Expression and SNP Genotyping Assays. Some of the PANTHER system's key features include:

- Gene function browser
- List-oriented workspace
- List conversion
- Pie and bar chart visualization, and navigation
- Statistical comparison of gene lists with respect to function

6.6 Results

6.6.1 Distinguishing Benign thyroid lesions from PTC

6.6.2 Clustering and Bonferroni analysis

Initial analysis of the data consisted of using a t-test to compare average normalised signal values for benign and malignant groups, with a p value setting <0.05. In addition, selection for genes showing significant increased or decreased expression was made by filtering for genes showing at least 2-fold expression change between the two groups. This analysis gives a large list of genes (N=1139) that are potential markers of benign and malignant (PTC) phenotypes. Initial hierarchical clustering of these 1139 genes generates a heat map and cluster dendrogram, which clearly separated benign lesions and PTC into distinct hierarchies (Figure 6.4).

For data reduction purposes, further analysis of this gene group was performed by using the stringent Bonferroni correction. As discussed above, the Bonferroni correction is a very stringent control of the FWER. Using both the classic Bonferroni correction and the Holm Bonferroni correction for FWER limitation, a list of 23 genes with high statistical significance was generated from the initial t-tests. Only two of these showed increased expression in PTC (Table 6.2). A further 21 showed decreased expression in PTC relative to benign conditions (Table 6.3).

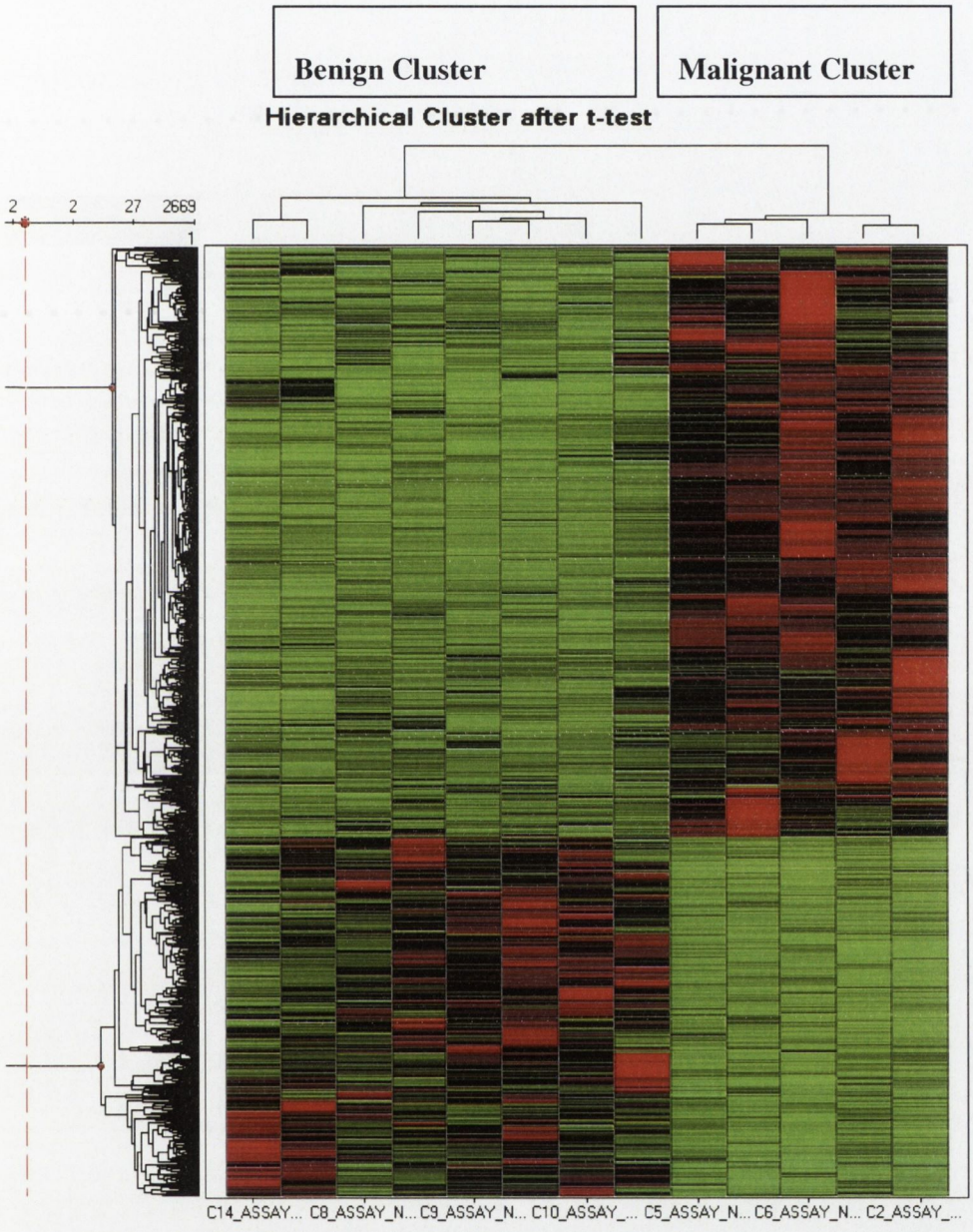

Figure 6.4 Hierarchical clustering of 1139 genes after *t*-test ($p<0.05$). The column dendrogram clearly shows benign cases clustering to the left with PTC cases (both FVPTC and classic PTC) in a distinct right-sided cluster. Red denotes genes with relative increased expression and green denotes genes with relative decreased expression.

GENE ID	Symbol	Gene Name
hCG227163	CSNK1G2	Casein kinase 1, gamma 2
hCG211083	IRF3	Interferon regulatory factor 3

Table 6.2 Genes showing increased expression in malignancy after *t*-test and Bonferroni correction.

6.6.3 False Discovery Rate analysis

As described above a more reasonable way to control the FWER is to use an FDR calculation. For this data series the BY (Benjamini Yekutieli) correction was utilised for control of the FDR (Benjamini, 2001). Because this chapter is concerned with biomarkers of malignancy and because positive biomarkers are potentially far more useful than negative biomarkers, only those genes showing increased expression in PTC are shown in Table 6.4. However, it is noteworthy that several genes related to thyroid function were shown to be down regulated in malignancy in comparison to benign lesions e.g. Thyroid Peroxidase (Data not shown) and TSH receptor. Decreased expression of TSH receptor has been shown by this group previously using RTPCR (Sheils, 1999).

GENE ID	Symbol	Gene Name
NM_015713.1	RRM2B	Ribonucleotide reductase M2 B (TP53 inducible)
hCG21956.3	PRPF4B	PRP4 pre-mRNA processing factor 4 homolog B (yeast)
hCG27386.3	GOLGA1	Golgi autoantigen, golgin subfamily a, 1
hCG32808.3	STARD13	START domain containing 13
hCG37787.3	HSPC129	Hypothetical protein HSPC129
hCG401089.3	NXP2	Nuclear matrix protein NXP2
hCG15721.2	ATF2	Activating transcription factor 2
hCG17135.2	RAB23	RAB23, member RAS oncogene family
hCG22528.3	MAP3K7IP2	Mitogen-activated protein kinase kinase kinase 7 interacting protein 2
hCG40040.3	ADAM10	A disintegrin and metalloproteinase domain 10
NM_003226.1	TFF3	Trefoil factor 3 (intestinal)
hCG17257.3	MATN2	Matrilin 2
hCG1782506.1	FLJ10876	Hypothetical protein FLJ10876
hCG41077.3	FLJ31657	Hypothetical protein FLJ31657
hCG17370.3	SPTBN1	Spectrin, beta, non-erythrocytic 1
hCG2028767	TSHR	Thyroid stimulating hormone receptor
hCG38870.2	HP1-BP74	HP1-BP74
hCG1785449.2	ChGn	Chondroitin beta1,4 N-acetylgalactosaminyltransferase
hCG1789399.2	ADD3	Adducin 3 (gamma)
hCG21995.4	FLJ36090	Hypothetical protein FLJ36090
hCG37490.3	GRPEL2	GrpE-like 2, mitochondrial (E. coli)

Table 6.3 Genes with decreased expression in malignancy relative to benign conditions after t test with Bonferroni Correction ($p<0.05$). Average fold change>2. Shaded rows depict genes previously described in the literature as having relevance in thyroid pathology.

Gene ID	Symbol	Gene Name	Fold Change
hCG37681.3	GALE	Galactose-4-epimerase, UDP-	11.64269912
hCG38360.3	STK4	Serine/threonine kinase 4	6.342844203
hCG24743.3	RCOR	REST corepressor	5.216942149
hCG2028338	SLC30A7	Solute carrier family 30 (zinc transporter), member 7	4.906655844
hCG33216.2	TIP-1	Tax interaction protein 1	4.794661874
hCG2016952	FLJ22531	Hypothetical protein FLJ22531	4.718543046
hCG14731.3	KRAS2	v-Ki-ras2 Kirsten rat sarcoma 2 viral oncogene homolog	4.569817537
hCG201158.4	CDC2L2	cell division cycle 2-like 2	4.549507473
hCG1991625	FLJ20294	Hypothetical protein FLJ20294	3.972039474
hCG39980.2	FRABIN	Actin-filament binding protein frabin	3.733552632
hCG32920.3	WASL	Wiskott-Aldrich syndrome-like	3.732317737
hCG29944.2	CORO2A	Coronin, actin binding protein, 2A	3.539719626
hCG25594.3	FXYD5	FXYD domain containing ion transport regulator 5	3.524730216
hCG1811182.2	CD44	CD44 antigen (homing function and Indian blood group system)	3.162339098
hCG25594.3	FXYD5	FXYD domain containing ion transport regulator 5	3.08531746
hCG17680.2	PHLDA3	Pleckstrin homology-like domain, family A, member 3	3.029057018
hCG22629.2	BACH	Brain acyl-CoA hydrolase	2.987820297
hCG14678.2	RAD23B	RAD23 homolog B (S. cerevisiae)	2.949014591
hCG25086.4	CTBS	Chitobiase, di-N-acetyl-	2.911768096
hCG37487.3	HSU84971|FLJ10283	Fetal hypothetical protein|hypothetical protein FLJ10283	2.885919921
hCG1979691	GEMIN5	Gem (nuclear organelle) associated protein 5	2.884615385
hCG25177.3	DDB2	Damage-specific DNA binding protein 2, 48kDa	2.855351171
hCG2018239.1	C20orf40	Chromosome 20 open reading frame 40	2.806712963
hCG23527.3	PIASY	Protein inhibitor of activated STAT protein PIASy	2.80027933
hCG20857.3	F11R	F11 receptor	2.791524239
hCG1640926.3	GNG12	Guanine nucleotide binding protein (G protein), gamma 12	2.770794173
hCG22321.3	TGFB1	Transforming growth factor, beta 1 (Camurati-Engelmann disease)	2.709503745
hCG16921.3	S100A11	S100 calcium binding protein A11 (calgizzarin)	2.628953221
hCG32783.2	P5CR2	Pyrroline 5-carboxylate reductase isoform	2.486046512
hCG1770706.3	PPP4C	Protein phosphatase 4 (formerly X), catalytic subunit	2.399813123
hCG23133.3	FLJ10898	KIAA1685 protein	2.296883995
hCG1990006	RPS2	Ribosomal protein S2	2.267844301
hCG42017.3	CHRNB1	cholinergic receptor, nicotinic, beta polypeptide 1 (muscle)	2.256410256
hCG22716.3	CSNK1G2	casein kinase 1, gamma 2	2.209770115
hCG24776.3	MAD2L2	MAD2 mitotic arrest deficient-like 2 (yeast)	2.13576779
hCG21108.3	IRF3	Interferon regulatory factor 3	2.123655914
hCG29191.3	RGS3	Regulator of G-protein signalling 3	2.107344021
hCG24097.2	CENTD2	Centaurin, delta 2	2.06139329
hCG20449.2	GNB2	Guanine nucleotide binding protein (G protein), beta polypeptide 2	2.036783645
hCG39019.2	LOC92689	Hypothetical protein BC001096	2.013343799

Table 6.4. Genes showing increased expression in PTC relative to benign lesions after BY control of FDR with a p value of 0.01.

The genes have been sorted in descending order of maximal fold change. Shaded rows depict genes previously described in the literature as having relevance in thyroid pathology.

6.6.4 Distinction Analysis

It can be seen that the strict Bonferroni and FDR calculations yield a relatively small number of potential biomarkers in this data set. Figure 6.5 shows a profile chart generated after using the Distinction Analysis discussed above. Benign cases lie to the left of the Y-axis and malignant cases to the right. The diagram illustrates the concept of Distinction calculation, which relies on an analysis of how different parts of a profile appear to be. Using the distinction method a larger group of genes may be identified as potential biomarkers. Table 6.5 shows candidate genes the expression of which is increased in PTC relative to benign thyroid tissue (by distinction). Figure 6.6 shows a pie chart documenting the cellular processes upregulated in malignancy after a distinction calculation has been applied (Panther classification). Nucleic acid binding and membrane transport functions are the most frequently upregulated processes in PTC relative to benign conditions.

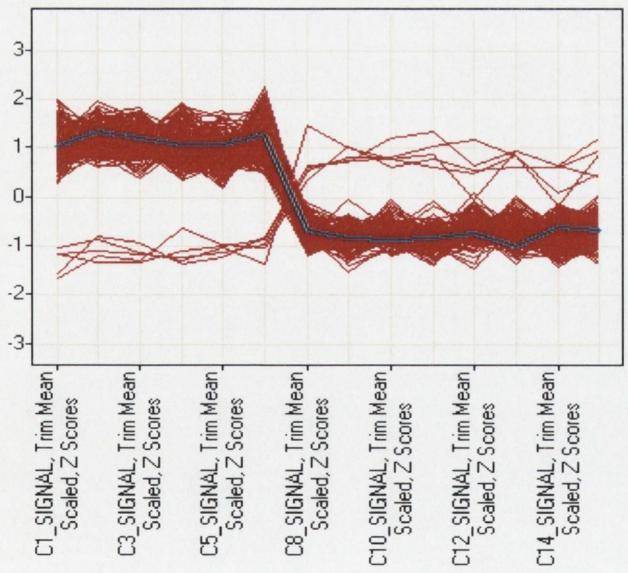

Figure 6.5 Profile chart of genes showing increased and decreased expression in PTC with clear distinction patterns.

On the Y-axis are all the arrays normalized using a Z score (Cheadle, 2003), which facilitates depiction of the data. The X-axis shows the actual value of the Z-score. A single gene is highlighted and shows increased expression in the benign group (C1-C6) relative to the malignant group (C8-C14)

Gene ID	Symbol	Gene Name
hCG14731.3	KRAS2	v-Ki-ras2 Kirsten rat sarcoma 2 viral oncogene homolog
hCG14678.2	RAD23B	RAD23 homolog B (S. cerevisiae)
hCG2005611.1	CLIC1	Chloride intracellular channel 1
hCG22690.3	LSM7	LSM7 homolog, U6 small nuclear RNA associated (S. cerevisiae)
hCG2039426.1	GNG5	Guanine nucleotide binding protein (G protein), gamma 5
hCG1811614.1	BAX	BCL2-associated X protein
hCG37681.3	GALE	Galactose-4-epimerase, UDP-
hCG41682.3	C14orf52	Chromosome 14 open reading frame 52
hCG25739.3	BPNT1	3'(2'), 5'-bisphosphate nucleotidase 1
hCG15302.3	LYRIC	LYRIC/3D3
hCG16921.3	S100A11	S100 calcium binding protein A11 (calgizzarin)
hCG42687.4	UBE2I	Ubiquitin-conjugating enzyme E2I (UBC9 homolog, yeast)
NM_018841.1	GNG12	Guanine nucleotide binding protein (G protein), gamma 12
hCG34619.2	LOC51255	Hypothetical protein LOC51255
hCG34333.2	PSMD1	Proteasome (prosome, macropain) 26S subunit, non-ATPase, 1
hCG2018239.1	C20orf40	Chromosome 20 open reading frame 40
hCG1770706.3	PPP4C	Protein phosphatase 4 (formerly X), catalytic subunit
hCG17176.3	RIT1	Ras-like without CAAX 1
hCG20857.3	F11R	F11 receptor
hCG401112.3	NSAP1	NS1-associated protein 1
hCG37487.3	HSU84971|FLJ10283	Fetal hypothetical protein|hypothetical protein FLJ10283
hCG25086.4	CTBS	Chitobiase, di-N-acetyl-
hCG21857.3	SNAPC2	Small nuclear RNA activating complex, polypeptide 2, 45kDa
hCG201158.4	CDC2L2	Cell division cycle 2-like 2
hCG1640926.3	GNG12	Guanine nucleotide binding protein (G protein), gamma 12
hCG23133.3	FLJ10898	KIAA1685 protein
hCG1642370.3	CXX1	CAAX box 1
hCG20224.2	SEPW1	selenoprotein W, 1
hCG2016179	CIP29|DRIP78	Cytokine induced protein 29 kDa|dopamine receptor interacting protein
hCG32920.3	WASL	Wiskott-Aldrich syndrome-like
hCG1992163	TAF15	TAF15 RNA polymerase II, TATA box binding protein (TBP)-associated factor, 68kDa
hCG28059.3	CLTA	clathrin, light polypeptide (Lca)
hCG1640491.3	CNO	Cappuccino
hCG1782977.2	PAK1IP1	PAK1 interacting protein 1
hCG17610.3	CITED1	Cbp/p300-interacting transactivator, with Glu/Asp-rich carboxy-terminal domain, 1
hCG1812038.1	USP31	Ubiquitin specific protease 31
hCG23000.4	GENX-3414	genethonin 1
hCG1775207.1	CGI-147	CGI-147 protein
hCG1811182.2	CD44	CD44 antigen (homing function and Indian blood group system)
hCG20722.4	SNRPD2	Small nuclear ribonucleoprotein D2 polypeptide 16.5kDa
hCG38329.2	H2AFY	H2A histone family, member Y

hCG2002898.1	IL6ST	Interleukin 6 signal transducer (gp130, oncostatin M receptor)
hCG1811421.1	LOC51319	Hypothetical protein LOC51319
hCG17527.3	HKE2	HLA class II region expressed gene KE2
hCG17111.3	NRCAM	Neuronal cell adhesion molecule
hCG16901.3	QPCT	glutaminyl-peptide cyclotransferase (glutaminyl cyclase)
hCG21108.3	IRF3	Interferon regulatory factor 3
hCG23840.2	SCARB2	Scavenger receptor class B, member 2
hCG34605.3	TGOLN2	Trans-golgi network protein 2
hCG41557.2	PHF5A	PHD finger protein 5A
hCG38577.3	TRA16	TR4 orphan receptor associated protein TRA16
hCG1817741.1	LOC55580|FLJ10392	Hypothetical protein LOC55580|hypothetical protein FLJ10392
hCG96444.4	CD2BP2	CD2 antigen (cytoplasmic tail) binding protein 2
hCG1811270.2	MI-ER1	Mesoderm induction early response 1
hCG2023423	PDAP1	PDGFA associated protein 1
hCG1741224.1	PSMD4	Proteasome (prosome, macropain) 26S subunit, non-ATPase, 4
NM_018845.1	LOC55974	Stromal cell protein
hCG33216.2	TIP-1	Tax interaction protein 1
hCG30332.3	RAB14	RAB14, member RAS oncogene family
hCG18034.3	RFC2	Replication factor C (activator 1) 2, 40kDa
hCG17314.3	JWA	Cytoskeleton related vitamin A responsive protein
hCG1785781.2	DKFZp761K1423	Hypothetical protein DKFZp761K1423
hCG17104.3	MRAS	Muscle RAS oncogene homolog
hCG37772.3	PLEKHB2	Pleckstrin homology domain containing, family B (evectins) member 2
hCG22119.2	LGALS3	lectin, galactoside-binding, soluble, 3 (galectin 3)
hCG1995572	RPS19	Ribosomal protein S19
hCG27698.3	DDX47	DEAD (Asp-Glu-Ala-Asp) box polypeptide 47
hCG1815074.1	GALNT7	UDP-N-acetyl-alpha-D-galactosamine:polypeptide N-acetylgalactosaminyltransferase 7 (GalNAc-T7)
hCG1743052.1	HIST1H4J	histone 1, H4j
hCG28475.3	EIF3S4	Eukaryotic translation initiation factor 3, subunit 4 delta, 44kDa
hCG41504.3	PRKAG1	protein kinase, AMP-activated, gamma 1 non-catalytic subunit
hCG23733.3	PRKCL2	protein kinase C-like 2
hCG1736747.2	HSPC163	HSPC163 protein
hCG15268.3	CA11	carbonic anhydrase XI
hCG23832.3	TAF1B	TATA box binding protein (TBP)-associated factor, RNA polymerase I, B, 63kDa
hCG2019614	NSFL1C	NSFL1 (p97) cofactor (p47)
hCG20131.3	USP4	Ubiquitin specific protease 4 (proto-oncogene)
hCG2006519	PSMD7	Proteasome (prosome, macropain) 26S subunit, non-ATPase, 7 (Mov34 homolog)
hCG15540.2	LOC113174	Hypothetical protein BC012010
hCG38464.3	CAPZA1	Capping protein (actin filament) muscle Z-line, alpha 1
hCG17666.2	PPARD	peroxisome proliferative activated receptor, delta
NM_153810.1	MGC33215	Hypothetical protein MGC33215
hCG1778767.2	AF1Q	ALL1-fused gene from chromosome 1q

hCG22629.2	BACH	Brain acyl-CoA hydrolase
hCG27511.3	FLJ13855	Hypothetical protein FLJ13855
hCG2028156	DMXL1	Dmx-like 1
hCG25594.3	FXYD5	FXYD domain containing ion transport regulator 5
hCG29947.3	TBC1D2	TBC1 domain family, member 2
hCG41772.4	PSMA7	Proteasome (prosome, macropain) subunit, alpha type, 7
hCG1997687.1	YAF2	YY1 associated factor 2
hCG1993933	IDS	Iduronate 2-sulfatase (Hunter syndrome)
hCG1787380.1	HIST1H4C	Histone 1, H4c
hCG1640439.3	MAP4K4|FLJ20373	Mitogen-activated protein kinase kinase kinase kinase 4|hypothetical protein FLJ20373
hCG20743.3	CD63	CD63 antigen (melanoma 1 antigen)
hCG1811074.1	EPS8	Epidermal growth factor receptor pathway substrate 8
hCG24410.2	FLJ10849	Hypothetical protein FLJ10849
hCG28251.3	EFA6R	ADP-ribosylation factor guanine nucleotide factor 6
hCG2028720	SYNJ2BP	Synaptojanin 2 binding protein
hCG22716.3	CSNK1G2	Casein kinase 1, gamma 2
hCG18409.4	CGI-32	CGI-32 protein
hCG29982.3	MGC4549	Hypothetical protein MGC4549
hCG25167.4	MGST1	Microsomal glutathione S-transferase 1
hCG25594.3	FXYD5	FXYD domain containing ion transport regulator 5
hCG29393.3	EVER1	Epidermodysplasia verruciformis 1
hCG1787850.1	ARPC3	Actin related protein 2/3 complex, subunit 3, 21kDa
hCG24125.2	RAD50	RAD50 homolog (S. cerevisiae)
hCG21844.4	GSTTLp28	Glutathione-S-transferase like; glutathione transferase omega
hCG2023566	COL8A1	Collagen, type VIII, alpha 1
hCG24776.3	MAD2L2	MAD2 mitotic arrest deficient-like 2 (yeast)
hCG29191.3	RGS3	Regulator of G-protein signalling 3
hCG24883.2	C10orf7	Chromosome 10 open reading frame 7
hCG1640463.2	HIST1H2AI	Histone 1, H2ai
hCG2016616	MGC29649	Hypothetical protein MGC29649
NM_173810.2	MGC29649	Hypothetical protein MGC29649
hCG2029168.1	SERPINA1	Serine (or cysteine) proteinase inhibitor, clade A (alpha-1 antiproteinase, antitrypsin), member 1
hCG32783.2	P5CR2	Pyrroline 5-carboxylate reductase isoform
hCG14635.2	TMSB4Y	thymosin, beta 4, Y chromosome
hCG1810958.2	LYN	v-yes-1 Yamaguchi sarcoma viral related oncogene homolog
hCG21576.3	GPX4	Glutathione peroxidase 4 (phospholipid hydroperoxidase)
hCG18636.2	HDAC8	histone deacetylase 8
hCG1790710.2	C14orf147	Chromosome 14 open reading frame 147
hCG1640844.3	C8orf4	Chromosome 8 open reading frame 4
hCG25270.2	RBBP2	Retinoblastoma binding protein 2
hCG22576.2	FLJ11175	Hypothetical protein FLJ11175
hCG1980223	HSPC111	Hypothetical protein HSPC111
NM_004454.1	ETV5	Ets variant gene 5 (ets-related molecule)
hCG39977.3	BICD1	Bicaudal D homolog 1 (Drosophila)
hCG2010805	KDELR3	KDEL (endoplasmic reticulum protein retention receptor 3

hCG14678.2	RAD23B	RAD23 homolog B (S. cerevisiae)
hCG21771.2	KIAA0677	KIAA0677 gene product
hCG21149.3	STX4A	Syntaxin 4A (placental)
hCG34610.4	SIAT9	Sialyltransferase 9 (CMP-NeuAc:lactosylceramide alpha-2,3-sialyltransferase; GM3 synthase)
hCG2016647	CCND1	Cyclin D1 (PRAD1: parathyroid adenomatosis 1)
hCG25185.2	PSMC3	Proteasome (prosome, macropain) 26S subunit, ATPase, 3
hCG1999622.1	SCOTIN	scotin
hCG2024976	RRP4	Homolog of Yeast RRP4 (ribosomal RNA processing 4), 3'-5'-exoribonuclease

Table 6.5 Genes with increased expression in PTC relative to benign conditions using the Distinction Calculation. Shaded rows depict genes previously described in the literature as having relevance in thyroid pathology.

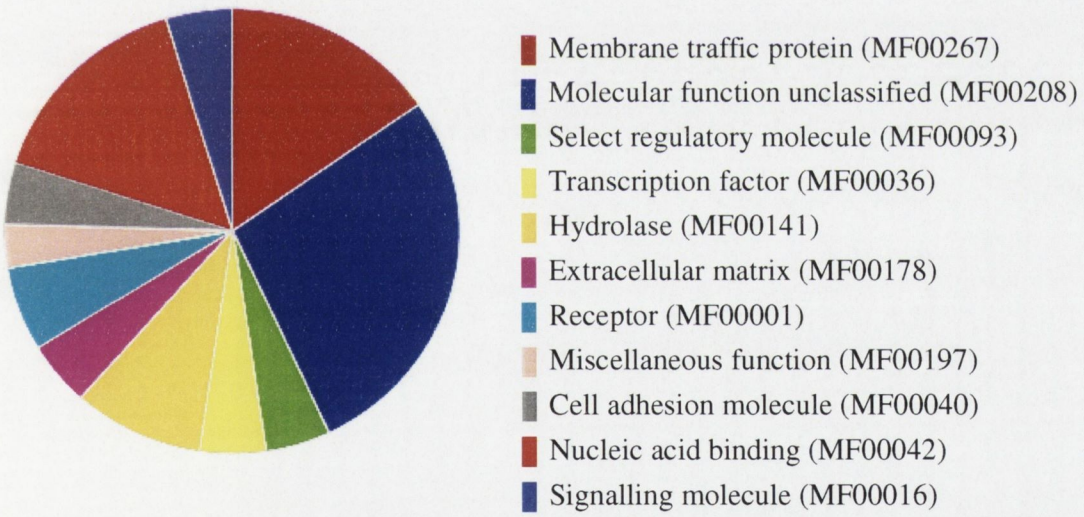

Figure 6.6 Panther Classification of transcripts seen in Table 6.5.

6.6.5 Benign and malignant follicular patterned lesions

A key clinical requirement may be the ability to differentiate malignant follicular patterned lesions (Follicular carcinoma and FVPTC) from benign follicular patterned lesions. In practice, using FNA, this problem is more often encountered as a clinical dilemma (because classic morphology PTC is more easily diagnosed by FNA). While it would have been worthwhile to include expression profiles from Follicular Carcinoma, we were restricted to analysis of Follicular Variant PTC and discrimination of this lesion from other benign follicular patterned lesions.

Again using a t-test it was possible to generate a list of 2639 genes with significant fold change between the two groups and to demonstrate that FVPTC and Benign follicular patterned lesions cluster distinctly as is seen in Figure 6.5

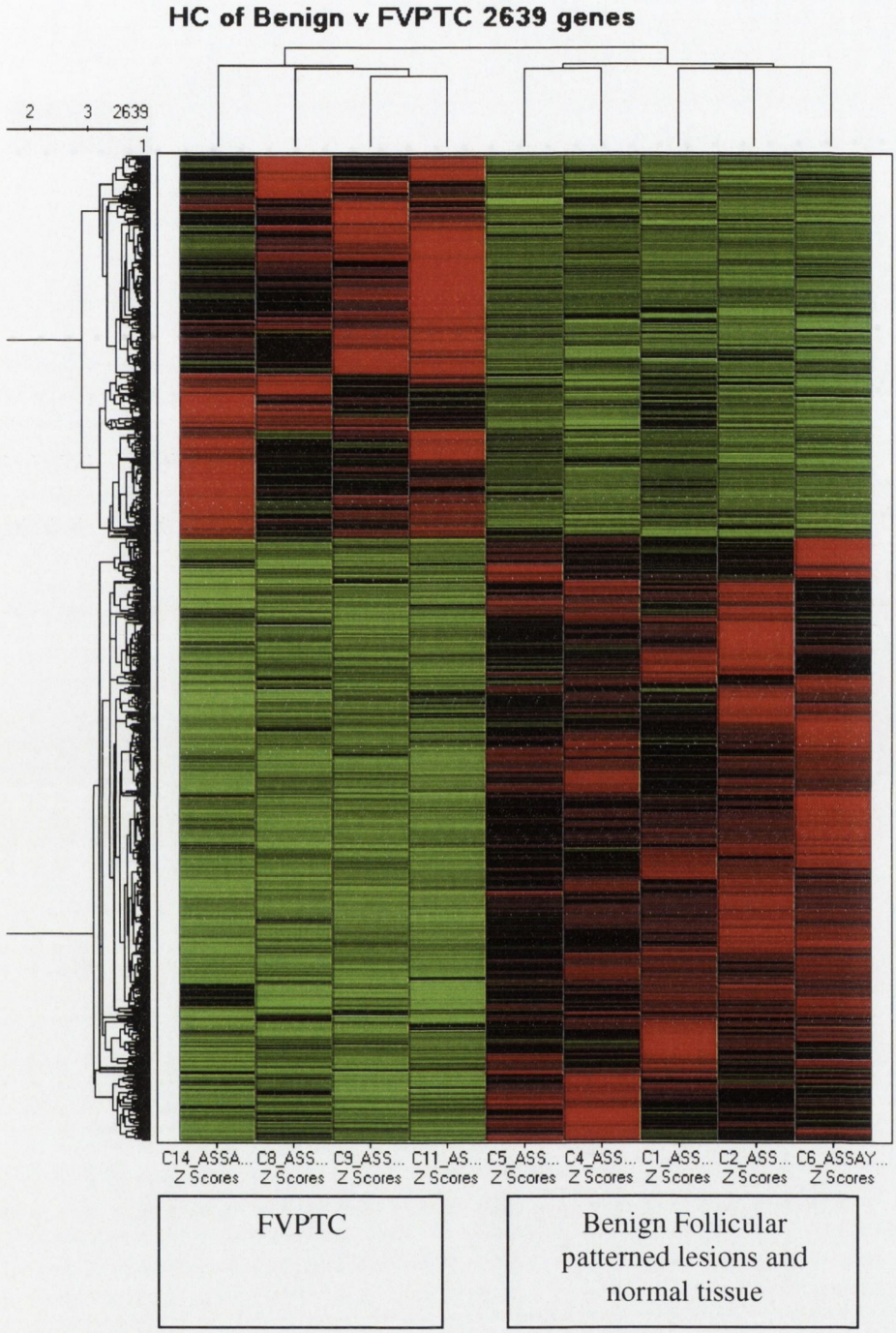

Figure 6.5 Hierarchical clustering of 2639 genes that distinguish FVPTC and other benign patterned follicular lesions. A Z score transformation was used to make genes comparable. There is a clear pattern of expression, Genes showing relatively increased expression are highlighted in red and those showing relative decreased expression are highlighted in green.

Bonferroni correction proved too stringent to identify significant biomarkers but using a *p*-value <0.001 a list of 64 genes demonstrated marked increased expression in FVPTC compared to benign follicular tissue and lesions. However, using FDR (BY method, q = 0.05), it was possible to identify genes showing more than 2 fold-increased expression in FVPTC compared to benign follicular patterned lesions and normal thyroid tissue (Table 6.6).

Gene ID	Gene Symbol	Gene Name
hCG38538.3	SPP1	Secreted phosphoprotein 1 (osteopontin, bone sialoprotein I, early T-lymphocyte activation 1)
hCG39680.3	PCSK2	Proprotein convertase subtilisin/kexin type 2
hCG29297.1	CCL13	Chemokine (C-C motif) ligand 13
hCG2010805	KDELR3	KDEL (Lys-Asp-Glu-Leu) endoplasmic reticulum protein retention receptor 3
hCG37504.2	DPYSL3	dihydropyrimidinase-like 3
hCG1811156.1	SORCS1	VPS10 domain receptor protein SORCS 1
hCG2002898.1	IL6ST	Interleukin 6 signal transducer (gp130, oncostatin M receptor)
hCG21094.3	SLC1A5	Solute carrier family 1 (neutral amino acid transporter), member 5
hCG2016952	FLJ22531	Hypothetical protein FLJ22531
hCG24743.3	RCOR	REST corepressor
hCG14731.3	KRAS2	v-Ki-ras2 Kirsten rat sarcoma 2 viral oncogene homolog
NM_006021.1	DLEU2	Deleted in lymphocytic leukemia, 2
hCG40173.3	CPNE6	Copine VI (neuronal)
hCG21529.3	BID	BH3 interacting domain death agonist
hCG24334.2	CTSH	Cathepsin H
hCG29393.3	EVER1	Epidermodysplasia verruciformis 1
NM_007200.3	AKAP13	A kinase (PRKA) anchor protein 13
hCG2004778	FLJ12541	Stimulated by retinoic acid gene 6
hCG32707.3	CXCL16	Chemokine (C-X-C motif) ligand 16
hCG1991625	FLJ20294	Hypothetical protein FLJ20294
hCG28476.2	ICAM1	Intercellular adhesion molecule 1 (CD54), human rhinovirus receptor
hCG20166.2	C1orf38	Chromosome 1 open reading frame 38
hCG24420.3	ARHGDIB	Rho GDP dissociation inhibitor (GDI) beta
hCG1811614.1	BAX	BCL2-associated X protein
hCG1811182.2	CD44	CD44 antigen (homing function and Indian blood group system)
NM_002675.2	PML	Promyelocytic leukemia
hCG25379.4	MGC4342	Hypothetical protein MGC4342
hCG2033276	CD109	CD109 antigen (Gov platelet alloantigens)
hCG1995506	PLD3	Phospholipase D3
hCG38865.4	RAB27A	RAB27A, member RAS oncogene family
hCG23527.3	PIASY	Protein inhibitor of activated STAT protein PIASy
hCG16921.3	S100A11	S100 calcium binding protein A11 (calgizzarin)
hCG2036531	MDN1	MDN1, midasin homolog (yeast)
hCG29982.3	MGC4549	Hypothetical protein MGC4549
hCG17457.4	CISH	Cytokine inducible SH2-containing protein
hCG18703.4	RCP9	Calcitonin gene-related peptide-receptor component protein
hCG25177.3	DDB2	Damage-specific DNA binding protein 2, 48kDa
hCG17680.2	PHLDA3	Pleckstrin homology-like domain, family A, member 3
hCG25147.3	RHBDL2	Rhomboid, veinlet-like 2 (Drosophila)
hCG27314.2	OSTF1	Osteoclast stimulating factor 1

Gene ID	Gene Symbol	Gene Name
hCG37487.3	HSU84971|FLJ10283	Fetal hypothetical protein|hypothetical protein FLJ10283
hCG1790710.2	C14orf147	Chromosome 14 open reading frame 147
hCG22321.3	TGFB1	Transforming growth factor, beta 1 (Camurati-Engelmann disease)
hCG27151.3	NAT2	N-acetyltransferase 2 (arylamine N-acetyltransferase)
hCG2018239.1	C20orf40	Chromosome 20 open reading frame 40
hCG1985644.1	MVP	Major vault protein
hCG37772.3	PLEKHB2	Pleckstrin homology domain containing, family B (evectins) member 2
hCG22216.3	PPP3R1	Protein phosphatase 3 (formerly 2B), regulatory subunit B, 19kDa, alpha isoform (calcineurin B, type I)
hCG40952.3	PTPRE	Protein tyrosine phosphatase, receptor type, E
hCG37772.3	PLEKHB2	Pleckstrin homology domain containing, family B (evectins) member 2
hCG38642.3	HNOEL-iso	HNOEL-iso protein
hCG17211.3	BAL	B aggressive lymphoma gene
hCG1770706.3	PPP4C	Protein phosphatase 4 (formerly X), catalytic subunit
hCG1990006	RPS2	Ribosomal protein S2
hCG22716.3	CSNK1G2	Casein kinase 1, gamma 2
hCG1992628	DKFZp547D065	Hypothetical protein DKFZp547D065
hCG17104.3	MRAS	Muscle RAS oncogene homolog
hCG37135.3	PROCR	Protein C receptor, endothelial (EPCR)
hCG2032359	ASML3B	Acid sphingomyelinase-like phosphodiesterase
hCG1999622.1	SCOTIN	scotin
hCG42425.3	ACAA1	Acetyl-Coenzyme A acyltransferase 1 (peroxisomal 3-oxoacyl-Coenzyme A thiolase)
hCG1778022.2	KIAA0152	KIAA0152 gene product
hCG2006519	PSMD7	Proteasome (prosome, macropain) 26S subunit, non-ATPase, 7 (Mov34 homolog)

Table 6.6 Genes showing increased expression in FVPTC compared to normal thyroid tissue and benign follicular patterned thyroid lesions using the BY statistic with p = 0.05

6.6.6 Panther analysis to assess functional differences between the follicular variant of PTC and classic morphology PTC

As discussed above, the Panther system uses a library of Hidden Markov Models (HMMs) to annotate sequences with information from homologous sequences. The PANTHER library contains HMMs not only for families, but also for functionally distinct subfamilies. A key function of the Panther system is the ability to analyse gene lists for over or under represented biological processes among each cluster. From a biological point it would be fascinating to assess which biological processes are relatively over and under represented in a comparison of FVPTC and classic morphology PTC. By generating lists of genes that show increased or decreased fold change in FVPTC relative to classic morphology PTC we can use Panther to assess which molecular functions are significantly associated with each phenotype.

When comparing genes showing increased expression in FVPTC in comparison to classic morphology PTC, two categories were significantly overrepresented (Table 6.7).

Panther Category	P-value
Microtubule family cytoskeletal Protein and microtubule binding motor protein	1.15E-4
Chemokine	2.69E-3

Table 6.7 Functional comparison of genes showing increased expression in FVPTC and relative decreased expression in classic morphology PTC

Specific genes of each category are discussed below

Using the same strategy, and by looking at genes showing increased expression in classic morphology PTC in comparison to FVPTC a further two categories of genes show statistically significant over representation in the classic morphology phenotype (Table 6.8).

Panther Category	P-value
Kinase activator/modulator	1.16E-3
Glycosyltransferase	1.85E-3

Table 6.8 Functional comparison of genes showing increased expression in classic morphology and relative decreased expression in FVPTC

Specific genes of each category are discussed below

6.7 Discussion

PTC accounts for up to 80% of all differentiated thyroid carcinomas. In many cases diagnosis and treatment planning are relatively straightforward after FNA, especially when the tumour shows classical papillary architecture and classic nuclear features. However, in a significant proportion of cases, FNA leads to suspicious or indeterminate diagnosis and surgical treatment planning and patient prognosis are set on an unsure footing. This is particularly true of lesions with follicular morphology and with inflammatory lesions with secondary Hurthle cell changes and nuclear abnormalities. For these reasons there is a need to develop biomarkers of malignancy in order to make the preoperative diagnosis more accurate and allow more appropriate treatment planning (Segev, 2003; Baloch, 2003).

In the recent thyroid literature there has been an emphasis on identification of various biomarkers using a variety of techniques. Mutant BRAF (Xing, 2004), MUC-1 (Wreesman, 2004; Pineda, 2003), Galectin-3 (Volante, 2004; Rosai, 2003; Kovacs, 2003; Giannini, 2003; Herrman, 2002; Lloyd, 2001), Cytokeratin 19, high molecular weight Cytokeratin, HBME-1 (Rosai, 2003; Casey, 2003), ECM-1 (Pauws, 2004), nicotinamide N-methyltransferase (Xu, 2003), c-met in Tall cell variant (Nardone, 2003), CD10 (Tomoda, 2003), Dipeptidyl peptidase IV/CD63 (Kholova, 2003; Aratake, 2002) and Cox 2 (Specht, 2002) among others have all been suggested as potential biomarkers of malignancy or differentiation. Despite the promise of markers such as Galectin-3, no single biomarker has become widely used and accepted in wide clinical practice.

Microarray technology provides a very powerful tool for biomarker identification. The first step to identifying a biomarker or a panel of biomarkers is to develop a "training set" using lesions with well-defined morphological diagnoses and well-defined molecular biological features. Having identified potential biomarkers, their utility must be analysed in a large cohort of lesions to examine sensitivity and specificity. Finally a selected group of biomarkers must be assessed in clinical FNA material from patients presenting prospectively to the clinical service.

In this study, we have performed the first step in this pathway. Numerous genes have been identified, within each of the study groups, from a range of host cell pathways that show significant changes in expression levels when compared with control samples. These preliminary results identify novel genes that may be implicated in the pathogenesis of PTC and in future may prove to be biomarkers of malignancy.
Hierarchical cluster analysis permitted us to distinguish benign thyroid lesions from PTC (both FVPTC and classic morphology PTC). Additionally, hierarchical clustering permitted distinction of the clinically problematic FVPTC from benign thyroid lesions.

Many of the genes identified in this study are entirely novel in the context of thyroid neoplasia. This is to be expected since there are no publications in the literature making use of an expression array platform with as many well-curated transcripts as this one.

However, it is reassuring that a subset of genes previously identified in the literature as being relevant to PTC are identified in this study. Of note, increased expression of CITED 1 in PTC (Huang, 2001; Prasad, 2004b), LGAL 3 (Galectin-3) and CD63 (Kholova, 2003; Aratake, 2002) in malignant thyroid lesions have been suggested from the literature and are reproduced in the current data set. Osteoclast stimulating factor, LYN (V-yes-1 Yamaguchi sarcoma viral related oncogene), PDGFA (Platelet derived growth factor A and the H2A Histone family were all shown in a previous study to show increased expression in PTC compared to benign thyroid neoplasms and normal thyroid tissue (Yano, 2004). While all of these genes show increased expression in PTC (Distinction tables) in the current data set, none was near the top of the gene lists either by maximal fold change or Bonferroni correction. In the case of the study by Yano *et al* this finding no doubt reflects the limited scale of the array used by the authors (4000 cDNA) in comparison to the full genome available on the ABI 1700 system.

An alternative reason may be the relative abundance of formerly poorly curated genes present on other microarray platforms and if that is the case, then the present study has the potential to uncover many more potential biomarkers than has previously been possible. Most other array platforms contain numerous probes for Expressed Sequence Tags (ESTs). More than 5 million ESTs have been generated, however, the sequences of ESTs are fragmented (400-600 bases) and often inaccurate (1-3% coding errors). For these reasons, assigning each of these ESTs to a particular gene has been elusive. The Affymetrix total human gene chip (U133) contains as many as 8000 ESTs or uncharacterised genes. A key advantage of the array system used in this

chapter is that the probe set is highly curated both to publicly known and curated genes and to the private Celera gene set.

A number of the genes showing increased expression deserve special note. Calgizzarin is a member of the S100 family. Tanaka *et al* identified and sequenced a cDNA encoding a human calgizzarin homolog (Tanaka, 1995). They found that the expression of human calgizzarin was remarkably elevated in colorectal cancers compared with that in normal colorectal mucosa. Tomasetto reported that Calgizzarin was one of several genes expressed in breast cancer-derived metastatic axillary lymph nodes but not in normal lymph nodes or breast fibroadenomas (Tomasetto, 1995). This literature suggests that Calgizzarin may represent a marker of malignancy, at least in some tumour types. Of interest, S100 immunohistochemistry (clone and epitope unspecified) has been suggested as a marker of PTC in comparison to benign papillary hyperplasia (Mitselou, 2002).

Osteopontin (OPN) has been shown to be a major RET/PTC-induced transcriptional target in PCCl3 thyroid follicular cells Castellone, 2004). RET/PTC also induced a strong overexpression of CD44, a cell surface signalling receptor for OPN. Thus, RET/PTC signalling triggers an autocrine loop involving OPN and CD44 that sustains proliferation and invasion of transformed PCCl3 thyrocytes. Although ret rearrangements were not detected in any of the cases included in this study it is intriguing that increased expression of both Osteopontin and CD 44 could be demonstrated in the tissues examined and suggests perhaps that expression of Osteopontin in thyroid carcinoma may occur independently of ret rearrangement or as a result of another kinase activating mechanism. Osteopontin may be a promising

marker of malignancy because expression has been demonstrated in human tumours from different body sites, suggesting involvement of this protein in tumour formation (Coppola, 2004).

Of the genes showing decreased expression in malignancy increased expression of Trefoil factor 3 has been implicated in the pathogenesis of both gastric and prostatic carcinoma. However, a recent paper comparing follicular adenoma with follicular thyroid carcinoma has shown marked decreased expression of trefoil factor 3 in follicular carcinoma relative to follicular adenoma (Takano, 2004) data, which is mirrored in this chapter.

The Panther system allowed for analysis of functional correlates of the genes detected. Figure 6.6 shows that "membrane traffic proteins" and "DNA binding proteins" were the Panther families containing the highest number of up-regulated genes in malignancy. It is not very surprising that genes belonging to either of these two families would show increased expression in malignancy relative to benign conditions and it is tempting to suggest that the increased expression of various DNA binding proteins might be responsible for the distinct nuclear morphology of these tumours.
A more powerful use of The Panther system was the ability to compare statistically over and under represented gene families in the phenotypically distinct PTC variants (FVPTC and Classic morphology PTC). The morphological differences between the two variants are clearly a reflection of gene expression patterns. The overexpression in FVPTC of microtubule family cytoskeletal proteins such as the Tubulin β chain, cytoplasmic dynein heavy chain 2 and the dynein heavy chain and of chemokines including CCL20 (chemokine ligand 20), CCL 27 (chemokine ligand 27) and

SPBPBP (DNA-binding protein amplifying expression of surfactant protein B) may account for the architectural differences between FVPTC and classic PTC.

Over representation of genes of the kinase category such as DUSP4 (dual specificity phosphatase 4), AKAP10 (A kinase anchor protein 10), MADHIP (mothers against decapentaplegic homolog (Drosophila) interacting protein, receptor activation anchor) and the Glycosylasetransferase category such as BGALT6 (beta 1,4-galactosyltransferase, polypeptide 6), GBE1 (glucan (1,4-alpha-), branching enzyme 1), ART5 (ADP-ribosyltransferase 5), ARHJ (ras homolog gene family, member J) and SIAT6 (sialyltransferase 6 (N-acetyllacosaminide alpha 2,3-sialyltransferase) in classic morphology PTC relative to FVPTC is an intriguing finding but of uncertain significance currently.

6.6 Conclusion

In this chapter, many candidate biomarkers of malignancy have been identified. However, although data mining has allowed a relatively small number of relevant genes to be isolated from the entire human genome, further investigation will be required to even further hone these lists. Genes showing decreased expression are less attractive as biomarkers than those showing increased expression, however these genes are no less relevant because it is plausible that no single biomarker of malignancy may be predictive and a matrix of markers may be required which may well include negative markers in association with positive markers. In order to refine the gene lists presented in this chapter, further validation must be performed on selected tissues using a larger number of thyroid lesions. Low-density TaqMan arrays are based on microfluidic technology and are available in a variety of formats that

allow validation of gene expression experiments using small PCR volumes and multiple assays. They are effectively a low density PCR array. The next step will be to perform low-density TaqMan arrays to further refine these data. Subsequent to that, retrospective and prospective trials of the validated biomarkers will be performed to continue the search for clinically relevant biomarkers.

6.9 References

Aratake Y, Umeki K, Kiyoyama K, Hinoura Y, Sato S, Ohno A, Kuribayashi T, Hirai K, Nabeshima K, Kotani T. 2002. Diagnostic utility of galectin-3 and CD26/DPPIV as preoperative diagnostic markers for thyroid nodules. Diagn Cytopathol 26(6): 366-72.

Baloch ZW, LiVolsi VA. 2002. The quest for a magic tumor marker: continuing saga in the diagnosis of the follicular lesions of thyroid. Am J Clin Pathol. 118(2): 165-6.

Bartolazzi A, Gasbarri A, Papotti M, Bussolati G, Lucante T, Khan A, Inohara H, Marandino F, Orlandi F, Nardi F, Vecchione A, Tecce R, Larsson O. 2001. Application of an immunodiagnostic method for improving preoperative diagnosis of nodular thyroid lesions. Lancet. 357(9269): 1644-50.

Barden CB, Shister KW, Zhu B, Guiter G, Greenblatt DY, Zeiger MA, Fahey TJ 3rd. 2003. Classification of follicular thyroid tumors by molecular signature: results of gene profiling. Clin Cancer Res. 9(5): 1792-800.

Beesley MF, McLaren KM. 2002. Cytokeratin 19 and galectin-3 immunohistochemistry in the differential diagnosis of solitary thyroid nodules. Histopathology. 41(3):236-43

Benjamini Y, Hochberg Y. 1995. Controlling the false discovery rate: a practical and powerful approach to multiple testing. J R Stat Soc Ser B 57: 289-300.

Benjamini Y, Yekutieli D. 2001. The control of the false discovery rate in multiple testing under dependency. Ann Stat 29: 1165-1188.

Bonferroni CE. 1936. Teoria statistica delle classi e calcalo delle probabilitá. Pubblicazioni del R Instituto Superiore di Scienze Economiche e Commerciali di Firenze, 8:3-62

Caruso D, Mazzaferri EL. 1991. Fine needle aspiration biopsy in the management of thyroid nodules. Endocrinologist 1:194-202

Casey MB, Lohse CM, Lloyd RV. 2003. Distinction between papillary thyroid hyperplasia and papillary thyroid carcinoma by immunohistochemical staining for cytokeratin 19, galectin-3, and HBME-1. Endocr Pathol. 14(1): 55-60.

Castellone MD, Celetti A, Guarino V, Cirafici AM, Basolo F, Giannini R, Medico E, Kruhoffer M, Orntoft TF, Curcio F, Fusco A, Melillo RM, Santoro M. 2004. Autocrine stimulation by osteopontin plays a pivotal role in the expression of the mitogenic and invasive phenotype of RET/PTC-transformed thyroid cells. Oncogene 23(12): 2188-96

Cerutti JM, Delcelo R, Amadei MJ, Nakabashi C, Maciel RM, Peterson B, Shoemaker J, Riggins GJ. 2004. A preoperative diagnostic test that distinguishes benign from malignant thyroid carcinoma based on gene expression. J Clin Invest. 113(8): 1234-42

Cheadle C, Vawter MP, Freed WJ, Becker KG. 2003. Analysis of microarray data using Z-score transformation. Journal of molecular Diagnostics 5 (2): 73-81

Coppola D, Szabo M, Boulware D, Muraca P, Alsarraj M, Chambers AF, Yeatman TJ. 2004. Correlation of osteopontin protein expression and pathological stage across a wide variety of tumor histologies. Clin Cancer Res. 10:184-90.

Eberwine J, 1996. Amplification of mRNA populations using cRNA generated from immobilized oligo(dT)-T7 primed cDNA. Biotechniques. 4:584-91

Finley DJ, Zhu B, Barden CB, Fahey TJ 3rd. 2004a. Discrimination of Benign and Malignant Thyroid Nodules by Molecular Profiling. Ann Surg. 240(3): 425-437.

Finley DJ, Arora N, Zhu B, Gallagher L, Fahey TJ 3rd. 2004b. Molecular profiling distinguishes papillary carcinoma from benign thyroid nodules. J Clin Endocrinol Metab. 89(7): 3214-23

Feilchenfeldt J, Totsch M, Sheu SY, Robert J, Spiliopoulos A, Frilling A, Schmid KW, Meier CA. 2003. Expression of galectin-3 in normal and malignant thyroid tissue by quantitative PCR and immunohistochemistry. Mod Pathol. 16(11):1117-23

Giannini R, Faviana P, Cavinato T, Elisei R, Pacini F, Berti P, Fontanini G, Ugolini C, Camacci T, De Ieso K, Miccoli P, Pinchera A, Basolo F. 2003. Galectin-3 and oncofetal-fibronectin expression in thyroid neoplasia as assessed by reverse

transcription-polymerase chain reaction and immunochemistry in cytologic and pathologic specimens. Thyroid. 13(8): 765-70

Golub TR, Slonim DK, Tamayo P, Huard C, Gaasenbeek M, Mesirov JP, Coller H, Loh ML, Downing JR, Caligiuri MA, Bloomfield CD, Lander ES. 1999. Molecular classification of cancer: class discovery and class prediction by gene expression monitoring. Science 286(5439): 531-7

Hamberger B, Gharib H, Melton LJ III, Goellner JR, Zinsmeister AR. 1982. Fine-needle aspiration biopsy of thyroid nodules: impact on thyroid practice and cost of care. Am J Med 73:381-384

Herrmann ME, LiVolsi VA, Pasha TL, Roberts SA, Wojcik EM, Baloch ZW. 2002. Immunohistochemical expression of galectin-3 in benign and malignant thyroid lesions. Arch Pathol Lab Med.126 (6): 710-3

Huang Y, Prasad M, Lemon WJ, Hampel H, Wright FA, Kornacker K, LiVolsi V, Frankel W, Kloos RT, Eng C, Pellegata NS, de la Chapelle A. 2001. Gene expression in papillary thyroid carcinoma reveals highly consistent profiles. Proc Natl Acad Sci U S A. 98(26): 15044-9.

Goellner JR, Gharib H, Grant CS, Johnson DA. 1987. Fine needle aspiration cytology of the thyroid, 1980 to 1986. Acta Cytol. 31(5): 587-90

Inohara H, Honjo Y, Yoshii T, Akahani S, Yoshida J, Hattori K, Okamoto S, Sawada T, Raz A, Kubo T. 1999. Expression of galectin-3 in fine-needle aspirates as a diagnostic marker differentiating benign from malignant thyroid neoplasms. Cancer 85(11): 2475-84

Kholova I, Ryska A, Ludvikova M, Cap J, Pecen L. 2003. Dipeptidyl peptidase IV expression in thyroid cytology: retrospective histologically confirmed study. Cytopathology. 14(1): 27-31.

Kovacs RB, Foldes J, Winkler G, Bodo M, Sapi Z. 2003. The investigation of galectin-3 in diseases of the thyroid gland. Eur J Endocrinol. 149(5): 449-53.

Leung YF, Cavalieri D. 2003. Fundamentals of cDNA microarray analysis. Trends in Genetics 19(11): 649-659

Lloyd RV. 2001. Distinguishing benign from malignant thyroid lesions: galectin 3 as the latest candidate. Endocr Pathol. 12(3): 255-7

Mazzaferri EL. 1993. Management of a solitary thyroid nodule. NEJM 328:553-559

Mazzanti C, Zeiger MA, Costourous N, Umbricht C, Westra WH, Smith D, Somervell H, Bevilacqua G, Alexander HR, Libutti SK. 2004. Using gene expression profiling to differentiate benign versus malignant thyroid tumors. Cancer Res. 64(8): 2898-903

Mitselou A, Vougiouklakis TG, Peschos D, Dallas P, Boumba VA, Agnantis NJ. 2002. Immunohistochemical study of the expression of S-100 protein, epithelial membrane antigen, cytokeratin and carcinoembryonic antigen in thyroid lesions. Anticancer Res. 2002 22(3): 1777-80.

Nardone HC, Ziober AF, LiVolsi VA, Mandel SJ, Baloch ZW, Weber RS, Mick R, Ziober BL. 2003. c-Met expression in tall cell variant papillary carcinoma of the thyroid. Cancer. 98(7): 1386-93.

Pauws E, Veenboer GJ, Smit JW, de Vijlder JJ, Morreau H, Ris-Stalpers C. 2004. Genes differentially expressed in thyroid carcinoma identified by comparison of SAGE expression profiles. FASEB J.18 (3): 560-1.

Pineda P, Rojas P, Liberman C, Moyano L, Goecke I. 2003. [Detection of malignancy markers in thyroid nodules by reverse transcriptase polymerase chain reaction (RT-PCR)]. Article in Spanish. Rev Med Chil. 131(9): 965-72

Pisani T, Vecchione A, Giovagnolii MR. 2004. Galectin-3 immunodetection may improve cytological diagnosis of occult papillary thyroid carcinoma. Anticancer Res. 24(2C): 1111-2

Prasad ML, Pellegata NS, Huang Y, Nagaraja HN, Chapelle Ad A, Kloos RT. 2004 Galectin-3, fibronectin-1, CITED-1, HBME1 and cytokeratin-19 immunohistochemistry is useful for the differential diagnosis of thyroid tumors. Mod Pathol. [Epub ahead of print]

Prasad ML, Pellegata NS, Kloos RT, Barbacioru C, Huang Y, de la Chapelle A. 2004b. CITED1 protein expression suggests Papillary Thyroid Carcinoma in high throughput tissue microarray-based study. Thyroid. (3): 169-75.

Ravetto C, Colombo L, Dottorini ME. 2000. Usefulness of fine-needle aspiration in the diagnosis of thyroid carcinoma: a retrospective study in 37,895 patients. Cancer. 2000 90(6): 357-63

Rosai J. 2003. Immunohistochemical markers of thyroid tumors: significance and diagnostic applications. Tumori. 89(5): 517-9

Saggiorato E, Aversa S, Deandreis D, Arecco F, Mussa A, Puligheddu B, Cappia S, Conticello S, Papotti M, Orlandi F. 2004. Galectin-3: presurgical marker of thyroid follicular epithelial cell-derived carcinomas. J Endocrinol Invest. 27(4):311-7

Saggiorato E, Cappia S, De Giuli P, Mussa A, Pancani G, Caraci P, Angeli A, Orlandi F. 2001. Galectin-3 as a presurgical immunocytodiagnostic marker of minimally invasive follicular thyroid carcinoma. Clin Endocrinol Metab. (11): 5152-8

Segev DL, Clark DP, Zeiger MA, Umbricht C. 2003. Beyond the suspicious thyroid fine needle aspirate. A review. Acta Cytol. 47(5): 709-22.

Sheils OM, Sweeney EC. 1999. TSH receptor status of thyroid neoplasms-TaqMan RT-PCR analysis of archival material. J Pathol 188(1):87-92.

Specht MC, Tucker ON, Hocever M, Gonzalez D, Teng L, Fahey TJ 3rd. 2002. Cyclooxygenase-2 expression in thyroid nodules. J Clin Endocrinol Metab. 87(1): 358-63

Storey JD. 2001. A direct approach to false discovery rates. J R Stat Soc Ser B 64: 479-498.

Takano T, Miyauchi A, Yoshida H, Kuma K, Amino N. 2004. High-throughput differential screening of mRNAs by serial analysis of gene expression: decreased expression of trefoil factor 3 mRNA in thyroid follicular carcinomas. Br J Cancer. 90(8): 1600-5.

Tanaka M, Adzuma K, Iwami M, Yoshimoto K, Monden Y, Itakura M. 1995. Human calgizzarin: one colorectal cancer-related gene selected by a large scale random cDNA sequencing and northern blot analysis. Cancer Lett 89: 195-200

Thomas PD, Campbell MJ, Kejariwal A, Mi H, Karlak B, Daverman R, Diemer K, Muruganujan A, Narechania A. 2003. PANTHER: a library of protein families and subfamilies indexed by function. Genome Res. (9): 2129-41

Tomasetto C, Regnier C, Moog-Lutz C, Mattei MG, Chenard MP, Lidereau R, Basset P, Rio MC. 1995. Identification of four novel human genes amplified and overexpressed in breast carcinoma and localized to the q11-q21.3 region of chromosome 17. Genomics 28(3): 367-76

Tomoda C, Kushima R, Takeuti E, Mukaisho K, Hattori T, Kitano H. 2003. CD10 expression is useful in the diagnosis of follicular carcinoma and follicular variant of papillary thyroid carcinoma. Thyroid.13 (3): 291-5.

Van 't Veer LJ, De Jong D. 2002. The microarray way to tailored cancer treatment. Nat Med. 8(1): 13-4

Volante M, Bozzalla-Cassione F, DePompa R, Saggiorato E, Bartolazzi A, Orlandi F, Papotti M. 2004. Galectin-3 and HBME-1 expression in oncocytic cell tumors of the thyroid. Virchows Arch. 445(2): 183-8

West M, Blanchette C, Dressman H, Huang E, Ishida S, Spang R, Zuzan H, Olson JA Jr, Marks JR, Nevins JR. 2001. Predicting the clinical status of human breast cancer by using gene expression profiles. Proc Natl Acad Sci U S A. 98(20): 11462-7

Wreesmann VB, Sieczka EM, Socci ND, Hezel M, Belbin TJ, Childs G, Patel SG, Patel KN, Tallini G, Prystowsky M, Shaha AR, Kraus D, Shah JP, Rao PH, Ghossein R, Singh B. 2004. Genome-wide profiling of papillary thyroid cancer identifies MUC1 as an independent prognostic marker. Cancer Res. 64(11): 3780-9

Xing M, Tufano RP, Tufaro AP, Basaria S, Ewertz M, Rosenbaum E, Byrne PJ, Wang J, Sidransky D, Ladenson PW. 2004. Detection of BRAF mutation on fine needle aspiration biopsy specimens: a new diagnostic tool for papillary thyroid cancer. J Clin Endocrinol Metab. 89(6): 2867-72

Xu J, Moatamed F, Caldwell JS, Walker JR, Kraiem Z, Taki K, Brent GA, Hershman JM. 2003. Enhanced expression of nicotinamide N-methyltransferase in human papillary thyroid carcinoma cells. J Clin Endocrinol Metab. 88(10): 4990-6

Yano Y, Uematsu N, Yashiro T, Hara H, Ueno E, Miwa M, Tsujimoto G, Aiyoshi Y, Uchida K. 2004. Gene expression profiling identifies platelet-derived growth factor as a diagnostic molecular marker for papillary thyroid carcinoma. Clin Cancer Res.10 (6):2035-43

Chapter 7

General Discussion, Future work and Conclusions

7.1 Review of results and conclusions

The knowledge of the molecular basis of both PTC and FTC has increased significantly in a relatively short period. Undoubtedly, the Chernobyl Disaster and the resulting increased incidence of PTC that occurred because of that accident, has led to an exponential increase in the knowledge of the molecular basis of the malignancy. However, even since the initial work of this thesis began, the rate of acquisition of molecular knowledge has been startling. When the work for the chapter 3 of this thesis began in 2002, rearrangements of the ret oncogene were firmly established as the central and only well described molecular event in PTC. At that time, there was little doubt that ret rearrangements were associated with radiation induced PTC and that ret/PTC-3 was strongly associated with the morphologically distinct solid variant occurring in Chernobyl fallout exposed children. However, in spite of this knowledge, the molecular pathogenesis of the majority of PTC was largely unknown.

Several studies from around the world suggested that ret rearrangements were detectable in PTCs from geographically disparate areas of the world remote from Chernobyl. In previous work, our group had shown that highly sensitive TaqMan RTPCR could be used to identify transcripts of ret/PTC-1 in PTC and somewhat controversially demonstrated the association of the ret/PTC-1 rearrangement with Hashimoto thyroiditis (Sheils, 2000a; Sheils 2000b; Sheils, 2002).

This work prompted several further avenues of research, including:

1) Assessment of the relationship of ret/PTC-1 activation to cell adhesion molecule expression e.g. E-cadherin (Smyth, 2001) and β and γ-Catenin (Smyth, 2003)
2) Assessments of the prevalence of the next most common rearrangement (ret/PTC-3) in our sporadic cohort of PTC, with comparison of morphological features of the tumour to specific ret rearrangements (Finn, 2003).

This latter study forms the basis of chapter 3 of this thesis and has been published (Finn, 2003). In this study, highly sensitive TaqMan RTPCR was used to detect ret/PTC-1 and ret/PTC-3 transcripts in the cohort, which included PTCs of varying morphology, accessioned over a 20-year period. Transcripts of ret/PTC-1 and ret/PTC-3 were detected in 43% and 18% of PTCs, respectively. Ret/PTC-3 was detected exclusively in follicular variant subtype (60%) and was not detected in classic PTC. Although the cohort was small the finding of an association of tumour morphology with specific ret rearrangement in a sporadic group has been borne out subsequently. The significant role of mutant BRAF (T1799A leading to V600E) as a possible alternative event in the pathogenesis of PTC has been demonstrated and its association almost exclusively with classic morphology PTC has been striking (Trovisco, 2004). A subsequent study of our cohort has confirmed this impression, with mutant BRAF status strongly associated with classic morphology PTC (Smyth, 2004, in press), although in our series occasional cases of FVPTC demonstrate a

BRAF mutation. Incidentally, mutated BRAF was not detected in a single case of Hashimoto thyroiditis. Our group has noted a small number of tumours that express ret/PTC and mutant BRAF concomitantly (Smyth, 2005,). This is a significant finding because, while some groups have viewed ret activation and BRAF mutation as mutually exclusive molecular events (Soares, 2003; Kimura, 2003), other groups (Xu, 2003, Nikiforova, 2004; Smyth 2005) have shown the presence of both mutant BRAF and a ret rearrangement within the same neoplasms. Although this occurs in a small minority of tumours and generally the mutation and the rearrangement are mutually exclusive, it is, perhaps, more plausible to expect that concomitant occurrence of these molecular events can occur in rare cases, rather than to consider them mutually exclusive molecular events. Biological systems rarely behave in such a strict uncompromising 'black and white' fashion and 'shades of grey' are more often observed.

Recent literature has suggested that ret/PTC is either a secondary event in PTC tumourigenesis or that some PTCs are of multiclonal origin. In one of the most elegant and significant papers to date in this area, Unger *et al* used an elegant Fluorescent in Situ Hybridisation technique to demonstrate heterogeneity in the distribution of ret/PTC rearrangements within individual post-Chernobyl PTCs (Unger, 2004). However, our own group had noted heterogeneity of ret/PTC expression in our cohort and we suggested that this heterogeneity either reflects geographical variation or clonal heterogeneity within the tumours examined (Finn, 2003). The finding was exemplified by a case of Tall Cell Variant PTC that recurred on several occasions and demonstrated chimeric expression of both ret/PTC-1 and ret/PTC-3 transcripts within the same tumour on one occasion and absence of both

rearrangements on another occasion. We have also experienced finding ret/PTC within one microdissected area and absent from another discrete microdissected area within the same tumour each area with identical morphology. Again, this demonstrates the occurrence of intra-tumoural heterogeneity. Prior to the Unger's study, such expression heterogeneity could have been ascribed to an epigenetic phenomenon, whereby the rearrangement is present at the genomic DNA level but subsequently becomes "switched off" by epigenetic mechanisms with repressed expression. However, the approach used by Unger *et al* demonstrates that in fact there is real and verifiable heterogeneity occurring at the genomic level. As time passes it seems that the role of ret rearrangements as initiators of thyroid carcinogenesis is being undermined increasingly by the literature. Indeed, although PTC is known to be associated with Hashimoto thyroiditis and our group has demonstrated ret/PTC-1 in association with Hashimoto thyroiditis (Sheils, 2000b), our group has speculated that ret/PTC expression may be responsible for the lymphocytic infiltrate in Hashimoto thyroiditis and may render the cells liable to immune mediated elimination, curtailing the development of PTC.

The finding of 'radiation signature' ret/PTC-3 activation in a significant minority of the tumours examined in our cohort prompted further research into the effects of radiation on thyroid epithelial cells. Array CGH is a powerful molecular technique that may potentially identify oncogenes and tumour suppressor genes. To make full use of the technology it was decided to attempt to develop a model of Chernobyl carcinogenesis with a focus on the role of gamma irradiation.

Gamma radiation as a potential cause of ret rearrangement has been largely ignored or overlooked. This may be because the most abundant type of radiation occurring initially after Chernobyl was Iodine 131 (I^{131}), emitting β-radiation. Ingestion of contaminated milk by children with actively growing thyroid glands in the context of moderate Iodine deficiency was assumed to be the most likely reason for the marked increase in PTC that subsequently occurred (Williams, 2002). In the past, after much debate, therapeutic radioiodine had not been considered to represent a risk factor for PTC. Although it is reasonable to suggest that I^{131} at a very high level and acting on thyroid glands of young patients in a relatively iodine deficient environment might be the cause of PTC, no direct causal link has been established and the dogma has never been challenged.

In-vitro experiments demonstrated that X-irradiation could induce ret rearrangements (Mizuno, 2000; Ito, 2003) but only at high doses and in those experiments ret/PTC-1 was preferentially induced. However, there is no evidence that abundance of X-irradiation was present after Chernobyl. Therefore, the role of gamma irradiation, the second most abundant contaminant in Chernobyl and one of the most persistent contaminants deserved investigation and consideration as a potential cause of ret rearrangements. In order to closely model Chernobyl, we used Caesium 137 as the radiation source. Caesium is a well-documented post Chernobyl contaminant and decays primarily by emission of gamma radiation.

We expected that cells with induced ret/PTC would enjoy a growth advantage over their counterparts and form dominant clones and relatively stable cell lines for future research. This did not occur and was puzzling because the paradigm in

carcinogenesis was that induction of a ret rearrangement should bestow a selective growth and survival advantage on the cells, which would lead to them forming a clonally expanded population. In fact, ret/PTC-3 transcripts were transiently expressed at low levels by a minority of the cells irradiated. Although this was difficult to rationalise, it can now be understood more easily in the context of the recent literature, which as discussed above now suggests that ret/PTC rearrangements may be a secondary non-clonal event or sub-clonal event, even in Chernobyl PTCs.

However, the experiment did provide proof of principle by demonstrating that gamma radiation at a dose comparable to that received by Chernobyl inhabitants was capable of inducing a ret rearrangement (Finn, 2004). Even more interesting was the exclusive detection of ret/PTC-3 with no expression of ret/PTC-1 at any stage. This finding further supports the concept of ret/PTC-3 as a Chernobyl associated rearrangement. As discussed in chapter 4 it seems likely that ret/PTC-1 is a rearrangement associated with X-ray exposure and ret/PTC-3 associated with gamma or other radiation exposure. This is supported by Mizuno's in-vitro experiments and by the occurrence of ret/PTC-1 transcripts in tumours of children exposed to therapeutic radiation in childhood. Recently our group has demonstrated ret/PTC-1 rearrangements in papillary serous carcinoma of the ovary in a small number of patients with a history of prolonged X-ray exposure. This is the first description of ret rearrangements occurring in non-thyroid malignancies (Flavin, 2004 abstract) and again is suggestive that ret rearrangements are markers of radiation exposure and resulting genomic damage but may not necessarily be the central molecular event in clonal neoplasms.

Array CGH performed on irradiated cells expressing ret/PTC-3 demonstrated a predominant pattern of loss or deletion of genetic material. The array CGH profiles of SV40 large T antigen epithelial transformation were also documented. The data from the array CGH experiment suggest that the subtelomeric regions of chromosomes are particularly vulnerable to radiation induced genomic instability and it was also noteworthy that chromosome 10 appears to represent a hotspot for radiation induced genomic damage in thyroid follicular cells. This is important because of the known association of rearrangements of chromosome 10 with PTC and the demonstration that the spatial architecture of chromosomes within the nucleus may account for specific patterns of radiation damage (Nikiforova, 2000).

As discussed above, array CGH is a powerful tool for the analysis of DNA copy number and loss in tumours. Although, chromosomal instability in PTC has been shown to be low (Kitamura, 2000; Gillespie, 2000), and microsatellite stable (Soares, 1997), the combination of arrayed clones and laser capture microdissection is likely to represent one of the most sensitive methods for identifying potential oncogenes and tumour suppressor genes in neoplasms. For this reason, in chapter five we decided to assess copy gain and loss in well-characterised PTC (i.e. known BRAF and ret/PTC status). The study focussed on potentially clinically significant aberrations in tumours with no currently well-defined molecular trigger.

The primary finding of the study was that DNA copy gain and loss appears to occur in all cases of PTC when tumours are examined using a combination of laser capture microdissection and sensitive array based CGH. Copy gain and loss is more frequent

in cell lines, which no doubt reflects the ease with which aggressive behaving tumours can be maintained in immortal culture, leading to a selection bias for highly genomically unstable tumours. Taking the surgical cases, which more accurately reflect true biology, the study confirmed previous LOH and CGH findings suggesting that genomic instability occurs at a low level in PTC. Aberrations occurred at a mean percentage of aberrations of 6% of all loci examined (Range, 1.45%-11.35%). While this confirms the relative genomic stability of PTC in comparison to other neoplasms and to FTC, it does not mean that the recurrent aberrations that were documented are not significant players in the pathogenesis of at least a sub-group of PTCs. A recent CGH paper has suggested a correlation between gains and losses seen in FVPTC with Follicular Adenoma and FTC (Wreesman, 2004). The current study found no significant pattern of genomic aberration associated with either FVPTC or classic PTC and the aberrations highlighted by Wreesman *et al* were uncommon in our cohort.

However, the occurrence of copy gain of Platelet derived growth factor receptor β (PDGFRB) may well be an extremely significant finding, because this gain occurred exclusively in PTC without BRAF mutation or ret/PTC activation. PDGFRB acts upstream of BRAF and results in activation of the mitogen activated protein kinase cascade (MAPK) (Figure 7.1). This occurs after binding of its ligands leads to dimerisation and subsequent phosphorylation. The activation of MAPK appears to represent one of the most common and central events in PTC pathogenesis. Furthermore, oncogenic mutations that affect V600E in BRAF have also been discovered in members of the platelet derived growth factor receptor family of receptor tyrosine kinases (Dibb, 2004). BRAF V600E and Aspβ9 of the PDGRF-

family kinases occur at identical positions within a region of the kinase domains of these proteins known as the activation segment, which is crucial for regulating enzyme activity in all kinases. The finding of copy gain of PDGRFβ in PTC without evidence of BRAF mutation or either of the common ret rearrangements may represent a further mechanism of upstream activation of BRAF and the MAPK cascade in thyroid carcinogenesis. The parallels are too significant to ignore and further assessment of copy gain of PDGFRB and perhaps mutations of the kinase domain deserve further analysis in a larger cohort of PTC. Like BRAF, PDGFRB has been implicated in the pathogenesis of a number of other neoplasms such as acute myeloid leukaemia and chronic myelomonocytic leukaemia (Reilly, 2002; Pietras, 2003).

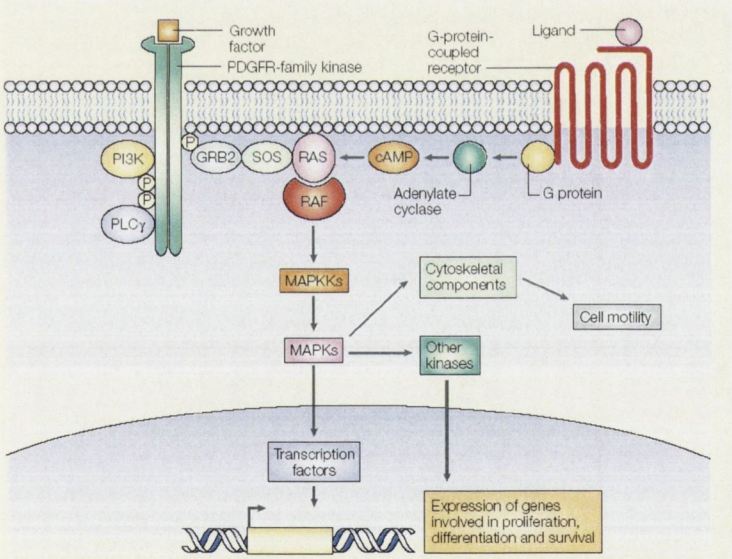

Figure 1 | **Signal transduction by PDGFR-family kinases and BRAF.** BRAF is a component of the RAS–RAF–MAPK (mitogen-activated protein kinase) signalling cascade, which is activated by many external stimuli, including growth-factor binding to receptor tyrosine kinases and G-protein-coupled receptors. Activation of this pathway ultimately results in the phosphorylation of MAPKs, which phosphorylate and regulate the activities of substrates such as transcription factors, cytoskeletal components and other kinases, which in turn regulate cell survival, proliferation, differentiation and motility. In addition to stimulating MAPK signalling, platelet-derived growth factor receptor (PDGFR)-family kinases also activate other signalling pathways — such as those involving phosphatidylinositol 3-kinase (PI3K) and phospholipase-Cγ (PLCγ) — which also lead to changes such as increased proliferation and survival (not shown). MAPKK, MAPK kinase.

Figure 7.1 Signal transduction by PDGRF family kinases and BRAF. Nature Cancer Reviews, Dibb, 2004

Approximately 10% of the population develop palpable thyroid nodules during their lifetime. More than 12,000 new cases of thyroid cancer develop each year in the US, for which scant information on cytogenetic abnormalities is available. The diagnostic tools available to distinguish benign from malignant neoplasms are not always reliable. This results in a large number of patients having to undergo unnecessary surgery. The identification of expressed biomarkers of PTC and other thyroid carcinomas would assist the diagnosis of these neoplasms using minimally invasive FNAC techniques and may eventually give prognostic information that would be of relevance to the patient. In chapter 6, the initial steps of this evaluation were presented. Using sophisticated mathematical approaches and the most completely curated library of expression array ever assembled many potential biomarkers of malignancy have been identified. The system is novel and is the first expression microarray system to utilise chemiluminescence for target quantitation.

It is reassuring that such a new system reliably identified increased expression of targets previously validated as potential biomarkers of malignancy in the literature e.g. Galectin 3, CITED 1, LYN, SERPINA1, LSM7, CD44 and PDAP1 (platelet derived growth factor A associated protein). In addition, the decreased expression of TFF3 and TSHR shows that the system can assess both up and down regulated transcripts. The most exciting findings, however, must be the many transcripts identified that have never previously been associated with thyroid cancer or indeed in many cases have never been associated with any malignancy at all. These targets will provide the basis of ongoing research within our group for the near future. The ability to use low-density microfluidic card TaqMan assays to further investigate the expression array results in a larger cohort of tumours will facilitate this aim.

7.2 Thyroid Cancer: A view of the future

7.2.1 The disappointment of the present

'The discussion of the role that morphology plays and in all likelihood will continue to play for long time to come in "the molecular age", can be divided into two separate categories, i.e., those of diagnostic pathology and investigative pathology. Regarding the former, it is my contention that as of today there is no technique in all of medicine that provides so much information so quickly and for such little cost as the H&E technique. Before too many eyebrows are raised, let me back up this statement with an example. Consider a biopsy of a cervical lymph node in a 25-year-old woman that shows a papillary carcinoma featuring nuclear pseudoinclusions and psammoma bodies. The pathologist examining that section will be able to tell the clinician:

"This patient has a metastatic tumor in this lymph node. The primary tumor is located in the thyroid gland, most likely in the homolateral lobe. It may be very small and not detectable by clinical or radiographic means but trust me, it is there. It is made up of epithelial, more specifically glandular, and even more specifically thyroidal follicular cells. It is likely to be accompanied by multicentric microscopic foci throughout the gland. If radiation had been administered to the neck of this patient during infancy, you should assume a causal relationship with the tumor. Other cervical lymph nodes are likely to be involved, particularly those in the central compartment. The lung is the other site you should look at for additional metastases, but other organs are not likely to be affected at this point. These tumor cells have the capacity to incorporate iodine. This means that if there are any additional tumor foci in this patient, they are likely to show up with a small dose of radioactive iodine, and to regress if a larger dose were to be administered. Most notably, despite the presence of a malignant tumor that has spread out beyond its original site, I can confidently tell you that 10 years from now this patient will probably be alive and well.'

Professor Juan Rosai (Rosai, 2001).

There is no doubt that currently the diagnosis and assessment of prognosis of thyroid carcinoma is based almost exclusively on gross and microscopic examination of H&E stained glass slides and fine needle aspiration cytology material, in a manner that has not appreciably changed for many years. In spite of the massive strides that have occurred in the knowledge of the molecular basis of the PTC and other forms of thyroid cancer, not a single clinically essential diagnostic or prognostic marker has emerged in what for many is a difficult area of morphological pathology with many challenging diagnostic dilemmas. That the great promise of molecular pathology as it is applied to daily clinical thyroid pathology practice has never been fulfilled is extremely disappointing.

7.2.2 The promise of the future

It is inconceivable that thyroid molecular pathology will continue to have a negligible role in daily thyroid pathology practice. It is unfashionable for pathologists to predict the end of classic surgical pathology but if pathology practice is to move forward then our aim as pathologists should be to increasingly evolve our practice and incorporate molecular knowledge into real clinical practice. Some morphologists decried the advent of immunohistochemical technology. However, currently there is no soft tissue or haematolymphoid pathologist who would not have at least 20 immunohistochemical markers in his or her armamentarium for the diagnosis of these challenging lesions. It can only be a matter of time before molecular techniques and molecular biomarkers play as big a role as immunohistochemical stains do now and eventually even thyroid pathology will require molecular input for diagnostic practice. Not only might the results of

microarray analysis one day prevail over histopathological diagnoses with respect to the guidance of treatment and the assessment of prognosis, but it is also possible that, in the near future, histopathological entities will be redefined on the basis of genomic and gene expression patterns at a much higher rate than is happening already. If pathologists neglect the potential of these processes at this early stage, it is not unimaginable that in the future their task will be limited to the assessment of whether or not a sample contains adequate material for microarray analysis or whether a tumour's histology is compatible with the more precise diagnosis made by geneticists or chemists, or just handing over samples to specialists from other disciplines after dissection! This latter situation is not only a worst case scenario for pathology as a profession, but it may also be harmful to the patient, because adequate sampling of representative tissue for diagnostic molecular analysis certainly requires the expertise of a trained pathologist (Snijders, 2000).

7.2.3 Magic Bullets

In the future, a patient presenting with a thyroid lesion will be diagnosed using both classical and molecular techniques. Cells, aspirated from the lesion, will be examined both cytologically and classified using ancillary technologies that may include immuncytochemistry, FISH, RTPCR, expression microarray studies and proteomic arrays. Therapy will be tailored to individual patients needs. Furthermore, eventually an in depth knowledge of the genome, transcriptome and proteome of thyroid carcinoma may allow us to identify potential therapeutic targets for future manipulation by target specific drugs, so-called 'magic bullets'. Such an approach has been highly successful recently with the use of Gleevec (a tyrosine

kinase inhibitor) in Gastro-intestinal stromal tumours (GIST) and chronic myeloid leukaemia (CML). PTC is a relatively indolent neoplasm, in comparison to malignant GIST and CML, and it seems unreasonable that a relatively biologically indolent neoplasm should require disfiguring surgery to the neck for eradication in some cases. Medical 'magic bullet' therapy would be a more attractive treatment modality. In addition, a minority of these tumours behave in an aggressive fashion and tumour specific biomolecules may provide useful targets for disease control in the small group of patients with aggressive disease. The methods used for the analysis of PTC in this thesis may be widened to target aggressive fatal neoplasms such as anaplastic thyroid carcinoma, widely invasive FTC and poorly differentiated thyroid carcinoma. Even now, research is underway to explore potential for viral mediated gene therapy for the management of metastatic thyroid carcinoma (DeGroot, 2004), dendritic cell-based immunotherapy in thyroid malignancies (Schott, 2003) and redifferentiation therapy in advanced thyroid cancer (Haugen, 2004).

Albert Einstein may have the last word.

"I never think of the future: it comes soon enough!"

7.3 References

DeGroot LJ, Zhang R. 2004. Viral mediated gene therapy for the management of metastatic thyroid carcinoma. Curr Drug Targets Immune Endocr Metabol Disord. (3):235-44

Dibb NJ, Dilworth SM, Mol CD. 2004. Switching on kinases: oncogenic activation of BRAF and the PDGFR family. Nat Rev Cancer. (9): 718-27.

Finn SP, Smyth P, O'Leary J, Sweeney EC, Sheils O. 2003. Ret/PTC chimeric transcripts in an Irish cohort of sporadic papillary thyroid carcinoma. J Clin Endocrinol Metab. 88(2):938-41

Finn SP, Smyth P, O'Regan EM, Cahill S, Flavin R, O'Leary JJ, Sheils OM. 2004. Array comparative genomic hybridisation analysis of gamma-irradiated human thyrocytes. Virchows Archiv. 445: 396-404

Flavin RJ, Finn SP, Smyth P, O'Regan EM, Gaffney E, O'Leary JJ, Sheils OM. 2004. Ret/PTC-1 a novel chimeric transcript occurring in Ovarian Serous surface Carcinomas: Preliminary Results. Abstract published Modern Pathology Vol. 17 no. 1 (Supplement).

Gillespie JW, Nasir A, Kaiser HE. 2000. Loss of heterozygosity in papillary and follicular thyroid carcinoma: a mini review. In Vivo. 14(1):139-40

Haugen BR. 2004. Redifferentiation therapy in advanced thyroid cancer. Curr Drug Targets Immune Endocr Metabol Disord. (3):175-80.

Ito T, Seyama T, Iwamoto KS, Hayashi T, Mizuno T, Tsuyama N, Dohi K, Nakamura N, Akiyama M. 1993. In vitro irradiation is able to cause RET oncogene rearrangement. Cancer Res. 53(13):2940-3

Kimura ET, Nikiforova MN, Zhu Z, Knauf JA, Nikiforov YE, Fagin JA. 2003. High prevalence of BRAF mutations in thyroid cancer: genetic evidence for constitutive activation of the RET/PTC-RAS-BRAF signaling pathway in papillary thyroid carcinoma. Cancer Res 63(7): 1454-7

Kitamura Y, Shimizu K, Tanaka S, Ito K, Emi M. 2000. Association of allelic loss on 1q, 4p, 7q, 9p, 9q, and 16q with postoperative death in papillary thyroid carcinoma. Clin Cancer Res. 6(5): 1819-25

Mizuno T, Iwamoto KS, Kyoizumi S, Nagamura H, Shinohara T, Koyama K, Seyama T, Hamatani K. 2000. Preferential induction of RET/PTC1 rearrangement by X-ray irradiation. Oncogene. 19(3): 438-43

Nikiforova MN, Stringer JR, Blough R, Medvedovic M, Fagin JA, Nikiforov YE. 2000. Proximity of chromosomal loci that participate in radiation-induced rearrangements in human cells. Science. 290(5489): 138-41.

Nikiforova MN, Ciampi R, Salvatore G, Santoro M, Gandhi M, Knauf JA, Thomas GA, Jeremiah S, Bogdanova TI, Tronko MD, Fagin JA, Nikiforov YE. 2004. Low prevalence of BRAF mutations in radiation-induced thyroid tumors in contrast to sporadic papillary carcinomas. Cancer Lett. 209(1): 1-6.

Pietras K, Sjoblom T, Rubin K, Heldin CH, Ostman A. 2003. PDGF receptors as cancer drug targets. Cancer Cell. (5):439-43.

Reilly JT. 2002. Class III receptor tyrosine kinases: role in leukaemogenesis. Br J Haematol. 116(4): 744-57

Rosai J. 2001. The continuing role of morphology in the molecular age. Mod Pathol. 14(3): 258-60

Schott M, Seissler J. 2003. Dendritic cell vaccination: new hope for the treatment of metastasized endocrine malignancies. Trends Endocrinol Metab. 14(4): 156-62

Sheils OM, O'Leary JJ, Sweeney EC. 2000a. Assessment of ret/PTC-1 rearrangements in neoplastic thyroid tissue using TaqMan RT-PCR. J Pathol. 192(1): 32-6.

Sheils OM, O'Leary JJ, Uhlmann V, Lattich K, Sweeney EC. 2000b. ret/PTC-1 Activation in Hashimoto Thyroiditis. Int J Surg Pathol. 8(3): 185-189

Sheils O, Smyth P, Finn S, Sweeney EC, O'Leary JJ. 2002. RET/PTC rearrangements in Hashimoto's thyroiditis. Int J Surg Pathol. 10(2): 167-8

Smyth P, Sheils O, Finn S, Martin C, O'Leary J, Sweeney EC. 2001. Real-time quantitative analysis of E-cadherin expression in ret/PTC-1-activated thyroid neoplasms. Int J Surg Pathol. 9(4):265-72.

Smyth P, Finn S, O'Leary J, Sheils O. 2003. Real-time analysis of beta- and gamma-catenin mRNA expression in ret/PTC-1 activated and nonactivated thyroid tissues. Diagn Mol Pathol. 12(1):44-9

Smyth P, Finn SP, Cahill S, Flavin R, O'Regan EM, O'Leary JJ, Sheils OM. 2005. Ret/PTC and BRAF act as distinct molecular time dependent triggers in a sporadic cohort of papillary thyroid carcinoma. Int J Surg Pathol 13(1): 1-8

Snijders AM, Meijer GA, Brakenhoff RH, van den Brule AJ, van Diest PJ. 2000. Microarray techniques in pathology: tool or toy? Mol Pathol. 53(6):289-94.

Soares P, dos Santos NR, Seruca R, Lothe RA, Sobrinho-Simoes M. 1997. Benign and malignant thyroid lesions show instability at microsatellite loci. Eur J Cancer. 33(2):293-6

Unger K, Zitzelsberger H, Salvatore G, Santoro M, Bogdanova T, Braselmann H, Kastner P, Zurnadzhy L, Tronko N, Hutzler P, Thomas G. 2004. Heterogeneity in the distribution of RET/PTC rearrangements within individual post-Chernobyl papillary thyroid carcinomas. J Clin Endocrinol Metab. 89(9):4272-9

Soares P, Trovisco V, Rocha AS, Lima J, Castro P, Preto A, Maximo V, Botelho T, Seruca R, Sobrinho-Simoes M. 2003. BRAF mutations and RET/PTC rearrangements are alternative events in the etiopathogenesis of PTC. Oncogene 22(29): 4578-80

Trovisco V, Vieira de Castro I, Soares P, Maximo V, Silva P, Magalhaes J, Abrosimov A, Guiu XM, Sobrinho-Simoes. 2004. BRAF mutations are associated with some histological types of papillary thyroid carcinoma. J Pathol. 202(2): 247-51

Williams ED. Cancer after nuclear fallout: lessons from the Chernobyl accident. 2002. Nature Reviews Cancer 2: 543-549

Wreesmann VB, Ghossein RA, Hezel M, Banerjee D, Shaha AR, Tuttle RM, Shah JP, Rao PH, Singh B. 2004. Follicular variant of papillary thyroid carcinoma: genome-wide appraisal of a controversial entity. Genes Chromosomes Cancer (4): 355-64.

Xu X, Quiros RM, Gattuso P, Ain KB, Prinz RA. 2003. High prevalence of BRAF gene mutation in papillary thyroid carcinomas and thyroid tumor cell lines. Cancer Res. 63(15): 4561-7.

Appendix

No.	Standard Name	Description	Cyto Loc
1	CEB108/T7	1p tel; CEB108/T7	1p tel
2	1PTEL06	1PTEL06; 1p tel-2	1p tel
3	CDC2L1 (p58)	P58, CDC2L1	1p36
4	PRKCZ	D1S243 (AFM214yg7), PRKCZ	1p36.33
5	TP73	TP73	1p36.33
6	D1S2660	D1S2660 (AFMa203yc1)	1p36.32
7	D1S214	D1S214	1p36.31
8	D1S1635	D1S1635 (CHLC.ATA9B08)	1p36.22
9	D1S199	D1S199	1p36.13
10	FGR (SRC2)	FGR (SRC2)	1p36.2-p36.1
11	MYCL1 (LMYC)	MYCL1 (LMYC)	1p34.3
12	D1S427, FAF1	D1S427, FAF1	1p32.3
13	D1S500	D1S500 (AFM343vf9)	1p31.1
14	D1S418	D1S418 (AFM197yg1)	1p13.1
15	NRAS	NRAS	1p13.2
16	D1S2465, D1S3402	D1S2465, D1S3402	1p12
17	WI-5663, WI-13414	WI-5663, WI-13414	1q21
18	LAMC2	LAMC2	1q25-q31
19	PTGS2(COX2)	PTGS2(COX2)	1q31.1
20	TGFB2	TGFB2	1q41
21	AKT3	AKT3	1q44
22	SHGC-18290	SHGC-18290; 1q tel-2	1q tel
23	1QTEL10	1q tel; 1QTEL10	1q tel
24	U32389	2 p tel; U32389	2p tel
25	2PTEL27	D2S2983 (2PTEL27)	2p tel
26	MYCN(N-myc)	MYCN (N-myc)	2p24.1
27	MSH2, KCNK12	MSH2, KCNK12	2p22.3-2p22.1
28	REL	REL	2p13-p12
29	GNLY	GNLY	2p12-q11
30	SGC34236	2q paracentric	2q13
31	BIN1	BIN1	2q14
32	LRP1B	LRP1B	2q21.2
33	TBR1	TBR1	2q23-q37
34	ITGA4	ITGA4	2q31-q32
35	CASP8	CASP8	2q33-q34
36	ERBB4(HER-4)	HER-4	2q33.3-q34
37	WI-6310	WI-6310; 2qtel-2	2q tel
38	D2S447	2q tel; D2S447	2q tel
39	3PTEL25	D3S4559 (3PTEL25)	3p tel

40	3PTEL01,CHL1	CHL1, 3PTEL01, 3PTEL02; 3ptel-2	3p tel
41	VHL	VHL	3p25-p26
42	RAF1	RAF1	3p25
43	THRB	THRB	3p24.3
44	MLH1	MLH1	3p21.3-p23
45	RASSF1	RASSF1	3p21.3
46	FHIT	FHIT	3p14.2
47	p44S10	p44S10	3p14.1
48	D3S1274, ROBO1	D3S1274, ROBO1 (DUTT1)	3p12-3p13
49	RBP1, RBP2	RBP1, RBP2	3q21-q22
50	TERC	TERC (hTR)	3q26
51	EIF5A2	EIF5A2	3q26.2
52	PIK3CA	PIK3CA	3q26.3
53	TP63	TP63	3q27-q29
54	MFI2	sts-M12154; 3q tel-2	3q tel
55	3QTEL05	D3S4560 (3QTEL05)	3q tel
56	GS10K2/T7	4p tel	4p tel
57	SHGC4-207	4p tel-2	4p tel
58	D4S114	Wolf-Hirschhorn clone #2	4p16.3
59	WHSC1	WHSCR(WHSC1)	4p16.3
60	DDX15	DDX15	4p15.3
61	KIT	c-KIT	4q11-q12
62	PDGFRA	PDGFRA	4q11-q13
63	EIF4E	EIF4E	4q24 (by ucsc)
64	PGRMC2	PGRMC2	4q26
65	PDZ-GEF1	PDZ-GEF1 (KIAA0313)	4q32.1
66	4QTEL11	4QTEL11; 4q tel-2	4q tel
67	D4S2930	4q tel	4q tel
68	C84C11/T3	5p tel	5p tel
69	D5S23	D5S23	5p15.2
70	D5S2064	D5S2064 2nd Cri du chat	5p15.2
71	DAB2	DAB2 (DOC-2)	5p13
72	DHFR, MSH3	DHFR, MSH3	5q11.2-q13.2
73	APC	APC	5q21-q22
74	EGR1	EGR1	5q31.1
75	CSF1R	CSF1R	5q33-q35
76	NIB1408	NIB1408; 5q tel-2	5q tel
77	5QTEL70	5q tel	5q tel
78	6PTEL48	6p tel	6p tel
79	PIM1	PIM1	6p21.2
80	CCND3	CCND3	6p21

81	D6S414	D6S414	6p12.1-p21.1
82	HTR1B	HTR1B	6q13
83	D6S434	D6S434	6q16.3
84	D6S268	D6S268	6q16.3-q21
85	MYB	MYB	6q22-q23
86	D6S311	D6S311	6q23-24
87	ESR1	ESR (ER)	6q25.1
88	6QTEL54	6q tel	6q tel
89	G31341	7p tel	7p tel
90	IL6	IL6	7p21
91	EGFR	EGFR (ERBB1)	7p12.3-p12.1
92	ELN	ELN (Elastin)	7q11.23
93	RFC2,CYLN2	WBSCR5, RFC2, CYLN2	7q11.23
94	ABCB1 (MDR1)	PGY1 (MDR1, ABC20)	7q21.1
95	CDK6	CDK6	7q21-q22
96	SERPINE1	PLANH1(PAI-1)	7q21.3-q22
97	MET	MET	7q31
98	TIF1	TIF1	7q32-q34
99	stSG48460	StSG48460; 7qtel-2	7q tel
100	7QTEL20	7q tel	7q tel
101	D8S504	8p tel	8p tel
102	D8S596	D8S596; 8ptel-2	8p tel
103	CTSB	CTSB	8p22
104	PDGRL	PRLTS	8p22-p21.3
105	LPL	LPL	8p22
106	FGFR1	FGFR1(FLG)	8p11.2-p11.1
107	MOS	MOS	8q11
108	E2F5	E2F5	8p22-q21.3
109	EXT1	EXT1	8q24.11-q24.13
110	MYC	MYC (c-myc)	8q24.12-q24.13
111	PTK2	FAK	8q24-qter
112	SHGC-31110	SHGC-31110; 8qtel-2	8q tel
113	U11829	8q tel	8q tel
114	AF170276	9p tel	9p tel
115	D9S913	D9S913, SHGC-140396; 9p tel-2	9ptel
116	MTAP	MTAP	9p21.3
117	CDKN2A (p16), MTAP	CDKN2A (INK4A, p16), CDKN2B (INK4B, p15), MTAP	9p21
118	AFM137XA11	AFM137XA11	9p11.2
119	D9S166	D9S166	9p12-q21
120	PTCH	PTCH	9q22.3

121	DBCCR1	DBCCR1	9q33.2
122	TSC1	TSC1	9q34
123	ABL1	ABL1 (ABL)	9q34.1
124	H18962	embl-H18962; 9q tel-2	9q tel
125	D9S325	9q tel	9q tel
126	10PTEL006	10p tel	10p tel
127	SHGC-44253	SHGC-44253; 10ptel-2	10p tel
128	D10S249, D10S533	D10S249, D10S533	10p15
129	GATA3	GATA3	10p15
130	WI-2389, D10S1260	WI-2389, D10S1260 (Di George chromosome region2)	10p14-p13
131	BMI1	BMI1	10p13
132	D10S167	D10S167	10p11-10q11
133	EGR2	EGR2,SHGC-145038	10q21.3
134	PTEN	PTEN (MMAC1)	10q23.3
135	FGFR2	FGFR2 (BEK, K-SAM)	10q26
136	DMBT1	DMBT1	10q25.3-q26.1
137	StSG27915	StSG27915;10q tel-2	10q tel
138	10QTEL24	10q tel	10q tel
139	11PTEL03	11p tel	11p tel
140	INS	INS, WIAF-1245; 11p tel-2	11p tel
141	HRAS	HRAS	11p15.5
142	CDKN1C (p57)	P57, KIP2	11p15.5
143	WT1	WT1	11p13
144	KAI1	KAI1	11p11.2
145	D11S461	D11S461	11q12.2
146	MEN1	MEN1	11q13
147	CCND1	CCND1 (BCL1)	11q13
148	FGF4,FGF3	FGF4 (HSTF1), FGF3 (INT2)	11q13
149	EMS1	EMS1	11q13
150	GARP	GARP (D11S833E)	11q13.5-q14
151	PAK1	PAK1	11q13-q14
152	RDX	RDX	11q22.3
153	ATM	ATM	11q22.3
154	MLL	MLL	11q23
155	WI-6509	WI-6509;11q tel-2	11q tel
156	AF240622	11q tel, VIJ-YRM2072	11q tel
157	8M16/SP6	12p tel	12p tel
158	SHGC-5557	SHGC-5557; 12p tel-2	12p tel
159	CCND2	CCND2	12p13
160	CDKN1B(p27)	CDKN1B, (p27, KIP1)	12p13.1-p12

161	KRAS2	KRAS2	12p11.2
162	WNT1 (INT1)	WNT1 (INT1)	12q12-q13
163	CDK2, ERBB3	CDK2, HER-3	12q13
164	GLI	GLI	12q13.2-q13.3
165	SAS, CDK4	SAS, CDK4	12q13-q14
166	MDM2	MDM2	12q14.3-q15
167	DRIM, ARL1	DRIM, ARL1	12q23
168	StSG8935	StSG8935; 12q tel-2	12q tel
169	U11838	12q tel	12q tel
170	BRCA2	BRCA2	13q12-q13
171	RB1	RB1, TGFBR1	13q14
172	D13S319	D13S319	13q14.2
173	D13S25	D13S25	13q14.3
174	D13S327	13q tel	13q tel
175	PNN (DRS)	PNN (Pinin, DRS, memA)	14q13
176	TCL1A	TCL1 (D14S62)	14q32.1
177	AKT1	AKT1	14q32.32
178	IGH (D14S308)	14q tel-2	14q tel
179	IGH (SHGC-36156)	14q tel	14q tel
180	D15S11	D15S11	15q11-q13
181	SNRPN	SNRPN	15q12
182	UBE3A, D15S10	UBE3A, D15S10	15q11-q13
183	GABRB3	GABRB3	15q11.2-q12
184	MAP2K5	MAP2K5	15q23
185	FES	FES	15q26.1
186	IGF1R	IGF1R	15q25-q26
187	PACE4C	PACE4C; 15q tel-2	15q tel
188	WI-5214	15q tel	15q tel
189	16PTEL03	16p tel	16p tel
190	StSG48414	StSG48414; 16ptel-2	16p tel
191	CREBBP	CREB	16p13.3
192	EMP2	EMP2 (SHGC-147579)	16p13.3
193	ABCC1 (MRP1)	ABCC1 (MRP, MRP, ABC29)	16p13.1
194	CYLD	CYLD1	16q12-q13
195	CDH1	CDH1	16q22.1
196	FRA16D	FRA16D	16q23.2
197	CDH13	CDH13	16q24.2-q24.3
198	LZ16	LZ16 (D16S3026)	16q24.2
199	FANCA	FANCA	16q24.3
200	StSG30213	StSG30213; 16qtel-2	16q tel
201	16QTEL013	16q tel	16q tel

202	282M15/SP6	17p tel	17p tel
203	WI-14673	WI-14673; 17ptel-2	17p tel
204	HIC1	HIC1	17p13.3
205	D17S379, MNT	D17S379, MNT	17p13.3
206	PAFAH1B1 (LIS1)	LIS1	17p13.3
207	TP53 (p53)	TP53(p53)	17p13.1
208	D17S125,D17S61	D17S125, D17S61	17p12-p11.2
209	D17S1296, D17S1523	D17S1296, D17S1523	17p12-p11.2
210	LLGL1	LLGL1	17p12-17p11.2
211	FLI, TOP3A	FLI, TOP3A	17p12-17p11.2
212	NF1 5'	NF1 5'	17q11.2
213	NF1 3'	NF1 3'	17q11.2
214	BRCA1	BRCA1	17q21
215	PPARBP (PBP)	PBP	17q12
216	ERBB2 (HER-2)	ERBB2 (HER-2/neu, EGFR2)	17q11.2-17q12
217	THRA	THRA	17q11.2
218	TOP2A	TOP2A	17q21-q22
219	NME1 (NME23)	NME1 (NME2, NM23)	17q21.3
220	RPS6KB1 (STK14A)	RPS6KB1 (STK14A)	17q23
221	D17S1670	D17S1670, WI-6857	17q23
222	TK1	TK1	17q23.2-q25.3
223	SHGC-103396	17qtel-2	17q tel
224	AFM217YD10	17q tel	17q tel
225	D18S552	18p tel, VIJ-YRM2102	18p tel
226	SHGC17327	18ptel-2	18p tel
227	YES1	YES1	18p11.31-p11.21
228	TYMS (TS)	TS	18p11.32
229	LAMA3	LAMA3	18q11.2
230	FRA18A(D18S978)	FRA18A, D18S978	18q12.3
231	DCC	DCC	18q21.3
232	MADH4(DPC4)	DPC4, SMAD4	18q21.1
233	BCL2 3'	BCL2-3'	18q21.3
234	CTDP1, SHGC-145820	CTDP1, SHGC-145820; 18qtel-2(formerlyRH1664)	18q tel
235	18QTEL11	18q tel	18q tel
236	129F16/SP6	19p tel	19p tel
237	StSG42796	StSG42796; 19p tel-2	19p tel
238	INSR	INSR	19p13.2
239	JUNB	JUNB	19p13.2
240	CCNE1	CCNE1	19q12

241	AKT2	AKT2	19q13.1-q13.2
242	GLTSCR2,SULT2A1	WI-11704, D19S902	19q13.32
243	D19S238E	19q tel	19 q tel
244	20PTEL18	20p tel	20p tel
245	SOX22	Sox-22,WI-14697,WI-15102; 20p tel-2	20p tel
246	JAG1	JAG1	20p12.1-p11.23
247	MKKS, SHGC-79896	SHGC-79896 2nd Alagille	20p12.1-p11.23
248	TOP1	TOP1	20q12-q13.1
249	NCOA3(AIB1)	NCOA3 (AIB1, RAC3, TRAM-1)	20q12
250	MYBL2	MYBL2	20q13.1
251	CSE1L(CAS)	CSE1L (CAS)	20q13
252	PTPN1	PTPN1	20q13.1-q13.2
253	STK6(STK15)	STK6 (STK15, BTAK, aurora 2)	20q13.2-q13.3
254	ZNF217(ZABC1)	ZNF217 (ZABC1)	20q13.2
255	CYP24	CYP24	20q13.2
256	TNFRSF6B(DCR3)	DCR3	20q13
257	TPD52L2,TOM	RH-74935; 20q tel-2	20q tel
258	20QTEL14	20q tel	20q tel
259	D21S378	D21S378 (LSI 21q11.2)	21q11.2
260	RUNX1(AML1)	AML1	21q22.3
261	DYRK1A	DYRK1	21q22
262	D21S341,D21S342	D21S341, D21S342	21q22.3
263	PCNT2(KEN)	KEN(PCN);21q tel-2	21q tel
264	21QTEL08	21q tel	21q tel
265	D22S543	D22S543	22q11
266	GSCL	GSCL	22q11.21
267	HIRA(TUPLE1)	HIRA (TUPLE 1, TUP1, DGCR1)	22q11.21
268	TBX1	TBX1 (GNB1L)	22q11.2
269	BCR	BCR (CML, PHL, BCR1, D22S11, D22S662)	22q11.23
270	NF2	NF2	22q12.2
271	PDGFB(SIS)	PDGFB (SIS)	22q13.1
272	ARHGAP8	ARHGAP8	22q13.3
273	ARSA	ARSA; 22q tel-2nd	22q tel
274	22QTEL31	22q tel	22q tel
275	DXYS129	X/Y p tel	X/Yp tel
276	STS 3'	STS	Xp22.3
277	STS 5'	STS 2nd STSclone	Xp22.3
278	KAL	KAL	Xp22.3
279	DMD exon 45-51	DMD exon 45-51	Xp21.1
280	DXS580	DXS580	Xp11.2
281	DXS7132	DXS7132	Xq12

282	AR 3'	AR 3'	Xq11-q12
283	XIST	XIST	Xq13.2
284	OCRL1	OCRL1	Xq25
285	EST CDY16c07	X/Yq tel	X/Yq tel
286	SRY	SRY	Yp11.3
287	AZFa region	AZFa region	Yq11